THE UNIVERSITY
of EDINBURGH

Studies on the intracellular life of the melioidosis pathogen *Burkholderia pseudomallei*

Nurhamimah Zainal Abidin

Doctor of Philosophy
University of Edinburgh
2018

DECLARATION OF AUTHORSHIP

I hereby declare that this thesis is composed entirely by myself, and it contains no material previously submitted in substance for any other degree. The work reported in this thesis herein is my own, except where due acknowledgement or reference is made in the text.

Nurhamimah Zainal Abidin

THESIS ABSTRACT

Melioidosis, caused by the environmental Gram negative bacillus *Burkholderia pseudomallei*, is an emerging infectious disease affecting both animals and humans. *B. pseudomallei* has the ability to enter the host cell and escape from the phagosome. Once in the cytoplasm, the pathogen proliferates and expresses a virulence-associated protein known as BimA which polymerises cellular actin at the pole of the bacterium to promote its movement inter- and intracellularly, a process known as actin-based motility. This actin-based motility is also used as a strategy to evade host immune responses and survive intracellularly.

In the first part of the thesis, we demonstrate that a *B. pseudomallei* Δ*bimA* mutant displays impaired intracellular survival compared to the isogenic parent strain in BALB/C bone-marrow derived macrophages (BMDMs), notably at later time points post-infection. Macrophages are the key innate immune cells that control *B. pseudomallei in vivo* and *in vitro*, and BALB/C mice provide an excellent model of acute human melioidosis. We also have determined that in BMDMs, the Δ*bimA* mutant is able to escape from the phagosome and enters the cytosol where it is unable to form actin tails. We used targeted, hypothesis-driven experiments to identify potential cell-autonomous innate mechanism/s of killing the mutant. First, we speculated that BimA mediates escape from autophagy. However our studies, including LC3-conversion assays, and bacterial co-localisation studies, failed to demonstrate a role for autophagy in clearance of the Δ*bimA* mutant from infected BMDMs.

In the second part of this thesis, we investigated the role of Toll-like Receptors (TLR) in recognition and elimination of *B. pseudomallei*. MyD88 (Myeloid differentiation primary-response gene 88) and TRIF (TIR-domain-containing adaptor protein inducing IFNβ) are the main adaptor proteins involved in TLR signalling. We utilised the gene silencing technique using short interfering RNAs (siRNAs) to knockdown MyD88 transcript, and in a separate experiment used MyD88- or TRIF-blocking peptides. In addition, we investigated the involvement of canonical and non-canonical inflammasome pathways in cell-autonomous immunity of the BMDMs. However, none of these pathways were shown to be involved in clearance of the Δ*bimA* mutant from infected BMDMs.

Finally we took an unbiased approach by microarray to characterise the global host transcriptome in BALB/C BMDMs upon *B. pseudomallei* infection, and to identify specific responses to the Δ*bimA* mutant. Analyses performed at the gene level revealed that several

interferon signalling-related pathways are activated in cells infected with either the WT or Δ*bimA* mutant strains. A number of other pro-inflammatory mediators that are commonly seen in general inflammatory infections, such as IL-1α, IL-1β, IL-12β, and IL-6, were also upregulated. Interestingly, the cytoplasmic RNA sensors RIG-1 and MDA-5, thought primarily to be involved in the detection of RNA viruses, were also induced upon *B. pseudomallei* infection. Very few pathways were associated with a specific macrophage response to the Δ*bimA* mutant, indicating that an as yet undescribed pathway may play a role in sensing and eliminating the Δ*bimA* mutant.

We conclude that actin-based motility mediates escape of *B. pseudomallei* from macrophage intracellular killing through a novel pathway which has yet to be unravelled.

LAY SUMMARY

Melioidosis, an emerging infectious disease that can affect both animals and humans, is caused by the bacterium *Burkholderia pseudomallei*. Melioidosis is endemic in tropical regions particularly in Southeast Asia and Northern Australia. Current diagnostic methods have limitations, no licensed vaccine is available and antibiotic therapy is often ineffective.

Macrophages are phagocytes that play a central role in the innate immune response to infection, including *B. pseudomallei*. After invading macrophages, *B. pseudomallei* escapes from the phagosome and enters the cytoplasm. Once in the cytoplasm, *B. pseudomallei* replicates and moves within and between the host cells via a mechanism known as actin-based motility. Actin-based motility is mediated by a bacterial protein called BimA which allows *B. pseudomallei* to avoid macrophage recognition and hence, to survive in the host cells. In this thesis we attempt to identify the immune surveillance pathways in macrophages that could be involved in detecting and killing the bacterium. We use a murine bone-marrow derived macrophage (BMDM) cell model system where we compare the ability of *B. pseudomallei* and a Δ*bimA* mutant strain which is unable to form actin tails to survive and replicate.

Autophagy is a process that deals with cellular stress, destroys unwanted proteins and organelles, and hence, maintains cellular homeostasis. Several studies have shown that autophagy also helps to eliminate intracellular pathogens, but some pathogens subvert this autophagic pathway to establish a persistent infection, including *B. pseudomallei*. Here we hypothesised that the BimA protein mediates the escape from autophagy, however, our findings did not agree with this hypothesis. We then investigated the role of Toll-like Receptors (TLR)-signalling in recognition and elimination of *B. pseudomallei*. TLRs are one of the major innate immune sensors which recognise pathogen-associated molecular patterns (PAMPs) and initiates immune responses to resolve infections. Activated TLRs also link to the activation of the canonical and non-canonical inflammasomes. Inflammasomes are multiprotein oligomers which assemble upon activation to promote the maturation and secretion of inflammatory cytokines and induce the cell death. However, none of these pathways were involved in the clearance of the Δ*bimA* mutant from infected cells.

We also took an unbiased approach to characterise which cellular genes are switched on upon infection of cells with *B. pseudomallei* infection and to identify specific responses to the Δ*bimA* mutant. Our analysis identified pro-inflammatory mediators, that are commonly

associated with general inflammatory infections, were upregulated in cells infected with either WT or Δ*bimA* mutant. Several Interferon Signalling-related pathways along with cytoplasmic RNA sensors, were also induced upon *B. pseudomallei* infection. Very few pathways were associated with a specific macrophage response to the Δ*bimA* mutant, indicating that an as yet undescribed pathway may play a role in sensing the Δ*bimA* mutant.

These studies allow us to conclude that actin-based motility mediates escape of *B. pseudomallei* from macrophage intracellular killing through a novel pathway which has yet to be unravelled.

ACKNOWLEDGEMENTS

This thesis becomes a reality with amazing support from many individuals who were instrumental to my PhD journey. It is my pleasure to extend my sincere thanks to all of them.

First and foremost, I would like to express my special gratitude to my supervisor, Dr Jo Stevens who never failed to motivate me from inception to completion, and always has confidence in my abilities as a developing research student. Her generous supports and guidance as well as constant supervision made it possible for me to complete this doctoral studies.

I would also like to acknowledge the invaluable guidance of members of thesis committee; Dr Denis Headon (thesis chair), Prof Mark Stevens (thesis internal advisor) and Prof Ross Fitzgerald (second supervisor). They have contributed many discussions and given helpful suggestions that shape this project.

I would also like to recognise the important roles of my research lab colleagues especially Dr Kirsty Jensen who never failed to guide me in immunology both in theory and lab works. My greatest thanks also goes to the group research assistant Dr Charles Vander-Broek whom I always discussed with on the result analysis. I would also like to thank Declan King who I always bothered with microarray questions from sample preparation to the analysis and also Dr Clare Pridans who was invaluable for teaching me on bone-marrow isolation and the preparation of bone-marrow derived macrophages (BMDMs). The work in this thesis would not have been possible without the support and friendship of my lab mates. Their kindness and also good humour have made my lab experiences incredibly enjoyable. It was a pleasure working with them. I would like to acknowledge Malaysia Scholarship MARA (Majlis Amanah Rakyat) for financially sponsoring my doctoral studies and had believe in me to make this journey a success.

A thousand thanks are sent to my family and friends for their understanding and patience along this journey. I would want to express my deepest appreciation and love towards my parents Zainal Abidin Ali and Fauziah Sanudin for their endless encouragement to follow my dreams. Thank you to the love of my life, my husband Shafiee Mohd Yusop. You were always there amazingly supportive from the day I received an unconditional offer to pursue PhD. Thank you for patiently dealing with my difficulties I had, and filling my life with happiness.

TABLE OF CONTENTS

DECLARATION OF AUTHORSHIP……i
THESIS ABSTRACT...…… ……..…….ii
LAY SUMMARY…… iv
ACKNOWLEDGEMENTS……...….vi
TABLE OF CONTENTS…….....…….vii
LIST OF FIGURES……xi
LIST OF TABLES…….....…….....xiv
LIST OF COMMONLY USED ABBREVIATIONS…….....…….xvi

1 CHAPTER 1: INTRODUCTION 1

1.1 *Burkholderia pseudomallei* and melioidosis 1

1.1.1 History, Background and Epidemiology 1

1.1.2 Routes of infection 3

1.1.3 Host risk factors, clinical presentations and treatment 3

1.1.4 Taxonomy and related species 4

1.2 Pathogenesis and intracellular lifestyle of *Burkholderia pseudomallei* 6

1.2.1 Adhesion to host cells 7

1.2.2 Entry into host cells 7

1.2.3 Escape from endocytic vesicles 9

1.2.4 Actin-based motility 10

1.2.5 Multi-nucleated giant cell (MNGC) formation 16

1.3 *Burkholderia pseudomallei* and host immune responses 19

1.3.1 Murine models of melioidosis 19

1.3.2 Role of neutrophils and macrophages in melioidosis 20

1.4 Host cell-autonomous immunity in response to microbial infection 22

1.4.1 Toll-Like receptor signalling pathways in melioidosis 26

1.4.2 Canonical inflammasome pathways in counteracting *Burkholderia pseudomallei* 30

1.4.3 The non-canonical inflammasome, an indispensable defence against *Burkholderia pseudomallei* 33

1.4.4 Interferon response to *Burkholderia pseudomallei* and other intracellular pathogens .. 34

1.4.5 Autophagy as a host innate mechanism against *Burkholderia pseudomallei* 39

1.5 Central hypothesis and objectives of thesis 45

2 CHAPTER 2: MATERIALS AND METHODS 46
2.1 Preparation of murine bone marrow cells 46
2.2 Differentiation of bone marrow-derived macrophages (BMDMs) 46
2.3 Phenotypic characterisation of BMDM cells by Flow Cytometry 47
2.4 Phagocytosis assay 47
2.5 Bacterial strains 48
2.6 Cell infection studies 48
2.7 Kanamycin and chloroquine protection assay 49
2.8 Cell cytotoxicity assay 49
2.9 Immunostaining and confocal microscopy 50
2.10 Protein gels and Western blots 51
2.11 ELISA (Enzyme-linked immunosorbent assays) 52
2.12 Proteome Profiler Mouse Cytokine Array 53
2.12.1 Sample preparation and protein concentration measurement 53
2.12.2 Proteome Profile Mouse Cytokine Array 54
2.13 Griess assay 54
2.14 Methods for evaluation of siRNA-mediated gene silencing 55
2.14.1 siRNA transfection 55
2.14.2 Total RNA isolation and reverse-transcriptase PCR (RT-PCR) 55
2.15 TLR-blocking peptide treatment 57
2.16 Total RNA extraction using the RNAeasy® Plus Micro Kit (Qiagen) 57
2.17 Reverse Transcription of RNA into cDNA 58
2.18 Design of the real-time PCR (qPCR) primers 59
2.19 Quantitative Real-Time PCR (qPCR) 60
2.20 Standard PCR to generate PCR products for standard curves 61
2.21 qPCR analysis software 61
2.22 Affymetrix microarray technology 61
2.22.1 Generation of RNA samples, labelling, hybridisation and scanning 61

2.22.2 General software used for Microarray analysis 62

2.23 General Statistical Analysis of Data 63

3 CHAPTER 3: ASSESSING THE ROLE OF AUTOPHAGY IN THE MACROPHAGE RESPONSE TO INTRACELLULAR *BURKHOLDERIA PSEUDOMALLEI* 64

3.1 INTRODUCTION 64

3.2 RESULTS 67

3.2.1 Phenotypic characterisation of BALB/C BMDMs 67

3.2.2 Intracellular survival of *B. pseudomallei* WT, Δ*bimA* mutant and the trans-complemented Δ*bimA* mutant strain in BALB/C BMDMs 72

3.2.3 The Δ*bimA* mutant strain displays no difference in bacterial uptake nor phagosomal escape compared to the WT strain 77

3.2.4 Autophagy does not play a role in the clearance of the Δ*bimA* mutant in infected BMDMs 80

3.3 DISCUSSION 90

4 CHAPTER 4 INVESTIGATING THE CONTRIBUTION OF MyD88- AND TRIF-DEPENDENT PATHWAYS, AND INFLAMMASOME ACTIVATION, IN CONTROLLING THE INTRACELLULAR FATE OF *BURKHOLDERIA PSEUDOMALLEI* 96

4.1 INTRODUCTION 96

4.2 RESULTS 99

4.2.1 BALB/C macrophages are activated upon infection with *B. pseudomallei*, as indicated by TNF-α secretion 99

4.2.2 Several other *B. pseudomallei*-induced cytokines and chemokines can be detected in infected BMDM lysates using the Profiler Mouse Cytokine Array 102

4.2.3 MyD88 depletion and inhibition do not affect the intracellular survival of *B. pseudomallei* 106

4.2.4 The TRIF-dependent pathway may be involved in the intracellular survival of *B. pseudomallei* 116

4.2.5 Non-canonical inflammasome activation upon *B. pseudomallei* infection of BALB/C BMDMs 121

4.3 DISCUSSION 129

5 CHAPTER 5 PROFILING MACROPHAGE TRANSCRIPTOMIC RESPONSES TO INFECTION WITH *BURKHOLDERIA PSEUDOMALLEI* 134

5.1 INTRODUCTION 134

5.2 RESULTS 137

5.2.1 Introduction to the microarray technology and choice of optimal time points for sampling 137

5.2.2 Assessing the quality of the cellular RNA 139

5.2.3 Affymetrix Expression Console Software: Preprocessing steps 144

5.2.4 Principal Component Analysis 148

5.2.5 Identifying the Differentially Expressed Genes using Affymetrix TAC Software 150

5.2.6 Functional Classification of Differentially Expressed Genes by IPA 164

5.2.7 Validating Differential Expressed Genes by SYBR-Green Real-Time PCR 176

5.2.8 Investigating the role of FNBP1L in limiting the intracellular survival of Δ*bimA* in BMDMs 189

5.3 DISCUSSION 192

6 CHAPTER 6 GENERAL DISCUSSION 199

6.1 Autophagy and future directions 200

6.2 Cellular signalling pathways and future directions 201

6.3 Host transcriptomic studies and future directions 202

6.4 Final conclusions 204

7 BIBLIOGRAPHY 205

LIST OF FIGURES

CHAPTER 1 INTRODUCTION

Figure 1.1 Predicted global distribution of melioidosis. 2

Figure 1.2 The intracellular lifestyle of *Burkholderia pseudomallei*. 6

Figure 1.3 Proposed structural model of the *Burkholderia* T3SS3 needle complex 9

Figure 1.4 Actin-based motility of *B. pseudomallei* requires BimA in J774.2 murine macrophage-like cells. 11

Figure 1.5 BimA is required for intracellular survival, inter-cellular spread and virulence in mice 12

Figure 1.6 The putative domain organisation of $BimA_{ps}$, $BimA_{ma}$ and $BimA_{th.}$ 15

Figure 1.7 Recognition of PAMPs and DAMPs by TLR and NLR signalling pathways 25

Figure 1.8 Cytosolic nucleic acid sensors 26

Figure 1.9 Type I and II interferon receptors and their respective signalling pathways… 35

Figure 1.10 Molecular pathway of autophagy. 41

CHAPTER 3 ASSESSING THE ROLE OF AUTOPHAGY IN THE MACROPHAGE RESPONSE TO INTRACELLULAR *BURKHOLDERIA PSEUDOMALLEI*

Figure 3.1 Phenotypic characterisation of BALB/C BMDMs by FACS 69

Figure 3.2 BALB/C BMDMs display high phagocytic activity. 70

Figure 3.3 Intracellular survival of WT *B. pseudomallei* (blue), Δ*bimA* mutant (orange) and the trans-complemented strain (grey) in BALB/C BMDMs. 73

Figure 3.4 Cytotoxicity level of uninfected (light green), infected BMDMs with WT (blue) and Δ*bimA* mutant (orange). 75

Figure 3.5 Representative z-stack confocal images of BMDMs infected with *B. pseudomallei* WT, Δ*bimA* mutant or the trans-complemented Δ*bimA* mutant strain under IPTG induction. 76

Figure 3.6 Proportion of cytoplasmic bacteria after 5 hours post infection. 79

Figure 3.7 Schematic diagram illustrating how autophagy acts as an innate mechanism against cytoplasmic bacteria. 81

Figure 3.8 Immunoblot analysis of LC3 conversion in BMDMs treated with the autophagy inducer rapamycin. 84

Figure 3.9 Immunoblot analysis of LC3 conversion in cell lysates from uninfected BMDMs (UN) and cells infected either with *B. pseudomallei* WT and Δ*bimA* mutant. 85

Figure 3.10 LC3 co-localisation analysis of BMDMs infected with *B. pseudomallei* WT or Δ*bimA* mutant bacteria. 86
Figure 3.11 Ubiquitin co-localisation analysis of BALB/C BMDMs infected with the WT or Δ*bimA* mutant. 88
Figure 3.12 p62 co-localisation analysis of BALB/C BMDMs infected with the WT or Δ*bimA* mutant bacteria. 89

CHAPTER 4 INVESTIGATING THE CONTRIBUTION OF MyD88- AND TRIF-DEPENDENT PATHWAYS, AND INFLAMMASOME ACTIVATION, IN CONTROLLING THE INTRACELLULAR FATE OF *BURKHOLDERIA PSEUDOMALLEI*

Figure 4.1 Secretion of the inflammatory cytokine TNF-α by infected BMDMs. 101
Figure 4.2 Global cytokine and chemokine response determined using a Proteome Profiler Mouse Cytokine Array 104
Figure 4.3 Relative levels of different cytokines/chemokines using a Proteome Profiler Cytokine Array 105
Figure 4.4 Knockdown efficiency of siRNA targeting MyD88 in BALB/C BMDMs and phagocytosis assay of siRNA-treated BMDMs. 108
Figure 4.5 Bacterial intracellular survival in siRNA-treated BMDMs. 109
Figure 4.6 Relative expression of IL-1β (top) and IL-6 (bottom) as determined by qPCR in the presence of TLR2 agonist Pam3CSK4 as compared to unstimulated BMDMs 112
Figure 4.7 Relative expression of IL-1β (top) and IL-6 (bottom) genes as determined by qPCR upon different peptide treatments 113
Figure 4.8 Phagocytosis assay of BMDMs pre-treated with control peptide (left) or MyD88-blocking peptide (right). 114
Figure 4.9 Bacterial intracellular survival in BMDMs pre-treated with MyD88-control peptide (checked bar) or MyD88-blocking peptide (horizontal-striped bar). 115
Figure 4.10 Relative expression of IFNβ in BMDMs as determined by qPCR in the presence of TLR3 agonist poly(I:C) as compared to unstimulated BMDMs. 118
Figure 4.11 Relative expression of IFNβ and phagocytosis assay of BMDMs treated with different peptides. 119
Figure 4.12 Bacterial intracellular survival in BMDMs pre-treated with Pepinh-control (left-bar) or Pepinh-TRIF (right bar). 120
Figure 4.13 Proposed integrative model of TLR and NLR pathways during the inflammatory response to Gram-negative bacteria 122

Figure 4.14 Immunoblot analysis of pro-caspase 11 and cleaved caspase 11 in BMDMs upon *B. pseudomallei* infection. 124
Figure 4.15 Secretion of the inflammatory cytokine IL-1α by ELISA.. 126
Figure 4.16 Western blot of pro-caspase 1 in BMDMs upon *B. pseudomallei* infection.. 128

CHAPTER 5 PROFILING MACROPHAGE TRANSCRIPTOMIC RESPONSES TO INFECTION WITH *BURKHOLDERIA PSEUDOMALLEI*

Figure 5.1 Intracellular survival of WT (blue) and Δ*bimA* mutant (orange) in BALB/C BMDMs. 138
Figure 5.2 Electropherograms of RNA samples generated by the Agilent Bioanalyser. 142
Figure 5.3 Flowchart of a typical genechip system microarray experiment. 143
Figure 5.4 Boxplots of log-intensity distribution across all 18 GeneChips. 146
Figure 5.5 Hybridisation and polyA controls. 147
Figure 5.6 Principal component analysis (PCA) of 18 samples 149
Figure 5.7 Workflow of microarray data analyses 151
Figure 5.8 Venn diagram comparison of DEGs identified from Affymetrix TAC software 152
Figure 5.9 Volcano Plots of each comparison pair. 153
Figure 5.10 Agarose gel electrophoresis of cDNA template. 177
Figure 5.11 Melt curves from qPCR of IL-1α gene from 18 samples over the entire temperature range 180
Figure 5.12 Average expression stability values of reference genes 183
Figure 5.13 geNorm V bar chart shows the optimal number of reference targets 184
Figure 5.14 Representative z-stack confocal microscopy images of BMDMs infected with *B. pseudomallei* WT and Δ*bimA* mutant bacteria for FNBP1L co-localisation 191

LIST OF TABLES

CHAPTER 1 INTRODUCTION

Table 1.1 Summary of the roles of different motifs in $BimA_{ps}$. 16

CHAPTER 2 MATERIALS AND METHODS

Table 2.1 Primary antibodies used in immunofluorescence 50
Table 2.2 Phalloidin conjugates for staining actin 51
Table 2.3 List of primary antibodies for Western Blot 52
Table 2.4 Primers for RT-PCR 57
Table 2.5 Primers for qPCR 60

CHAPTER 5 PROFILING MACROPHAGE TRANSCRIPTOMIC RESPONSES TO INFECTION WITH *BURKHOLDERIA PSEUDOMALLEI*

Table 5.1 RNA integrity and quality of the samples 141
Table 5.2 Number of differential expressed genes (DEGs) that met the criteria of p-value <0.05 and fold change exceeding 1.5 for each pairwise comparison 152
Table 5.3 Top 30 upregulated transcripts in BMDMs infected with WT versus uninfected at 8 hpi 156
Table 5.4 Top 30 downregulated transcripts in BMDMs infected with WT versus uninfected at 8hpi 157
Table 5.5 Top 30 upregulated transcripts in BMDMs infected with Δ*bimA* versus uninfected at 8hpi 158
Table 5.6 Top 30 downregulated transcripts in BMDMs infected with Δ*bimA* versus uninfected at 8hpi 159
Table 5.7 Top 30 upregulated transcripts in BMDMs infected with WT versus uninfected at 12hpi 160
Table 5.8 Top 30 downregulated transcripts in BMDMs infected with WT versus uninfected at 12hpi 161
Table 5.9 Top 30 upregulated transcripts in BMDMs infected with Δ*bimA* versus uninfected at 12hpi 162
Table 5.10 Top 30 downregulated transcripts in BMDMs infected with Δ*bimA* versus uninfected at 12hpi 163

Table 5.11 Top 30 IPA canonical pathways of common host responses to infection by *B. pseudomallei* at 8hpi. 168
Table 5.12 Top 30 IPA canonical pathways of common host responses to infection by *B. pseudomallei* at 12hpi. 170
Table 5.13 Top 30 IPA canonical pathways exclusive to the WT strain of *B. pseudomallei* at 8hpi. 172
Table 5.14 Top 30 IPA canonical pathways exclusive to the WT strain of *B. pseudomallei* at 12hpi. 173
Table 5.15 IPA canonical pathways exclusive to the Δ*bimA* strain of *B. pseudomallei* at 8hpi 175
Table 5.16 IPA canonical pathways exclusive to the Δ*bimA* strain of *B. pseudomallei* at 12hpi. 175
Table 5.17 Genes selected for validation of the microarray data by qPCR 188

LIST OF COMMONLY USED ABBREVIATIONS

ABM	Actin-based motility
ALR	Absent in melanoma (AIM2)-like receptors
AMPK	5'-AMP-activated protein kinase
AP1	Activation protein-1
BCA	Bicinchoninic acid
BMDM	Bone-marrow derived macrophage
BRT	Boosted regression tree
BSA	Bovine serum albumin
Bsa	*Burkholderia* secretion apparatus
CA	Central and acidic domain
CD14	Cluster of differentiation 14
cDC	Conventional dendritic cells
cDNA	Complementary DNA
CIS	Cytokine-Inducible Src Homology 2-containing protein
CL3	Containment Level 3
CLR	C-type lectin-binding domain receptor
cRNA	Complementary RNA
CRISPR-Cas9	Clustered Regularly Interspaced Short Palindromic Repeats- CRISPR associated protein-9 nuclease
CTD	C-terminal domain
DAMP	Damage-associated molecular pattern
DAPI	4', 6-Diamidino-2-Phenylindole
DAI	DNA-dependent activator of IRFs
DDX58	DEAD (Asp-Glu-Ala-Asp) Box Polypeptide 58
DEG	Differentially expressed gene
DMEM	Dulbecco's modified eagle medium
DNA	Deoxyribonucleic acid
dNTP	Deoxyribonucleotides
dsRNA	Double-stranded ribonucleic acid
ELISA	Enzyme-linked immunosorbent assay
ER	Endoplasmic reticulum
ERK	Extracellular-signal regulated kinase
EC	Expression Console software
FACS	Fluorescence-activated cell sorting
FBS/FCS	Foetal bovine serum/ Foetal calf serum
GAPDH	Glyceraldehyde 3-phosphate dehydrogenase
GAS	Interferon gamma activated site
GBP	Guanylate-binding protein
gDNA	Genomic DNA
GEF	Guanine nucleotide exchange factor
GM-CSF	Granulocyte macrophage colony stimulating factor
GO	Gene ontology
HEK293	Human embryonic kidney cell 293
Hcp	Haemolysin co-regulated protein
HMGB1	High mobility group protein B1
Hpi	Hours post infection
HRP	Horseradish peroxidase

IFIH1	Interferon Induced With Helicase C Domain 1
IFN	Interferon
IFNα	Interferon-alpha
IFNβ	Interferon-beta
IFNγ	Interferon-gamma
IFNAR	Type I Interferon receptor
IFNGR	Interferon gamma receptor
IL	Interleukin
IL-1α	Interleukin-1 alpha
IL-1β	Interleukin-1 beta
IL-1R	Interleukin-1 receptor
IL-1ra	Interleukin-1 receptor antagonist
IPA	Ingenuity pathway analysis
IPTG	Isopropyl β-D-1-thiogalactopyranoside
IQGAP1	IQ motif containing GTPase activating protein 1
IRF	Interferon regulatory factor
ISG	Interferon-stimulated gene
ISGF3	Interferon-stimulated gene factor 3
ISRE	IFN-stimulated response element
JAK	Janus activated kinase
LAMP-1	Lysosome-associated membrane glycoprotein-1
LAP	LC3-associated phagocytosis
LB	Luria-Bertani
LC3	Microtubule-associated protein 1A/1B-light chain 3
LDH	Lactate dehydrogenase
LIR	LC3-interacting region
LPS	Lipopolysaccharide
mAb	Monoclonal antibody
MAL	MyD88-adaptor-like
MAPK	Mitogen-activated protein kinase
MAVS	Mitochondrial anti-viral signalling
MCP-1	Monocyte chemoattractant protein-1
M-CSF	Macrophage colony stimulating factor
MEF	Murine embryonic fibroblast
MDA-5	Melanoma differentiation antigen 5
MDP	Muramyl dipeptide
MIP2β	Macrophage inflammatory protein 2β
MIQE	Minimum information for publication of quantitative real-time PCR experiments
MLST	Multilocus sequence typing
MNGC	Multinucleated giant cells
MOI	Multiplicity of infection
mRNA	Messenger ribonucleic acid
MS	Mass spectrometry
mTOR	Mechanistic target of rapamycin
MyD88	Myeloid differentiation primary response gene 88
NDP52	Nuclear dot protein 52 kDa
NF-κB	Nuclear factor kappa-light-chain-enhancer of activated B cells
NLR	Nucleotide-binding oligomerisation domain (NOD) and leucine-rich repeat
NO	Nitric oxide

OAS	Oligoadenylate synthetase
OASL	Oligoadenylate synthetase-like
NPF	Nucleation promoting factor
PARP	poly(ADP-ribose)-polymerase
Pam3CSK4	Pam3-Cys-Ser-Lys4
PAMP	Pathogen-associated molecular pattern
PBS	Phosphate buffered saline
PCR	Polymerase chain reaction
pDC	Plasmacytoid dendritic cells
PE	Phosphatidylethanolamine
PFA	Paraformaldehyde
PI3K	Phosphatidylinositol 3-kinase
PMN	Polymorphonuclear cell
PRM	Proline-rich motif
PTGS2	Prostaglandin-endoperoxide synthase 2
PTM	Post-translational modification
poly(I:C)	Polyinosinic-polyctidylic acid
PRR	Pattern recognition receptor
QC	Quality control
qPCR	Quantitative real time polymerase chain reaction
RIG-1	RNA helicase Retinoic-acid inducible gene-1
RLR	Retinoic-acid inducible gene I-like receptor
RNA	Ribonucleic acid
ROS	Reactive oxygen species
RPMI	Roswell park memorial institute
RT	Reverse transcriptase
RT-PCR	Reverse transcription polymerase chain reaction
SARM	Sterile α- and armadillo-motif containing protein
SEM	Standard error of the mean
SDS-PAGE	Sodium dodecyl sulphate polyacrylamide gel electrophoresis
siRNA	Short interfering RNA
SLR	Sequestome 1-like receptors
SOCS3	Suppressor of cytokine signaling 3
SQSTM1	Sequestome 1
STAT	Signal transducer and activator of transcription
STING	Stimulator of interferon genes
SUMO	Small ubiquitin-related modifier
TAC	Transcriptome analysis console software
TBK1	TANK-binding kinase 1
T3SS	Type three secretion system
T6SS	Type six secretion system
TEM	Transmission electron microscopy
TIR	Toll/interleukin-1 receptor-like domain
TIRAP	TIR domain-containing adaptor protein
TLR	Toll-like receptor
TNFα	Tumor necrosis factor α
TOR	Target of rapamycin
TRAM	TRIF related adaptor molecule
TRIF	TIR-domain-containing adapter-inducing interferon-β
TYK2	Tyrosine kinase 2

VASP	Vasodilator-stimulated phosphoprotein
VgrG	Valine-glycine repeat protein
WASP	Wiskott-Aldrich syndrome protein
WH2	WASP homology domain 2
ZBP-1	Z-DNA binding protein 1

1 CHAPTER 1: INTRODUCTION

1.1 *Burkholderia pseudomallei* and melioidosis

1.1.1 History, background and epidemiology

Melioidosis was first described by the pathologist Alfred Whitmore in 1912 as a "glanders-like" disease from autopsies on deceased opium addicts he conducted in Rangoon, Burma (Whitmore & Krishnaswami, 1912). The term was derived from the Greek "melis" (distemper of asses) and "eidos" (resemblance) by Stanton & Fletcher (1932). Melioidosis is a disease caused by the motile Gram-negative bacterium *Burkholderia pseudomallei*. *B. pseudomallei* is an environmental saprophyte commonly isolated from wet soil or surface water such as in rice paddy fields, in the endemic areas (reviewed in Inglis *et al*, 2001). Geographical factors namely high rainfall and temperature, anthrosol and acrisol soil types, soil with high salinity and a high proportion of gravel are strongly associated with the presence of *B. pseudomallei* (Limmathurotsakul *et al*, 2016). Recently, the global burden of human melioidosis was estimated to be approximately 165,000 cases per year worldwide with a high mortality rate of approximately 50%, from which 89,000 people will be expected to die. This estimation was generated using a formal modelling framework using the current map of human and animal melioidosis occurrences and also the environmental suitability for *B. pseudomallei,* predicted by a boosted regression tree (BRT) statistical model (Limmathurotsakul *et al*, 2016). The number of melioidosis cases is likely to be considerably underestimated as its clinical manifestations can mimic several other disorders and also due to inadequate laboratory facilities and poor reporting systems. The apparent emergence of melioidosis cases in new countries such as India, Southern China, Brazil and Malawi, is likely due to the upgrade of research facilities and microbiological laboratories. It has been suggested that melioidosis is severely underreported in 45 countries in which melioidosis is known to be endemic, and a further 24 countries are potentially endemic but have never reported the disease (Limmathurotsakul *et al*, 2016). Highest risk zones have been identified in Southeast and South Asia, tropical Australia, Western sub-Saharan Africa and South America. Besides, risk zones are also observed in Central America, Southern Africa and the Middle East (Figure 1.1) (Limmathurotsakul *et al*, 2016). The high number of estimated cases and fatalities highlight the need for this disease to be given renewed attention by health workers, international health organisations and policy makers.

The ability of *B. pseudomallei* to survive inside phagocytic cells for prolonged periods demonstrates that it is a facultative intracellular bacterium (Pruksachartvuthi, Aswapokee & Thankerngpol, 1990). Some early studies showed that inhalation is the main route of infection. For example, in 1941 many American servicemen (~225,000) in Vietnam were infected with *B. pseudomallei*, through inhalation of aerosolised infectious dust generated by helicopter blades (Howe, Sampath & Spotnitz, 1971). Interestingly, a small proportion of them were reported to have late-onset infections up to 62 years after leaving Southeast Asia which led to the name 'Vietnamese Time Bomb', and illustrates the prolonged latency and recrudescence of the disease (Mays & Ricketss, 1975; Ngauy *et al*, 2005).

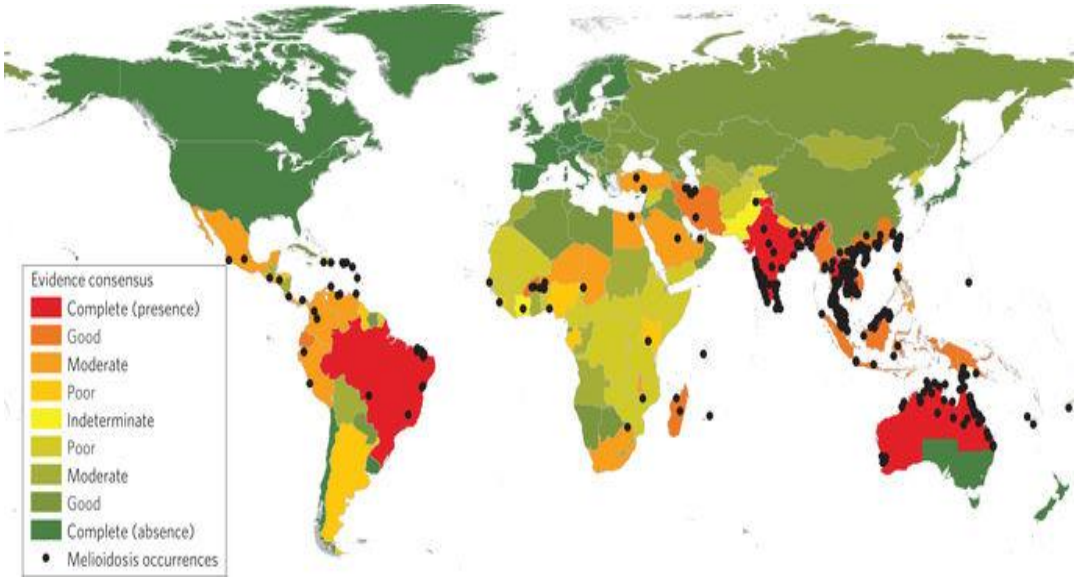

Figure 1.1 Predicted global distribution of melioidosis. The strength of evidence for melioidosis endemicity was assessed at national level, ranging from complete consensus on absence (green) and complete consensus on presence (red) (figure reprinted from Limmathurotsakul, D. *et al* (2016). Predicted global distribution of *Burkholderia pseudomallei* and burden of melioidosis. *Nature Microbiology*, 1, 1–5. Copyright © 2016 with permission from Macmillan Publishers Ltd: Nature Publishing Group).

1.1.2 Routes of infection

Melioidosis has a strong correlation with occupational (18%) or recreational exposure (75%) to environmental *B. pseudomallei* in water and soil, with 81% of cases presenting during the monsoon season (Currie, Ward & Cheng, 2010; Currie & Jacups, 2003). Higher rainfall is significantly associated with melioidosis sepsis and pneumonia, supporting the role of inhalation as a mode of acquisition with more severe pneumonic presentations (Currie *et al*, 2010). By contrast, epidemiology in Northern Australia has supported the predominant mode of transmission in this region to be through percutaneous inoculation of *B. pseudomallei* after exposure to wet soil or contaminated water (Currie *et al*, 2000). In addition, two recent clusters of melioidosis in Northern Australia have been linked to contaminated community water supplies, highlighting the possibility of ingestion as a route of transmission (Currie *et al* , 2001; Inglis *et al*, 2000). Human-to-human transmission of melioidosis has been reported previously, but such cases are exceedingly uncommon (Abbink *et al*, 2001; Kunakorn, Jayanetra, & Tanphaichitra, 1991; McCormick *et al*, 1975). There is no evidence suggesting transmission occurs through biting insects in nature, despite Sulaiman *et al* (2000) reporting that *B. pseudomallei* can be isolated from synanthropic flies.

1.1.3 Host risk factors, clinical presentations and treatment

In the majority of cases, the incubation period for melioidosis is between 1 and 21 days (with an average of 9 days) (Currie *et al*, 2000). The incubation period and clinical presentation depends on several factors including infecting dose, the bacterial strain, routes of transmission and importantly, host risk factors (reviewed in Currie, 2008). Melioidosis often affects individuals with one or more pre-existing conditions associated with an altered immune response, the most common being diabetes mellitus (which accounts for 50% of cases) followed by alcoholism, chronic lung disease and chronic renal disease. Other predisposing factors to melioidosis include malignancy, immunosuppression and thalassemia (Currie *et al*, 2010). Cystic fibrosis patients should avoid travel to endemic regions as they are at substantial risk of infection with *B. pseudomallei* (Currie *et al*, 2010). Melioidosis septicaemia is the most severe clinical manifestation which is often associated with pneumonia, resulting in high

mortality rates of 49%. Other presentations range from skin lesions to abscess formation in internal organs (for example the liver, lungs or spleen) and also soft tissues that can progress to septic shock (Currie *et al*, 2010).

There is no licensed vaccine available for melioidosis at present, while the therapeutic options are very limited. *B. pseudomallei* is highly resistant to wide groups of antibiotics, including penicillins, third-generation cephalosporins, rifamycins, aminoglycosides, quinolones and macrolides. Current post-exposure prophylaxis against melioidosis include ceftazidime, imipenem or meropenem with co-trimoxazole (reviewed in Dance, 2014; Sivalingam *et al*, 2008; Cheng & Currie, 2005). The antibiotic treatment falls into two distinct categories; phase 1 (acute infection) and phase 2 (eradication or maintenance therapy). The principal choice for the first acute-phase therapy includes a cephalosporin, usually Ceftazidime, or a carbapenem, usually Meropenem. Co-trimoxazole (trimethoprim/sulfamethoxazole) or co-amoxiclav (amoxicillin/clavulanic acid) therapy is suitable for the eradication phase for a minimum of 12 weeks based on international consensus guidelines (reviewed in Dance, 2014). This antibiotic regimen has been shown to be effective to eradicate *B. pseudomallei* and reduce the chance of relapse (reviewed in Dance, 2014; Sarovich *et al*, 2014; Sivalingam *et al*, 2008). Non-antibiotic intervention using a statin has shown potential in treatment for phase 1, but this intervention is still under study and clinical efficacy for melioidosis has not yet been reported (Inglis, 2010). The severe course of infection, aerosol infectivity, intrinsic antibiotic resistance and lack of a vaccine has resulted in the listing of *B. pseudomallei* as a category B bioterrorism agent by the US Centres for Disease Control and Prevention (Patel *et al,* 2011). As such, continuous investigation on disease pathogenesis is crucial and may increase the likelihood of identifying new therapeutic targets for disease treatment.

1.1.4 Taxonomy and related species

The genus *Burkholderia* contains >30 species, many of which are plant-associated inhabitants of the rhizosphere and plant pathogens. In exception, some members are pathogens of humans and animals namely *B. pseudomallei, B. mallei* and, in certain clinical conditions such as cystic fibrosis, *Burkholderia cepacia* (Coenye & Vandamme, 2003).

Environmental isolates previously considered to be "*B. pseudomallei*- like" are now known as *Burkholderia thailandensis. B. thailandensis* can be differentiated from *B. pseudomallei* on the basis of their different abilities to assimilate arabinose and also based on a comprehensive 16S rDNA analysis. *B. thailandensis*, but not *B. pseudomallei,* can assimilate arabinose (ara^+) (Godoy *et al*, 2003; Brett *et al*, 1998). Even though *B. thailandensis* and *B. pseudomallei* are closely related, *B. thailandensis* is relatively avirulent, at least in animal models of infection, requiring significantly higher doses of *B. thailandensis* than *B. pseudomallei* to cause disease or death in animal models (DeShazer, 2007; Brett *et al*, 1998). Although there have been reports of a few *B. thailandensis* infected patients in Thailand and in the United States, none were fatal (Glass *et al*, 2006; Lertpatanasuwan *et al*, 1999).

Burkholderia mallei is very closely related to *B. pseudomallei* and is the etiological agent of glanders in horses and other equines and, occasionally, can be transmitted to humans and other animals. It was originally demonstrated that *B. pseudomallei* and *B. mallei* are closely related genetically by DNA-DNA hybridisation experiments (Rogul *et al,* 1970). This similarity has been studied further by Godoy *et al,* 2003 using multilocus sequence typing (MLST). They found five isolates of *B. mallei* clustered within the *B. pseudomallei* strains, unambiguously classifying *B. mallei* as a clone of *B. pseudomallei* and not as a separate species. However, both were proven to be clearly distinct from *B. thailandensis* (Godoy *et al*, 2003). Glanders is now a very rare disease in Europe and North America and is largely an animal disease restricted to parts of Africa, Asia, the Middle East, and Central and South America. It has been reported that *B. mallei* was used during World War I by the German Army and may have been the first biological weapon of the 20th century (Srinivasan *et al,* 2001).

1.2 Pathogenesis and intracellular lifestyle of *Burkholderia pseudomallei*

As a facultative intracellular pathogen, *B. pseudomallei* has the ability to enter, survive, and replicate in both phagocytic and non-phagocytic cells (Jones *et al*, 1996). Indeed, this remarkable behaviour of *B. pseudomallei* to survive intracellularly may explain numerous features of melioidosis, namely, treatment difficulty, recrudescence and latency (Wiersinga *et al*, 2012). Numerous strategies have been employed by *B. pseudomallei* to survive in such a specialised niche as the intracellular environment.

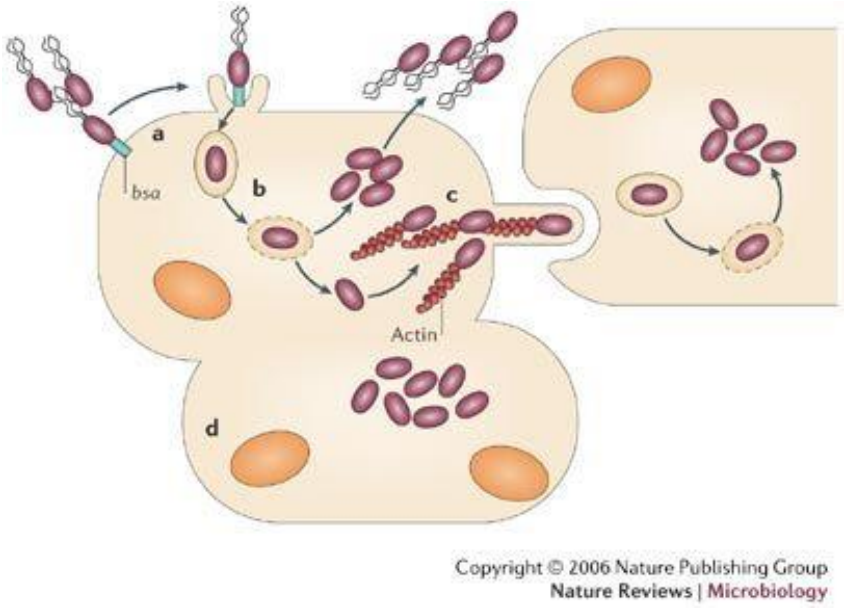

Figure 1.2 The intracellular lifestyle of *Burkholderia pseudomallei*. a) The *Burkholderia* secretion apparatus (*bsa*) system encodes proteins mediating host cell invasion, and also escape from the endocytic vacuole. (b) The bacterium is internalised into the endocytic vacuole or phagosome in the case of a phagocytic cell such as a macrophage. Once the bacterium escapes into the cytoplasm, *B. pseudomallei* proliferates. (c) *B. pseudomallei* can be propelled via BimA-dependent actin-based motility to protrude into the neighbouring cell and form a secondary vacuole in this new cell. Consequently, *B. pseudomallei* escapes from the secondary vacuole and enters the new cell cytoplasm and proliferates. (d) *B. pseudomallei* can induce cell fusion and form multinucleated giant cells (Figure reprinted from Wiersinga, W.J. *et al* (2006). Melioidosis: insights into the pathogenicity of *Burkholderia pseudomallei. Nature Reviews Microbiology*, 4, 272–282, Copyright © 2006 with permission from Macmillan Publishers Ltd: Nature Publishing Group).

1.2.1 Adhesion to host cells

Adhesion of the bacteria to the host cell is an essential early step in the pathogenesis of all intracellular bacteria, including *B. pseudomallei*. It has been demonstrated previously that the ability to adhere to the host cell is associated with the virulence of the bacteria. Kespichayawattana *et al* (2004) showed that *B. pseudomallei* has higher adherence capacity to human A549 lung epithelial cells than the avirulent *B. thailandensis*, resulting in more extensive cellular damage as represented by plaque formation. But, the molecular basis of this observation was not studied. Type IV fimbria (pili) and flagellum have been demonstrated previously as putative virulence factors required for cell adhesion of *B. pseudomallei* (Essex-Lopresti *et al*, 2005; Inglis *et al*, 2003). Recently, two novel adhesins in *B. pseudomallei* were identified; BoaA and BoaB. Single *boaA* and *boaB* mutants showed a reduction in attachment to both A549 and Hep2 epithelial cell lines. A double *boa/boaB* mutant displayed a lack of synergism as the adherence level of the double mutant was similar to that of the single mutants, suggesting multiple adhesins are required for cell adhesion (Balder *et al*, 2010).

1.2.2 Entry into host cells

The Type Three Secretion System (T3SS) is a central virulence factor in many Gram-negative bacteria. The T3SS comprises a cell-surface located complex nanomachine that allows a set of bacterial protein translocators and effectors to be injected directly into eukaryotic target cells (Figure 1.3). *B. pseudomallei* has at least three T3SS gene clusters (Rainbow *et al,* 2002). Clusters 1 (T3SS1) and 2 (T3SS2) are related to the T3SS gene clusters encoding Hrp secretion systems of the plant pathogens *Ralstonia* (formerly *Burkholderia)*, *Solanacearum* and *Xanthomonas spp* (Rainbow *et al*, 2002). Some studies demonstrated that these two gene clusters are involved in *B. pseudomallei* infection of tomato plants (Lee *et al*, 2010; Sun & Gan, 2010), but neither T3SS1 nor T3SS2 is needed for virulence in Syrian hamsters (Warawa & Woods, 2005). Cluster 3 (T3SS3) encodes the animal virulence-associated Bsa (*Burkholderia* secretion apparatus) T3SS which shares homology with the Inv/Mxi-Spa T3SS in *Salmonella* and *Shigella* (Stevens *et al*, 2002). Interestingly, T3SS2 and T3SS3 are present

in *B. pseudomallei, B. mallei* and *B. thailandensis*, but T3SS1 is unique to *B. pseudomallei* (Rainbow *et al,* 2002).

Several studies have demonstrated the importance of Bsa T3SS encoded proteins in various aspects of the intracellular lifestyle of *B. pseudomallei*, including invasion of host cells and escape from endocytic vacuoles (Figure 1.2). Invasion of *B. pseudomallei* into non-phagocytic cells is facilitated by its secreted effector protein BopE. BopE, a homologue of SopE/SopE2 in *Salmonella*, acts as a guanine nucleotide exchange factor (GEF) for Rho GTPases that regulate the actin network (Cdc42 and Rac1) and subsequently, induces the cytoskeletal rearrangements that engulf bacteria, promoting invasion (Stevens *et al*, 2003). As BopE needs to be translocated into the host cytosol, BopE requires other Bsa proteins to act in concert to assist the translocation and hence, bacterial invasion. BipD, a translocator protein located at the tip of the needle (Figure 1.3), was shown to be important in cell invasion as a *bipD* mutant showed greater impairment in invading HeLa cells than a *bopE* mutant (Stevens *et al*, 2003). Additionally, Bsa structural proteins BsaQ and BsaZ, and the translocator protein BipD, are also essential for secretion of the BopE (Muangsombut *et al*, 2008; Stevens *et al*, 2004). Interestingly, investigation of invasion of phagocytic cells, namely J774.2 murine macrophage-like cells, revealed that BopE was not required in invasion (Stevens *et al,* 2002), indicating that the T3SS may not be required for the invasion of phagocytic cells (Stevens *et al,* 2002). Moreover, the *bopE* mutant was not significantly attenuated in BALB/C mice following intraperitoneal or intranasal infection, suggesting BopE is not required for virulence and other effectors may be involved during both systemic and mucosal infection (Stevens *et al,* 2004). Conversely, the *bipD* mutant showed strong *in vivo* attenuation in the BALB/C mouse model of melioidosis and reduced bacterial colonisation of the liver and spleen at the early phase of infection (Stevens *et al*, 2004), however, immunisation with purified BipD protein failed to confer protection against challenge with wild type *B. pseudomallei* (Stevens *et al*, 2004).

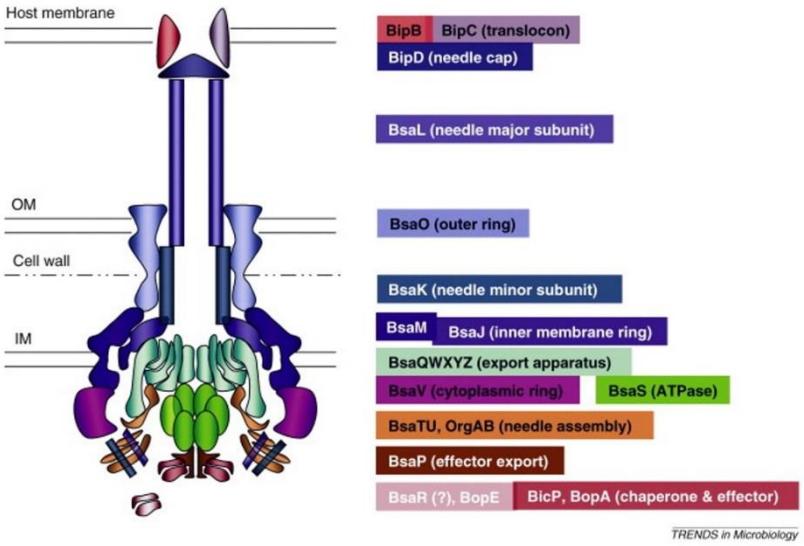

Figure 1.3 Proposed structural model of the *Burkholderia* T3SS3 needle complex. Putative function of proteins and their position in the needle complex are based on information of homologous proteins found in other well-studied systems. *Burkholderia* T3SS3 consists of a basal body that spans across both the inner membrane (IM) and outer membrane (OM) and a hollow needle extending from the bacterial surface to form a translocation pore in the host cell membrane (figure reprinted from Sun, G. W., & Gan, Y.-H. (2010). Unraveling type III secretion systems in the highly versatile *Burkholderia pseudomallei*. *Trends in Microbiology*, *18*(12), 561–568, Copyright © 2010, with permission from Elsevier).

1.2.3 Escape from endocytic vesicles

Escape from endocytic vesicles is essential for the bacteria to subsequently survive intracellularly. As early as 15 minutes following internalisation, *B. pseudomallei* lyses the endosomal membrane and escapes from the endocytic vacuole (Harley *et al,* 1998) in a Bsa T3SS-dependent manner (Stevens *et al,* 2002). *bsaZ*, similar to *Salmonella spaS*, is the last gene in the *bsa* gene cluster encoding a putative constituent of the T3SS apparatus (Stevens *et al,* 2002). *bsaZ* and *bipD* mutants are trapped in endocytic vesicles in J774.2 cells up to 6 hours post-infection (hpi) (Stevens *et al*, 2002). In RAW264.7 cells, the majority of the *bsaZ* mutant showed delayed escape from endocytic vacuoles, becoming visible in the cytoplasm of infected cells at 18hpi (Burtnick *et al,* 2011). More specifically, the T3SS effector BopA has been shown to be required for efficient escape of *B. pseudomallei* from phagosomes (Gong *et al*, 2011). In addition, the structural protein BsaQ is also involved in exiting endocytic vacuoles

(Muangsombut *et al,* 2008). Taken together these data suggest that the Bsa T3SS is not the only factor needed for phagosomal escape, but requires other bacterial-encoded proteins for this step in pathogenesis.

1.2.4 Actin-based motility

1.2.4.1 Actin-based motility in *B. pseudomallei* is mediated by BimA

Once in the host cell cytoplasm, the bacteria replicate and subvert the host cytoskeleton machinery to promote cell-to-cell spread, enabling pathogen dissemination while evading immune surveillance. Such actin-based motility is mediated by a bacterial factor known as BimA (*Burkholderia* intracellular motility A) which induces the formation of actin tails at one pole of the bacterial cell. Mutation of *bimA* abolished actin-based motility (ABM) of the pathogen in a macrophage-like J774.2 cell line, a phenotype that could be restored by inducible expression of the *bimA* gene on a pME6032 plasmid, showing the importance of the *bimA* gene in actin-based motility (Figure 1.4) (Stevens *et al,* 2005). Extensive investigations were then performed by our laboratory to determine if such actin-based motility contributes to the virulence of *B. pseudomallei,* as observed in other intracellular pathogens. As a result, *bimA* mutants exhibit attenuation in a murine model of melioidosis (Figure 1.5(C)) (unpublished data, G. Bancroft, LSHTM) and in a *Galleria mellonella* model system (unpublished data, J. Stevens and C. Vander Broek, The Roslin Institute). In addition, intracellular survival of a *B. pseudomallei bimA* mutant was found to be totally diminished in infected monolayers of A549 lung epithelial carcinoma cells, a phenotype that could be restored when the *bimA* gene was provided *in trans* (Figure 1.5(A)) (unpublished data, J. Stevens, The Roslin Institute). Intracellular actin-based motility is believed to underlie the ability of *B. pseudomallei* to spread intercellularly and promote multinucleated giant cell (MNGC) formation. Plaque formation in the same cell line was found to require *bimA*, suggesting that actin-associated membrane protrusion facilitates cell-to-cell spreading (Figure 1.4(B)). These collectively increase the intracellular survival of *B. pseudomallei* in both phagocytes and non-phagocytes.

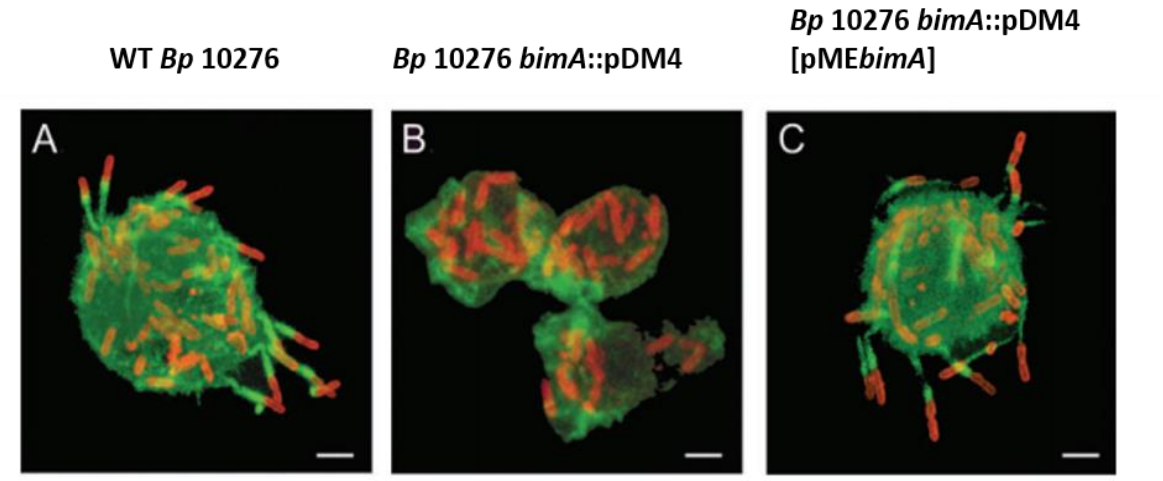

Figure 1.4 Actin-based motility of *B. pseudomallei* requires BimA in J774.2 murine macrophage-like cells. The figure shows representative confocal micrographs of J774.2 cells infected with (a) WT *Bp* 10276, (b) *Bp* 10276 *bimA*::pDM4, and (c) *Bp* 10276 *bimA*::pDM4 pME*bimA*. Mutation of *bimA* abolishes membrane protrusions in macrophage-like J774.2 cells. Bacteria were stained red, while filamentous actin was stained green with FITC-phalloidin. Scale bar = 5μM (Figure reprinted from Stevens, M. P. *et al* (2005). Identification of a bacterial factor required for actin-based motility of *Burkholderia pseudomallei*. *Molecular Microbiology*, 56(1), 40–53, Copyright © 2005 with permission from John Wiley & Sons, Inc.).

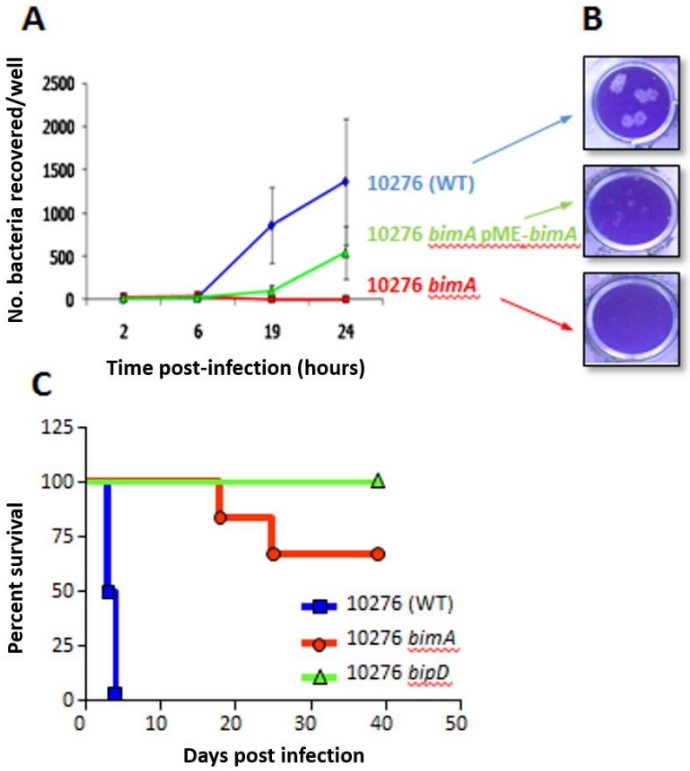

Figure 1.5 BimA is required for intracellular survival, inter-cellular spread and virulence in mice. (A) Intracellular survival of *B. pseudomallei* 10276 (blue), a *bimA* mutant (red) and a *bimA* mutant transcomplemented with an IPTG-inducible vector expressing BimA (green), in A549 cells. The mean bacterial recoveries (CFU ± SEM) from three independent experiments with triplicate measurements at 2, 6, 19, and 24 hours post-infection (hpi) were shown. The number of intracellular bacteria of the WT remained almost unchanged up to 6 hpi, but had increased at 19 and 24 hpi. In contrast, the intracellular survival of *bimA* mutant was totally diminished up to 24 hpi, but the phenotype could be restored when the *bimA* gene was provided *in trans*. (B) Ability of the same strains to spread from cell-to-cell and form plaques in A549 cell monolayers. Plaques were visualised by crystal violet staining of the monolayers. Plaques were formed by the cell monolayers infected with WT 10276 strain (blue) as well as the transcomplemented strain (green), indicating these strains were capable of spreading intercellularly. In contrast, intracellular *bimA* (red) mutant has a defect in cell-to-cell spreading as no plaque was observed by the infected cell monolayer. (C) Comparison of the virulence of a *bimA* mutant to the WT and a TTSS mutant (*bipD*), in a murine intranasal model of melioidosis. 10 mice were inoculated for each strain at day 0 and the survival of mice were investigated for 40 days. Mice inoculated with WT 10276 strain at day 0 all died by day 4 post-inoculation, while mice inoculated with an isogenic *bipD* mutant were all survived throughout the 40-days of experiment. For the mice inoculated with an isogenic *bimA* mutant, 6 out of 10 mice were survived until 40-days of experiment (unpublished data, Jo Stevens, Roslin Institute, reprinted with permission).

1.2.4.2 The mechanism of actin-based motility of *Burkholderia pseudomallei* is distinct from other intracellular pathogens

Actin-based motility (ABM) is common in members of several genera, including *Burkholderia, Listeria, Shigella, Rickettsia* and *Mycobacterium* (reviewed in Stevens *et al* 2006). The majority of pathogens capable of actin-based motility do so by exploiting the cellular Arp2/3 complex and have developed several mechanisms to activate this complex. The conserved Arp2/3 complex consists of seven polypeptides and acts as a nucleating factor to facilitate *de novo* actin polymerisation in host cells. The Arp2/3 complex itself has weak biochemical activity and is activated by a nucleation promoting factor (NPF), in particular members of the Wiskott-Aldrich syndrome protein (WASP) family. This activation leads to conformational stabilisation and promotes actin monomer delivery for actin nucleation (Goley *et al*, 2004). The *Listeria* ActA protein mimics the action of N-WASP in activating the Arp2/3 complex (Welch *et al*, 1997), while *Shigella* expresses the surface protein IcsA that recruits host cell WASP family proteins to the bacterial surface (Egile *et al*, 1999), facilitating the co-localisation with Arp2/3 complex and hence, actin polymerisation. In contrast, BimA can stimulate actin polymerisation *in vitro* in a manner that is independent of the cellular Arp2/3 complex, therefore the mechanism of *B. pseudomallei* ABM is different from those previously described for *Listeria* and *Shigella* (Benanti *et al,* 2015; Stevens *et al,* 2005). Moreover, over-expression of a dominant negative domain of the cellular NPF Scar1, which inhibits actin tail formation by *S. flexneri* and *L. monocytogenes*, did not block actin tail formation by *B. pseudomallei* (Breitbach *et al,* 2003). Additionally, neither WASP nor the host elongation factor Ena/VASP protein are important as *B. pseudomallei* ABM was not impaired in knockout N-WASP$^{-/-}$ nor Ena/VASP$^{-/-}$ cells (Breitbach *et al,* 2003).

Recently, it has been revealed that *B. pseudomallei* establishes BimA-mediated ABM through a novel mechanism by mimicking the host Ena/VASP actin polymerases (Benanti *et al,* 2015). It has been demonstrated that BimA in *B. pseudomallei* and the closely related species *B. mallei* can oligomerise into trimers to initiate actin nucleation and elongation, similar in fashion for the requirement for tetramerisation and clustering for Ena/VASP actin polymerase activity. The actin monomer-binding motif WH2 (WASP homology domain 2) of BimA recruits actin subunits and brings them into close proximity so that actin nucleation can

occur. BimA also demonstrates similar anti-capping activity of host Ena/VASP which removes the CapZ inhibition from barbed ends to enable actin elongation (Benanti *et al,* 2015). It has been described recently that the cellular cytoskeletal scaffold protein Ras GTPase-activating-like protein IQGAP1 is recruited to the actin tails of *B. pseudomallei* (Jitprasutwit *et al*, 2016), a protein that has so far not been linked with ABM of any other intra-cytoplasmic microbe. IQGAP1 plays a functional role in regulating tail length and actin density of *B. pseudomallei* (Jitprasutwit *et al*, 2016). However, the interaction of *B. pseudomallei* BimA and IQGAP1 is believed to be indirect as confirmed by the yeast-two hybrid assay (Jitprasutwit *et al*, 2016). In addition to IQGAP1, the cellular protein α-actinin is also present in *B. pseudomallei* actin tails as observed by Breitbach *et al* (2003) by confocal microscopy, however the functional role in *B. pseudomallei* actin-tails has not been characterised. In fact, 30 cellular proteins have been identified to be recruited to BimA-expressing bacteria including actin, actin-depolymerising factor and capping protein under actin polymerising conditions *in vitro* (Jitprasutwit *et al*, 2016). However, investigation of whether these proteins are essential for actin-tail formation in *B. pseudomallei* is warranted.

1.2.4.3 Studies of BimA in different *Burkholderia* species

Studies on the BimA protein of *B. pseudomallei* were extended to its related species, *B. mallei* and *B. thailandensis* (Figure 1.6). *B. mallei* and *B. thailandensis* also exhibit actin tail membrane protrusion in infected cells, despite their BimA proteins showing no sequence identity to the BimA protein of *B. pseudomallei* (designated as $BimA_{ps}$) at the N-terminus (Stevens *et al*, 2005a). It has been shown that the BimA proteins from *B. mallei* and *B. thailandensis* can functionally compensate for the ABM defect of a *Burkholderia pseudomallei bimA* mutant. Hence, it was of interest to identify motifs or factors required for the subversion of actin dynamics in intracellular actin-based motility. Initially, *B. pseudomallei* BimA was identified by searching the translated *B. pseudomallei* genome for proline-rich Type V autosecreted proteins for similarity to the IcsA/VirG virulence-associated protein required for ABM in *Shigella flexneri*. BimA is a putative autosecreted protein which is homologous to the C-terminal region of the *Yersinia enterocolitica* adhesin YadA and *Haemophilus influenzae* Hia autotransporters (Stevens *et al*, 2005b). Later, the BimA proteins in *B. mallei* and *B. thailandensis* (designated as $BimA_{ma}$ and $BimA_{th}$ respectively) were identified based on this conserved C-terminal region, corresponding to the putative membrane targeting and anchoring motifs in $BimA_{ps}$ (Stevens *et al*. 2005a).

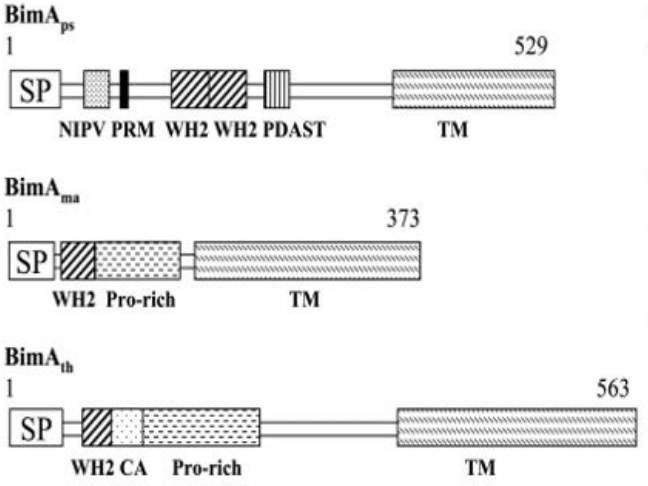

Abbreviation:

SP	Predicted signal peptide
NIPV	Repeat sequence with homology to human diaphanous 1 (hDia1)
PRM	Proline rich motif 1 (IP_7)
WH2	WASP homology domain-2, actin monomer binding motif
PDAST	Repeat sequence, predicted casein kinase II sites for phosphorylation
TM	Putative transmembrane anchor, containing homology to YadA and HiA type V autotransporters
CA	Central and acidic domains, role with WH2 domain involved in binding for actin and Arp2/3 for inducing actin polymerisation

Figure 1.6 The putative domain organisation of BimA$_{ps}$, BimA$_{ma}$ and BimA$_{th}$. The domains are drawn to scale and the abbreviation and predicted signal sequence are shown in the table (Figure reprinted from Stevens, J.M. *et al* (2005a). Actin-binding proteins from *Burkholderia mallei* and *Burkholderia thailandensis* can functionally compensate for the actin-based motility defect of a *Burkholderia pseudomallei bimA* mutant. *Journal of Bacteriology*, 187(22), 7857–7862. Copyright © 2005 with permission from American Society Microbiology).

WH2 and proline-rich motifs (PRMs) are present in all three BimA proteins. In BimA$_{ps}$, the WH2 domains were found to be required for actin-binding, actin polymerisation and ABM (Benanti *et al,* 2015; Sitthidet *et al*, 2011). The CA domain is unique to BimA$_{th}$, recruiting and activating the Arp2/3 complex for actin polymerisation, and is required for ABM in *B. thailandensis*. BimA$_{ps}$ lacks this CA domain, consistent with the finding that *B. pseudomallei* polymerises actin in an Arp2/3-independent manner (Benanti *et al,* 2015; Sitthidet *et al*, 2011). A PRM is known to interact with profilin, a G-actin-binding protein that aids in funnelling monomeric actin to the tip of actin filaments for incorporation into growing filaments (Haglund *et al,* 2010; Holt, 2001). In BimA$_{ps}$, a tandem repeat of 13 amino acids (NIPKVPPPMPGGGA) is adjacent to the PRM1 motif (also known as IP7) at the amino-terminus of the protein (Figure 1.6) (Stevens *et al,* 2005a). Both the PRM1 motif and 13 amino acid repeat are conserved in most *B. pseudomallei* strains, but are not essential for ABM of *B. pseudomallei in vitro* (Sitthidet *et al*, 2011; Sitthidet *et al,* 2010). Interestingly, BimA$_{ps}$ that lacks the 13-aa direct repeat abrogated plaque formation (cell to cell spread) and intracellular survival, despite retaining the ability to undergo ABM. It has been speculated that the 13aa repeats may be responsible for recruiting bacterial or cellular factors that may mask BimA from recognition by the host autophagic pathway (Sitthidet *et al*, 2008). Putative consensus sites for cellular

casein kinase II phosphorylation are found adjacent to the WH2 domains. The number of PDASX repeats vary within sequenced *B. pseudomallei* strains (between 2 and 7 copies) (Sitthidet *et al*, 2008). These PDASX repeats are required for polymerisation of actin but not for actin binding. Interestingly, the rate of polymerisation increased in a step-wise manner as the number of repeats increased, indicating that the repeats stimulate actin polymerisation *in vitro* in an additive fashion (Sitthidet *et al*, 2011). The roles of the different $BimA_{ps}$ motifs as studied by Sitthidet *et al* (2011) using the *B. pseudomallei* strain 10276 are summarised in table 1.

Table 1.1 Summary of the roles of different motifs in $BimA_{ps}$. The functional roles of each motif are determined using the plasmid-borne *bimA* variants with in-frame deletions of specific motifs, followed by *in vitro* experiments on actin-based motility, intercellular spreading and the actin binding and polymerisation as studied by Sitthidet *et al* (2011).

$BimA_{ps}$ variant with specific motif deletion	Actin-tail formation	Plaque formation	Actin binding	Pyrene-actin polymerisation
Δ13-aa	Yes	No	Yes	Yes
ΔPRM1	Yes	Yes	Yes	Yes
ΔWH2 domains	No	No	No	No
ΔPDASX repeats	No	No	Yes	No

1.2.5 Multi-nucleated giant cell (MNGC) formation

Inter-cellular spreading mediated by BimA contributes to the phenomenon of cell fusion, inducing the formation of multi-nucleated giant cells (MNGC). This MNGC formation is not observed in other intracellular bacterial pathogens such as *Salmonella enterica* Typhimurium or *Shigella flexneri* (Kespichayawattana *et al*, 2000), but is common in viral infection such as human immunodeficiency virus (HIV), cytomegalovirus (CMV) and herpes simplex virus (HSV) (reviewed in Allwood *et al*, 2011). Cell fusion is thought to represent a strategy to facilitate cell-to-cell spreading, evasion of host-immune responses and persistence of *B. pseudomallei* within a host, which collectively increases the intracellular survival of *B. pseudomallei* in both phagocytes and non-phagocytes (Kespichayawattana *et al*, 2000; Harley *et al,* 1998). Moreover, MNGC formation has been observed in tissues from melioidosis patients (Wong *et al*, 1995), suggesting that MNGC formation is a part of pathogenesis.

In *B. pseudomallei*, MNGC formation has been associated with RpoS (RNA polymerase, sigma S) (Utaisincharoen *et al,* 2006), BipB (Suparak *et al*, 2005), and T6SS-1 (Burtnick *et al*, 2011), however, the molecular mechanisms involved are poorly understood. Sigma factor

RpoS is the key transcriptional regulator in response to general stress and also during stationary phase. Utaisincharoean *et al* (2006) demonstrated that in comparison to the WT strain, a *B. pseudomallei rpoS* mutant is significantly impaired in its ability to induce MNGC formation in RAW264.7 cells, despite demonstrating no difference in intracellular survival and replication at a late time point of 18 hpi. Suparak *et al* (2005) demonstrated that a strain with mutation of the gene encoding the T3SS translocon protein *bipB* was deficient in forming MNGC in J774A.1 macrophage-like cells at 6 hpi but was restored by complementation with intact *bipB* on a plasmid. However, both the *rpoS* and *bipB* mutants were not tested for their ability to escape the endocytic compartment or for their ability to promote actin-based motility.

Besides T3SS, The Type VI secretion system (T6SS) is another contact-dependent protein translocation system commonly expressed by many Gram negative bacteria. *B. pseudomallei* possesses six evolutionarily distinct T6SSs and specifically, T6SS cluster 5 (T6SS-5) is strictly required for MNGC formation (Schwarz *et al*, 2010). Hcp (Haemolysin co-regulated protein) and VgrG (valine-glycine repeat protein) are hallmark proteins of T6SS activity. Hcp polymerises into tubules in a hexameric ring formation to translocate bacterial proteins across the membrane of the host cells, while VgrG forms a trimer at the tip of the T6SS apparatus for membrane puncturing, analogous to the structural counterparts of bacteriophage (Schwarz *et al*, 2014; Toesca *et al*, 2014). Studies by Burtnick *et al* (2011) showed that infection with the Δ*hcp1* mutant in RAW264.7 cells resulted in no MNGC formation, despite an increase in bacterial replication by 18 hpi and no difference in CFU counts when compared with the WT strain (Burtnick *et al*, 2011). On the other hand, mass spectrometry secretomic analysis by Schwarz *et al* (2014) identified VgrG-5 as a novel secreted protein whose export is dependent on T6SS-5 function. VgrG-5 is a specialised VgrG protein that harbours a C-terminal domain (CTD) conserved within *B. pseudomallei*, *B. mallei* and *B. thailandensis* (Schwarz *et al*, 2014). T6SS VgrG-5 is required for cell fusion and intercellular spread as a *vgrG-5* mutant in *B. pseudomallei* failed to show MNGC in HEK293 (Toesca *et al,* 2014) and RAW264.7 cell lines (Schwarz *et al*, 2014), but is dispensable for endosomal escape and actin polymerisation (Toesca *et al,* 2014). Both studies documented that the VgrG-5 CTD specifically was responsible for T6SS-5-dependent MNGC formation (Schwarz *et al*, 2014; Toesca *et al,* 2014). The authors proposed that the force generated by the bacterial propulsion into the neighbouring cell facilitates bacteria-plasma membrane contact, bringing adjacent membranes into close apposition. The membrane contact may release some cue to deploy the T6SS-5, and the resulting energy drives the VgrG-5 CTD to be inserted across one or both cell surfaces, creating

a disordered “hemifusion zone” and subsequently membrane fusion. However, VgrG-5 CTD alone is unlikely to be sufficient for cell fusion and additional bacterial factors such as surface proteins and host factors such as adhesin may be required (Toesca *et al,* 2014). In fact, inhibition of several macrophage surface proteins namely integrin-associated protein (CD47), E-selectin (CD62E), a fusion regulatory protein (CD98), and E-cadherin (CD324) with blocking monoclonal antibodies, were each able to suppress MNGC formation in a concentration-dependent manner, supporting the possible involvement of those host factors during *B. pseudomallei*-induced MNGC formation (Suparak *et al*, 2011).

1.3 *Burkholderia pseudomallei* and host immune responses

1.3.1 Murine models of melioidosis

The laboratory mouse represents an excellent surrogate for the study of clinical melioidosis with respect to the disease presentation and immune response (Warawa *et al*, 2010). Two inbred mouse strains, BALB/C and C57BL/6, have been extensively used to investigate the immunopathogenesis of several intracellular pathogens such as *Listeria monocytogenes* (Liu *et al*, 2000), *Chlamydia muridarum* (Jiang *et al*, 2010), *Yersinia enterocolitica* (Hancock *et al*, 1986) and *Mycobacterium avium* (Roque *et al*, 2007). In many of these mouse models, BALB/C mice are relatively susceptible compared to C57BL/6 mice. In melioidosis, several studies have shown that BALB/C mice are also highly susceptible to infection with *B. pseudomallei*, while C57BL/6 mice are considerably more resistant (Liu *et al*, 2002; Hoppe *et al*, 1999; Leakey *et al,* 1998). Intravenous administration of as few as 37 CFU of *B. pseudomallei* in BALB/C mice resulted in substantial bacterial colonisation in liver and spleen, that progressively developed into bacteraemia within 48 hours, causing death of the animal within 72 to 96 hours (Leakey *et al*, 1998). However, bacteraemia is absent in infected C57BL/6 animals indicating that some innate resistance mechanisms may play important roles in controlling *B. pseudomallei* at early time points. However, considerable bacterial burden in the liver and spleen eventually leads to a fatal outcome in C57BL/6 mice and implies incomplete resistance (Leakey *et al*, 1998). Further studies indicate that acute melioidosis observed in BALB/C mice is characterised by hypersecretion of proinflammatory cytokines namely TNF-α, IL-1β and IL-6 (Ulett *et al*, 2000), resulting in an inappropriate cell response, multiple organ failure and failure to control the infection. The relative resistance of C57BL/6 correlates with a more protective interferon-gamma (IFN-γ) mediated macrophage response (Breitbach *et al*, 2006), an effective NADPH oxidase (Breitbach *et al*, 2006), and a higher immunoglobulin IgG2a/IgG1 ratio (Hoppe *et al*, 1999). This differential susceptibility to infection classifies BALB/C and C57BL/6 mice as excellent models for the acute and chronic forms of human melioidosis respectively.

1.3.2 Role of neutrophils and macrophages in melioidosis

Neutrophils and macrophages are key components of the innate immune response in the control of acute melioidosis (Breitbach *et al*, 2011; Barnes *et al*, 2008; Easton *et al*, 2007; Breitbach *et al*, 2006; Leakey *et al,* 1998). A role for macrophages in control of acute melioidosis in murine models has been established by *in vivo* depletion studies where the mice were administered clodronate-containing liposomes intravenously to eliminate macrophages in the spleen and liver, the organs known to accommodate *B. pseudomallei* (Breitbach *et al*, 2006). Macrophage-depleted mice were significantly more susceptible to disease and death indicating that macrophages are essential to control early *B. pseudomallei* infection in both BALB/C and C57BL/6 mice (Breitbach *et al*, 2006)**.** In a study of a murine model of pulmonary *B. pseudomallei* infection, neutrophils were shown to be rapidly recruited to the primary site of infection in the lung, showing a critical role in early resistance to invading bacteria and to prevent dissemination to distal organs (Easton *et al*, 2007). In the same studies, *in vivo* depletion of neutrophils using monoclonal antibody RB6 rendered mice exquisitely susceptible to experimental *B. pseudomallei* infection (Easton *et al*, 2007), which was accompanied with a decrease in early proinflammatory cytokines namely TNF-α, IL-6 and IFN-γ in the lungs (Easton *et al*, 2007). Riyapa *et al*. (2012) have demonstrated that neutrophils are capable of neutralising extracellular bacteria through the secretion of 'neutrophil extracellular traps'. Recently, it has been demonstrated that autophagy in primary neutrophils clears intracellular *B. pseudomallei* through novel membraneous structures composed of partial phagosome-like single membranes and partial elongated membranes (Rinchai *et al*, 2015).

The importance of the host innate immune responses in melioidosis can also be evidenced from studies using a murine model of Type 2 Diabetes (*diabetes mellitus*) (Hodgson *et al*, 2013; Hodgson *et al*, 2011) as well as polymorphonuclear cells (PMNs) from diabetic subjects (Chanchamroen *et al*, 2009). Macrophages and neutrophils from diabetic patients have decreased chemotaxis, phagocytosis and antimicrobial mechanisms (Geerlings & Hoepelman, 1999). This impaired innate immune response is assumed to underlie the diabetics' susceptibility to infection with *B. pseudomallei* (Hodgson *et al*, 2011; Chanchamroen *et al*, 2009), and also other bacteria such as *Klebsiella pneumonia* (Lin *et al*, 2013), *Mycobacterium tuberculosis* (reviewed in Dooley & Chaisson, 2009) and *Staphylococcus aureus* (reviewed in Breen & Karchmer, 1995). A defective innate immune response allows the pathogen to resist

killing within immune cells which then could lead to persistence of the bacteria and dissemination of infection, followed by progression to sepsis. Hodgson *et al* (2011) demonstrate that macrophages from diabetic mice have a significantly impaired ability to phagocytose and kill *B. pseudomallei in vitro*. Similarly, PMNs from diabetics subjects also exhibited reduced phagocytosis of *B. pseudomallei* (Chanchamroen *et al*, 2009). The bactericidal activity was also reduced in infected macrophages from diabetic mice as they secreted significantly lower nitric oxide (NO) compared to infected macrophages from non-diabetic mice (Hodgson *et al*, 2011). While in diabetic patient PMNs, the oxidative killing seemed to be decreased compared to healthy volunteer PMNs in response to *B. pseudomallei* (Chanchamroen *et al*, 2009).

In vivo, two different diabetic mouse models are used to mimic human Type 2 Diabetes and melioidosis comorbidity namely the monogenic *db/db* model that has a genetic mutation in leptin signalling and secondly, the polygenic diet-induced HFD (high-fat-diet-fed) mouse models (Hodgson *et al*, 2013; Hodgson *et al*, 2011). Subcutaneous infection of monogenic and polygenic diabetic mice with *B. pseudomallei* resulted in 100% and 40% mortality rate respectively, while the infected non-diabetic mice survived during the 10-day experimental period (Hodgson *et al*, 2013; Hodgson *et al*, 2011). This increased mortality of diabetic mice was accompanied by earlier dissemination of *B. pseudomallei* to several organs as early as 24 hpi (Hodgson *et al*, 2013; Hodgson *et al*, 2011). These findings together show that the impaired host innate functions in diabetics could contribute to an increased susceptibility to melioidosis, corresponding to their role as a first line of host defence against bacterial infections.

1.4 Host cell-autonomous immunity in response to microbial infection

In response to microbial infection, cell-autonomous immunity is activated as a first line of defence to eliminate an invasive infectious agent. The host cell surveys the presence of microbial PAMPs (Pathogen Associated Microbial Patterns) or DAMPs (danger-associated molecular patterns) in the extracellular, vacuolar and cytoplasmic compartments using germline-encoded specialised sensor proteins known as pattern-recognition receptors (PRRs). Activation of these PRRs is dependent on the ligands and signals detected, and triggers downstream innate immune signalling networks to eliminate the pathogen. Classification of PRRs include Toll-like receptors (TLRs), retinoic acid-inducible gene 1 (RIG-I)-like receptors (RLRs), nucleotide-binding and oligomerisation domain (NOD)- and leucine-rich repeat containing proteins (NLRs), absent in melanoma (AIM2)-like receptors (ALRs), C-type lectin receptors (CLRs) and sequestome 1-like receptors (SLRs) (Figure 1.7). Some of these PRRs are not exclusively expressed by immune cells like macrophages and dendritic cells, but are also expressed in other cell populations such as endothelial and epithelial cells (Irving *et al*, 2014; reviewed in Bäckhed & Hornef, 2003), which allow these cells to engage in immune-surveillance and host defence.

CLRs and TLRs belong to the family of membrane anchored PRRs that are either located on the cell surface or within phagosomal/endosomal compartments. CLRs, which consist of Dectin-1 and Dectin-2, recognise complex carbohydrate structures such as the cell wall of fungi. These CLRs signal through adapter kinase Syk and CARD9 via nuclear factor κB (NF-κB) transcription factor to express inflammatory cytokines (Saijo *et al*, 2010; Taylor *et al*, 2007). Some TLRs detect bacterial components such as lipopolysaccharide (LPS), bacterial flagellin, lipoteichoic acid of the Gram-positive bacteria cell wall and many others, while some TLRs namely TLR3, TLR7 and TLR9 detect 'non-self' nucleic acids. Upon ligand binding, an individual TLR triggers distinctive downstream signalling depending on the recruitment of the adaptor proteins MyD88 or TRIF (Figure 1.7). MyD88 is employed by all TLRs except TLR3 and certain TLR4, while TRIF is an exclusive adaptor used by TLR3 as well as the TLR4-induced MyD88-independent pathway (reviewed by Kawai and Akira, 2010). There are other adaptor proteins that either serve as bridging adaptors (MyD88-adaptor-like (MAL) and TRIF-related adaptor molecule (TRAM)) or as a TLR-negative regulator (sterile α- and armadillo-motif containing protein (SARM)). MAL bridges TLR2 and TLR4 to recruit MyD88, and

TRAM is exclusively used by TLR4 to bridge TRIF to allow for IFN regulatory factor (IRF) 3 activation (reviewed in Kawai & Akira, 2011). SARM inhibits the TRIF signalling pathway, functioning as a negative regulator of TRIF (Peng *et al*, 2010). Ligand binding and TLR activation triggers the transcription of Type I interferon (IFN) and various inflammatory cytokines and chemokines through the transcription factors nuclear factor κB (NF-κB), activation protein-1 (AP1) and IRF (reviewed in Schattgen & Fitzgerald, 2011) (Figure 1.7). Transcription of these immune molecules are crucial for cell-intrinsic control of bacterial pathogens as well as activation of adaptive immunity (reviewed in von Moltke *et al*, 2013).

Sensing of PAMPs or DAMPs in the cytosol is mediated by the family of NOD receptors (NOD1 and NOD2), NOD-like receptors (NLRs), RNA-sensing RLRs (RIG-1 and MDA-5) and other nucleic acid receptors. NOD receptors (NOD1 and NOD2) recognise bacterial cell wall fragments such as peptidoglycan containing muramyl dipeptide (MDP). Upon ligand binding, cytosolic NOD receptors activate NF-κB for induction of inflammatory cytokine production (Figure 1.7) (Ogura *et al*, 2001). Cytosolic 'non-self' RNA can be recognised by the cytosolic sensor RIG-1 or MDA-5, which then associates with the adaptor protein MAVS (mitochondrial anti-viral signalling, also known as IPS-1) to induce expression of Type I IFNs and inflammatory cytokines via IRF3 and NF-κB signalling pathways respectively (Figure 1.8). Activation of IRF3 requires upstream signalling through TBK1 (Tank-binding Kinase) to induce transcription of Type I IFN. Besides MAVS, STING (stimulator of interferon genes) is another essential adaptor protein that functions upstream of TBK1 and IRF3 to induce Type I IFN (Figure 1.8). In addition to STING, ZBP-1 (Z-DNA binding protein 1, also known as DNA-dependent activator of IRFs (DAI)) is another DNA-sensor which leads to the production of Type I IFN. Several other DNA sensors can induce the production of inflammatory cytokines and Type I IFNs in a STING-dependent and independent manner.

In addition to cytosolic NOD-receptors and RLRs, activation of cytosolic NLR (NLRP3, NLRP1 and NLRC4) and some ALR (AIM2) can lead to the assembly of oligomeric multiprotein complexes known as inflammasomes upon recognition of 'non-self' nucleic acids or upon recognition of certain danger signals. Inflammasomes provide signalling platforms to catalytically activate pro-caspase 1 into its active subunit caspase 1. This cleaved caspase-1 promotes the maturation and release of biologically active pro-inflammatory IL-1β and IL-18 (reviewed in von Moltke *et al*, 2013; Nikolov *et al*, 1992). Also, inflammasome-induced activation of caspase-1 induces pyroptotic cell death, an inflammatory programmed cell death to prevent the establishment and dissemination of intracellular pathogens (Miao *et al*, 2010).

Pyroptosis is distinct from the programmed cell death known as apoptosis, which is dependent on activation of caspase-3 and caspase-7 and is non-inflammatory (Miao *et al*, 2010). Inflammatory pyroptosis can also be mediated in a non-canonical manner through activation of murine caspase-11, which is known as caspase 4/5 in humans. Downstream signalling of this non-canonical activation pathway results in the maturation of pro-inflammatory interleukin-1 alpha (IL-1α), which is distinct from the scenarios following activation of the canonical inflammasome pathway (Groß *et al*, 2012).

SLRs such as p62 (also known as sequestome 1) and nuclear dot protein 52 (NDP52) promote host defence by selectively targeting ubiquitinated substrates or cytoplasmic bacteria such as *Listeria, Shigella* and *Mycobacterium tuberculosis* for destruction by the autophagy pathway (reviewed in Vojo and Kliewer, 2012). All in all, closely interlinked networks between multiple PRRs facilitate bacterial recognition, however, an appropriate scaling of these PRRs is crucial to control the infection, but also to avoid excessive inflammation.

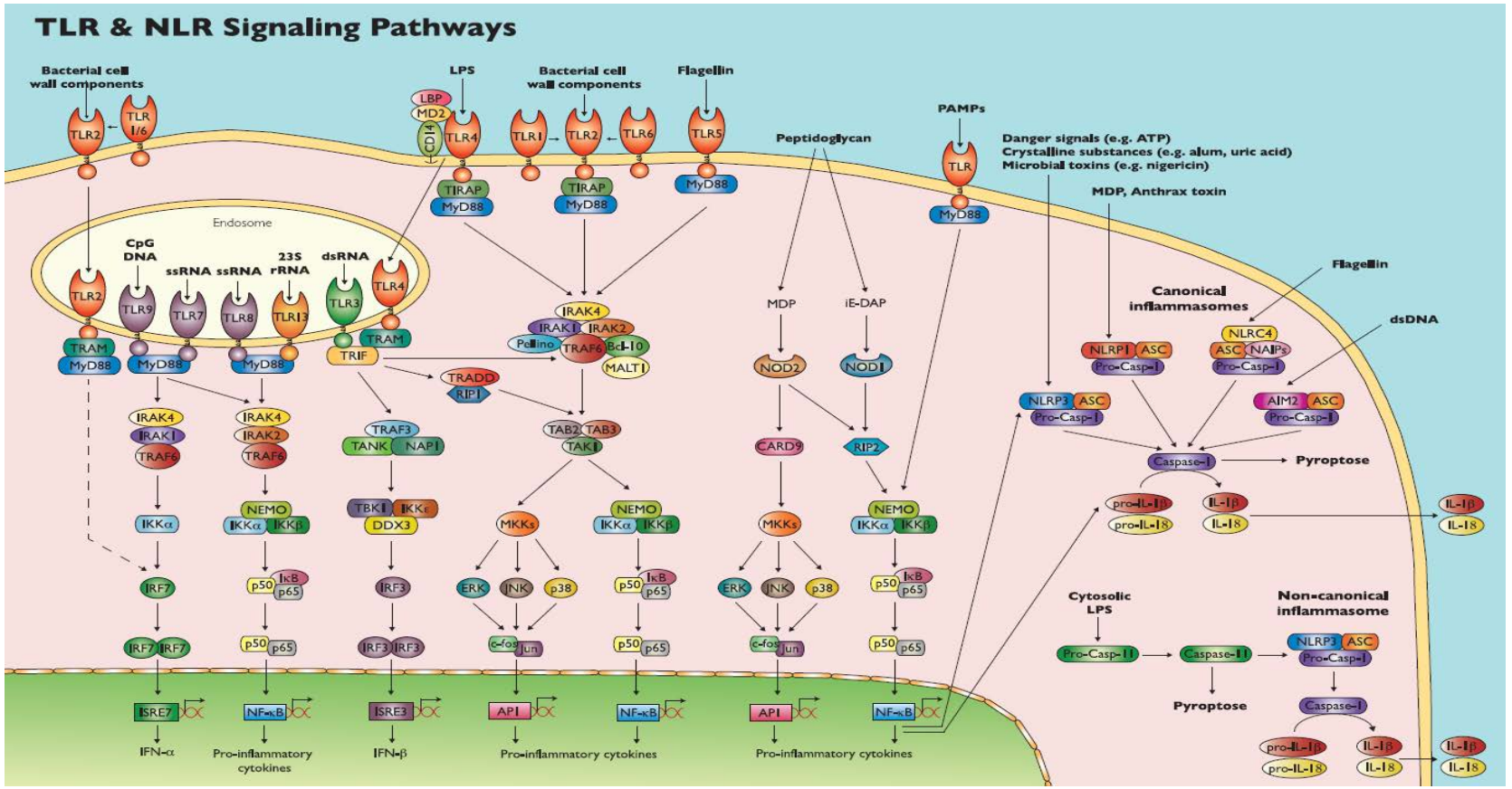

Figure 1.7 Recognition of PAMPs and DAMPs by TLR and NLR signalling pathways. Toll-like receptors (TLRs) are located on the surface membrane and also within endosomal compartments. Some TLRs are non-nucleic sensors detecting several bacterial components while some TLRs namely TLR3, TLR7, TLR8 and TLR9 recognise only the presence of certain nucleic acid. Activation of the TLR signalling pathway induces transcription of inflammatory cytokines and Type I IFN through transcription factor NF-κB, AP1 or IRF. NOD receptors recognise peptidoglycan components and signal via API and NF-κB. Inflammasome activation is achieved by different NLRs characterised by caspase-1-mediated proteolytic cleavage of matured IL- 1β and IL-18. NLRP3 inflammasome can also be activated in a non-canonical way by cytosolic LPS, mediated by an inflammatory caspase-11. Source of diagram: http://www.invivogen.com/review-innate-immunity, reprinted with permission from InvivoGen)

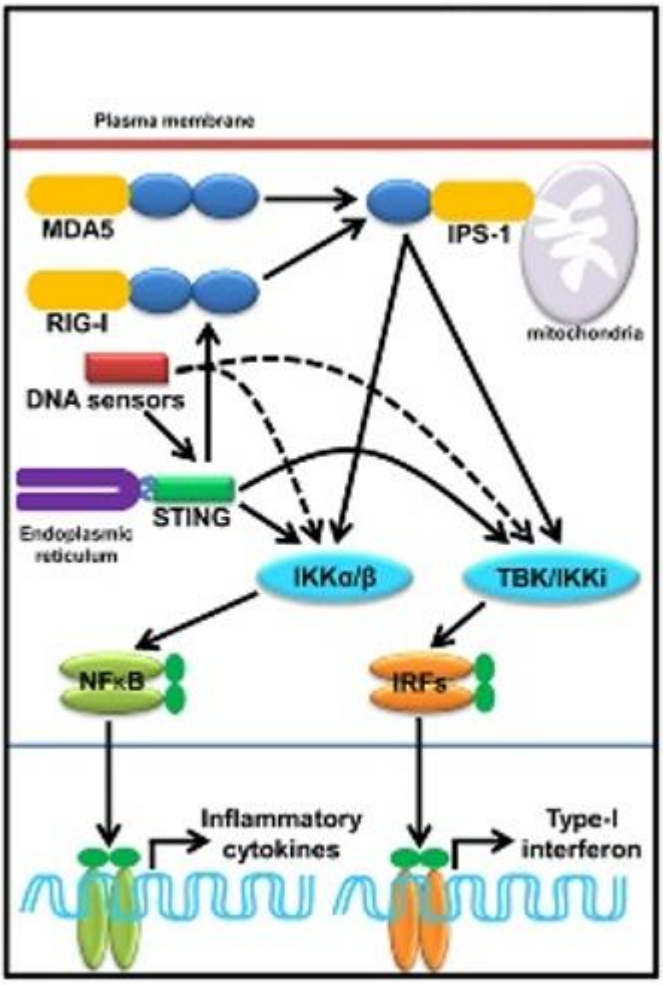

Figure 1.8 Cytosolic nucleic acid sensors. RIG-1 and MDA5 sense 'non-self' RNA, recruits an adaptor IPS-1 (MAVS) for induction of Type I IFNs and inflammatory cytokines via IRFs and NF-κB signalling pathways respectively. Several DNA sensors can induce the production of inflammatory cytokines and Type I IFNs in a STING-dependent and independent manner. (Figure reprinted from Mahla, R.S. *et al* (2013) Sweeten PAMPs: Role of sugar complexed PAMPs in innate immunity and vaccine biology. *Frontiers in Immunology*, 4(SEP), 1–16, Copyright © 2013 with permission under Creative Commons Attribution License (CC BY)).

1.4.1 Toll-Like receptor signalling pathways in melioidosis

TLRs occupy a prominent position in the innate immune system by virtue of their ability to recognise various bacterial components. Engagement of TLRs with their ligands leads to the production of many inflammatory cytokines, chemokines and effector molecules which

together orchestrate the inflammatory response. In septicaemic melioidosis, there is an increase in mRNA encoding TLR1, TLR2, TLR3, TLR4, TLR5, TLR8, TLR10, CD14 and MD-2 in leukocytes (Wiersinga *et al*, 2007). Expression of TLR2 and TLR4 along with CD14 and TLR1 were shown to be upregulated on the surface of circulating monocytes and granulocytes, indicating the importance of TLR2 and TLR4 in response to the presence of *B. pseudomallei*. In melioidosis research, TLR2, TLR4 and TLR5 were given much attention to study the innate immune response both *in vivo* and *in vitro*. Gram-negative lipopolysaccharide (LPS) comprises of a core polysaccharide, O-antigen and lipid A (endotoxin) which is the canonical bacterial ligand for TLR4. Lipid A is the endotoxic centre of an LPS molecule where this region interacts with TLR4 in association with MD-2 and CD14 to induce a pro-inflammatory signal. Charuchaimontri *et al* (1999) found high levels of serum antibodies to LPS are associated with improved survival in severe melioidosis, suggesting the importance of *B. pseudomallei* LPS for an appropriate response. Furthermore, administration of monoclonal or polyclonal antibodies (mAb) to *B. pseudomallei* LPS proved to be protective upon aerosol challenge in murine melioidosis (Nelson *et al*, 2004). In fact, in humans, polymorphisms in the gene encoding TLR4 are associated with susceptibility to melioidosis (West *et al*, 2012). However, *B. pseudomallei* LPS is reported to be less immunostimulatory compared to pathogenic enterobacterial LPS (Matsuura *et al*, 1996). The differences in such immunological activities can be further explained by the unique three-dimensional shape of the lipid A moiety of *B. pseudomallei* LPS which has different disaccharide backbone, different fatty acyl-chains as well as the presence of modified phosphate group (Novem *et al*, 2009). In the RAW264.7 macrophage-like cell line, *B. pseudomallei* LPS exhibits slower and weaker kinetics of macrophage-activating activity compared to *E. coli* LPS, in which the delayed onset of cytokines production may serve as a way to evade host defence (Utaisincharoen *et al*, 2000). In addition, human and murine macrophages stimulated with *B. pseudomallei* LPS secrete less inflammatory cytokines TNFα, IL-6 and IL-10 when compared to cells stimulated with LPS from avirulent *B. thailandensis* (Novem *et al*, 2009). In a separate study, *B. pseudomallei* LPS has been demonstrated to possess weaker pyrogenic activity in rodents than enterobacterial LPS but stronger mitogenic activity in murine splenocytes (Matsuura *et al*, 1996). *In vivo*, TLR4 knock out has no obvious effect on mouse survival upon *B. pseudomallei* infection (Wiersinga *et al*, 2007).

TLR2 is a promiscuous receptor which heterodimerises with either TLR1 or TLR6 upon recognition of a bacterial cell wall component; lipotechoic acid, peptidoglycans or lipoproteins

(reviewed in Kawai and Akira, 2010). Though TLR2 is predominantly regarded as a receptor for Gram-positive bacteria, the unique LPS structure derived from *B. pseudomallei* has been shown to signal via TLR2 (Feterl *et al*, 2008; Wiersinga *et al*, 2007). Activation of TLR2 been reported in response to LPS from a range of other Gram-negative bacteria such as *Legionella pneumophila* (Katz *et al*, 2006), *Porphyromonas gingivalis* (Darveau *et al*, 2004) and *Helicobacter pylori* (Smith *et al*, 2003). *In vitro* study using HEK294 cells transfected transiently with murine or human TLRs demonstrated that both TLR2 and TLR4 are activated in the presence of *B. pseudomallei,* illustrated by an increased level of NF-κB signalling (Weehuizen *et al*, 2015). Wiersinga *et al* (2007) showed similar observations where TLR2 and TLR4 were found to contribute to cellular responsiveness to *B. pseudomallei in vitro*.

In contrast with *in vitro* studies showing the importance of both TLR2 and TLR4 in response to *B. pseudomallei,* West and colleagues (2008) characterised *B. pseudomallei* LPS as solely a TLR4 ligand , and macrophage cytokines TNFα and IL-10 production were shown to be dependent on TLR4 alone. These findings are contrary to the *in vivo* studies of Wiersinga *et al* (2007) which described that only the TLR2 receptor recognised *B. pseudomallei* LPS. Significantly less cytokine levels of TNFα, IL-6 and IL-10 were observed in TLR2 knockout mice compared to WT mice. Nevertheless, the TLR2 signalling induced upon recognition of *B. pseudomallei* LPS resulted in an uncontrolled stimulation that impaired the protective immune response against the pathogen (Wiersinga *et al*, 2007). TLR2 knockout mice were found to be less susceptible to lethal infection with less bacterial growth, diminished dissemination and reduced distant organ injury (Wiersinga *et al*, 2007). This is in accordance with the genome-wide expression study where the overwhelming induction of TLR2 was observed to counteract *B. pseudomallei* (Chin *et al*, 2010). Though undoubtedly TLR signalling responses play a crucial role in eliminating invading pathogens, uncontrolled stimulation that exceeds the threshold of immune homoeostasis may cause excessive inflammation, as in the case of sepsis.

In addition to the role of TLR2 and TLR4 as innate mechanisms in the pathogenesis of melioidosis, TLR5 that detects bacterial flagellin has also been shown to be activated in response to *B. pseudomallei*. In infected CHO cells *in vitro*, *B. pseudomallei* induces a TLR5-dependent innate immune response through NF-κB signalling (West *et al*, 2013). In fact, polymorphisms in TLR5 are associated with survival from melioidosis (West *et al*, 2013). A hypofunctional TLR5 variant that is insensitive to flagellin has been postulated to generate an impaired inflammatory response during melioidosis infection, and therefore reduced sepsis-induced organ failure and lower mortality (West *et al*, 2013). *In vivo* studies using TLR5

knockout mice showed significantly more susceptibility to *B. pseudomallei* by intranasal challenge (West *et al*, 2014), a phenotype that contrasts with that observed in TLR2 and TLR4 knockout mice (Wiersinga *et al*, 2007).

The key roles of TLR2, TLR4 and TLR5 in the pathogenesis of melioidosis are underscored by the finding that mice deficient of the main adaptor protein MyD88, but not TRIF, show a strong lethality upon intranasal infection with *B. pseudomallei* (Wiersinga *et al*, 2008). MyD88, which is the key adaptor for all TLRs except TLR3 and certain TLR4s, was shown to give protection through recruitment and activation of neutrophils at the site of primary infection *in vivo* (Wiersinga *et al*, 2008). This is in accordance with *in vitro* studies in RAW macrophage-like cells where *B. pseudomallei* induced expression of genes downstream of the MyD88-dependent pathway only, and not through the TRIF-dependent signalling pathway (Tangsudjai *et al*, 2010). Conversely, an LPS mutant was able to stimulate both MyD88-dependent and -independent pathways. It was shown that only the MyD88-dependent pathway is needed to control the WT infection, but, the survival of the LPS mutant was suppressed by MyD88-independent activation (Tangsudjai *et al*, 2010). Additionally, an LPS mutant of *B. pseudomallei* is able to activate IFN-β production in macrophage-like cell lines leading to the expression of iNOS for nitric oxide-mediated killing, a pathway that is not stimulated by the WT strain (Arjcharoen *et al,* 2007). These findings suggest that the LPS mutant strain may induce a different TLR signalling pathway from the WT strain. The failure to activate the MyD88-independent pathway may facilitate B. *pseudomallei* survival within macrophages (Tangsudjai *et al*, 2010).

1.4.2 Canonical inflammasome pathways in counteracting *Burkholderia pseudomallei*

Inflammasomes, of which several different types have been identified, are multiprotein complexes containing PRRs belonging to the Nod-like receptor family (NLR family; NLRP1, NLRP3, NLRC4) or the PYHIN family (such as AIM2), together with ASC adaptor and the protease caspase-1. Different inflammasomes are triggered by different microbial components or endogenous 'danger signals'. Upon activation, the procaspase-1 will be auto-cleaved into its active form of p10 and p20 caspase-1. Active caspase-1 mediates the maturation of the pro-inflammatory cytokines pro-IL-1β and pro-IL-18 into their respective biologically active IL-1β and IL-18 (von Moltke *et al*, 2013; Schattgen and Fitzgerald, 2011). Additionally, the inflammasome can regulate the innate immune pathway through the induction of programmed cell death known as pyroptosis, which destroys the intracellular niche and prevents the subsequent dissemination of the pathogen.

Caspase-1 activation is triggered in macrophages by many intracellular pathogens including *Salmonella* (Jarvelainen *et al*, 2003)*, Shigella* (Suzuki *et al*, 2007)*,* and *Listeria* (Warren *et al*, 2008), causing rapid cell death. Similarly, an *in vitro* experiment by Sun *et al* (2005) demonstrated that *B. pseudomallei* is also capable of inducing pyroptotic caspase-1-dependent cell death in the human THP-1 monocytic-like cell line, along with the secretion of IL-1β. In other *in vitro* studies, Caspase1$^{-/-}$ macrophages infected with *B. pseudomallei* showed slower cell cytotoxicity as demonstrated by Breitbach *et al* (2009). This suggests that prolonged cell death in the absence of caspase-1 benefits the pathogen by allowing it to survive and replicate in a cell displaying reduced bactericidal capacity. An *in vivo* experiment showed that caspase-1 mediates resistance towards intranasal challenge of *B. pseudomallei*, where caspase-1 knockout mice reached 100% mortality as early as 3 days post-infection, with significantly higher bacterial load in spleen, liver and lung when compared to WT mice (Aachoui *et al*, 2013; Breitbach *et al*, 2009). Likewise, caspase-1 also protects from the closely related, but far less virulent *B. thailandensis* as *Casp-1*$^{-/-}$ mice succumbed to *B. thailandensis* infection, whereas the WT mice survived (Aachoui *et al*, 2013). Consistent with these findings, *in vitro* experiments showed that bone marrow-derived macrophages (BMDMs) which lack caspase-1/11 contained higher bacterial loads compared to WT macrophages at 3 hpi, the difference became more pronounced at 6hpi (Bast *et al*, 2014). Collectively, the canonical caspase-1-

dependent inflammasome pathway seems to play an important role in controlling *B. pseudomallei* at the early phase of infection, which is crucial for host survival.

In terms of which inflammasome receptors are involved in the recognition of *B. pseudomallei*, Ceballos-Olvera and co-workers revealed that *B. pseudomallei* can induce the activation of caspase-1 inflammasome via both NLRP3 and NLRC4 (Ceballos-Olvera *et al*, 2011). NLRP3 triggers caspase-1 activation in response to host-derived 'danger signals' (DAMPs), multiple pathogens including bacteria, virus and fungi, and also to several non-infectious crystals. These crystals are also termed as particulate matter which can be endogenous such as monosodium urate (MSU) crystals, cholesterol crystals and amyloid β structures, or exogenous as for examples, silica crystals, asbestosis fibers and aluminium salts. These crystals can cause chronic diseases like gout disease, Alzheimer's disease, atherosclerosis and silicosis (reviewed by Kazazian, 2014). Perturbation of cell membrane integrity such as phagosomal or vacuolar rupture is also a common event which is triggered by NLRP3 activation. NLRC4 specifically responds to Type III secretion system (T3SS) inner rod/needle components and also the cytoplasmically delivered bacterial flagellin, in which the specificity is determined by its interaction with the NAIP molecules NAIP2 or NAIP5, respectively. In a murine model of melioidosis, both *Nlrc4*$^{-/-}$ and *Nlrp3*$^{-/-}$ inflammasome-deficient mice were dramatically susceptible to aerosolised *B. pseudomallei* infection compared to WT mice, showing the importance of inflammasomes in controlling *B. pseudomallei*. NLRC4 was shown to mainly regulate pyroptosis, whereas NLRP3 was required for the production of IL-1β and IL-18 (Ceballos-Olvera *et al*, 2011). *Nlrc4*$^{-/-}$ BMDMs, but not *Nlrp3*$^{-/-}$ BMDMs, exhibited substantially reduced pyroptosis when infected with *B. pseudomallei* when compared to macrophages from WT animals. Consistent with the role of pyroptosis in restricting the intracellular bacterial growth, substantially higher numbers of bacteria were recovered from inflammasome-deficient *Nlrc4*$^{-/-}$ BMDMs compared to the WT and *Nlrp3*$^{-/-}$ BMDMs (Ceballos-Olvera *et al,* 2011). This result is paralleled with the *in vivo* studies where infected *Nlrc4*$^{-/-}$ mice carried considerably higher bacterial load in the spleen, liver and lungs at 24hpi and 48hpi than WT and *Nlrp3*$^{-/-}$ mice (Ceballos-Olvera *et al*, 2011).

The studies described above were then extended to investigate the role of inflammasome-mediated cytokines IL-1β and IL-18 during murine melioidosis. *IL-18*$^{-/-}$ mice were extremely vulnerable to *B. pseudomallei* even at a low dose of infection (Ceballos-Olvera *et al*, 2011). This finding is parallel to the *in vivo* experiment by Wiersinga *et al* (2007) where upon intranasal challenge with a lethal dose of *B. pseudomallei*, *IL-18*$^{-/-}$ mice displayed enhanced

bacterial growth in the lungs and liver as compared to the WT mice as early as 24 hours post-infection. This protective role of IL-18 was then shown to be associated with the induction of IFN-γ production (Ceballos-Olvera *et al,* 2011; Wiersinga *et al,* 2007). However, unexpectedly mice deficient in interleukin-1 receptor (*Il-1r*$^{-/-}$) displayed better resistance to lung infection compared to WT mice, with reduced neutrophil influx into the lungs, lower bacterial burden, and less severe lung pathology (Ceballos-Olvera *et al*, 2011). The IL-1β cytokine was found to be deleterious by causing excessive neutrophil recruitment, leading to excessive inflammation and subsequently tissue damage (Ceballos-Olvera *et al*, 2011). The detrimental effect of IL-1β was further confirmed when the administration of recombinant IL-1β significantly increased the bacterial burden, inflammation and mortality, while administration of IL-1 receptor antagonist IL-1ra protected WT mice from mortality (Ceballos-Olvera *et al*, 2011). It has been argued that neutrophils might be permissive for *B. pseudomallei* growth and the continuous production of IL-1β excessively increased the influx of neutrophils which benefits the bacteria for dissemination (Ceballos-Olvera *et al*, 2011). Therefore, the host innate immune response must be tailored accordingly to each pathogen to elicit the correct inflammatory response, otherwise it may lead to excessive inflammation that results in severe morbidity and mortality.

1.4.3 The non-canonical inflammasome, an indispensable defence against *Burkholderia pseudomallei*

Pyroptotic cell death can also occur through activation of the non-canonical inflammasome. This non-canonical inflammasome pathway is mediated by murine caspase-11 (known as caspase-4/5 in humans). The non-canonical inflammasome pathway requires priming by TLR4 in a TRIF-dependent manner and with an IFNβ-responsive factor. TLR4 recognises cytosolic LPS in a TRIF-dependent manner, leading to upregulation of Type I IFN expression, commonly IFN-β. The released Type I IFN is recognised by Type1 IFN receptor, activates the STAT (Signal transducer and activator of transcription) interferon signalling pathway and leads to expression of more procaspase-11 protein. Whether pro-caspase-11 expression itself is sufficient for caspase-11 auto-activation (Rathinam *et al*, 2012) or requires additional yet unknown bacterial signals for activation (Broz *et al*, 2012), still remains a controversy. Upon activation, procaspase-11 is cleaved into its active form of p20 and p10, or partially cleaved into p30, similar to the mechanism of caspase-1 activation. Caspase-11 activation also leads to release of pro-inflammatory cytokine IL-1α and high mobility group protein B1 (HMGB1) in a caspase 1-independent manner. Caspase-11 also promotes assembly of the NLRP3 inflammasome and IL-1β secretion in a caspase-1 dependent manner (Maltez and Miao, 2016; Man and Kanneganti, 2015).

This pyroptotic cell death pathway via caspase-11 contributes to a novel cell autonomous response that is reserved exclusively to detect cytosolic, but not vacuolar, bacteria. It has been demonstrated previously that the specific *sifA* mutant of *Salmonella* that aberrantly enters the cytosol, triggers caspase-11 to enhance clearance of *Salmonella* Typhimurium, independently from all known canonical inflammasomes NLRP3, NLRC4 and ASC. On the other hand, the WT *Salmonella* Typhimurium that remains within the vacuole can effectively escape from Caspase-11 pyroptotic killing (Aachoui *et al*, 2013). In response to naturally cytosolic *B. pseudomallei*, inflammasome activation is key for protection of the host, as $Casp1^{-/-}Casp11^{-/-}$ mice succumb more readily to infection *in vivo* (Kayagaki *et al*, 2011). This finding is consistent with the evidence from Aachoui *et al* (2013) where $Casp11^{-/-}$ knockout mice exhibited greater mortality *in vivo* when infected with *B. pseudomallei*, indicating that a novel pyroptosis-inducing pathway via Caspase-11 is also critical for host survival against *B. pseudomallei.*

1.4.4 Interferon response to *Burkholderia pseudomallei* and other intracellular pathogens

Interferons (IFNs) are secreted cytokines that orchestrate diverse immune responses to viruses and other intracellular microbes. Type I interferon family members include a single IFNβ protein, as well as numerous IFNα and other family members namely IFN-ε, IFN-κ, IFN-ω, IFN-δ, IFN-ι and IFN-ξ (reviewed in Platanias, 2005). All Type I IFNs signal via a common heterodimeric cell surface receptor (IFNAR), comprised of IFNAR1 and IFNAR2 which are associated with tyrosine kinase 2 (TYK2) and Janus Activated Kinase 1 (JAK1), respectively (Figure 1.9). Type II IFN mainly consists of IFNγ, and the IFNγ receptor (IFNGR) consists of heterodimeric IFNGR1 and IFNGR2 subunits which are associated with JAK1 and JAK2, respectively (Figure 1.9). Activation of JAK leads to the phosphorylation of STATs which rapidly translocate to the nucleus and initiate gene transcription. Both Type I and II IFNs can induce the formation of STAT1-STAT1 homodimers which then enter the nucleus and bind to a GAS (IFNγ-activated site) element, a specific motif in the promoters of various Interferon-Stimulating Genes (ISGs) and initiates transcription. However, only the Type I IFN signalling pathway results in the formation of STAT1-STAT2 heterodimers, which forms a heterotrimeric transcription complex with IRF9 known as ISGF3 (interferon-stimulated gene factor 3). This ISG3 complex is then transported to the nucleus and recognises IFN-stimulated response elements (ISREs) in DNA, which is distinct from GAS elements, to initiate transcription of another set of ISGs (reviewed in Platanias, 2005).

Although typically considered to be the most important antiviral immune response, it is increasingly evident that stimulation of Type I IFNs correlates with host susceptibility to infections with several bacterial pathogens such as *Listeria monocytogenes* (O'Connell *et al*, 2004), *Mycobacterium tuberculosis* (Novikov *et al*, 2011) and *Francisella tularensis* (Henry *et al*, 2007). This bacterial induction of Type I IFNs can occur via TLR-dependent or TLR-independent pathways using cytosolic sensors (reviewed in Perry *et al*, 2005). TLR3 and TLR4 sense dsRNA and lipopolysaccharide (LPS) respectively, and stimulate Type I IFN in a TRIF-dependent manner. While other nucleic acid recognising TLRs namely TLR7, TLR8 and TLR9 can induce Type I IFNs in a MYD88-dependent pathway. Several studies reported that they are restricted to cell types such as plasmacytoid dendritic cells (pDCs) and conventional dendritic cells (cDCs) (reviewed in Perry *et al*, 2005).

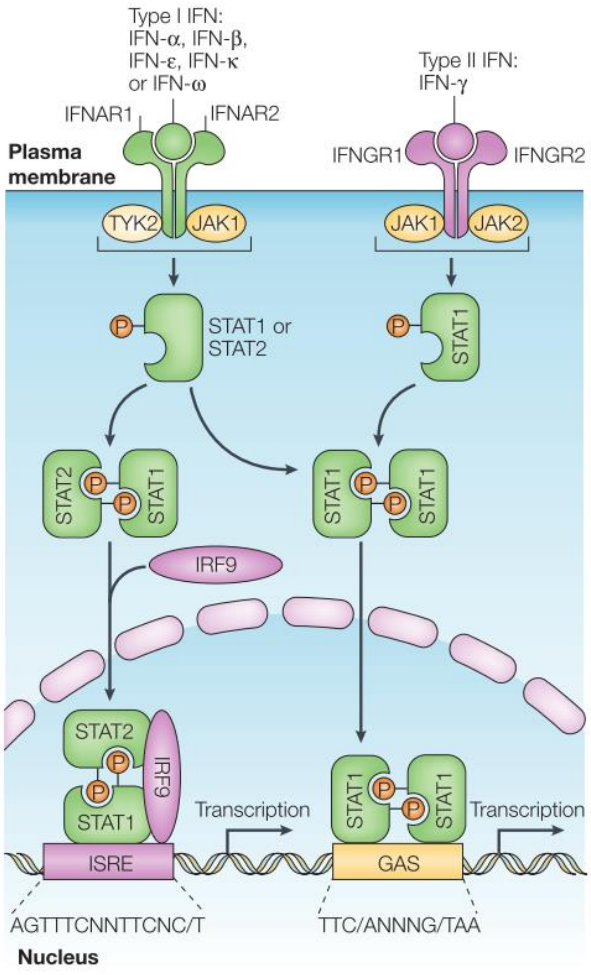

Figure 1.9 Type I and II interferon receptors and their respective signalling pathways. Type I IFNs utilise heterodimeric cell surface receptors (IFNAR) which consist of IFNAR1 and IFNAR2 chains to signal through a canonical JAK/STAT cascade involving JAK1, Tyk2, STAT1 and STAT2 proteins. A similar mechanism is used by Type II IFN (IFNγ) but requires different receptor subunits and proteins during activation. Type II IFN receptors (IFNGR) consist of IFNGR1 and IFNGR2, where upon binding with IFNγ they activate the canonical JAK/STAT pathway involving JAK1, JAK2 and STAT1 proteins. Different STAT complexes are formed in response to different types of interferons resulting in distinct gene-expression programmes. STAT1 and STAT2 complexes together with IFN-regulatory factor 9 bind to IFN-stimulated response element (ISRE) sequences to activate classical antiviral genes. In contrast, downstream signalling cascade of STAT1 homodimers bind to gamma-activated sequences (GASs) to induce pro-inflammatory genes (figure reprinted from Platanias, L.C. (2005). Mechanisms of type-I- and type-II-interferon-mediated signalling. *Nature Reviews Immunology*, 5(5), 375–86. Copyright © 2005 with permission from Macmillan Publishers Ltd: Nature Publishing Group).

Type I IFN can also be induced in a TLR-independent cytosolic pathogen receptor manner. Cytosolic RNA is detected by RNA helicase Retinoic-acid inducible gene-1 (RIG-1), or RIG-1-like receptors (RLR) such as MDA-5 (melanoma differentiation antigen 5). RIG-1 and MDA-5 recognise RNA via a DExD/H box-containing RNA helicase domain. Upon ligand recognition, RIG-1 and MDA-5 are recruited to mitochondria to bind with the adaptor protein MAVS to activate IRF3 as well as NF-κB transcription factors (Figure 1.8), subsequently inducing transcription of Type I IFNs and inflammatory cytokines respectively. Activation of IRF3 requires upstream signalling through TBK1. RLRs which are thought primarily to detect RNA viruses, have also been recently shown to detect RNA from intracellular bacteria such as *Listeria monocytogenes* (Hagmann *et al*, 2013), *Legionella pneumophila* (Monroe *et al*, 2009) and *Shigella flexneri* (Dixit & Kagan, 2013; Jehl *et al*, 2012). In addition to RNA sensors, Type I IFN also can be induced by cytosolic DNA-sensing pathway such as DNA sensor ZBP-1 which is activated in response to human cytomegalovirus (DeFilippis *et al*, 2010). However, ZBP-1 may not be a unique DNA sensor and its ability to stimulate IFNβ production may be redundant with other DNA sensors (Monroe *et al*, 2009; Lippmann *et al*, 2008). Besides MAVS, STING (stimulator of interferon genes) is another essential adaptor protein that functions upstream of TBK1 and IRF3 to induce Type I IFN (Figure 1.8). STING recognises the second messenger cyclic-diguanylate monophosphate (cGAMP) that is generated by nucleotidyltransferase cyclic GMP-AMP synthase (cGAS) in response to recognition of foreign DNA. STING also recognises cGAMP that is secreted directly from cytosolic bacteria (reviewed in Burdette and Vance, 2013). Bacterial pathogens such as *Listeria monocytogenes* (Ishikawa *et al*, 2009) and *Chlamydia trachomatis* (Barker *et al*, 2013) require STING for Type I induction *in vitro*. Interestingly, STING has been shown to be associated with autophagy during microbial infection. This novel STING-dependent autophagy-like response has been observed for the intracellular bacteria *Mycobacterium tuberculosis* (Watson *et al*, 2012) and also α-herpesvirus (Rasmussen *et al*, 2011).

B. pseudomallei by itself fails to stimulate IFNβ production in infected RAW264.7 cells (Utaisincharoen *et al*, 2003), resulting in better survival inside the host cell. It was reported that the inability to stimulate IFNβ also leads to a reduced expression of transcription factor IRF-1 and nitric oxide synthase (iNOS) for antimicrobial nitric oxide (NO) production (Utaisincharoen *et al*, 2003). In the presence of exogenous IFNβ, *B. pseudomallei*-infected macrophages express high levels of both IRF-1 and iNOS, and subsequently suppress the intracellular survival of *B. pseudomallei*, indicating the role of IFNβ as an antimicrobial by

upregulating NO production (Utaisincharoen *et al*, 2003). Which sensor is required for the production Type I IFN in response to *B. pseudomallei* is not well studied. Tangsudjai *et al* (2010) reported that *B. pseudomallei* is incapable of activating TRIF-dependent signalling for Type I IFN expression. Failure to induce IFNβ stimulation by *B. pseudomallei* itself may be related to the low activation of TLR4 due to the unique LPS structure of *B. pseudomallei* which is a poor macrophage activator (Utaisincharoen *et al*, 2000). In addition to this finding, *in vivo* global transcription profiling by microarray identified several highly induced Type I interferon related genes such as members of the oligoadenylate synthetase (OAS) family and Signal Transducer and Activator of Transcription (STAT1 and STAT2) in *B. pseudomallei*-infected mice (Chin *et al*, 2010). However, involvement of other cytosolic sensors such as RIG-1, MDA-5, ZBP-1 and others in relation to melioidosis have not been described so far.

Exposure of cells to Type I IFN during viral infection elicits an antiviral state that inhibits viral replication, but in bacterial infections, Type I IFN does not always participate in the host immune resistance against infection. Type I IFN has been regarded as the main cytokines which suppresses intracellular survival of *Legionella pneumophila* in infected murine macrophages, which is directly associated with the polarisation of macrophages toward the classically activated M1 phenotype, but independent from STAT1- and STAT2- mediated pathways (Plumlee *et al*, 2009). Similarly, Type I production in response to group B *Streptococci* increased the production of proinflammatory cytokines and hence, resistance to infection (Mancuso *et al*, 2007). Often, however, the production of Type I IFN causes susceptibility towards other bacterial infections. Indeed, Type I IFN receptor-knockout mice (IFNAR-/-) exhibit substantially increased resistance to infection with *Francisella tularensis* (Henry *et al*, 2010; Henry *et al*, 2007) and *Listeria monocytogenes* than WT mice (Stockinger *et al*, 2009).

Type II IFNγ is generally a more potent activator of phagocytic cells and is essential for host resistance to *Listeria monocytogenes* (Rayamajhi *et al*, 2010) and other intracellular pathogens. It has been shown that IFNγ is essential for resistance to *B. pseudomallei*. In one *in vivo* study, administration of neutralising monoclonal antibody (mAb) against IFNγ rendered the mice significantly more susceptible to death. Higher mortality observed in mAb-treated mice was due to significantly increased bacterial burden in liver and spleen compared to the control mice (Santanirand *et al*, 1999). In clinical samples, patients presenting with lethal melioidosis express high levels of IFNγ which correlates with mortality (Lauw *et al*, 1999; Brown *et al*, 1991). In addition, one of the IFNγ-inducing cytokines known as IL-12p40 was found to be significantly higher in melioidosis patients (Lauw *et al*, 1999). However, IFNγ

mediated resistance to *B. pseudomallei* is not complete and does not provide protective sterilising immunity as observed with resistance to *Listeria monocytogenes* (Utaisincharoen *et al*, 2004). Besides, Ekchariyawat *et al* (2005) documented that suppression of IFNγ responses in infected macrophages is possibly due to *B. pseudomallei*-induced expression of Suppressor of cytokine signalling 3 (SOCS3) and Cytokine-Inducible Src Homology 2-containing protein (CIS). Activation of these proteins inhibits phosphorylation of Y701-STAT and consequently, interferes with IFNγ signalling (Ekchariyawat *et al*, 2005).

1.4.5 Autophagy as a host innate mechanism against *Burkholderia pseudomallei*

1.4.5.1 The molecular autophagic pathway

Essential in the context of cellular homeostasis, autophagy involves the elimination of non-functional organelles and misfolded protein aggregates in response to various environmental and cellular stresses. The cellular autophagic activity is presumed to occur at low basal levels and can be rapidly regulated in response to various stimuli such as nutrient starvation, high-temperature, hypoxia and energy depletion. Autophagy suppression is often associated with certain diseases, including cancers, infectious diseases, aging and neurodegenerative disorders (reviewed in Levine & Kroemer, 2008). Recently, autophagy has been implicated as a part of the innate immune response by targeting intracellular pathogens residing in the cytoplasm or within vacuolar compartments to the host autophagic machinery for clearance. Intracellular *Streptococcus pyogenes* (Nakagawa *et al*, 2004) and *Mycobacterium tuberculosis* (Gutierrez *et al*, 2004) have been shown to be cleared by autophagy. Conversely, some pathogens such as *Listeria monocytogenes* (Yoshikawa *et al,* 2009; Py *et al*, 2007) and *Shigella* (Ogawa *et al,* 2005) actively subvert the autophagic process and survive within host cells. Such selective degradation of intracellular pathogens has resulted in a new class of innate immunity receptors known as SLR (sequestome-like receptor/p62) or LIR (LC3-interacting region)(reviewed in Wileman, 2013).

Autophagy is initiated by formation of an isolated membrane phagophore (vesicle nucleation), which then elongates into a double-membrane vesicle known as an autophagosome (vesicle elongation). This process is then followed by fusion with lysosomes to form autolysosomes and subsequently, degradation of the autophagosome contents by a series of lysosomal proteases. The autophagosome can also fuse with an endosome before fusion with the lysosome, to form a structure known as an amphisome. Amino acids and other small molecules can be recycled and delivered to the cytoplasm for reuse (Figure 1.10) (reviewed in Jo *et al*, 2013).

Autophagosome formation involves different enzymatic pathways (Figure 1.10). This begins with a serine/threonine protein kinase complex that responds to upstream inhibitory signals like TOR kinase (Target Of Rapamycin kinase). TOR kinase senses amino acids levels in cells and in the presence of abundant nutrients, this major inhibitor shuts off autophagy. However, when amino acid levels fall during starvation, the TOR kinase becomes inactive and

autophagy is switched on (reviewed in Levine & Kroemer, 2008). The pharmacological inducer rapamycin mimics autophagy starvation by inhibiting the negative regulatory signal of TOR kinase, hence inducing autophagy. The second part of the pathway is vesicle nucleation which requires a class III phosphatidylinositol 3-kinase (PI3K) enzymatic complex. In yeast, PI3K Vps34 activation depends on its binding partners Beclin1/Atg6 (**A**u**T**opha**G**y 6), Atg14 and Vps15 to generate a PI3P complex. This complex localises other autophagy proteins to the forming autophagosomes as well as phosphorylates lipids at autophagosome sites (Kihara *et al*, 2001). Many membrane sources can generate autophagosomes including ER (Endoplasmic Reticulum), mitochondria and Golgi apparatus. Some regulatory molecules such as AMPK (5'-AMP-activated protein kinase) which responds to low energy (low ATP (adenosine triphosphate)) can enhance autophagy at this step. Conversely, the drugs 3-MA and wortmannin can inhibit PI3K activity and suppress cell autophagy. The third element of the pathway is known as vesicle expansion. During the expansion process, LC3-I (microtubule-associated light chain 3) (a mammalian homologue of yeast Atg8) is conjugated to the highly lipophilic phosphatidylethanolamine (PE) moiety to generate LC3-II. LC3-II is then integrated into the lipid membranes of the autophagosome (Nakatogawa *et al*, 2009). This lipidation requires the Atg12-Atg5-Atg16 complex in which upon expansion, the autophagosomes are eventually released into the cytosol. Only LC3-II protein is known to be recruited to the autophagosome, hence it serves as a widely used marker for autophagosomes. LC3-II molecules are located both in the inner and outer membranes of autophagosomes, in which the outer one is cleaved by Atg4 to form LC3-I and recycled back into the cytoplasm, while the inner LC3-II is degraded.

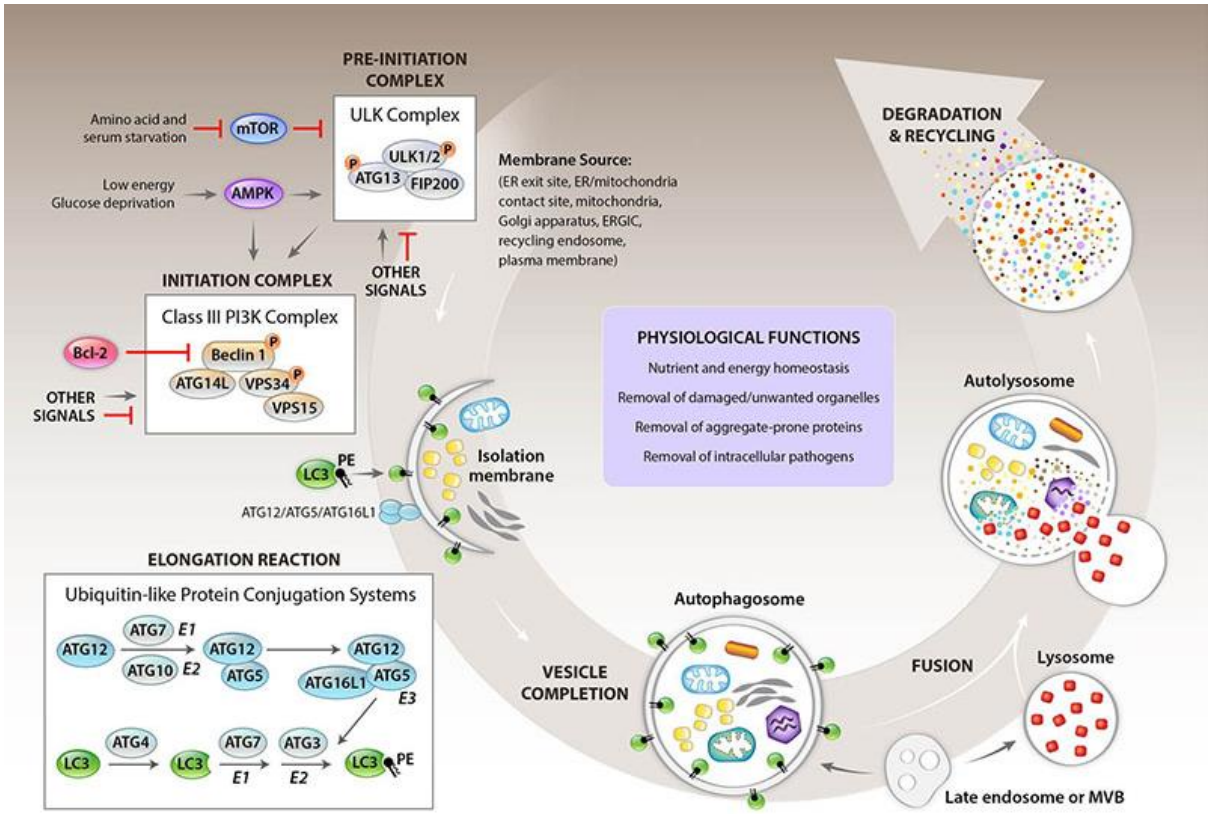

Figure 1.10 Molecular pathway of autophagy: Autophagy formation begins with vesicle nucleation (formation of the membrane/phagophore), which then elongates into a double-membrane autophagosome. An autophagosome fuses with a lysosome and to form an autolysosome. Enzymes that are present in the lysosome such as proteases and hydrolases degrade the content of autolysosome as well as lysis of the autophagosome inner membrane. Some of the degraded materials are recycled into the cytoplasm. Each step is regulated by different signalling pathways and Atg proteins (figure reprinted from Green, D. R. & Levine, B. (2014). To be or not to be? How selective autophagy and cell death govern cell fate. *Cell*, 157(1), 65–75, Copyright © 2014, with permission from Elsevier)

1.4.5.2 **Autophagy and *Burkholderia pseudomallei***

Antibacterial autophagy (xenophagy) is an autonomous immune response that can target intracellular pathogens that are residing both in the vacuolar and cytoplasmic compartments. Some bacteria such as *Mycobacterium tuberculosis* actively modify their endosome compartments to prevent lysosomal fusion, however they are eventually taken up into autophagosomes before being degraded by autophagy (Gutierrez *et al*, 2004). Bacteria such as *Streptococcus pyogenes* can exit from endosomes and enter the cytoplasm, but then the cytoplasmic *Streptococcus* can be captured by autophagosomes which fuse with lysosomes for degradation (Nakagawa *et al*, 2004). In other pathogens, autophagy is used for the bacterium's own benefit to survive and replicate, and their survival is decreased in host cells treated with autophagy inhibitors. For examples, *Mycobacterium marinum* generates double-membrane vacuoles independently of Atg5 and LC3, hence avoiding classical autophagy before entering the cytoplasm for replication (Collins *et al*, 2009). *Coxiella burnetti* is resistant to lysosomal degradation, but yet activates autophagy to fuse lysosomes and formation of a parasitophorous vacuole for replication (Gutierrez *et al*, 2004). Some cytosolic pathogens such as *Shigella* (Dupont *et al*, 2009) and *Listeria* (Yoshikawa *et al*, 2009), avoid recognition by the autophagy machinery.

In mammalian cell lines such as RAW264.7 and murine embryonic fibroblast (MEF), LC3 molecules have been shown to be recruited directly to *B. pseudomallei* localised in a single-membrane phagosome, a process termed as LC3-associated phagocytosis (LAP) (Gong *et al*, 2011; Cullinane *et al*, 2008). This LAP formation is distinct from the double-membrane canonical autophagosomes as LC3 molecules are recruited directly to the phagosome containing the pathogen rather than the phagophore or autophagosomes. LAP is used as a pathway to enhance pathogen degradation within phagosomes. LAP structures can fuse with lysosomes for phagosomal maturation, or alternatively deliver phagosomal cargo to PRRs, and also facilitate antigen presentation to MHC class II molecules (reviewed in Romao & Munz, 2014). The colocalisation of LC3 with phagosomal *B. pseudomallei* has been shown to be further increased in infected RAW264.7 cells when autophagy was pharmacologically induced using rapamycin, accompanied by a significant reduction in intracellular bacteria (Gong *et al*, 2011; Cullinane *et al*, 2008). These together implicate the importance of LAP-mediated autophagy in controlling phagosomal *B. pseudomallei* at early time points of infection.

Similarly, recruitment of LC3 molecules to phagosomal *B. pseudomallei* has also been observed *ex vivo* in primary human neutrophils, but through a novel elongated single-membrane structure that partially fuses with an autophagosome-like or a phagophore-like structure (Rinchai *et al*, 2015). In the same studies, inhibiting autophagy by treating neutrophils with 3MA, and also the lysosomal hydrolase inhibitors E64d and pepstatin A, enhanced the intracellular survival of *B. pseudomallei* in a time-dependent manner. However, it is worth noting that in infected primary human neutrophils, very few *B. pseudomallei* escape from the phagosomes and reach the cytoplasm, suggesting that autophagy is likely the second line of defence against cytoplasmic *B. pseudomallei* (Rinchai *et al*, 2015). Furthermore, those cytoplasmic *B. pseudomallei* did not form actin-tails unlike those observed in infected immortalised cell lines such as HeLa (Stevens *et al*, 2005b), A549 (Sitthidet *et al*, 2011), J744.2 (Sitthidet *et al*, 2011; Stevens *et al*, 2005b) and RAW264.3 (Burtnick *et al*, 2008). Therefore, the different cell-types used for these studies could account for the difference in the effect of the host autophagic machinery. Nevertheless, in those cells where *B. pseudomallei* is capable of escape from the phagosomes in a Bsa T3SS-dependent manner (Stevens *et al*, 2002), LAP targeting of *B. pseudomallei* becomes relatively ineffective. Cytoplasmic *B. pseudomallei* is rarely sequestered in a double-membrane canonical autophagosome as observed by transmission electron microscopy (TEM) (Rinchai *et al*, 2015; Gong *et al*, 2011), suggesting that *B. pseudomallei* actively evades the autophagy innate immune response. Such autophagy evasion could be mediated by bacterial actin-based motility as shown for intracellular *Listeria monocytogenes* and *Shigella flexneri*.

1.4.5.3 Actin-based motility allows *Listeria monocytogenes* and *Shigella flexneri* to evade autophagy

The intracellular pathogens *S. flexneri* (Ogawa *et al*, 2005) and *L. monocytogenes* (Yoshikawa *et al,* 2009; Py *et al*, 2007) have been shown to evade host autophagy through actin-based motility, but with distinct molecular mechanisms. *S. flexneri* evades autophagic recognition in the presence of the T3SS effector protein IcsB (Ogawa *et al*, 2005), while host protein recruitment to the actin-tail of *L. monocytogenes* camouflages the bacterium from being recognised by autophagy (Yoshikawa *et al,* 2009; Py *et al*, 2007). *S. flexneri* expresses IcsA on its surface to mediate actin polymerisation and appears to activate autophagy. IcsA has been

shown to interact with the autophagic protein, Atg5, which targets cytoplasmic *Shigella* for autophagy. However, virulent *Shigella* isolates expressing IcsB do not activate autophagy as the IcsB protein competes for the binding of Atg5 to IcsA, thus shielding *Shigella* against autophagic recognition (Ogawa *et al*, 2005)**.** In *B. pseudomallei*, BimA is unlikely to be a functional counterpart of *S. flexneri* IcsA in evading autophagy as the BimA protein lacks the 114 amino acid region of IcsA that is targeted by Atg5 (Gong *et al*, 2011). *B. pseudomallei* BopA has been predicted to be a homologue of *Shigella* IcsB and a *B. pseudomallei* mutant lacking *bopA* has an increased colocalisation with LC3 molecules (Gong *et al*, 2011). However, it appears unlikely that BopA assists in autophagy evasion in a manner analogous to IcsB. Instead, the *bopA* mutant has a reduced ability to escape from the phagosome and is targeted to autophagy in an LAP-dependent manner, but not cytoplasmic engulfment by autophagosomes (Gong *et al*, 2011; Cullinane *et al*, 2008). It has been suggested that the presence of the Rho GTPase inactivation domain at the BopA carboxyl terminus disrupts the phagosome membrane, assisting the sequestered bacteria to escape into the host cytosol (Gong *et al*, 2011). Alternatively, the BopA cholesterol binding domain leads to the accumulation of cholesterol on the phagosome membrane, which could prevent lysosomal recognition and hence, disrupts autophagy (Gong *et al*, 2011; Kayath *et al,* 2010).

When *L. monocytogenes* enters the cytoplasm, the bacterium expresses ActA which is required for actin-tail formation. It has been shown that ActA has binding sites for the host proteins Arp2/3 and Ena/VASP (Yoshikawa *et al,* 2009). Yoshikawa *et al* (2009) demonstrated that recruitment of Arp2/3 and Ena/VASP to the actin-tails on the bacterial surface camouflages the bacteria from autophagic recognition. On the other hand, *actA* mutants have been shown to be first ubiquitinated, which is followed by recruitment of LC3 and the adaptor protein p62, before finally entering the autophagic pathway (Yoshikawa *et al*, 2009). *B. pseudomallei* has been shown to form actin-tails independently from the host proteins Arp2/3 and Ena/VASP. In fact, *B. pseudomallei* BimA itself mimics Ena/VASP during actin polymerisation (Benanti *et al*, 2015). However, some host proteins that are postulated to be involved during the process of forming actin-tails such as IQGAP1 (Jitprasutwit *et al*, 2016) could disguise *B. pseudomallei* from host autophagy recognition. Whether *B. pseudomallei* employs a similar strategy to subvert host autophagy has yet to be determined.

1.5 Central hypothesis and objectives of thesis

Macrophages are important host immune cells in innate defence against *B. pseudomallei*, yet the pathogen has evolved multiple strategies to manipulate such cells to survive and replicate within the host. We hypothesise that *B. pseudomallei* utilises actin-based motility, which is mediated by the bacterial BimA protein, as a strategy to escape from macrophage innate defence pathways. Therefore, the broad aim of this thesis is to elucidate the macrophage response to infection with *B. pseudomallei*, and to discover the innate mechanisms that are avoided by *B. pseudomallei* in a BimA-dependent manner. Understanding the basis of such evasion could provide novel insights into potential host-directed therapies against this emerging pathogen. Primary BALB/C bone-marrow derived macrophages (BMDMs) have been utilised throughout this PhD project to address the following specific objectives:

1. To isolate and characterise the phenotype of BALB/C BMDMs (Chapter 3)
2. To compare the intracellular survival of *B. pseudomallei* with the isogenic Δ*bimA* mutant in BALB/C BMDMs (Chapter 3)
3. To investigate if *B. pseudomallei* evades autophagy in a BimA-dependent manner (Chapter 3)
4. To investigate the contribution of MyD88- and TRIF-dependent signalling in controlling the intracellular fate of *B. pseudomallei* and the Δ*bimA* mutant (Chapter 4)
5. To demonstrate whether cytosolic canonical- or non-canonical inflammasomes are activated in response to intracellular *B. pseudomallei* or the Δ*bimA* mutant in BALB/C BMDMs (Chapter 4)
6. To use Affymetrix gene expression profiling to characterise the global macrophage transcriptomic response to infection with *B. pseudomallei*, as well as to identify any specific macrophage response to infection with the Δ*bimA* mutant (chapter 5)

2 CHAPTER 2: MATERIALS AND METHODS

2.1 Preparation of murine bone marrow cells

12-week old BALB/C mice were obtained from Envigo Laboratory, UK. Briefly, tibias and femurs were aseptically removed with the whole bone intact, and dissected free of adhering tissues, in a class II Microbiological Safety Cabinet. The bones were then placed in 70% ethanol for a minute, washed in complete RPMI medium and kept in PBS (phosphate-buffered saline) solution. The complete RPMI medium (Sigma-Aldrich) was supplemented with 10% (vol/vol) heat-inactivated foetal calf serum (FCS) (Gibco Life Technologies) and 100U/ml penicillin, 100µg/ml streptomycin and 29.2mg/ml L-glutamine (Pen-Strep-Glu from Gibco Life Technologies). The bone ends were removed with a scalpel and bone marrow cells were flushed out using a syringe filled with complete RPMI medium into a sterile polypropylene Falcon tube. The medium containing the cells was suspended up and down to gently dissociate the cells. Fresh bone marrow cells were counted using a haemocytometer, and centrifuged at ~150 *x* g for 10 minutes. The pellet was then resuspended in recovery-cell culture freezing medium (Thermo Fisher Scientific) at a density of 6 x 10^6 cells per ml. 1ml aliquots of this suspension were dispensed into cryogenic storage vials. The vials were placed into a 'Mr Frosty' and stored at -80°C until needed.

2.2 Differentiation of bone marrow-derived macrophages (BMDMs)

To thaw the cells, cryovials were quickly transferred to a 37°C water bath until the suspension was completely thawed. For a 10cm-square petri dish, four vials were diluted into 17ml of complete medium containing 10ng/ml recombinant murine granulocyte-macrophage colony stimulating factor (GM-CSF) (Gibco Life Technologies), to give a density of 2.4 x 10^7 cells per plate. The cells were incubated at 37ºC in a 5% CO_2 atmosphere. On day 4, 10ml of fresh complete RPMI medium containing 10ng/ml GM-CSF was added per plate and cultivated for an additional 3 days. On day 7, the supernatants were discarded and the attached cells were washed with 10ml of sterile PBS. BMDMs were harvested gently using a rubber scraper. The cell suspension was then collected and centrifuged at ~150 *x* g for 10 minutes. The supernatant was then discarded and the pellet was resuspended in 10ml of complete RPMI medium containing 10ng/ml GM-CSF. The cells were counted using the haemocytometer before seeding into tissue culture plates for experiments. For 96 well plates, the BMDMs were seeded at a density of 1 x 10^5 cells per well, while BMDMs were seeded at a density of 5 x 10^5 cells

per well for 24 well-plates. 96-well plates were used for assaying intracellular survival of bacteria at different time points while other experiments were conducted in 24-well plates. BMDMs were incubated for 2 days before any further experimental procedure.

2.3 Phenotypic characterisation of BMDM cells by Flow Cytometry

BMDMs were harvested in FACS buffer [PBS with 2% FCS (Gibco Life Technologies)] using a cell scraper. The cells were pelleted by centrifugation at 450 *x g* for 5 minutes and supernatant was discarded. The pellet was then resuspended in FACS buffer and the number of cells were adjusted to 1 x 10^6 cells per 100µl. 100 µl aliquots were dispensed into microcentrifuge tubes for staining. Each aliquot was pelleted again at 450 *x g* for 5 minutes and supernatant was discarded. The pellet was resuspended in 100µl FACS buffer containing the Phycoerythrin (PE)-conjugated antibody for staining. Two antibodies were used to stain separate cell samples. The isotype control antibody (PE Rat IgG2a, κ Isotype Control from BD BioSciences, UK) and PE anti-mouse F4/80 antibody (BioLegend, UK) were both used at a final concentration of 0.5µg/ml. Unstained cells were used as a negative control. This staining step was carried out for 30 minutes at 4ºC, in the dark. Then, 500µl of ice-cold FACS buffer was added to stop the reaction. The cells were washed twice in 400µl of FACS buffer before being analysed using a FACS Calibur (BD Biosciences). The data was then analysed by FlowJo software.

2.4 Phagocytosis assay

BMDM cells were seeded on a coverslip in a 24-well plate in complete RPMI medium containing 10ng/ml GM-CSF. The medium was then removed and replaced with 350µl fresh medium containing approximately 2.5 x 10^7 fluorescein-conjugated Zymosan A (*Saccharomyces cerevisiae*) BioParticles (Molecular Probes). The Zymosan A BioParticles were not added to the control well. The cells were incubated for an hour at 37˚C to allow particle uptake. Phagocytosis was stopped by adding 550µl ice-cold PBS and BMDMs were washed with cold-PBS four times. The cells were then fixed with freshly prepared 4% (wt/vol) paraformaldehyde in PBS, and incubated for 30 minutes at room temperature. After fixing, cells were permeabilised with 0.5% (vol/vol) Triton X-100 in PBS for 15 minutes and non-specific binding sites were blocked with 0.5% (wt/vol) BSA in PBS (PBS/BSA) for 30 minutes. F-actin was stained using phalloidin conjugated to Alexa-Fluor 568 (Molecular Probes) at a concentration of 5U/ml diluted in PBS/BSA and incubated for 15 minutes in the dark at room temperature. Nuclei were counter-stained with DAPI (Molecular Probes) at a concentration of

0.17µg/ml. Coverslips were then mounted with ProLong Gold Antifade reagent (Life Technologies). Images were captured using a Zeiss LSM70 confocal laser scanning microscope and analysed with Image J software.

2.5 Bacterial strains

Burkholderia pseudomallei strain 10276 was isolated from a human melioidosis patient from Bangladesh (Maegraith & Leithead, 1964) and obtained from Ty Pitt, Health Protection Agency, Colindale, United Kingdom. A null mutant of this strain with a targeted deletion of *bpss1492* (Δ*bimA*) was generated by Charles Vander Broek in our laboratory (Jitprasutwit *et al*, 2016). Plasmid pME6032-*bimA* containing the intact *bimA* gene from *B. pseudomallei* strain 10276 has been described previously (Stevens *et al*, 2005a; Stevens *et al*, 2005b). The plasmid pME3062-*bimA* was transformed into the Δ*bimA* mutant strain and fully restored actin-based motility to 10276 Δ*bimA*. Strain 10276 *bsaZ*::pDM4 lacks a functional Bsa Type III secretion system and has been described previously (Stevens *et al*, 2003; Stevens *et al*, 2002). Wild-type and Δ*bimA* mutant bacterial strains were amplified in Luria-Bertani broth (LB) without antibiotics, while *bsaZ:*:pDM4 mutant required 15µg/ml chloramphenicol. The Δ*bimA* strain complemented with pME6032-*bimA* plasmid required 15µg/ml tetracycline. All cultures were incubated at 37^{o}C with shaking for 12 to 20 hours.

2.6 Cell infection studies

Bacterial strains were cultured to stationary phase in Luria-Bertani broth at 37 ^{o}C , with shaking at 200 rpm overnight, and adjusted to the same OD_{600} of 0.5 (for strain details and antibiotic selection refer to part 2.5 Bacterial Strains). To make the infection media, the bacterial suspension was diluted 1:500 in DMEM (Sigma-Aldrich) containing 10% (vol/vol) heat-inactivated FCS (Gibco Life Technologies) without antibiotics to give approximately 1 x 10^6 bacteria per ml. The BMDM cells were then inoculated with the infection media at an MOI of 2 (bacteria per cell) and the bacteria were pelleted onto the surface of the cells at 60 *x g*. The actual number of bacteria added was enumerated by retrospective plating of serial dilutions of each culture on LA plates. After 30 minutes of infection, cells were washed with PBS and overlaid with medium containing an inhibitory level of 250 µg/ml kanamycin to suppress the growth of residual extracellular bacteria (Stevens *et al*, 2005a). For the Δ*bimA* mutant strain complemented with the plasmid pME-*bimA*, 0.25mM isopropyl-βisopropyl-β-D-thiogalactoside (IPTG) was always included in the medium to induce the expression of the

bimA gene. In a small number of experiments, rapamycin (or solvent DMSO) was used at 4μM to induce autophagy.

At the indicated time point of infection, infected BMDMs were rinsed with PBS twice and lysed with 0.1% Triton X-100 in PBS for about 5 minutes at room temperature. Lysates were then diluted serially 10-fold with PBS and aliquots plated onto LA (Luria-Agar) plates which were incubated at 37 ^{o}C for 48 hours. The number of viable intracellular bacteria were counted and expressed as colony forming units (CFU) per well of a 96-well plate.

2.7 Kanamycin and chloroquine protection assay

BMDMs were seeded at 1 x 10^5 per well in a 96-well plate. Briefly, BMDM cells were infected at an MOI of 2 with bacterial strains. After 30 minutes of infection at 37°C in a 5% CO_2 atmosphere, the cells were washed and overlaid with medium containing 250 μg/ml kanamycin. The infection then proceeded for another 3 hours at 37°C in a 5% CO_2 atmosphere, before adding chloroquine at a concentration of 50 μg/ml. The cells were incubated for an additional 1.5 hours to allow killing of any bacteria that were trapped inside vacuoles by the action of the chloroquine. The cells were washed twice with PBS and lysed in 0.1% Triton X-100 in PBS. The lysates were serially diluted 10-fold with PBS and aliquots plated on LA agar plates to count the CFU after 48 hours incubation at 37°C.

2.8 Cell cytotoxicity assay

Cell cytotoxicity was determined using lactate dehydrogenase (LDH) assays purchased from Promega known as CytoTox 96 Non-Radioactive Cytotoxicity Assay, according to the manufacturer's instructions. Briefly, a 50μl aliquot of culture supernatant was transferred into a well of a 96-well plate. 50μl of CytoTox 96 Reagent was then added to each well and incubated for 30 minutes at room temperature. Control wells lacking any cells served as the negative control to determine culture medium background, whilst a Maximum LDH release Control was achieved by adding 1X Lysis solution to a confluent monolayer of cells 45 minutes before adding the CytoTox 96® Reagent. Lastly, 50μl of Stop solution was added and the absorbance was measured at 490nm. The percentage of cytotoxicity was calculated as follows: 100 X (A_{490} experimental-A_{490} background)/(A_{490} maximum-A_{490} background). The assay was performed on samples obtained from three independent experiments, each containing three technical replicates and the data reported as the mean ± SEM.

2.9 Immunostaining and confocal microscopy

BMDMs were seeded at 5 x 10^5 per well in a 24-well plate on coverslips. Briefly, BMDM cells were infected at an MOI of 2 with bacterial strains. At the indicated time point of infection, the medium was removed and the cells were washed with PBS twice before fixing with 4% paraformaldehyde, or methanol, for 30 minutes at room temperature or overnight at 4 ºC. After fixing, cells were permeabilised with 0.5% (vol/vol) Triton X-100 in PBS for 15 minutes and non-specific binding sites were blocked with 0.5% (wt/vol) bovine serum albumin (BSA) in PBS (PBS/BSA) for 30 minutes at room temperature. The primary antibody at the dilution indicated in Table 2.1 was added onto the coverslip in PBS/BSA for one hour at 37°C. The coverslips were then washed with PBS before adding the relevant secondary anti-species antibody conjugated with either Alexa Fluor 568 or 488 (Molecular Probes) at 10µg/ml in PBS/BSA for another hour at 37°C in the dark. On certain occasions, F-actin was stained with phalloidin diluted in PBS/BSA at room temperature for 15 minutes (Table 2.2) after washing the coverslips with PBS. Where necessary to counter-stain nuclei, the coverslips were then washed again in PBS and dipped in distilled water containing DAPI (4', 6-Diamidino-2-Phenylindole, Dihydrochloride) (Sigma-Aldrich) at a concentration of 500nM. Finally, the coverslips were rinsed with distilled water and mounted with ProLong Gold Antifade reagent (Life Technologies). The slides were stored in the dark at 4 ºC. Images were captured using a Zeiss LSM70 confocal laser scanning microscope and analysed with Image J software.

Table 2.1 Primary antibodies used in immunofluorescence

Detected antigen	Antibody	Species reactivity	Dilution/ concentration used	Supplier	Product code
B. pseudomallei LPS	Mouse monoclonal	*B. pseudomallei*	2µg/ml	Camlab, Cambridge, UK	
B. pseudomallei LPS	Rabbit polyclonal	*B. pseudomallei*	1:200	Ty Pitt, Health Protection Agency, London	
LC3B	Rabbit monoclonal	Mouse, Human, Rat	1:400	Cell Signalling Technology	2775S
p62/SQSTM1	Rabbit polyclonal	Mouse, Hamster, Human, Rat	1:100	MBL Medical and Biological Laboratories	PM045
Mono- and polyubiquitinylated proteins	Mouse monoclonal	Species independent	1:200	Enzo Life Sciences LTD	BMWL-PW8810-0100
TOCA-1	Rabbit polyclonal	Human, Mouse, Rat	20µg/ml	ProSci Inc	4373

Table 2.2 Phalloidin conjugates for staining actin

Actin-selective probe	Species reactivity	Dilution/ Concentration used	Supplier	Product code
Alexa Fluor 488 Phalloidin	All (species independent)	5U/ml	Molecular Probes	A12379
Alexa Fluor 568 Phalloidin	All (species independent)	5U/ml	Molecular Probes	B3475
CruzFluor 405 Phalloidin	All (species independent)	1:1000	Santa Cruz Biotechnology	Sc-363790

2.10 Protein gels and western blots

For preparation of BMDM cell lysates, the medium in each well was removed at the indicated time point, and cells washed with PBS twice. 50µl of BugBuster MasterMix (Novagen) was added directly to the cells (for cells plated in a 24-well plate). 10µl of 6x Laemmli buffer (300mM Tris pH8.8, 12% SDS, 0.6% Bromophenol blue and 20% glycerol) was added to each of the lysates, heated at 90 ºC for 10 minutes. This step of heating the samples was required to inactivate the bacteria and allow the samples to be removed from the Containment Level 3 laboratory for further procedures.

The lysates were first resolved by SDS-PAGE gel (Sodium dodecyl sulphate (SDS) polyacrylamide gel electrophoresis (PAGE)). Samples were separated either on ready-made any kDa Mini-Protean TGX Precast Gels (BioRad) or on self-prepared 15% polyacrylamide gels. The gels were electrophoresed in 1X Tris-Glycine-SDS PAGE (FlowGen BioScience) running buffer for 50 minutes at 160V or until the loading dye front reached the bottom of the gel.

The proteins were transferred from the gel matrix onto a nitrocellulose membrane (BioRad) using a Trans-Blot Turbo Transfer System for 30 minutes at 25V. Both filter papers and membrane were pre-wetted and equilibrated in 1X transfer buffer containing 20% v/v EtOH (BioRad) for about 5 minutes. After the protein transfer was completed, the blot was then blocked in PBS containing 5% (wt/vol) Blotto milk protein for 30 minutes at room temperature on a rocking platform. The blot was washed three times (15 minutes each) with PBS-T (PBS containing 0.1% (vol/vol) Tween 20) before being incubated with primary antibody diluted in PBS-T (Table 2.3) at 4 ºC overnight on a rocking platform. This was

followed by washing three times with PBS-T (first 15 minutes and then 2 x 5 minutes) and then incubated with secondary IRDye (Cell Signalling Technology) anti-mouse, anti-rabbit or anti-goat IgG antibody (1:10,000) diluted in PBS-T for 45 minutes, at room temperature on a rocking platform. After washing a further 4 times (5 minutes each), the bound antibodies were detected using a LI-COR Odyssey Infrared Imaging System (LI-COR BioSciences), according to the manufacturer's instructions. The images were processed using Image Studio Lite 4.0 software (LI-COR BioSciences).

Table 2.3 List of primary antibodies for Western Blot

Detected antigen	Antibody	Species reactivity	Dilution/ concentration used	Supplier	Product Code
LC3B	Rabbit monoclonal	Mouse, Human, Rat	1:1000	Cell Signalling Technology®	2775S
GAPDH	Mouse monoclonal	Yeast, Rabbit, Rat, Pig, Human ,Mouse	0.5µg/ml	Thermo Scientific	MA5-15738
Caspase-1	Rabbit polyclonal	Mouse, Pig, Rat, Worm	0.2µg/ml	Santa Cruz Biotechnology	sc-514
Caspase-11/ caspase-4	Rabbit polyclonal	Mouse, Rat	1.0µg/ml	Bioss Inc	bs-6858R

2.11 ELISA (Enzyme-linked immunosorbent assays)

To detect qualitatively the amount of secreted cytokines TNF-α, IL-1α and IL-1β in cell supernatants, commercially available ELISA Ready-SET-Go! sets from eBioscience (UK) were used, essentially as described in the manufacturer's protocol. Cell culture supernatants from the infected cells were filtered through a 0.22µM Millipore filter prior to analysis. This is an important step to ensure the supernatants were free from bacterial contamination before removing from the Containment Level 3 Laboratory for processing.

Briefly, high-binding 96-well ELISA plates (Corning Costar) were coated with 100µL per well of the capture antibody (IL-1α, TNFα, IL-1β) in Coating Buffer, overnight at 4°C. The wells were washed three times with 200µl/well Wash Buffer (1X PBS, 0.05% Tween-20) with an interval of 1 minute soaking in between the washes. Next, 200µl of blocking solution (1X Assay Diluent as provided in the kit) was added per well and incubated at room temperature for 1 hour. The cytokine standards were serially diluted 2-fold in 1X Assay Diluent to make the standard curve ranging from 4-500 pg/ml. 100µl of each dilution or supernatant was added to the coated plate and incubated overnight at 4°C. The plate was washed 5 times with Wash

Buffer before adding 100µl of detection antibody (as provided in the kit) into each well. After incubation at room temperature for 1 hour, the plate was washed 5 times with Wash Buffer. Next, 100µl of 1X avidin-horseradish peroxidase HRP in Assay diluent was added to each well and incubated for 30 minutes at room temperature. This was followed by washing with Wash Buffer 7 times to remove any unbound enzyme, before adding 100µl/well of Substrate Solution (TMB solution) for the next 15 minutes at room temperature. Lastly, the reaction was stopped by adding 50µl of stop solution (2N H_2SO_4). The cytokine levels were assessed by taking OD_{450} measurements using a microplate spectrophotometer, and quantified based on the standard curve drawn from the standards described above. The assay was performed on samples obtained from three independent experiments, each containing three technical replicates and the data reported as the mean $\pm$ SEM (standard error of mean).

2.12 Proteome Profiler Mouse Cytokine Array

2.12.1 Sample preparation and protein concentration measurement

BMDMs were infected with *B. pseudomallei* WT or Δ*bimA* strain as described in section 2.6 for 8 hpi and 16 hpi. For the positive control, BMDMs were stimulated with 500ng/ml *E. coli* LPS for 8 hours. Uninfected BMDMs at respective time points served as a baseline for measuring cytokine and chemokine concentration fold-change. Cell lysates were obtained by lysing the cells using 500µl of 1% Triton X-100 in PBS per well of a 24-well plate for 5 minutes. The lysates were then filtered through a 0.22µm membrane filter (Millipore). Some of the filtrate were plated onto an LA plate for sterility testing to ensure no intact bacteria were present in the samples. This step was required before bringing the sample out of the containment level 3 laboratory.

Total protein concentration of lysates were then determined using a Pierce BCA (bicinchoninic acid) Protein Assay Kit (Thermo Fisher Scientific) according to the manufacturer's instructions. Briefly, BCA working reagent was prepared by mixing 50 parts of BCA reagent A with 1 part of BCA reagent B. Proteins standards were prepared from Bovine Serum Albumin (BSA) (Sigma) at different concentrations 25, 125, 250, 500, 750, 1000, 1500 and 2000µg/ml. 25µl of each standard or sample was added into each microplate well in duplicate. 200µl of working reagent was then added into each well and mixed on a plate shaker for 30 seconds, followed by incubation at 37°C for 30 minutes. Finally, the absorbance was measured at 562nm. The protein concentrations were determined based on the BSA standard curve.

2.12.2 Proteome Profile Mouse Cytokine Array

Cytokine and chemokine profiling in BMDM cell lysates was performed using a Proteome Profiler Mouse Cytokine Array Kit, Panel A (R&D Systems) according to the manufacturer's instructions. Firstly, the array membranes were placed carefully in a separate well of a Multi-Dish containing 2.0ml of Array Buffer 6 to block any non-specific binding. The membranes were placed with the number on the membranes facing upwards. The membranes were incubated for an hour on a rocking platform, at room temperature. While the membranes were blocking, samples were prepared by mixing 1ml of each sample containing 100µg of protein lysate with 0.5ml of Array Buffer 4. Next, 15µl of reconstituted Detection Antibody cocktail was added to each prepared sample, mixed and incubated at room temperature for an hour. When the incubation period elapsed, Array Buffer 6 was aspirated from the wells and the sample:antibody mixtures were then added into each well. The membranes were incubated overnight at 4°C on a rocking platform. The next day, each membrane was washed three times with 20ml of 1x Wash Buffer on a rocking platform for 10 minutes each. After washing, each membrane was carefully removed from its wash container and the lower edge blotted onto absorbent paper to drain excess buffer from the membrane. Afterwards, each membrane was placed back into the well containing 2ml of IRDye 800CW Streptavidin (LI-COR Biosciences) that was diluted 1:2000 in Array Buffer 6. The membranes were then incubated for 30 minutes at room temperature on a rocking platform. After incubation, each membrane was washed as described previously. Finally, each membrane was blotted onto absorbent paper to drain excess buffer before scanning using a LI-COR Odyssey Infrared Imaging System (LI-COR BioSciences). The images were processed using Image Studio Lite 4.0 software (LI-COR BioSciences).

2.13 Griess assay

Nitric oxide (NO) is synthesised by iNOS (inducible nitric oxide synthase), and is an important antimicrobial mediator and physiological messenger in many biological systems. NO_2^- (nitrite) is one of the primary, stable breakdown products of NO, hence measuring the nitrite concentration by Griess assay gives an indication of NO production in the sample. For this assay 100µl of cell supernatant was aliquoted into each well of a clear, flat-bottomed 96-well plate, followed by 50µl of Griess assay R1 and R2 reagent (Cayman Chemical). The reaction was incubated for 10 minutes at room temperature before values were obtained at OD_{540} using a microplate spectrophotometer. A nitrite standard curve was produced by serially diluting 2-fold sodium nitrite, ranging from 100µM to 1.56µM. The nitrite concentration in

each sample was then quantified in comparison to the reference curve of sodium nitrite standards. The assay was performed on samples obtained from three independent experiments, each containing three technical replicates and the data reported as the mean ± SEM.

2.14 Methods for evaluation of siRNA-mediated gene silencing

2.14.1 siRNA transfection

For MyD88 gene silencing in BALB/C BMDMs, Pre-designed Silencer siRNA duplexes specific for mouse MyD88 (RefSeq Accession No. NM_010851.2) were obtained from Ambion (Thermo Fisher Scientific) (5'-GGAUAUACUGAAGGAGCUG-3'). MISSION Universal Negative siRNA control (Sigma-Aldrich), which does not share homology with any known mammalian gene, was included at the same concentration in each experiment as a non-target siRNA control.

MyD88 siRNA transfection into BALB/C BMDMs was performed using Lipofectamine RNAiMAX reagent (InvitrogenTM, Life Technologies), following the manufacturer's recommendations. Briefly, 6µl RNAiMAX was mixed with 6µl of 20µM siRNA in 200µl of Opti-MEM I reduced serum medium (Invitrogen), and incubated at room temperature for 20 minutes. Meanwhile, the medium was removed from each well containing BMDMs and replaced with fresh RPMI medium (supplemented with 20% FCS, 50µM β-mercaptoethanol and 5mM L-glutamine). BMDMs were seeded at 1 x 10^5 cells per well of a 96-well plate for assessing intracellular bacterial survival. Cells were seeded in wells of a 12-well plate at a density of 7.5 x 10^5 cells per well to harvest RNA for subsequent gene analysis. The RNAiMAX-siRNA mixture was added dropwise to give a final concentration of 75nM siRNA per well, and incubated at 37°C. After 24 hours, the medium was replaced with fresh supplemented RPMI medium, and incubated for another 24 hours at 37°C in a 5% CO2 atmosphere, before infection as described in section 2.6, or RNA isolation as described in 2.14.2.

2.14.2 Total RNA isolation and reverse-transcriptase PCR (RT-PCR)

Total cellular RNA was isolated from 1 x 10^6 cells using a ReliaPrep RNA Cell Miniprep kit (Promega), according to the manufacturer's recommendations. Briefly, 200µl of lysis buffer (BL) containing 0.1% 1-thioglycerol (TG) was added to each well. The sample was pipetted repeatedly to lyse the cells and transferred to a new tube. The lysate was centrifuged at 300 *x g* for 5 minutes. Addition of TG to the BL helps to inactivate the ribonucleases present in cell

lysate. The cell lysate was then washed with ice-cold PBS and centrifuged again at 300 *x* g for 5 minutes. Next, 250µl of BL + TG was added to the washed cell lysate, mixed with 85µl of isopropanol and vortexed for 5 seconds. The lysate was then transferred to a ReliaPrep Minicolumn and centrifuged at 13, 000 *x* g for 30 seconds. Nucleic acids in the lysates adsorb rapidly to the column in this step. The column was then washed with 500µl of RNA Wash solution containing 60% ethanol, centrifuged again at 13,000 *x* g for 30 seconds. The contaminating genomic DNA was then removed by adding 30µl of freshly prepared DNase I incubation mix (80% Yellow Core Buffer, 9mM $MnCl_2$ and 10% DNase I enzyme) directly to the membrane of the column and incubated for 15 minutes before washing with 200µl of Column Wash solution. The column was then washed twice with RNA Wash solution to further purify the bound RNA from contaminating salts, proteins and cellular components. Finally, 30µl of nuclease-free water was added to the membrane and centrifuged at 13,000 *x* g for 60 seconds to elute the total RNA. The total RNA was stored at -20°C until used in downstream experiments.

RNA samples were subjected to one-step RT-PCR using 10ng of RNA using the Access RT-PCR System (Promega), according to the manufacturer's recommendations. This kit uses a two-enzyme system in which the first enzyme AMV Reverse Transcriptase (AMV RT) from Avian Myeloblastosis Virus synthesises first-strand complementary DNA (cDNA) from the RNA. This is followed by second-strand cDNA synthesis and DNA amplification by the second enzyme *Tfl* DNA polymerase from *Thermus flavus*. Briefly, the reaction mixture contained 10ng of sample RNA, 1X AMV/*Tfl* Reaction Buffer, 0.2mM dNTP mix, 1µM forward primer, 1µM reverse primer, 1mM MgSO4, 0.1u AMV Reverse Transcriptase and 0.1U of Tfl DNA polymerase. The RT-PCR reaction consisted of incubation at 45°C for 45 minutes and 94°C for 2 minutes for the first cDNA synthesis step, followed by 40 cycles of 94°C for 30 seconds, 60°C for 1 minute and 68°C for 2 minutes for second strand synthesis and PCR amplification. Finally, a final extension step was carried out at 68°C for 7 minutes. 30µl of the amplified reaction was electrophoresed on a 2.5% TAE agarose gel (UltraPure Agarose from Thermo Fisher Scientific) and DNA was visualised by adding 1X Invitrogen SYBR Safe DNA Gel Stain directly to the gel. Primer sequences for MyD88 and β-actin are shown in the Table 2.4.

Table 2.4 Primers for RT-PCR

Target	Primer sequence
MyD88	Forward:5' CCCACTCGCAGTTTGTTGGATGCCTGG 3' Reverse: 5' GGTGGTGATGCCTCCCAGTTCCTTTGT 3'
β-actin	Forward: 5' GGATGACGATATCGCTGCGCTGGT 3' Reverse: 5' TCTTTTCACGGTTGGCCTTAGGGTTC 3'

2.15 TLR-blocking peptide treatment

TRIF-blocking peptide (Pepinh-TRIF) and the negative control peptide (Pepinh-Control) (InvivoGen) were prepared as 1mM stock solutions by dissolving peptides in endotoxin-free water and used at final concentrations of 20μM. The MyD88-dependent pathway was blocked with the MyD88 Homodimerisation Inhibitor Peptide NBP2-29328, which was purchased from Novus Biologicals. Stock solutions of NBP2-29328 and the negative control inhibitor were prepared to 5mM by dissolving in PBS and were used at final concentrations of 100μM. BMDM cells were pre-treated with TRIF- or MyD88- blocking peptides (or the corresponding negative control inhibitors), for 4 hours or 24hours respectively, at 37°C before stimulation with exogenous ligand or carrying out the bacterial infection experiment. To determine the effectiveness of the TRIF -blocking peptide, BMDMs were stimulated with 25μg/ml of polyI:C (polyinosinic-polyctidylic acid) (InvivoGen) for 6 hours before isolating the cellular RNA (refer to section 2.16) and carrying out quantitative RT-PCR (qPCR) for expression of the Interferon-β (IFN-β) gene. While to determine the effectiveness of the MyD88-blocking peptide, 4μg/ml of Pam3CSK4 (Bio-Techne) were used to stimulate BMDMs for 24 hours, followed by RNA isolation (refer to section 2.16) and qPCR for expression of the Interleukin-1β (IL-1β) and Interleukin-6 (IL-6) genes.

2.16 Total RNA extraction using the RNeasy Plus Micro Kit (Qiagen)

Prior to experiments involving TLR-blocking peptides and microarray, total RNA was extracted using the RNeasy Plus Micro Kit (Qiagen) according to the manufacturer's instructions. Approximately 5 x 10^5 cells were lysed using 350μl of RLT lysis buffer containing β-mercaptoethanol, followed by homogenisation using a QIAshredder (Qiagen) spin column. The lysates were recovered by centrifuging the spin columns for 2 minutes. All centrifugation steps were performed at 13, 000 *x* g at room temperature. The flow-through lysates were then transferred to gDNA Eliminator spin columns to eliminate gDNA contamination, and lysates recovered by centrifugation at 30 seconds. Next, 350μl of 70% ethanol was added to the flow-through, mixed and transferred to the RNeasy spin column which was centrifuged for 15

seconds. Addition of ethanol at this step provides the appropriate conditions for RNA to bind to the column. The column was then washed with 700µl of buffer RW1 and centrifuged for 15 seconds. The column was then rinsed with 500µl of buffer RPE and centrifuged for 15 seconds. The final wash involved the addition of 500µl of 80% ethanol, which was removed by centrifugation for 2 minutes. The column membrane was then dried by centrifugation for 5 minutes. Lastly, the RNA was eluted by adding 14µl of RNase-free water directly to the centre of the spin column membrane followed by centrifugation for 1 minute. The RNA concentration was quantified using a Nanodrop ND-100 (NanoDrop Technologies).

2.17 Reverse Transcription of RNA into cDNA

Total RNA was reverse transcribed using random oligo $(dT)_{15}$ primer (Promega) with Promega GoScript Reverse Transcriptase (Promega GoScript Reverse Transcription System). Firstly, 100ng of RNA was combined with 0.5µg of Oligo $(dT)_{15}$ primer and the primer/template mix was thermally denatured at 70°C for 5 minutes and immediately chilled on ice. The template-primer mixture was then added to the reaction mix containing 2.5mM $MgCl_2$, 1X RT buffer, 1mM dNTP and reverse transcriptase (RT) enzyme on ice. For the negative control reactions, RNAse free water was added instead of the RT-enzyme. The reactions were then incubated first at 25°C for 5 minutes for annealing, followed by extension at 42°C for 50 minutes and enzyme inactivation at 70°C for 15 minutes. The cDNA products were then stored at -80°C.

To determine if the RNA samples contained genomic DNA contaminants, PCR was carried out by amplifying β-actin in both the samples with and without the RT-enzyme. The forward and reverse primer sequence for β-actin were 5'-GGATGACGATATCGCTGCGCTGGT-3' and 5'-TCTTTTCACGGTTGGCCTTAGGGTTC-3' respectively. β-actin primers were designed spanning an exon-exon boundary, thus avoiding the detection of the target gene from residual genomic DNA in the initial RNA sample. 0.4U of Phusion high-fidelity polymerase (Thermo Scientific) was used for gene amplification with 1x Phusion buffer, 0.3µl DMSO, 0.2mM dNTPs, 1µM of primers and 2.5ng diluted cDNA product. The reaction conditions used were 98°C for 2 minutes, followed by 25 three step cycles (98°C for 10 seconds, 68°C for 20 seconds, and 72°C for 30 seconds) and a final extension of 72°C for 10 minutes. PCR products were visualised using agarose gel electrophoresis. Gel electrophoresis was performed using 2.5% TAE agarose gels (UltraPure Agarose from Thermo Fisher Scientific) and DNA was

visualised by adding 1X Invitrogen SYBR Safe DNA Gel Stain. The electrophoresis was performed at 80-90V for 45-60 minutes. Amplification of β-actin from cDNA gives a band product at approximately 350bp while amplification from genomic DNA gives a band about 420bp which indicates gDNA contamination in the RNA samples.

2.18 Design of the real-time PCR (qPCR) primers

The primers were carefully designed and analysed using Beacon Designer software (PREMIER Biosoft International) to identify if the primer set (forward and reverse primer of the target) could form any secondary DNA structure, namely a primer dimer (self-dimer, or cross-dimer) or hairpin structure. The software predicts the Gibbs free enthalpy (represented as ΔG) required to fully break a secondary DNA structure. Hence, the more negative value it is, the more energy required to separate the DNA structure. All the primer sets were designed with an energy value below -4.0 kcal/mol, which ensures that primers do not form stable dimers or hairpin structures. The primers were designed to span exon-exon boundaries (table 2.5), thus avoiding the detection of target genes from residual genomic DNA in the initial RNA sample. The primers were also checked with the NCBI BLAST database to ensure that they did not anneal to any non-specific DNA targets. Nine different concentrations of reverse and forward primers were tested (two-by-two combinations of 100, 200 or 300nM) to obtain the optimum concentration for each pair that gave the lowest threshold cycle (Ct) but maximum amplification (with minimum non-specific amplification). All the primers were ordered from Sigma-Aldrich. Below are the criteria that were taken into account when designing the primers:

1) GC content: 40-60%
2) Tm value: 60°C - 75°C
3) Product size: 100-250 base pairs
4) Primer length: 24-28 base pairs
5) Self-dimer, cross-dimer and hairpin energy value: ≤-4.0kcal/mol

Table 2.5 Primers for qPCR

Target	Primer sequences
FNBP1L / TOCA-1	Forward: 5' CAAACAGCAGTTGAACCTTCGTACG 3' Reverse: 5' CGTACGAAGGTTCAACTGCTGTTTG 3'
IL-12β	Forward: 5' CATAGGCTCTGGAAAGACCCTGACCATC3' Reverse: 5' AGTAATTTGGTGCTTCACACTTCA 3'
IL-1β	Forward: 5' TTTGACCTGGGCTGTCCTGATGAGAGC 3' Reverse: 5' ATTCTGTCCATTGAGGTGGAGAGCTTT 3'
IL-6	Forward: 5' TTCCATCCAGTTGCCTTCTTGGGACTA 3' Reverse: 5' ATCCAGTTTGGTAGCATCCATCATTTC 3'
TNF	Forward: 5' AGCACAGAAAGCATGATCCGCGACGTG 3' Reverse: 5' TGTGAGGGTCTGGGCCATAGAACTGAT 3'
NOS2	Forward: 5' AGAATCCCTGGACAAGCTGCATGT 3' Reverse: 5' AAGGAGCCATAATACTGGTTGATG 3'
IL-1α	Forward: 5' TGATGCAAGCTATGGCTCACTTCATGAG 3' Reverse: 5' GGTCATTTAACCAAGTGGTGCTGAGAT 3'
CD40	Forward: 5' CAAGGGCTTCGGGTTAAGAAGGAGGG 3' Reverse: 5' TTGTCCAGGGATAACACTTTTCGAAAA 3'
ISG15	Forward: 5' TAGTGGTACAGAACTGCAGCGAGCCTC 3' Reverse: 5' CTCAGGCGCAAATGCTTGATCACTGTG 3'
IFIH1/MDA-5	Forward: 5' CCAGAAGTTGTCAAATCTTACGATGTTATT 3' Reverse: 5' CTTGAGGTCATTGTTTCTCAGCTTCTG 3'
FAS	Forward: 5' CTTGAGCCGTGCACAGCAACCAGCAA 3' Reverse: 5' ACTGGAGGTTCTAGATTCAGGGTCATCC 3'
IFN-β	Forward: 5' GGAATGAGACTATTGTTGTACGTCTCCTGG 3' Reverse: 5' GTCTTCGAATGATGAGAAAGTTCCTGA 3'

Primer sets for the amplification of six different reference genes were purchased from PrimerDesign Ltd (Mouse geNormPLUS 6 gene kit) for use in qPCR. The reference genes provided in this kit were:

1. *Mus musculus* adaptor-related protein complex 3, delta 1 subunit (Ap3d1), mRNA
2. *Mus musculus* casein kinase 2, alpha prime polypeptide (Csnk2a2), mRNA
3. *Mus musculus* PAK1 interacting protein 1 (Pak1ip1), mRNA
4. *Mus musculus* 18S rRNA gene
5. *Mus musculus* actin, beta, cytoplasmic (ACTB), mRNA
6. *Mus musculus* glyceraldehyde-3-phosphate dehydrogenase (GAPDH), mRNA

2.19 Quantitative Real-Time PCR (qPCR)

Approximately 120ng of cDNA for each sample was mixed with Agilent Brilliant III Ultra-fast SYBR Green qPCR Master Mix (Agilent Technologies) containing SYBR Green I fluorescent dye, Taq DNA polymerase, Mg^{2+} and dNTPs, together with the optimal concentration of forward and reverse primers. An inert ROX reference dye (30nM) was

included to normalise the fluorescent signal between reactions. This normalisation was performed automatically by the MxPro software (Agilent Technologies), and was represented as dRn in the amplification plot. The thermal cycling was performed using the following temperature profile: Cycle 1 for 3 minutes at 95°C and 50 cycles of 10 seconds at 95°C followed by 22 seconds at 60°C. A dissociation curve was included in every PCR run; 95°C 1min, 60°C 30sec and 95°C 15 sec. A 'no template' control was also included as a negative control. The real-time PCR reactions were performed using a Stratagene Mx3000P qPCR System (Agilent Technologies).

2.20 Standard PCR to generate PCR products for standard curves

Standard PCR was used to generate PCR products for standard curves in qPCR reactions. PCR reactions contained 0.4U of Phusion high-fidelity polymerase (Thermo Scientific), 1X Phusion buffer, 0.3µl DMSO, 0.2mM dNTPs, 1µM of primers and 3ng diluted cDNA product. The reaction conditions used were 98ºC for 2 minutes, followed by 35 cycles of three steps reaction (98ºC for 10 seconds, 68ºC for 20 seconds, and 72°C for 30 seconds) and final extension of 72ºC for 10 minutes. The PCR products were diluted to give a range of 10^{-1} to 10^{-6} ng of PCR product for standard curve, quantified using a Nanodrop ND-100 (NanoDrop Technologies).

2.21 qPCR analysis software

qPCR data were analysed using MxPro QPCR software (Agilent Technologies). The validation of reference genes were assessed using the geNorm algorithm implemented in qBase+ software (BioGazelle).

2.22 Affymetrix microarray technology

2.22.1 Generation of RNA samples, labelling, hybridisation and scanning

BMDM cells in wells of a 24-well plate were infected at an MOI of 2 for 8 and 12 hours post infection. Total RNA was carefully extracted from uninfected BMDM cells, BMDM cells infected with WT 10276 strain and BMDM cells infected with the Δ*bimA* mutant strain using an RNeasy Plus Micro Kit as described above. Three biological replicates were performed for each sample at each time point, giving a total of 18 samples. The RNA integrity was verified using an Agilent 2100 Bioanalyser (Agilent Technologies) and the concentration was quantified using a Nanodrop ND-100 (NanoDrop Technologies). All the samples used for microarray passed the QC with an RIN >7, and ratios of OD 260/230 and OD 260/280 >1.7.

Samples were sent to Source BioScience GeneService (Nottingham, UK) for the downstream processes of biotin-labelling, hybridisation and scanning. Biotin-labelled cDNA was prepared from each sample using the GeneChip Whole Transcript Sense Target Labelling Assay (Affymetrix) and hybridised to Affymetrix GeneChip Mouse Gene 2.0 ST Arrays according to the manufacturer's instructions. Arrays were washed and stained using the GeneChip Hybridisation, Wash, and Stain Kit in a Fluidics Station 450 and scanned with a GeneChip Scanner 3000 according to the manufacturer's instructions. An output file known as a Cell Intensity File (*.*CEL*), containing intensity values for each probe cell on the array (probe-level data), was obtained from Source BioScience and analysed as described below.

2.22.2 General software used for Microarray analysis

The raw CEL files were imported into the Affymetrix Expression Console Software for data pre-processing and normalisation. The raw CEL files were background-adjusted, normalised and $\log_2$-transformed using the GC-RMA (robust-Multiarray average) algorithm. The intensity signal was standardised across arrays via the quantile normalisation algorithm. The quality control (QC) assessment of the arrays were performed using the same software. The normalised data were grouped on the basis of experimental conditions (uninfected or BMDM cells infected with different bacterial strains, and infection time points) using Affymetrix Transcriptome Analysis Console (TAC) Software. Pairwise comparison was then applied to find the differentially expressed transcripts of the infected BMDMs (with either WT strain or Δ*bimA* strain) versus uninfected BMDMs, at respective time points of infection. The comparison was carried out based on error-weighted one-way unpaired Analysis of Variances (ANOVA), and genes with $*p \leq 0.05$ and fold change of ≥ 1.5 were defined as significantly differentially expressed.

Venny 2.0 tool (http://bioinfogp.cnb.csic.es/tools/venny/) was then used to create Venn Diagrams to identify common subsets of genes that were differentially expressed in cells infected with both WT and Δ*bimA* bacteria. This group of overlapping genes represents the common host response of BMDMs towards *B. pseudomallei*. The software was also used to identify genes that were differentially expressed in *ΔbimA* infected cells compared to WT. Gene lists were evaluated using Ingenuity Pathway Analysis (IPA) (https://www.qiagenbioinformatics.com/products/ingenuity-pathway-analysis/). The IPA analysis categorised the list of DEGs into functions, interactions and pathways that reflect the underlying biological processes uniquely involved in the experiment.

2.23 General Statistical Analysis of Data

To determine significance, the student's t-test was used to compare samples using GraphPad Prism 5. A p value of 0.05 or less was considered to be statistically significant.

3 CHAPTER 3: ASSESSING THE ROLE OF AUTOPHAGY IN THE MACROPHAGE RESPONSE TO INTRACELLULAR *BURKHOLDERIA PSEUDOMALLEI*

3.1 INTRODUCTION

Macrophages and neutrophils are the key innate immune cells that control *B. pseudomallei in vivo* and *in vitro* (Breitbach *et al*, 2011; Barnes *et al*, 2008; Easton *et al*, 2007; Breitbach *et al*, 2006; Leakey *et al,* 1998). The essential role of macrophages has been revealed by *in vivo* studies where macrophage-depletion led to increased mortality in both BALB/C and C57BL/6 mice when challenged with *B. pseudomallei* (Barnes *et al*, 2008; Breitbach *et al*, 2006). Macrophages from melioidosis patients demonstrate reduced phagosome-lysosome fusion and the subsequent metabolic oxidative burst compared with healthy individuals, allowing bacterial proliferation in macrophages (Puthucheary & Nathan, 2006). Furthermore, an ineffective cellular innate immune response shown in diabetic mice (Hodgson *et al*, 2013; Hodgson *et al*, 2011) as well as human polymorphonuclear neutrophils (PMN) from diabetic patients (Chanchamroen *et al*, 2009) contribute to an increased susceptibility to melioidosis, and corresponds with their central role as a first line of host defence against bacterial infections.

The laboratory mouse represents a useful surrogate for the study of clinical melioidosis with respect to the disease presentation and immune response (Warawa *et al*, 2010). The establishment of a murine model demonstrating differential susceptibility towards *B. pseudomallei* infection allows us to examine the host innate mechanisms involved in control of this bacterium. Two inbred mouse strains, BALB/C and C57BL/6, have been extensively used to investigate the immunopathogenesis of *B. pseudomallei.* Several studies have shown that BALB/C mice are susceptible to infection with *B. pseudomallei*, while C57BL/6 mice are considerably more resistant (Breitbach *et al*, 2011; Barnes *et al*, 2008; Easton *et al*, 2007; Breitbach *et al*, 2006; Liu *et al*, 2002; Hoppe *et al*, 1999; Leakey *et al,* 1998). This differential susceptibility to infection classifies BALB/C and C57BL/6 mice as good models for the acute and chronic forms of human melioidosis respectively.

The higher susceptibility of BALB/C mice to infection with *B. pseudomallei* is mirrored in *in vitro* studies using bone-marrow derived macrophages (BMDMs). Breitbach *et al* (2006) showed that C57BL/6 BMDMs have lower numbers of *B. pseudomallei* compared to BMDMs differentiated from the susceptible BALB/C strain. The difference in macrophage killing

activity between C57BL/6 and BALB/C derived macrophages can be explained by the proteomic and transcriptomic analysis documented by Depke *et al* (2014). In comparison to BALB/C BMDMs, C57BL/6 BMDMs have more abundant respiratory complexes to generate more ROS (reactive oxygen species) and also more lysosomal membrane proteins and lysosomal enzymes, hence, have a more effective antimicrobial activity. In addition, components that protect cells from oxidative stress such as peroxiredoxin and mitochondrial superoxide dismutase are also more abundant in C57BL/6 BMDMs as compared to BALB/C BMDMs (Depke *et al*, 2014). This suggests that the differences observed *in vitro* using BMDMs from BALB/C and C57BL/6 mice might correlate with differences in susceptibility *in vivo* to several infections including *B. pseudomallei*.

The majority of human melioidosis cases present as acute disease (Currie *et al*, 2000). As described above, the BALB/C strain represents a mouse model for acute human melioidosis. As the broad aims for the thesis are to investigate the macrophage innate mechanisms in controlling intracellular bacterial survival, we decided to use BMDMs from BALB/C mice as an appropriate *in vitro* cell system.

As a facultative intracellular pathogen, *B. pseudomallei* has the ability to enter, survive, and replicate in both phagocytic and non-phagocytic cells (Jones *et al*, 1996), deploying a Type III secretion system (Bsa) to promote its entry into host cells (Stevens *et al*, 2003). Bsa also influences endosome lysis and escape into the cytosol (Stevens *et al*, 2002; Harley *et al*, 1998). Within the cytosol, *B. pseudomallei* replicates and subverts the host cytoskeleton machinery to nucleate actin at one pole, forming F-actin enriched tails that propel the organism within and between host cells in a BimA (*Burkholderia* intracellular motility protein A) -dependent manner (Stevens *et al*, 2005b). As with other pathogens, *B. pseudomallei* uses actin-based motility to disseminate between cells while evading immune surveillance. Following actin-based motility, and uniquely among bacteria, *B. pseudomallei* is able to induce fusion of adjacent cells forming multinucleated giant cells (MNGC) (Kespichayawattana *et al*, 2004) as observed in tissues from melioidosis patients (Wong *et al*, 1995).

The work described in this thesis aims to investigate the general response of macrophages to intracellular *B. pseudomallei*, and also to elucidate the role of BimA in aiding the bacterium to evade macrophage innate detection and elimination mechanisms. To address this second scientific question, a bacterial mutant lacking the *bimA* gene (Δ*bimA*) was included in the study as a comparison to the WT strain. In this chapter we hypothesised that autophagy plays a role

in the clearance of the Δ*bimA* mutant in infected BMDMs. The specific aims of the work described in this chapter are:

1. To generate and phenotype BALB/C BMDMs
2. To identify the time course of infection where the mutant Δ*bimA* strain shows an impaired intracellular survival compared to the WT strain
3. To demonstrate that the WT strain, but not the mutant Δ*bimA* strain, is able to form actin tails in BMDMs
4. To determine if the mutant Δ*bimA* strain has a defect in bacterial uptake or phagosomal escape in comparison to the WT strain
5. To investigate if autophagy is involved in targeting and killing the Δ*bimA* mutant in BMDMs

3.2 RESULTS

3.2.1 Phenotypic characterisation of BALB/C BMDMs

Many previous studies on the intracellular life of *B. pseudomallei* have utilised immortalised cell lines as model systems. However, it is clear that in some instances certain phenotypes described in these models are not relevant in a primary cell. An example is the finding by Rinchai *et al* (2015) that *B. pseudomallei* does not escape the phagosome of infected primary neutrophils and does not display actin-based motility. Selective pressure imposed by continual subculture of immortalised macrophage-like cells such as RAW cells usually results in the loss of genes that are not essential for cell division and replication, but are key for macrophage immune functions (Kaur & Dufour, 2012; Chamberlain *et al*, 2009). For example, Chamberlain *et al* (2009) demonstrated that in response to lipopolysaccharide (LPS), murine BMDMs produce significantly more inflammatory cytokines TNF-α, IL-6, IL-12 and MCP-1 compared to RAW264.7 cells. In addition, phenotypes of BMDMs and RAW264.7 cells often differ. For example, the immortalised RAW264.7 cell line express higher levels of CD14 than primary BMDMs (Berghaus *et al*, 2010; Chamberlain *et al*, 2009), but the macrophage marker F4/80 is significantly more highly expressed in primary BMDMs compared to RAW264.7 cells (Chamberlain *et al*, 2009). Studies on the intracellular life of *B. pseudomallei* should therefore be conducted in the most relevant cell system available. Studies by other laboratories have shown that BMDMs represent a more biologically relevant *in vitro* model for studies on the intracellular survival of *B. pseudomallei* (Breitbach *et al*, 2011; Breitbach *et al*, 2006). Hence, BALB/C bone-marrow derived macrophages (BMDMs) were used as an infection model system in the experiments described in this thesis.

This chapter begins with the description on the generation and phenotyping of BMDMs isolated from BALB/C mice. Briefly, the femur and tibia were dissected from the hind legs of BALB/C mice to obtain the bone-marrow cells. These were differentiated *in vitro* in RPMI media for 7-9 days in the presence of the growth factor GM-CSF (granulocyte macrophage-colony stimulating factor) as described in Section 2.1. The purity and the phagocytic activity of the BMDMs were then determined by FACS assay and assessment of uptake of Zymosan BioParticles respectively.

Fluorescence activated cell sorting (FACS) of live cells was utilised to phenotype the differentiated BMDMs by staining with specific antibody to detect the F4/80 antigen. F4/80 is

regarded as one of the most specific cell-surface markers for mature murine macrophages (Austyn & Gordon, 1981). To harvest the cells, BMDMs were scraped gently from the 10cm-square petri dish after rinsing with phosphate buffered saline (PBS). Of 2.5×10^7 bone marrow cells seeded per plate on day 0, approximately 20% (4.8×10^6) of the total cells matured into BMDMs and were harvested on day 7. The BMDMs were then stained separately with Phycoerythrin (PE)-conjugated F4/80 antibody and PE-conjugated isotype control as described in Section 2.3. Unstained cells were used as a negative control. Data was acquired and analysed using a FACS Calibur (BD Biosciences) and FlowJo software respectively. Histograms of isotype control, F4/80-specific stained cells as well as the unstained control, were overlaid after applying gating around the macrophage population. The percentage of F4/80-stained positive cells was determined using the software and a representative histogram is shown in Figure 3.1. From three independent experiments, the differentiated cells expressed high levels of F4/80 antigen with a percentage average of 83.5 % $\pm$ 2.2% (SEM).

The phagocytic activity of BMDMs was determined by assessing the ability of cells to engulf fluorescein-conjugated Zymosan BioParticles. Zymosan BioParticles were added to the BMDMs plated on a coverslip at a ratio of 50 beads per cell, and incubated for one hour at 37^{o}C to allow uptake. BMDMs were then fixed in 4% PFA in PBS before staining with phalloidin conjugated to Alexa-Fluor 568 (green) and DAPI. Images were captured using a Zeiss LSM70 confocal laser scanning microscope and analysed with Image J software. It is clear from the representative confocal images, that BALB/C BMDMs displayed high phagocytic activity with engulfment of numerous Zymosan BioParticles by each cell (Figure 3.2).

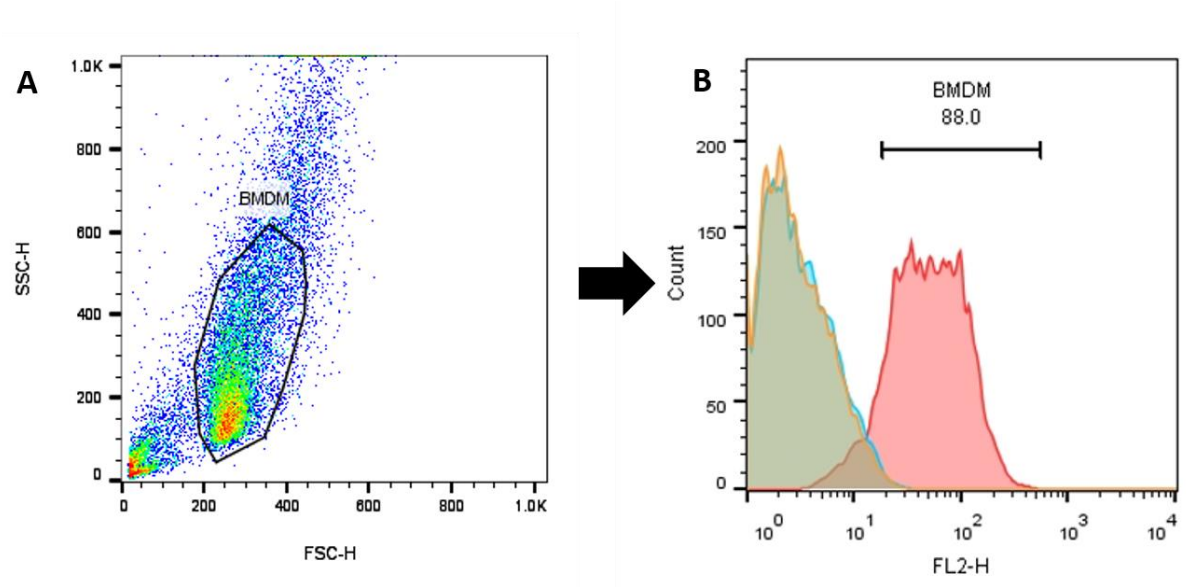

Figure 3.1 Phenotypic characterisation of BALB/C BMDMs by FACS. Cells were stained for the presence of macrophage marker F4/80 (red) and also the isotype antibody control (blue) as decribed in *Materials and Methods 2.3*. Unstained cells (orange) were also included as a negative control. (A) Population of BMDMs was first gated based on the forward (FSC; x-axis) and side scatter (SSC; y-axis) properties to remove cellular debris and dead cells, as shown in the light-scatter density plot (A). Each dot represents the individual cell that has passed through the laser. This gated population (BMDM) was then selected for the analysis of expression marker F4/80 as shown in (B). (B) Single parameter histograms display number of events (cell counts) (y-axis) versus fluorescence intensity (x-axis). Overlay of isotype control and unstained cells population together with the cells stained with F4/80 antibody identified that 88% of the gated BMDMs expressed F4/80 macrophage marker.

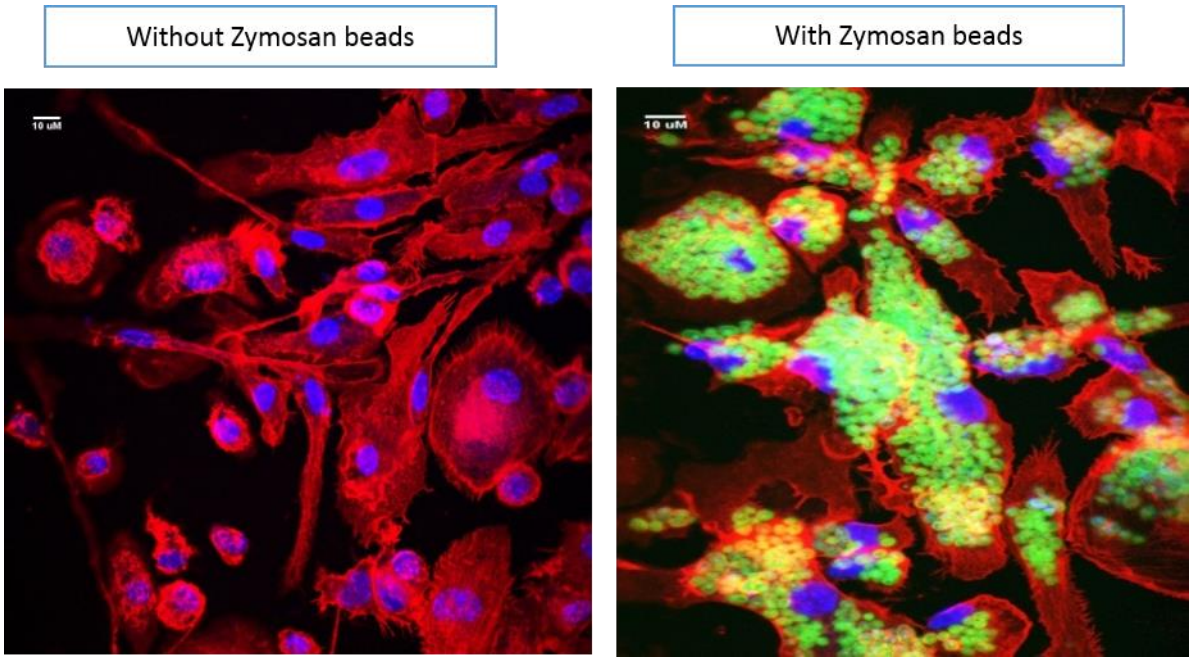

Figure 3.2 BALB/C BMDMs display high phagocytic activity. BALB/C BMDMs were grown on coverslips at a density of 5 x 10^5 cells. BMDMs were then incubated with fluorescently-labelled Zymosan BioParticles (green) (right image) at a ratio of 50 beads per cell for an hour before fixing and staining as demonstrated in *Materials and Methods 2.4*. No Zymosan BioParticles were added into the control well (left). The cell nuclei and the actin cytoskeleton were stained with DAPI (blue) and phalloidin (red) respectively. The images were captured using a Zeiss LSM70 confocal laser scanning microscope and figure shows a representative z-stack confocal image. Scale bar=10µm.

In this *in vitro* system, BMDMs were differentiated under the influence of GM-CSF as a growth factor. Another growth factor commonly used in the *in vitro* culture of BMDMs is M-CSF (macrophage-colony stimulating factor). CSFs are a heterogenous group of glycoproteins which promote the proliferation and differentiation of haematopoietic progenitor cells (Kruse *et al*, 1989). It has been reported that differentiating BMDMs under the influence of different CSFs polarise the macrophages into different sub-populations; M1 and M2 macrophages. M1 macrophages are polarised in the presence of GM-CSF while M2 macrophages are polarised in the presence of M-CSF (Martinez & Gordon, 2014; Verreck *et al*, 2004). The M1 macrophage is the 'classically-activated' anti-microbial macrophage, generated in response to interferon-gamma (IFN-γ) or lipopolysaccharide (LPS), or both, and also tumour necrosis factor (TNF-α). This population produces reactive oxygen and nitrogen species, secretes proinflammatory cytokines such as interleukin (IL)-23 and promotes type 1 immunity which is required for optimal host defence against intracellular pathogens (Martinez & Gordon, 2014; Barnett & Brundage, 2010). Conversely the M2 macrophage is the 'alternatively activated' macrophage, also known as the 'wound-healing' macrophage. This population is stimulated by IL-4, IL-13 (Th2 cytokines) and does not produce nitric oxide. This alternative activation leads to an anti-inflammatory phenotype, hallmarked by IL-10 as the signature cytokine (Verreck *et al*, 2004). M2 macrophages promote type 2 immunity responses such as dampening inflammation, tissue remodelling, wound healing but also tumour promotion (Martinez & Gordon, 2014). With this understanding, differentiating BM cells in the presence of GM-CSF is appropriate to produce M1 macrophages for the investigation of the intracellular survival of *B. pseudomallei* in phagocytes. This is consistent with the work by Ivo Steinmetz and colleagues on *B. pseudomallei* infection of BMDMs of susceptible BALB/C mice, which utilise GM-CSF as a growth factor in the differentiation process from bone marrow cells into BMDMs (Depke *et al*, 2014; Breitbach *et al*, 2011; Breitbach *et al*, 2006). Besides, based on our experiences on *in vitro* culturing BMDMs cells, differentiating BALB/C BMDMs in the presence of M-CSF was not successful, and the proportion of differentiated BMDMs cells was too small for subsequent experimentation. Difficulty in proliferating BALB/C BMDM cells in response to M-CSF has been reported by Kruse *et al* (1989) previously, who conclude that BALB/C mice can be regarded as a low responder to this growth factor.

3.2.2 Intracellular survival of *B. pseudomallei* WT, Δ*bimA* mutant and the trans-complemented Δ*bimA* mutant strain in BALB/C BMDMs

The second part of this chapter compares the intracellular survival of *B. pseudomallei* WT and Δ*bimA* mutant strains in the BALB/C BMDM infection model. Intracellular survival was assessed in a kanamycin protection assay where samples were taken over a time course (at 2, 8, 16 and 24 hours post infection: hpi) to identify the optimal time points showing a significant clearance of the Δ*bimA* mutant compared with the WT strain. BMDMs were infected at a multiplicity of infection (MOI) of 2 bacteria per cell for 30 minutes before being overlaid with medium containing an inhibitory level of kanamycin (250μg/ml) to kill any extracellular bacteria (Stevens *et al*, 2003; Stevens *et al*, 2002). At the indicated time point post-infection, the infected cell monolayers were subsequently lysed with 0.1% Triton X-100 in PBS, serially diluted and plated on Luria-Bertani (LB) agar. Bacterial colony forming unit (CFU) were recorded after 2 days incubation at 37ºC. This assay also included a trans-complemented Δ*bimA* mutant strain harbouring the inducible plasmid pME6032 containing the full length *bimA* gene from strain 10276 (simplified as Δ*bimA*+pME-*bimA*). This was used to investigate if the *bimA* gene provided *in trans* could restore the intracellular survival and complement the actin-based motility defect of the Δ*bimA* mutant in BMDMs. In this trans-complemented mutant strain, Isopropyl β-D-1-thiogalactopyranoside (IPTG) was present at all times during the assay to induce the expression of the *bimA* gene from the *tac* promoter in the pME6032 vector (Heeb *et al*, 2002), which stably replicates in *B. pseudomallei* (Stevens *et al*, 2005b). In addition, the infected cells were immunostained and imaged by confocal microscopy to identify if actin tail formation could be observed in BMDMs infected with the WT strain and the complement strain, as demonstrated previously in the macrophage-like cell line J774.1 (Stevens *et al*, 2005b).

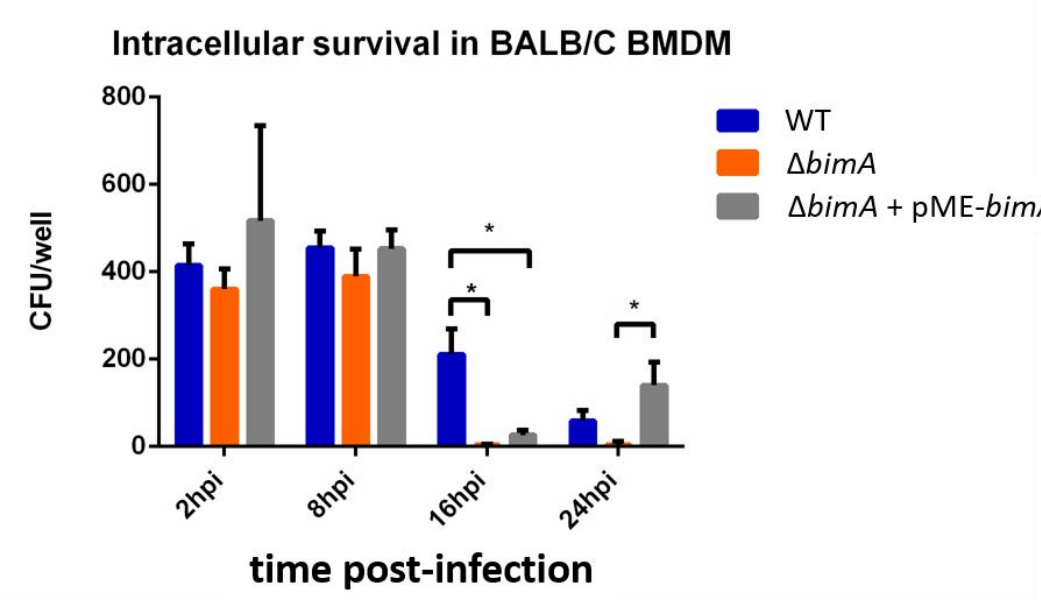

Figure 3.3 Intracellular survival of WT *B. pseudomallei* (blue), Δ*bimA* mutant (orange) and the trans-complemented strain (grey) in BALB/C BMDMs. The chart represents mean bacterial recoveries (cfu ± standard error) from four independent experiments, each with triplicate technical measurements. This assay was performed on BMDMs plated in a 96-well plate format which containing 1 x 10^5 cells per well. Kanamycin-resistant bacteria were recovered at 2 hpi, 8 hpi, 16 hpi and 24 hpi after infection of BALB/C BMDMs as described in *Materials and Methods 2.6*. Statistical significance was determined using an unpaired Student t-test (*) $p<0.05$.

The graph in Figure 3.3 demonstrates similar levels of net intracellular survival of both WT *B. pseudomallei* 10276 and the Δ*bimA* mutant at 2 hpi and 8 hpi in BALB/C BMDMs. However, there was a dramatic decrease in the net intracellular survival of the Δ*bimA* mutant at 16 hpi compared to the WT strain. Almost no Δ*bimA* mutants were recovered at 16 and 24 hpi (Figure 3.3). Reduced numbers of bacteria at later time points could result from cytotoxicity of the strains, which in turn would cause lysis of the infected cell, exposure of the intracellular bacteria to the kanamycin in the media and subsequent killing. The cellular cytotoxicity was assessed using a commercial Lactate-dehydrogenase(LDH)-release assay. LDH is a stable cytosolic enzyme that is released upon cell lysis into the surrounding medium. This enzyme converts its substrate lactate into pyruvate which results in the conversion of the tetrazolium salt iodonitrotetrazolium violet (INT) into a red formazan product, which can be measured at 490nm using a spectrophotometer. The absorbance of the sample is proportional to the amount of LDH released and hence, the number of lysed cells. The data displayed in Figure 3.4 indicates that the cytotoxicity measured in all samples was not significantly different compared to the uninfected control cells (<15%).

The infected BMDMs on the coverslip were then stained with anti-*B. pseudomallei* antibody and phalloidin to detect actin filaments. Analysis of confocal images revealed that numerous intracellular WT *B. pseudomallei* formed actin tails at 8 hpi, and some had formed membrane protrusions at the cells periphery, consistent with previous observations in the immortalised cell lines HeLa (Stevens *et al*, 2005b), A549 (Sitthidet *et al*, 2011), J744.2 (Sitthidet *et al*, 2011; Stevens *et al*, 2005b) and RAW264.3 (Burtnick *et al*, 2008). As expected, no actin tails were observed in cells infected with the Δ*bimA* mutant (Figure 3.5). Furthermore, the defect in actin-based motility of the Δ*bimA* mutant was partially restored by inducible expression of the native *bimA* allele in pME6032 at 24 hpi, but not at 16hpi, consistent with a role for the BimA protein in actin-based motility (Figure 3.3). The partial restoration of actin-based motility is likely due to imperfect *bimA* expression on the inducible plasmid. This is a common issue with complementation of genetic defects *in trans*. Confocal microscopy demonstrated that the trans-complemented strain formed actin-tails of a similar morphology to the WT strain at 8 hpi (Figure 3.5).

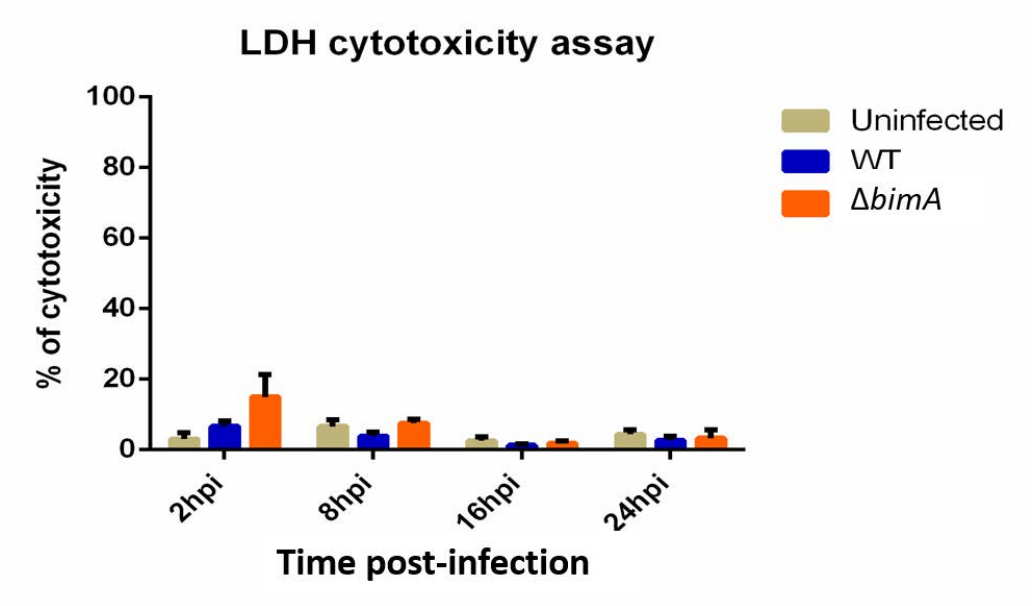

Figure 3.4 Cytotoxicity level of uninfected (light green), infected BMDMs with WT (blue) and Δ*bimA* mutant (orange). Bacterial cytotoxicity was determined from three independent experiments with triplicate measurements using a commercial LDH-release assay as described in *Materials and Methods 2.8.* Cytotoxicity was calculated by first subtracting the average absorbance values of the triplicates with the culture medium background control. These corrected values were then divided by the absorbance of maximum LDH release, followed by multiplication of 100% to give percentage of cytotoxicity. The maximum LDH release control was obtained by lysing the cells with Lysis solution containing 1% TritonX-100. Data expressed as the mean $\pm$ standard error.

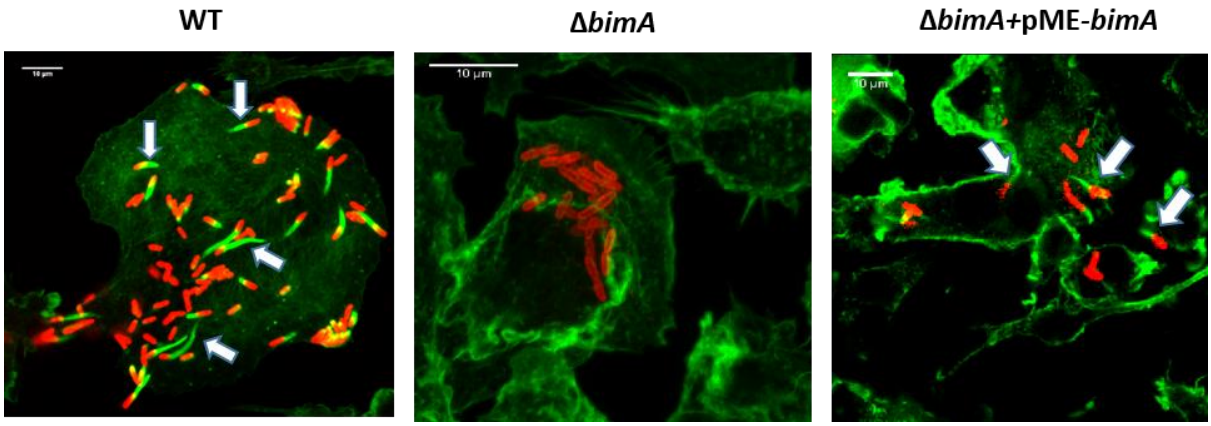

Figure 3.5 Representative z-stack confocal images of BMDMs infected with *B. pseudomallei* WT, Δ*bimA* mutant or the trans-complemented Δ*bimA* mutant strain under IPTG induction. BMDMs were seeded on coverslips and infected with bacterial strains at an MOI of 2 for 8 hpi before fixing and staining for confocal microscopy. Bacteria were stained red with mouse anti-*B. pseudomallei* LPS and anti-mouse Ig-Alexa 568. Filamentous actin was stained green with Alexa Fluor 488 Phalloidin. White arrows indicate actin tails. Scale bar = 10µm.

3.2.3 The Δ*bimA* mutant strain displays no difference in bacterial uptake nor phagosomal escape compared to the WT strain

Before investigating the macrophage innate mechanisms involved in killing the intracellular Δ*bimA* mutant, it was important first to determine if the defect observed in intracellular survival of the Δ*bimA* mutant in BALB/C BMDMs was a result of differences in bacterial uptake or escape from the phagosome between the strains. Bacterial uptake or invasion of *B. pseudomallei* is normally assessed at 2 hpi using the kanamycin-protection assay. Figure 3.3 confirms that the Δ*bimA* mutant does not have any defect in uptake by BALB/C BMDMs, as the intracellular bacterial number at 2 hpi is comparable between the WT and Δ*bimA* mutant strains.

In J77.4 murine macrophage-like cells, both WT strain 10276 and an insertion mutant (*bimA*::pDM4) were shown to escape into the cytosol, gaining access to this replicative niche at 3 hours post-infection (Stevens *et al*, 2005b). However these data were not analysed quantitatively. Here the ability of the Δ*bimA* mutant to escape the phagosome was determined using a chloroquine-protection assay as described by Marathe *et al* (2012) and Fernandez-Prada *et al* (2000). Chloroquine is a lysomotropic agent that enters the cell membrane at weak base state and becomes protonated within the acidic environment of the phagosome. Consequently, chloroquine becomes concentrated within the phagosomes and selectively kills the intracellular bacteria localised in the phagosomes, discriminating between the intracellular bacteria that are free in the cytoplasm which are not exposed to chloroquine. To assess the efficiency of the strains to escape the phagocytic compartment, infected BMDMs were either treated with kanamycin alone, or with both kanamycin and chloroquine. Kanamycin is used to kill extracellular bacteria, hence, CFU recovered from the infected cells lysed after kanamycin treatment without chloroquine represents the total number of intracellular bacteria that are localised in the phagosomes as well as within the cytoplasm. On the other hand, in the presence of both kanamycin and chloroquine treatment, the CFU recovered from the lysed macrophages represent only the cytoplasmic population of *B. pseudomallei*, since those within the phagosomes will have been killed by the chloroquine (Marathe *et al*, 2012; Fernandez-Prada *et al*, 2000). BMDMs were infected with WT, Δ*bimA* mutant or *bsaZ*::pDM4 (*bsaZ*) mutant strain at an MOI of 2 for 30 minutes. The *bsaZ* mutant strain is a Type III secretion system

(T3SS) mutant which has been described previously to be defective in phagosomal escape in immortalised macrophage-like cell lines (Burtnick *et al*, 2008; Stevens *et al*, 2002) hence acts as a positive control for the assay. After 30 minutes of incubation, the media were aspirated and the BMDMs were washed with PBS before replacing with new media containing 250μg/ml kanamycin for another 3 hours. Then chloroquine (50μg/ml) was added to relevant wells and the cells incubated for a further 1.5 hours. The concentration of chloroquine used in this study was optimised so that it exerted minimal cytotoxic effect on the BMDMs (data not shown). Cells were lysed at 5hpi and viable bacteria enumerated. In Figure 3.6, the percentage refers to the proportion of bacteria that were localised in the cytoplasm compared with the total number of bacteria localised both in phagosomes and cytoplasm (which was taken as 100%). No significant differences were observed in the recovery of WT and Δ*bimA* mutant bacteria in BALB/C macrophages, in the presence of kanamycin alone, or in the presence of both kanamycin and chloroquine. As expected, low numbers of bacteria were recovered from *bsaZ* infected BMDMs treated with both kanamycin and chloroquine, indicating that this is a robust assay for determining the ability of *B. pseudomallei* to escape from phagosomes into the cytoplasm of infected cells (Figure 3.6). It can therefore be concluded that the intracellular survival defect of the Δ*bimA* mutant in BMDMs is independent of uptake and macrophage phagosomal killing mechanisms. The findings here were consistent with previous observations by Stevens *et al* (2005b) in J774.2 cells. Using confocal microscopy, they observed that the intracellular *bimA*::pDM4 mutant bacteria did not significantly co-localise with the lysosome-associated membrane glycoprotein-1 (LAMP-1), a marker for late endosomes/lysosomes. This suggests that the *bimA*::pDM4 mutant was able to escape from endosomes and gain access to the cytoplasm. While in the same experiment, *bsaZ* mutant bacteria were almost exclusively colocalised with regions of LAMP-1 (Stevens *et al*, 2005b; Stevens *et al*, 2002).

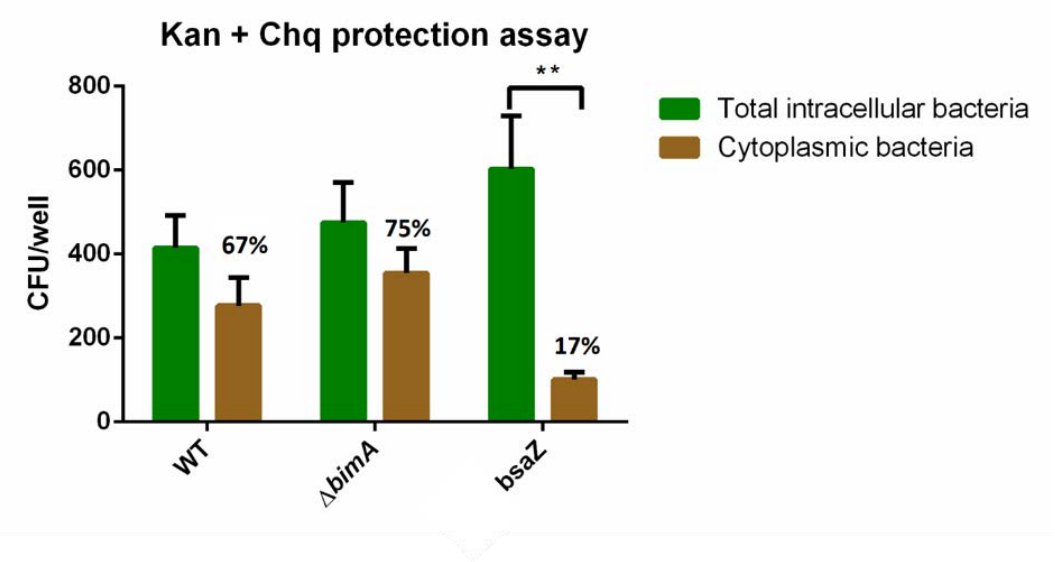

Figure 3.6 Proportion of cytoplasmic bacteria after 5 hours post infection. The bar chart shows the intracellular load of WT, Δ*bimA* mutant and T3SS *bsaZ* mutant in BALB/C BMDMs using a kanamycin-protection assay in the presence or absence of 50µg/ml chloroquine. The cells were infected at an MOI of 2 for 30 minutes. The media was then replaced with media containing kanamycin for a further 3 hours. Then, chloroquine was added in one set of samples while in the second set, cells were left with kanamycin alone, and incubated for a further 1.5 hours. Cells were lysed at 5 hours post infection. The percentage refers to the proportion of bacteria that were localised in the cytoplasm compared with the total number of bacteria localised both in phagosomes and cytoplasm. Data represents the mean bacterial recoveries (cfu + standard error per well of a 96-well plate) from four independent experiments with triplicate technical measurements. Statistical significance was determined using an unpaired Student t-test. ** = $p<0.01$.

3.2.4 Autophagy does not play a role in the clearance of the Δ*bimA* mutant in infected BMDMs

Autophagy is a tightly regulated host cell process of targeting unwanted molecules, damaged intracellular organelles and proteins to the degradation pathway. Autophagy is known to be involved in cell survival following nutrient deprivation, cell development and also tumour suppression (Mehrpour *et al*, 2010; Mizushima *et al*, 2010). Many studies have shown that autophagy is also important for controlling intracellular pathogens, being implicated as a key part of the cell-autonomous innate immune response (reviewed in Wileman, 2013). It has previously been demonstrated that *B. pseudomallei* induces autophagy in immortalised RAW264.7 macrophage-like cells at early stages of infection which can be further activated upon rapamycin treatment, an inducer of autophagy (Cullinane *et al*, 2008). Studies carried out by Cullinane and colleagues showed that *B. pseudomallei* is targeted in the phagosome through the non-canonical autophagy pathway known as LAP (LC3 associated phagosomes). LAP is a mechanism where LC3 molecules are recruited directly to the bacteria-containing phagosomes rather than sequestered in canonical double-membrane autophagosomes which can be observed by electron microscopy (Gong *et al*, 2011). *B. pseudomallei* has been shown to effectively evade autophagy upon escape from the phagosomal compartment (Gong *et al*, 2011). Phagosomal escape is dependent on a functional Bsa Type III secretion system (T3SS), mutants lacking the genes encoding the T3SS effector protein BopA or the translocator protein BipD, demonstrated a delay or lack of escape from phagosomes, with considerable co-localisation of the mutants with LC3 and reduced bacterial survival (Gong *et al*, 2011).

Gong *et al* (2011) reported that cytoplasmic WT *B. pseudomallei* was rarely taken up by canonical autophagosomes, however their experiments did not extend to time points later than 6 hpi. Once in the cytoplasm, *B. pseudomallei* replicates, disseminates both inter- and intracellularly, processes mediated by the BimA protein and fusion of adjacent cells to form multinucleated giant cells (MNGC) in a Type 6 Secretion System -dependent manner. It is possible that autophagy plays a role in the detection and elimination of these cytosolic bacteria. Indeed the avoidance of autophagy has been observed in cases of other intracellular and cytosolic bacterial pathogens. For example, for *Listeria monocytogenes,* the bacterial factor required for actin-based motility ActA has been shown to mask autophagic recognition of the bacterium by recruiting host cellular proteins Arp2/3 and VASP proteins, which results in

camouflage of the bacterium from being targeted by this host defence mechanism (figure 3.7). We speculated that BimA mediates escape of cytoplasmic *B. pseudomallei* from autophagy in infected cells leading to the observed reduction in intracellular Δ*bimA* numbers at 16hpi in BALB/C BMDMs (Figure 3.3).

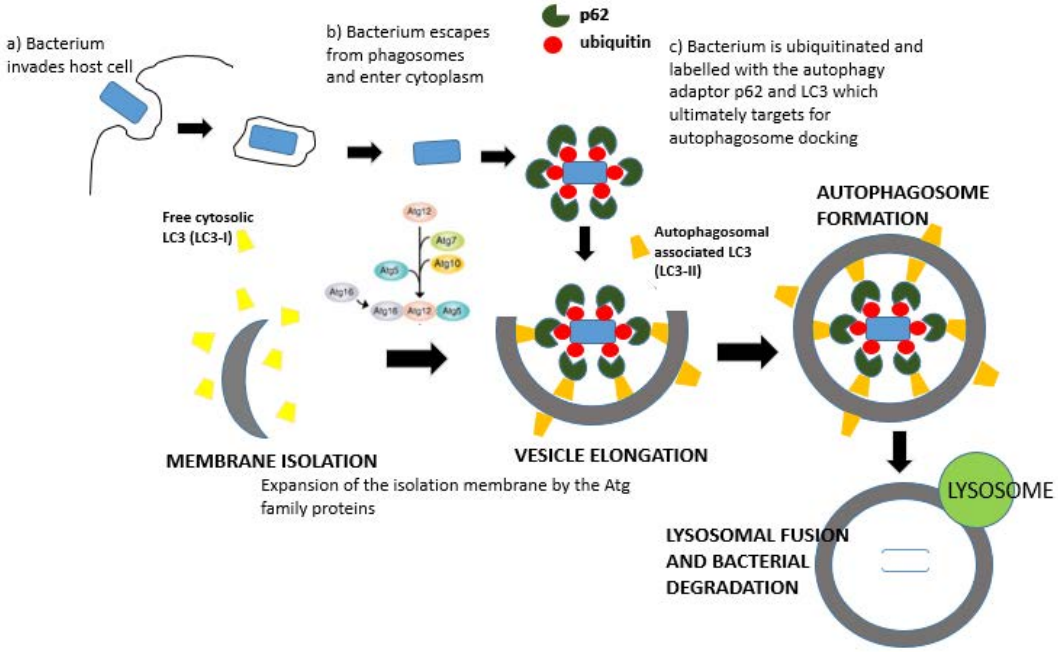

Figure 3.7 Schematic diagram illustrating how autophagy acts as an innate mechanism against cytoplasmic bacteria. Autophagy involves different stages starting from vesicle nucleation (formation of the isolation membrane), vesicle elongation and completion to form a double-membrane autophagosome. A lysosome then fuses with the autophagosome to form the autophagolysosome. This step is followed by the lysis of the autophagolysosome inner membrane and bacterial degradation. Using a *L. monocytogenes actA* mutant as a bacterial model for infection, Yoshikawa *et al* (2009) demonstrated that when the *L. monocytogenes actA* mutant escapes from the phagosome and gains access to the cytoplasm, the bacterium is ubiquitinated and labelled with the autophagy adaptor p62, followed by LC3 molecules. This subsequently targets the bacterium for autophagosome docking and degradation, indicating autophagy as an innate mechanism to suppress the survival of intracellular bacteria (figure adapted from Yoshikawa, Y. *et al* (2009). *Listeria monocytogenes* ActA-mediated escape from autophagic recognition. *Nature Cell Biology*, 11(10), 1233–1240. Copyright © 2009 with permission from Macmillan Publishers Ltd: Nature Publishing Groups).

The contribution of the autophagic pathway in the elimination of the Δ*bimA* mutant strain in macrophages can be monitored by measuring LC3-II conversion during infection. Upon autophagic induction in response to bacterial infection, the cytosolic form of LC3 (LC3-I) is conjugated to a highly lipophilic phosphatidylethanolamine (PE) moiety to generate the autophagosomal-associated form (LC3-II). In short, LC3-II correlates well with the formation of autophagosomes. Due to the higher hydrophobicity of LC3-II, this molecule migrates more rapidly in SDS-PAGE than LC3-I. This can be assayed by Western blotting analysis of infected cell lysates with anti-LC3B antibodies. There are three isoforms of LC3 in mammalian cells; LC3A, LC3B and LC3C, but only LC3B correlates with increased autophagic vesicle formation (Barth *et al*, 2010). The fold change in LC3-II conversion (LC3-II/ total LC3) of each sample relative to uninfected or untreated cells at respective time points can be determined by quantitative densitometric analysis. We first investigated if autophagy can be further activated above its basal level by treating BMDMs with the autophagy inducer, rapamycin for 2, 8 and 16 hours. Rapamycin was used at a concentration of 4μM, similar to previous studies by Cullinane *et al* (2008). The solvent Dimethyl sulfoxide (DMSO) was included as a vehicle control in this experiment. In the presence of rapamycin, autophagy could be stimulated up to 1.6 fold and 1.5 fold over basal levels in the untreated BMDMs at 2 hours and 8 hours respectively (figure 3.8). The slight decrease in LC3-II conversion over time could be explained by the balance of LC3-II formation and degradation, where LC3-II degradation is more rapid than its formation when cells were treated pharmacologically with rapamycin (Barth *et al*, 2010; Mizushima *et al*, 2010; Mizushima & Yoshimori, 2007).

To determine whether autophagy is involved in the detection and elimination of the Δ*bimA* mutant, BMDMs were infected with *B. pseudomallei* WT or the Δ*bimA* mutant at an MOI of 2 at 2 hpi, 8 hpi and 16 hpi in a kanamycin-protection manner as described previously. Uninfected BMDMs were also included as a control for basal levels of autophagy. At the indicated times post infection, BMDMs were lysed and subjected to SDS-PAGE and Western blotting as described in Section 2.10. Analysis of LC3-II conversion showed that there was no significant difference in the ratio of LC3-II: total LC3 signal among the non-infected BMDMs and BMDMs infected with WT and Δ*bimA* mutant at all time points (Figure 3.9). This suggests that autophagy is not involved in targeting *B. pseudomallei*, either WT or Δ*bimA* mutant strains, at any of the time points tested. Although Cullinane *et al* (2008) described that there was about a 2-fold increase in LC3 conversion upon infection with *B. pseudomallei* at 2hpi in immortalised RAW264.7 macrophage-like cells, we were unable to show that autophagy was

differentially activated in BMDMs infected either with WT or Δ*bimA* strains compared to uninfected cells. This may due to the differences in cell types and *B. pseudomallei* strains used for the studies.

Next, confocal microscopy was used to observe if there is any significant co-localisation of LC3 molecules with the Δ*bimA* mutant. Confocal microscopy confirmed that neither WT nor bacteria lacking *bimA* showed co-localisation with LC3 molecules (Figure 3.10). This confocal analysis corresponds to the immunoblot analysis in Figure 3.9, indicating that host autophagy is not differentially activated in cells infected with the Δ*bimA* mutant compared to those infected with WT bacteria.

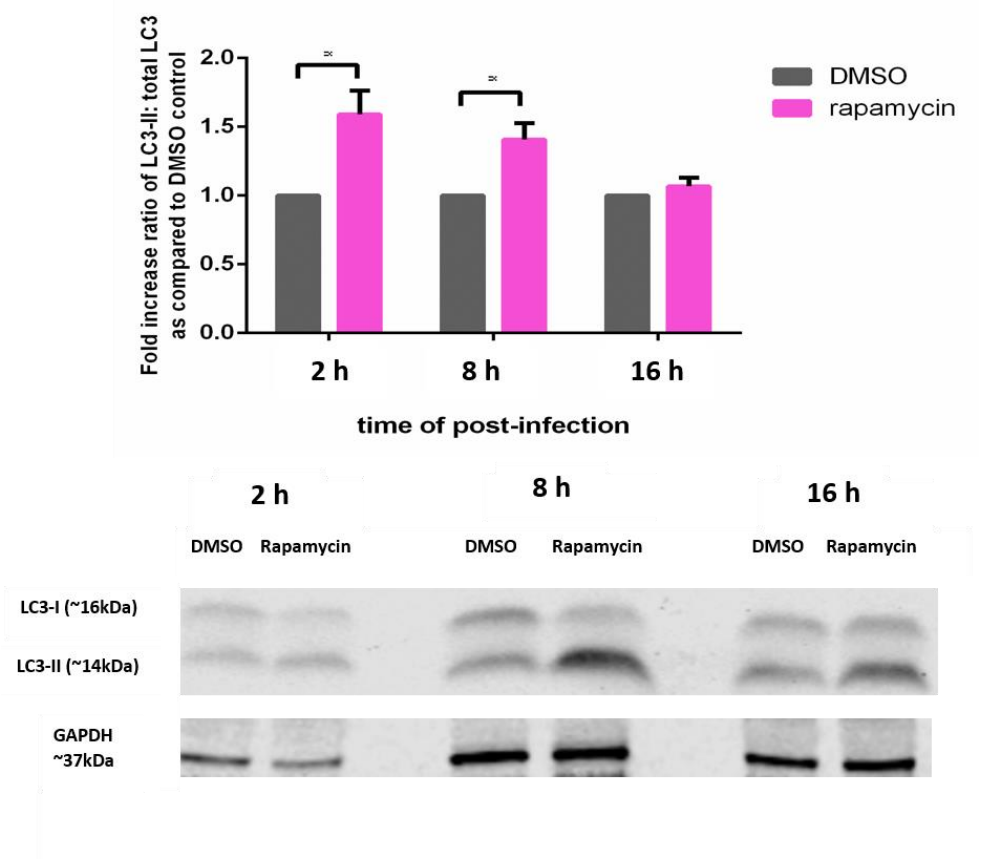

Figure 3.8 Immunoblot analysis of LC3 conversion in BMDMs treated with the autophagy inducer rapamycin. BMDMs were seeded at 5 x 10^5 per well in a 24-well plate. BMDMs were treated with 4μM of rapamycin or the control DMSO for 2, 8 and 16 hours before being lysed and proceeded for Western Blot as described in *Materials and Methods 2.10*. (A) Mean densitometric measurements of LC3-II conversion as compared to DMSO control from four independent experiments and the error bars represent the standard error. Significance was assessed using an unpaired Student's t-test, where * = $p<0.05$. (b) A representative immunoblot where the LC3-I (cytosolic) and LC3-II (lipid conjugated) were detected with a monoclonal antibody against LC3B. GAPDH is the loading control.

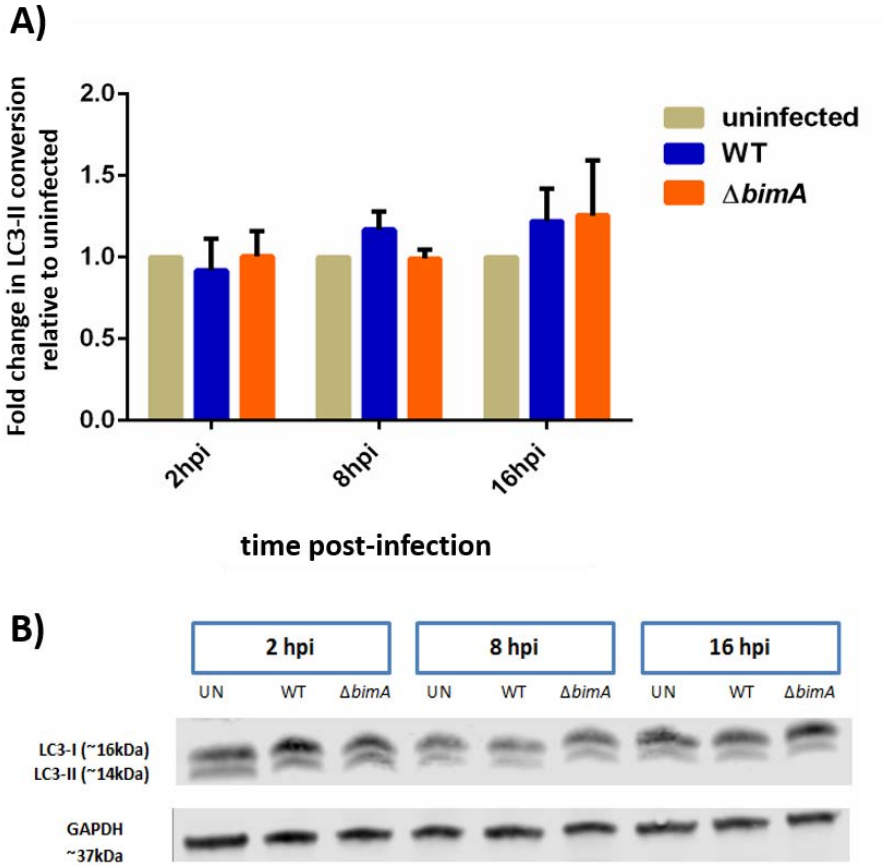

Figure 3.9 Immunoblot analysis of LC3 conversion in cell lysates from uninfected BMDMs (UN) and cells infected either with *B. pseudomallei* WT and Δ*bimA* mutant. (a) The mean densitometric measurements of the LC3-II conversion as compared to uninfected control from four independent experiments and the error bars represent the standard error. Statistical analysis was performed using an unpaired Student's t-test of two groups; infected with either *B. pseudomallei* WT or Δ*bimA* mutant, compared to the uninfected control cells at respective time points**.** (b) A representative immunoblot where the LC3-I (cytosolic) and LC3-II (lipid conjugated) forms were detected with a monoclonal antibody against LC3B. GAPDH is the loading control.

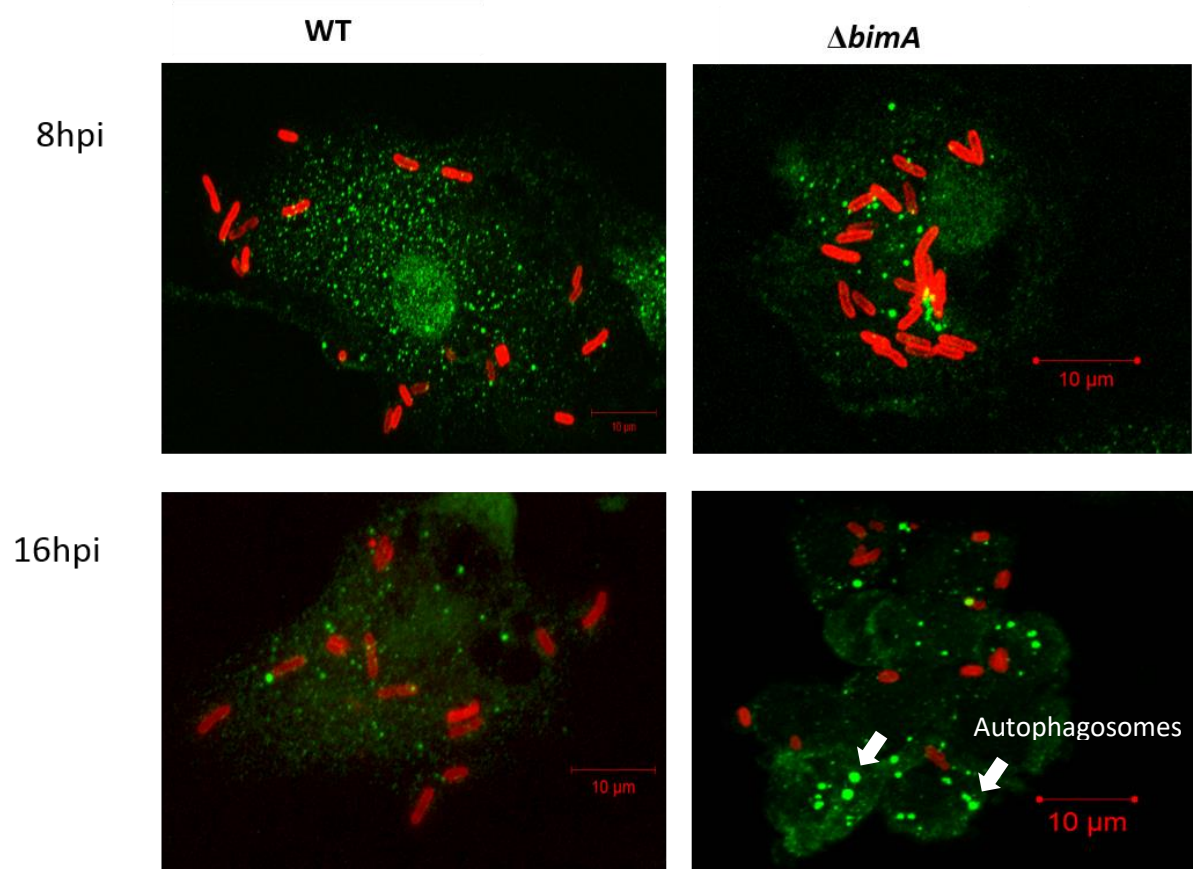

Figure 3.10 LC3 co-localisation analysis of BMDMs infected with *B. pseudomallei* WT or Δ*bimA* mutant bacteria. BMDMs were seeded on coverslips at 5 x 10^5 cells per well before infected with WT or Δ*bimA* mutant bacteria at an MOI of 2 in a kanamycin protection manner as described in *Materials and Methods 2.6*. BMDMs infected with WT or Δ*bimA* mutant bacteria were incubated for the indicated times before fixing and staining for confocal microscopy. Bacteria were stained red with mouse anti-*B. pseudomallei* LPS and anti-mouse Ig-Alexa 568 antibodies. LC3 molecules were stained green with rabbit anti-LC3B and anti-rabbit Ig-Alexa Fluor 488. Large green dots as indicated by arrows are autophagsomoes. Scale bar = 10µm.

To further investigate the role of autophagy-related processes in the clearance of the Δ*bimA* mutant in infected cells, we next carried out confocal microscopy to explore the ubiquitination of cytoplasmic bacteria as shown in Figure 3.7. It has recently been recognised that ubiquitination provides a signal for the autophagic targeting of bacteria for degradation. We stained the infected BMDMs with the FK2 monoclonal antibody, which has affinity for both mono- and poly-ubiquitinated proteins tagged regardless of ubiquitin linkage location, but does not react with free ubiquitin (Fujimuro *et al*, 1994). Interestingly, the cytosol-adapted pathogen *L. monocytogenes* has been shown previously to avoid recognition by the ubiquitin system by moving rapidly in the cytosol of host cells via actin-based motility (Yoshikawa *et al*, 2009; Perrin *et al*, 2004). These studies demonstrated that the Δ*actA* mutant showed extensive co-localisation with ubiquitin moieties compared to the WT bacteria (Yoshikawa *et al*, 2009; Perrin *et al*, 2004). However, in our confocal analysis, we observed a strong signal for ubiquitin that co-localised with the bacterial surface of the majority of both WT and Δ*bimA* mutant bacteria at 8 hpi and 16 hpi (Figure 3.11), with no obvious differences between strains or time points. This suggests that ubiquitination, which is part of the cellular innate surveillance system, however, does not specifically target the bacteria that are unable to undergo actin-based motility.

We then investigated if p62 (also known as sequestome 1, SQSTM1) molecules interact with these poly-ubiquitinated bacteria. p62 is an autophagy adaptor protein which has two domains; an ubiquitin-binding domain and an LC3-binding domain. In general, p62 interacts with poly-ubiquitinated protein aggregates through its ubiquitin-binding domain (UBA), targeting these aggregates for autophagy degradation through its LC3 binding domain (LIR). p62 has been shown to be involved in targeting ubiquitinated bacteria for autophagy (Zheng *et al*, 2009). Hence, if the bacteria are targeted for autophagy, we would observe co-localisation of p62 molecules with bacteria as demonstrated in Yoshikawa *et al* (2009) and Zheng *et al* (2009). However, neither WT nor Δ*bimA* mutant showed significant co-localisation with p62 by confocal microscopy analysis (Figure 3.12).

The experiments described in this chapter have included LC3-conversion assays, LC3-bacteria and p62-bacteria co-localisation studies, none of which explained the intracellular survival defect of the Δ*bimA* mutant. Hence, we hypothesise that actin-based motility mediates escape of *B. pseudomallei* from macrophage intracellular killing, through an as yet undefined mechanism.

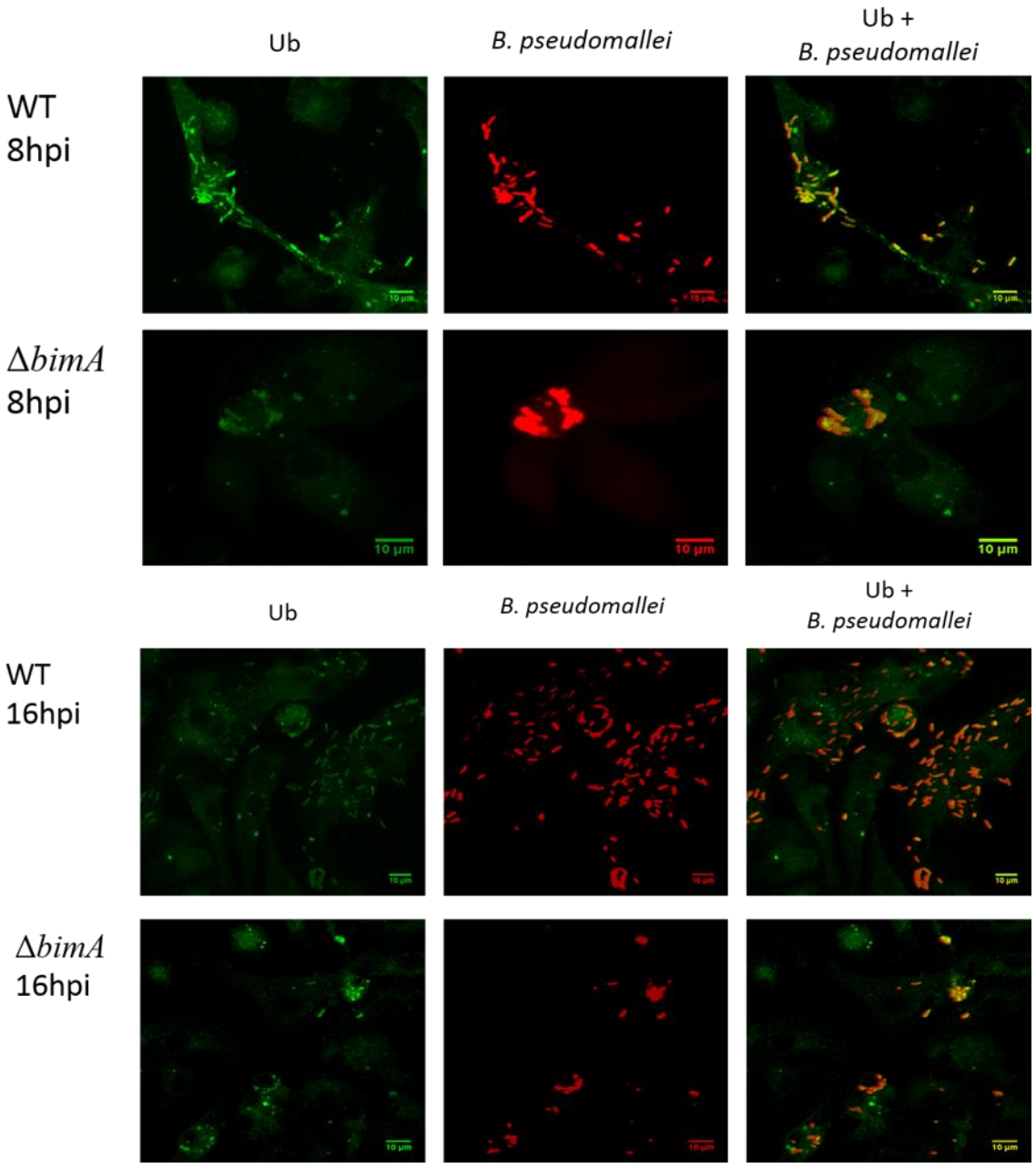

Figure 3.11 Ubiquitin co-localisation analysis of BALB/C BMDMs infected with the WT or Δ*bimA* mutant. BMDMs were seeded on coverslips at 5 x 10^5 cells per well before infected with WT or Δ*bimA* mutant bacteria at an MOI of 2 in a kanamycin protection manner as described in *Materials and Methods 2.6*. BMDMs infected with WT or Δ*bimA* mutant bacteria were incubated for the indicated times before fixing and staining for confocal microscopy. Bacteria were stained red with rabbit anti-*B. pseudomallei* LPS and anti-rabbit Ig-Alexa 568 antibodies. While Ub molecules were stained green with rabbit anti-LC3B and anti-rabbit Ig-Alexa Fluor 488. Scale bar = 10µm.

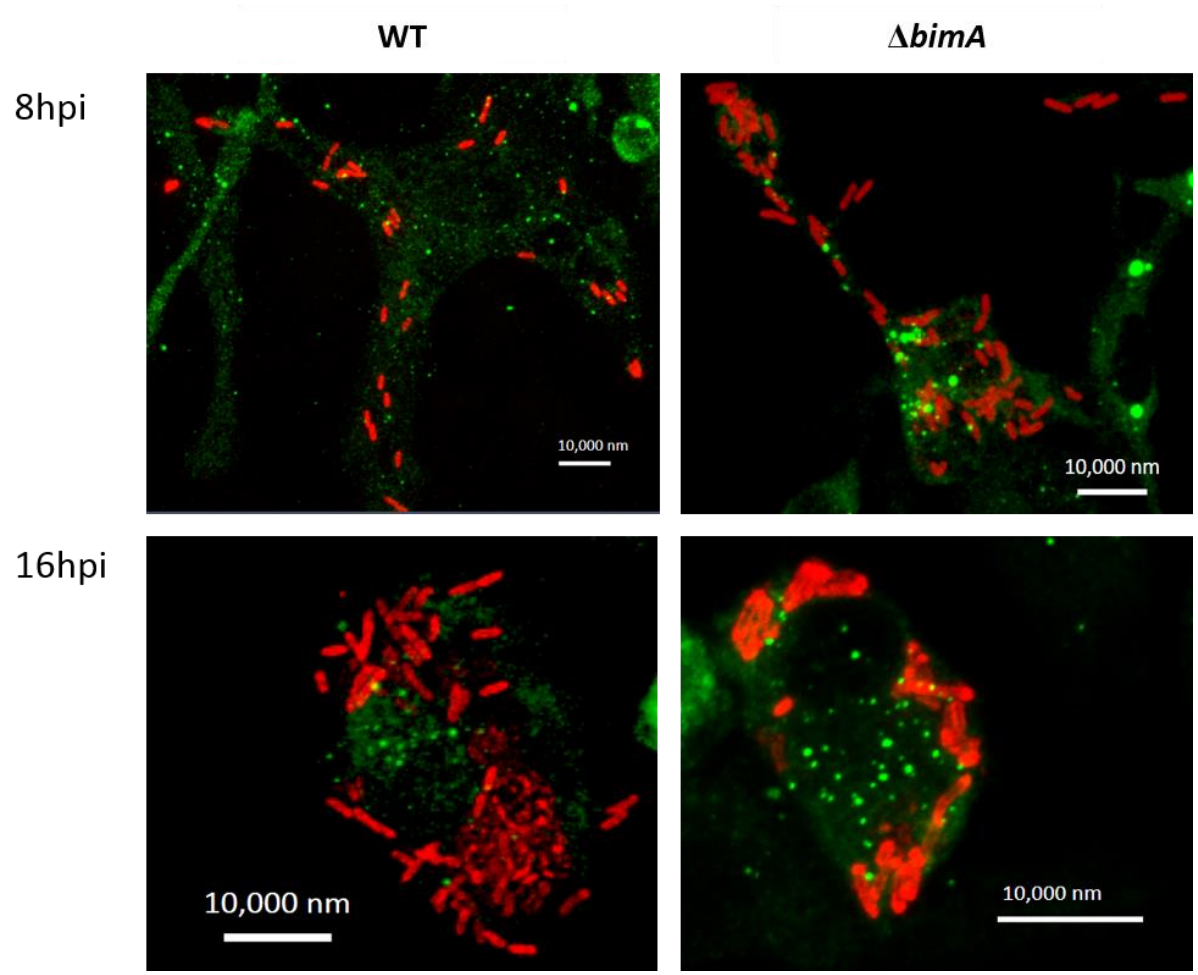

Figure 3.12 p62 co-localisation analysis of BALB/C BMDMs infected with the WT or Δ*bimA* mutant bacteria. BMDMs were seeded on coverslips at 5 x 10^5 cells per well before infected with WT or Δ*bimA* mutant bacteria at an MOI of 2 in a kanamycin protection manner as described in *Materials and Methods 2.6*. BALB/C BMDMs infected with WT or Δ*bimA* mutant bacteria were incubated for the indicated times before fixing and staining for confocal microscopy. Bacteria were stained red with mouse anti-*B. pseudomallei* LPS and anti-mouse Ig-Alexa 568 antibodies. p62 molecules were stained green with rabbit anti-LC3B and anti-rabbit Ig-Alexa Fluor 488. Scale bar = 10μm.

3.3 DISCUSSION

Infection with *Burkholderia pseudomallei* has a high mortality of up to 40% in endemic areas such as Thailand. To elucidate how the bacterium evades host defences, it is important to understand the pathogenesis in host macrophages, as they represent a first line of defence against many infectious agents. Intracellular bacteria such as *Listeria monocytogenes*, *Shigella flexneri* and *Burkholderia pseudomallei* have evolved to escape from the harsh environment of phagosomes and enter the nutrition-rich cytosol as a niche for replication. In the cytoplasm, they are continuously being exposed to multiple host innate mechanisms to restrict their intracellular survival. By moving from cell to cell by actin-based motility, *L. monocytogenes, S. flexneri* and *B. pseudomallei* escape from such host innate responses to continue to replicate and survive. In our *in vitro* system using murine bone marrow derived macrophages (BMDMs), a *B. pseudomallei* Δ*bimA* mutant which is unable to undergo actin-based motility showed a marked decrease in intracellular survival compared the WT strain, suggesting that cellular innate responses play a critical role in control of the cytoplasmic *B. pseudomallei* that lack the ability to undergo actin-based motility. This is in line with *in vivo* studies that have previously been conducted in our laboratory, where *bimA* mutant strains exhibit attenuation in both murine (unpublished data; Stevens, J.M. and Bancroft, G.) (Figure 5.5) and *Galleria mellonella* models of melioidosis (unpublished data, Stevens J.M.). BMDMs seem to be better able to control the intracellular survival of *B. pseudomallei* when compared to the immortalised murine macrophage-like RAW264.7 cells (Varintip Srinon, manuscript in preparation). Infection of RAW264.7 cells with either the WT or Δ*bimA* mutant strains resulted in identical patterns of replication and survival over time with no significant levels of killing (Varintip Srinon, manuscript in preparation), indicating that BMDMs are more relevant for the studies described in this thesis. This is perhaps predictable as selective pressure imposed by continual subculture of immortalised cells, usually results in the loss of genes that are not essential for multiplication but are key for macrophage immune functions. Chamberlain *et al* (2008) have demonstrated that murine BMDMs cells exhibit significantly higher expression of some inflammatory cytokines for example TNF-α, IL-6, IL-12 and MCP-1 compared to RAW264.7 cells in response to LPS stimulation. Our *in vitro* system using resting, non-primed/non-activated murine BALB/C BMDMs cells show that both WT and the Δ*bimA* mutant strains are capable of escaping from the phagosomes, and that the WT strain is capable of forming actin-tails as observed by confocal microscopy.

Antibacterial autophagy (xenophagy) is appreciated as a cell-autonomous immune response to invading intracellular bacteria namely *Salmonella* (Zheng *et al*, 2009), *Shigella* (Dupont *et al*, 2009) and *Listeria* (Yoshikawa *et al*, 2009). Upon invasion, some bacteria actively modify their vacuolar compartments to prevent autophagosomal fusion, while others escape into the cytosol for replication. Host autophagy is highly dynamic and can target pathogens at any intracellular stage, either when they are residing in the vacuolar compartment or within the cytosol. In RAW264.7 macrophage-like cells, LC3 was shown to be recruited directly to the bacteria localised in a single-membrane phagosome at early time point, a process termed LC3-associated phagocytosis (LAP), resulting in decreased intracellular survival of *B. pseudomallei* (Gong *et al*, 2011). This LAP formation is distinct from the double-membrane canonical autophagosomes observed during clearance of organelles or proteins, or elimination of other bacterial species. This recruitment of LC3 molecules to phagosomal *B. pseudomallei* has also been observed in primary human neutrophils, but through novel membranous structures composed of partial phagosome-like single membranes and partial elongated membranes (Rinchai *et al*, 2015). Both studies by Rinchai *et al* (2015) and Gong *et al* (2011) have determined that cytoplasmic *B. pseudomallei* is rarely sequestered in double-membrane canonical autophagosomes as observed by transmission electron microscope (TEM). This suggests that *B. pseudomallei* actively evades the autophagic innate immune response once the bacterium has successfully escaped from the phagosome, a process mediated by the Bsa Type III secretion system (Rinchai *et al*, 2015; Gong *et al*, 2011; Cullinane *et al*, 2008). Once *B. pseudomallei* enters the cytoplasm, *B. pseudomallei* forms actin tails in a BimA-dependent manner to propel itself to the neighbouring cell (Stevens *et al*, 2005) and also to escape from the host innate immune responses in order to survive. Hence, this is the first report investigating if the Δ*bimA* mutant is being targeted by autophagy in primary murine BMDMs. It has been shown that WT *B. pseudomallei* can form actin tails in infected BMDMs (Figure 3.5), unlike in *B. pseudomallei*-infected primary human neutrophils (Rinchai *et al*, 2015). On the other hand, the Δ*bimA* mutant strain did not form actin tails at all, but the phenotype was restored in the complemented strain (Figure 3.5).

In BALB/C BMDMs, the intracellular survival of the *B. pseudomallei* Δ*bimA* mutant was significantly impaired at 16 hpi when compared to the WT strain. However, both an LC3-conversion assay and LC3-co-localisation studies could not demonstrate a specific role for autophagy in this defect in intracellular survival. Notably, the low infection rate in BMDMs may limit the experimental power to investigate the autophagy pathway upon infection.

Approximately, 500 CFU was produced per 1 x 10^5 BMDMs (which accounts <0.5% of the BMDMs were infected) in the kanamycin protection assay whereas in the immortalised cell line RAW264.7, *B. pseudomallei* WT produced up to 10^6 CFU per 1 x10^5 BMDMs at 16 hpi using the same MOI (data not shown). Furthermore, in contrast to the RAW264.7 cells, there was no replication of intracellular *B. pseudomallei* over time in infected BMDMs (data not shown). Very few MNGC were formed in *B. pseudomallei* WT infected BMDMs at late times post-infection (16hpi) with less than 5 nuclei per MNGC, unlike infected RAW264.7 cells where the majority formed MNGC with tens of nuclei, as observed under the confocal microscopy (data not shown). As cell lines may not adequately represent primary cells as discussed above, differences in the ability to control intracellular bacterial survival and MNGC formation are perhaps predictable.

In several studies of autophagy, it is common to include drugs such as rapamycin or 3-methyladenine (3MA) to pharmacologically induce or inhibit autophagy activity respectively. For example, Rinchai *et al* (2015) successfully demonstrated that survival of *B. pseudomallei* in human neutrophils was greatly enhanced in 3MA-treated cells. While Cullinane *et al* (2008) reported that rapamycin stimulation of autophagy in RAW264.7 and murine embryonic fibroblast (MEF) cell lines resulted in increased co-localisation of *B. pseudomallei* with LC3, and subsequently reduced intracellular survival of the bacteria. Application of these drugs in our experimental conditions would only be essential and worthwhile if there is clear evidence showing that autophagy does play a role in controlling bacterial intracellular survival.

Interestingly, although we did not observe co-localisation of *B. pseudomallei* WT and Δ*bimA* mutant strains with LC3, we identified that both strains were ubiquitinated once they enter the cytoplasm. Although Yoshikawa *et al* (2009) and Perrin *et al* (2004) reported that *L. monocytogenes* evades host ubiquitin system via actin-based motility, in our analysis we found no evidence to suggest that *B. pseudomallei* avoids such recognition in the same manner. Based on our preliminary observation by confocal microscopy, we identified a similar level of co-localisation of ubiquitin with both WT and Δ*bimA* mutant strains in the cytosol. However, these studies need to be repeated over a time course and the data quantified. Ubiquitin has the ability to interact subsequently with several ubiquitin-binding proteins namely p62/SQSTM1, NDP52/CALCOCO2, NBR1 and optinuerin that facilitate ubiquitinated cargo engulfment by autophagosomes or degradation through the proteasomal pathway (Kraft *et al*, 2010). Several studies have reported that p62 is involved in targeting the polyubiqitinated bacteria to the autophagy pathway (Zheng *et al*, 2009; Yoshikawa *et al,* 2009). In *L. monocytogenes*, Perrin

et al (2004) demonstrated that the Δ*actA* mutant strain, lacking the ability to form actin-tails, co-localised extensively with ubiquitin molecules and Yoshikawa *et al* (2009) further demonstrated this mutant strain co-localised significantly with p62 molecules in the cytosol when compared to the WT strain. These together target the Δ*actA* mutant to the autophagic degradation machinery for destruction. However, our confocal microscopy analysis does not show any co-localisation of p62 molecules with either the *B. pseudomallei* WT or Δ*bimA* mutant strains. This suggests that although *B. pseudomallei* is ubiquitinated, the ubiquitin labelling does not target *B. pseudomallei* (neither WT strain nor Δ*bimA* mutant) for autophagy via p62/LC3. Alternatively, the ubiquitination of *B. pseudomallei* might direct the bacteria for degradation in proteasomes which has not been investigated in this chapter. This ubiquitin-proteosomal degradation can be investigated in future by observing the colocalisation of ubiquitin-coated *B. pseudomallei* with proteasome-associated molecules by confocal microscopy. In addition to p62 adaptor molecules, other adaptor proteins such as NDP52/CALCOCO2, NBR1 and optinuerin have not yet been investigated.

In contrast with our findings on the co-localisation of ubiquitin with *B. pseudomallei* 10276 (both WT and Δ*bimA* mutant), Pumirat *et al* (2014) and Tan *et al* (2010) reported low levels of Ubiquitin-bacteria co-localisation for *B. pseudomallei* strain K96243. This could be explained by the fact that different bacterial strains may express a different repertoire of virulence protein(s) to manipulate various host innate mechanisms. For example, *B. pseudomallei* K96243 expresses CHBP (cycle inhibiting factor), a bacterial protein that inhibits Ub ligase-catalysed Ub-chain synthesis by specifically deamidating Gln40 of ubiquitin (Pumirat *et al*, 2014). In addition, Boh *et al* (2011) demonstrated that CHBP may interfere with the interaction of ubiquitin with p62 molecules. However, the strain used in these studies (*B. pseudomallei* 10276) does not encode this effector protein (Pumirat *et al*, 2014). Tan *et al* (2010) have characterised another bacterial virulence protein involved in manipulating host ubiquitination-related pathways, TssM. The T6SS TssM effector protein possesses deubiquitinase activity which removes ubiquitin from proteins attached to the bacterial surface. Although polyubiquitin-labelled bacteria may be targeted by autophagy for destruction, there is no clear evidence yet to show that such ubiquitin manipulations by *B. pseudomallei* are relevant for autophagy evasion (reviewed in Allwood *et al*, 2011). In summary, the mechanism by which *B. pseudomallei* evades host autophagy remains to be defined.

In addition to recruitment of ubiquitin, p62, and LC3 molecules to cytoplasmic bacteria to target them for autophagy, Mostowy *et al* (2011) identified a novel septin-caging mechanism

that entraps cytosolic bacteria for autophagy destruction. Septins have been demonstrated to play a crucial role in the control of cytosolic *Shigella flexneri*. Septins are conserved GTP-binding and filament-forming proteins which are essential for cell division, cytoskeletal dynamics, vesicle trafficking and membrane remodelling (Hall & Russell, 2004). Septins are cytoskeletal components associating with cellular membranes, actin filaments and microtubules to form filaments. In epithelial cells infected with *Shigella flexneri,* septins are recruited around the bacterial bodies, and compartmentalise the bacteria within cage-like structures (Mostowy *et al*, 2010). This septin-caging entraps the cytosolic bacteria for destruction by autophagy, and hence prevents bacterial dissemination. SEPT2 and its binding partner SEPT9 were shown to be responsible for the septin ring assembly. Depletion of SEPT2 and SEPT9 resulted in significantly fewer cages and more actin tail formation by *Shigella*. To our knowledge, the role of septins in controlling cytosolic *B. pseudomallei* has not been investigated so far and it would be interesting to study in future. Interestingly, these cage-like structures have also been observed to compartmentalise *Shigella icsA* mutant bacteria which are defective in actin-based motility (Mostowy *et al*, 2010), leading us to predict that septin-caging might entrap the *B. pseudomallei* Δ*bimA* mutant. Hence, it would be interesting to investigate the co-localisation of septin proteins with *B. pseudomallei* WT and Δ*bimA* strains, and determine if such co-localisation is more prominent for the Δ*bimA* mutant. If there is a clear evidence showing that Δ*bimA* mutant significantly compartmentalises with septins, it would be desirable to knock down the appropriate septin gene(s) by siRNA and determine if the intracellular survival of the mutant could be restored.

In addition to the mechanisms of septin caging and autophagy, bacteria that successfully escape from vacuoles or phagosomes can be sensed by the innate sensors galectins. Galectins are evolutionary conserved β-galactoside-binding lectins implicated in inflammatory responses as well as in cell adhesion (Di Lella *et al*, 2011). Galectins are abundant in innate immune cells and epithelial cells, and an increase in galectin expression may be associated with their roles in host-pathogen interactions. Galectin-3 and galectin-8 are among the ones that are commonly associated with modulating the host immune response. For example, *in vivo* studies using mice reported heightened galectin-3 expression in the lungs of animals infected with *Francisella novida* (Mishra *et al*, 2013) and *Streptococcus pneumoniae* (Sato *et al*, 2002). Galectins can sense various bacterial molecular components such as glycans on the capsule polysaccharide of *Streptococcus pneumonia*, or LPS from *Klebsiella pneumonia* and *Escherichia coli* (reviewed in Chen *et al*, 2014). Binding of galectins to the bacteria can have bacteriostatic or

bactericidal effects. In relation to autophagy, galectin-8 was shown to be recruited to vacuoles containing *Salmonella* Typhimurium, interacting directly with NDP52 to target the bacteria for autophagy (Thurston *et al*, 2012). To our knowledge, the role of galectins in *B. pseudomallei* intracellular survival have not been reported so far. Therefore, it would be of interest in future to knock down the appropriate galectin gene(s) by siRNA and determine if the intracellular survival of the mutant could be restored. As ubiquitin, septin caging and certain galectins are crucial for cell-autonomous immunity mechanisms, elucidating their role in detection and elimination of *Burkholderia pseudomallei* would be interesting avenues of investigation in future.

4 CHAPTER 4: INVESTIGATING THE CONTRIBUTION OF MyD88- AND TRIF-DEPENDENT PATHWAYS, AND INFLAMMASOME ACTIVATION, IN CONTROLLING THE INTRACELLULAR FATE OF *BURKHOLDERIA PSEUDOMALLEI*

4.1 INTRODUCTION

The innate immune system plays a critical role in the early recognition of invading pathogens and subsequently activating the pro-inflammatory response against the pathogen. Activation of innate immune cells begins with the recognition of highly conserved microbial structures, termed pathogen-associated molecular patterns (PAMPs) or host derived molecules that signal the presence of tissue injury known as damage-associated molecular patterns (DAMPs), by a limited set of germline-encoded pattern recognition receptors (PRRs). Some PRRs such as TLRs (Toll-like receptors) are located on the cell surface or in endosomes, and some such as NLRs (nucleotide-binding oligomerisation domain-like receptors), RLRs (retinoic-acid inducible gene I-like receptors) and CLRs (C-type lectin-binding domain receptors) are present in the cytoplasm of innate immune cells (reviewed in Kawai & Akira, 2011). Upon PAMP recognition, PRRs relay the signal to the host cell and activate a multitude of intracellular signalling transduction pathways, including adaptor molecules, kinases and transcription factors. These ultimately switch-on gene expression and synthesis of different cytokines, chemokines, cell adhesion molecules and immunoreceptors that contribute to the innate host response to infection, and also links to the adaptive immune response (reviewed in Kawai & Akira, 2011).

Among PRRs, TLRs have been studied most extensively in melioidosis both *in vitro* and *in vivo*. Three TLRs namely TLR2, TLR4 and TLR5 have been implicated in the recognition of *Burkholderia pseudomallei* (West *et al*. 2013; West *et al*, 2012; West *et al*, 2008; Wiersinga *et al*, 2007). TLR2 is a receptor involved in the recognition of bacterial peptidoglycans, lipoteichoic acid and lipoproteins, while TLR4 and TLR5 are receptors for bacterial LPS and flagellin respectively. Upon ligand binding to TLRs, MyD88 (Myeloid differentiation primary response gene 88) adaptor-protein is recruited to activated TLRs, except TLR3 and certain TLR4s. The downstream cascade results in the activation of the MAPK and NF-κB pathways leading to the production of many cytokines and chemokines, and is known as the MyD88-

dependent pathway (reviewed in O'Neill & Bowie, 2007). Another major pathway emanating from TLRs depends on TIR-domain containing adaptor-inducing IFNβ protein (TRIF). This is known as the TRIF-dependent or MyD88-independent pathway which appears to be specifically induced by TLR3 and some TLR4. The downstream signalling mediates recruitment of IFN regulatory factors (IRF) transcription factor such as IRF3 and IRF7 to the nucleus, which induces expression of Type I IFN including IFNβ. The TRIF-dependent signalling pathway also mediates NF-κB and MAPK signalling pathways similar to the MyD88-dependent pathway, but with delayed kinetics (reviewed in O'Neill & Bowie, 2007).

Cooperation and cross-talk between innate immune receptors are common in macrophages which facilitate a tailored and optimal host response to a pathogen. An example of such cooperation is the synthesis and secretion of mature IL-1β. IL-1β mRNA expression is driven downstream of TLR-activation, but the release of pro-inflammatory IL-1β depends on the activation of caspase-1, which is regulated by an NLR-containing complex, known as the canonical inflammasome (reviewed in Netea *et al*, 2010). Hence, secretion of the mature IL-1β requires signals from different PRRs, one from the TLR system and one from the NLR system. In addition to this canonical inflammasome, there are several reports describing the involvement of a non-canonical inflammasome pathway during the immune response to Gram-negative bacteria (Oficjalska *et al*, 2015; Aachoui *et al*, 2013; Case *et al*, 2013; Gurung *et al*, 2012; Rathinam *et al*, 2012). Instead of caspase-1 activation, this non-canonical inflammasome is dependent on the activation of murine caspase-11 (a homologue of caspase 4 and caspase 5 in humans). Caspase-11 is a caspase-1-like inflammatory protease which upon activation, leads to the maturation of IL-1α and secretion of the danger signal high-mobility group box 1 (HMGB1). This pathway is initiated specifically by TLR4 via the TRIF-dependent signalling pathway. TLR4 senses cytosolic LPS and activation of the TRIF-cascade leads to expression of more Type I IFN commonly IFNβ. Whether the activation of the Type I IFN signalling pathway induces pro-caspase-11 expression, in which the expression itself is sufficient for caspase-11 autoactivation (Rathinam *et al*, 2012), or requires an additional as yet unknown bacterial signal (Broz *et al*, 2012), still remains in controversy. Last but not least, activation of caspase-1 and caspase-11 lead to pyroptotic cell death, an efficient strategy to limit bacterial replication and hence, intracellular survival of pathogens (Aachoui *et al*, 2013; Breitbach *et al*, 2009; Cervantes *et al*, 2008; Raupach *et al*, 2006).

In this study, we evaluated the contribution of MyD88- and TRIF- dependent signalling in controlling the intracellular fate of *B. pseudomallei* in BALB/C BMDMs. Despite the

importance of macrophages as innate immune cells, *B. pseudomallei* manipulates macrophages as a vehicle for bacterial dissemination and forms multi-nucleated giant cells (MNGC) (Kespichayawattana *et al*, 2000). *B. pseudomallei* uses actin-based motility to move intra- and intercellularly (Stevens *et al*, 2005), therefore evading recognition by macrophage cell-autonomous pathways and survives intracellularly. We observed an impaired survival of the Δ*bimA* mutant previously at 16 hpi, a mutant that is unable to establish actin-based motility. We would like to investigate if the impaired survival of the Δ*bimA* mutant at 16 hpi in BALB/C BMDMs could be mediated by the MyD88- or TRIF-signalling pathways. If one of these pathways is involved, inhibiting the pathway would restore the bacterial intracellular survival. To address this question, we utilised a gene silencing technique using short interfering RNAs (siRNAs) to knockdown the MyD88 transcripts, and in a separate experiment using MyD88- or TRIF-blocking peptides. Then we assayed the intracellular survival of *B. pseudomallei* WT and Δ*bimA* mutant strain as described previously.

Activation of a TLR signaling cascade leads to the downstream activation of canonical and non-canonical inflammasome pathways which are both essential for host innate immunity against *B. pseudomallei* (Bast *et al*, 2014; Aachoui *et al*, 2013; Breitbach *et al*, 2009). We investigated the maturation of caspase-1 and caspase-11 by Western blot. In addition, secretion of the proinflammatory cytokines IL-1α and IL-1β into the supernatant of infected macrophages were measured by enzyme-linked immunosorbent assay (ELISA). This thesis chapter aims to gain more insight into the role of MyD88- and TRIF-dependent signalling, as well as the inflammasomes, in BALB/C BMDMs during infection with *B. pseudomallei* WT and the Δ*bimA* mutant. The specific aims of the work described in this chapter are:

1) To assess macrophage activation by measuring TNF-α secretion
2) To identify other cytokines/chemokines expressed in *B. pseudomallei*-infected BMDMs using a Profiler Mouse Cytokine Array
3) To investigate if MyD88- or TRIF- dependent signalling pathway affect the intracellular survival of *B. pseudomallei* WT and Δ*bimA* strains in BMDMs
4) To investigate activation of the canonical and non-canonical inflammasomes upon infection of BMDMs with both WT and Δ*bimA B. pseudomallei* strains

4.2 RESULTS

4.2.1 BALB/C macrophages are activated upon infection with *B. pseudomallei*, as indicated by TNF-α secretion

Macrophages are major producers of pro-inflammatory cytokines such as TNFα. TNFα has been shown to play a central role in regulating the cytokine cascade in many inflammatory disease states and is therefore regarded as a 'master regulator' of inflammatory cytokine production (reviewed in Parameswaran & Patial, 2010). Here we measured the secretion of TNFα to indicate the activation of macrophages upon infection with *B. pseudomallei*. BMDMs were infected at an MOI of 2 with two different strains, the WT and the Δ*bimA* mutant at three different time points (2 hpi, 8 hpi and 16 hpi). TNFα secretion into the supernatant of the infected cells was measured by ELISA, and data from three independent experiments (each with duplicate technical replicates) plotted (Figure 4.1). At 2 hpi, secretion of TNFα was below the detection limit of the assay for all samples, suggesting a delay in macrophage activation. The TNFα concentration increased significantly at 8 hpi and 16 hpi in BMDMs infected with either WT or Δ*bimA* strain when compared to the uninfected control cells. At 8 hpi, BMDMs infected with the WT strain secreted about 115pg/ml of TNFα, a similar level to that observed at 16hpi (~111pg/ml). While in BMDM cells infected with the Δ*bimA* strain, the TNFα secretion at 8hpi was about 85pg/ml, and slightly decreased to 64pg/ml at 16 hpi. The observed delay in macrophage activation could be due to the absence of a priming agent such as IFNγ in our cell system. Pre-activation of macrophages with IFNγ would prevent the bacteria from escaping the phagosome and enter the cytosol as shown by Utaisincharoen *et al,* (2004) and Myers *et al* (2003). On the other hand, quiescent/resting macrophages ensures the survival of intracellular bacteria via rapid phagosomal escape followed by replication in the cytosol (Tsang *et al*, 2000). Therefore our *in vitro* system, where we do not use a priming agent, is more suitable for studies with the purpose of investigating innate mechanism/s involved in detection and clearance of cytosolic *B. pseudomallei*.

TNFα secretion in response to infection of BMDMs with WT *B. pseudomallei* was much less than the levels of TNFα secreted in response to *E.coli* LPS (500ng/ml), which produced about 587pg/ml of TNFα after 8 hours of stimulation (~5-fold higher)(Figure 4.1). It has been

suggested previously that the relatively weaker level of macrophage activation by *B. pseudomallei* may be correlated with its unique LPS structure, which is significantly different from that of other Gram-negative bacteria (Utaisincharoen *et al*, 2000).

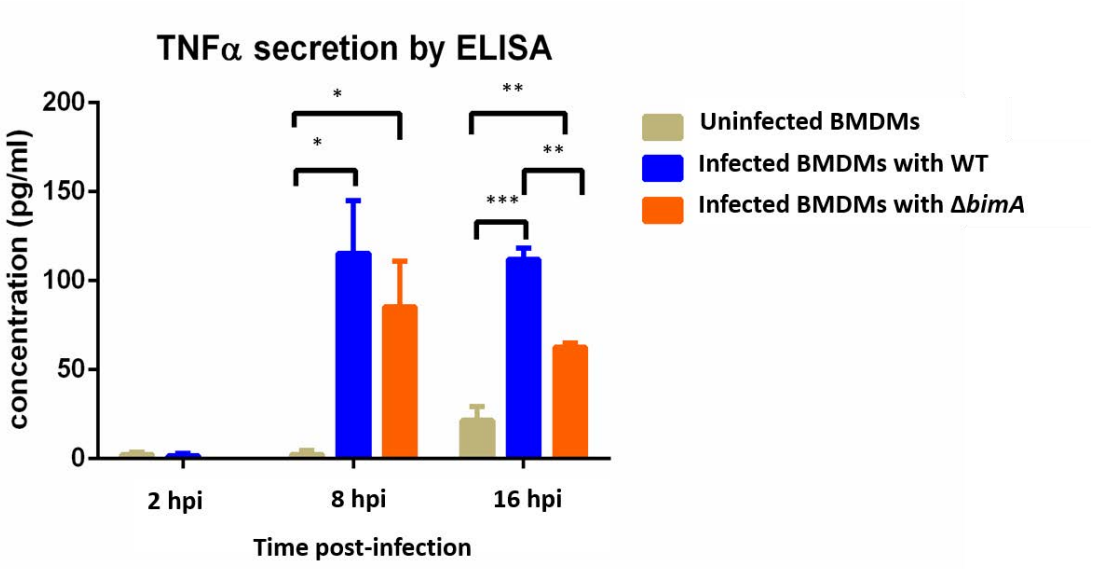

Figure 4.1 Secretion of the inflammatory cytokine TNF-α by infected BMDMs. BMDMs were seeded at 1 x 10^5 cells per well in 96-well plate, followed by infection with *B. pseudomallei* WT (blue) or the Δ*bimA* mutant (orange) at 2, 8 and 16 hpi. The concentration of TNFα (pg/ml) in the supernatant of uninfected BMDMs (beige) or infected BMDMs were then calculated at the indicated time points by ELISA as shown in *Materials and Methods 2.11*.The bar chart represents the mean + SE from three independent experiments. The statistical analysis was done using a Student's t-test between two groups as indicated where * = $p < 0.05$, ** = $p < 0.01$, *** = $p < 0.001$.

4.2.2 Several other *B. pseudomallei*-induced cytokines and chemokines can be detected in infected BMDM lysates using the Profiler Mouse Cytokine Array

Besides TNF- α, we were also interested in identifying other cytokines or chemokines produced in *B. pseudomallei*-infected BALB/C BMDMs, and to assess if their production is distinct in cells infected with the *B. pseudomallei* WT strain from those infected with the Δ*bimA* mutant strain at 8 hpi and 16 hpi. The high-throughput Mouse Cytokine Array (Panel A) can detect 40 cytokines and chemokines in a single array. This was utilised as an initial screen to identify any candidate differentially expressed molecules, which would later be validated on multiple samples using an alternative cost-effective assay, for example an ELISA. BMDMs were infected with *B. pseudomallei* WT or the Δ*bimA* strain as described in section 2.6 for 8 hpi and 16 hpi. For the positive control, BMDMs were stimulated with *E. coli* LPS for 8 hours. Uninfected BMDMs at respective time points served as a baseline for concentration fold-change calculations. At respective time points, cells were lysed in 1% Triton X-100 in PBS for 5 minutes. The cell lysates were mixed with a cocktail of biotinylated detection antibodies followed by incubation with the array, which is spotted in duplicate with capture antibodies to specific target proteins. The array was then incubated with IRDye 800CW Streptavidin and scanned using a LI-COR Odyssey Infrared Imaging System. After scanning, the spot intensities were quantified using Image Studio software (Figure 4.2 and Figure 4.3). The intensity of each spot is proportional to the amount of analyte bound.

We included BMDMs incubated with 500ng/ml LPS for 8 hours as a positive control to ensure that the BMDMs were competent and produced cytokines/chemokines in response to LPS. LPS is a ligand for TLR4 and can stimulate both MyD88- and TRIF-dependent pathways (reviewed in Takeda & Akira, 2004). In comparison with the uninfected cells 8 hpi, it is clear that the expression of many cytokines and chemokines increased in response to LPS treatment (Figure 4.2). The elevated cytokines include TNF-α, IFNγ, IL-1α, IL-1β, IL-2, IL-6, IL-10, IL-17, IL-23, of which all are pro-inflammatory except the anti-inflammatory cytokine IL-10. While the increased chemokines included CXCL10, CXCL1, CCL2, CCL12, CCL4, CXCL2, RANTES/CCL5. Some spots did not appear on the array of the samples from the uninfected cells, but appeared at high intensity for this positive control array.

At 8 hpi infection, BMDMs infected with either the *B. pseudomallei* WT or Δ*bimA* mutant strains displayed a slightly increased production of IL-1α, IL-1β, CXCL10, CXCL11, CXCL2 and TNFα with a fold-change exceeding 1.5, but less than 2.6. BMDMs infected with the WT strain demonstrated an increase in IL-12p70 and IL-13 proinflammatory cytokines, but these were not increased in cells infected with the Δ*bimA* mutant. While at 16hpi infection, pro-inflammatory cytokines IL-1α and IL-1β, and the chemokine CXCL12 were induced upon infection, both with *B. pseudomallei* WT and the Δ*bimA* mutant (<5.0 fold change). Furthermore, there were several other cytokines and chemokines that were elevated in response specifically to the Δ*bimA* mutant namely GM-CSF, IL-6, IL-17, IL-23, and RANTES/CCL5. IL-17 has been described previously as an inflammatory initiator as it can induce many pro-inflammatory cytokines such as TNFα, IL-1β and IL-6 in macrophages (reviewed in Gaffen, 2008; Jovanovic *et al*, 1998), while IL-23 could in turn increase the expression of IL-17. While RANTES/CCL5 plays an active role in recruiting immune cells including macrophages as a part of the inflammatory response (Hiura *et al*, 1999). We chose IL-1α and IL-1β to be validated with a more sensitive ELISA. ELISA data for the secretion of IL-1α and IL-1β, which are the downstream products of the activation of non-canonical and canonical inflammasomes respectively, is described in later sections.

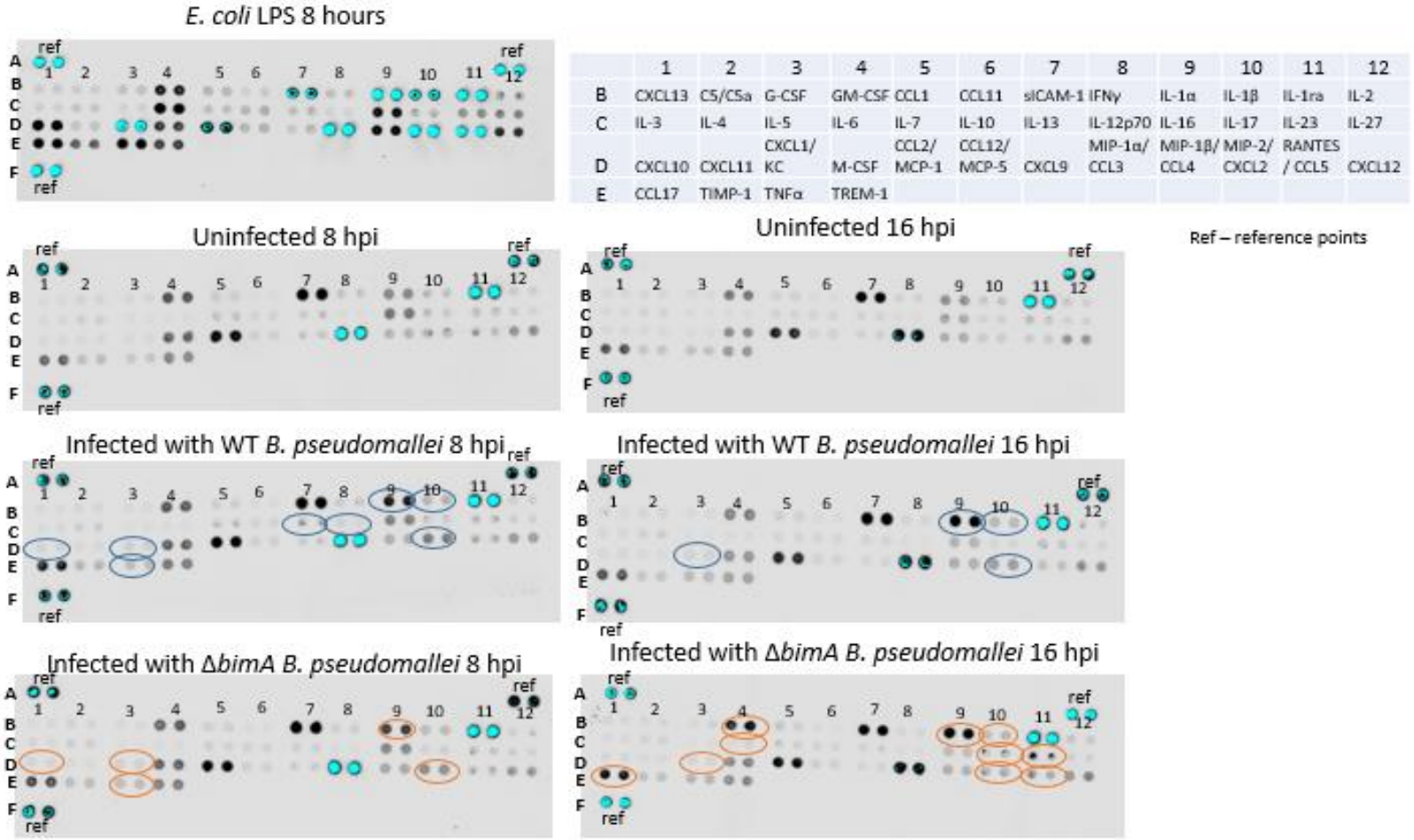

	1	2	3	4	5	6	7	8	9	10	11	12
B	CXCL13	C5/C5a	G-CSF	GM-CSF	CCL1	CCL11	sICAM-1	IFNγ	IL-1α	IL-1β	IL-1ra	IL-2
C	IL-3	IL-4	IL-5	IL-6	IL-7	IL-10	IL-13	IL-12p70	IL-16	IL-17	IL-23	IL-27
D	CXCL10	CXCL11	CXCL1/ KC	M-CSF	CCL2/ MCP-1	CCL12/ MCP-5	CXCL9	MIP-1α/ CCL3	MIP-1β/ CCL4	MIP-2/ CXCL2	RANTES / CCL5	CXCL12
E	CCL17	TIMP-1	TNFα	TREM-1								

Figure 4.2 Global cytokine and chemokine response determined using a Proteome Profiler Mouse Cytokine Array. The table on the upper right shows the analytes detected and their location on the membrane. The circled spots are those with increased levels of cytokine/chemokine (>1.5 fold change) in cell lysate from cells infected either with *B. pseudomallei* WT (blue circle) or Δ*bimA* (orange circle), as compared to the uninfected cell lysate at the respective hour post-infection (hpi). Images were obtained using an LI-COR Odyssey Infrared Imaging System and processed using Image Studio Lite 4.0 software. Blue spots = saturated signal.

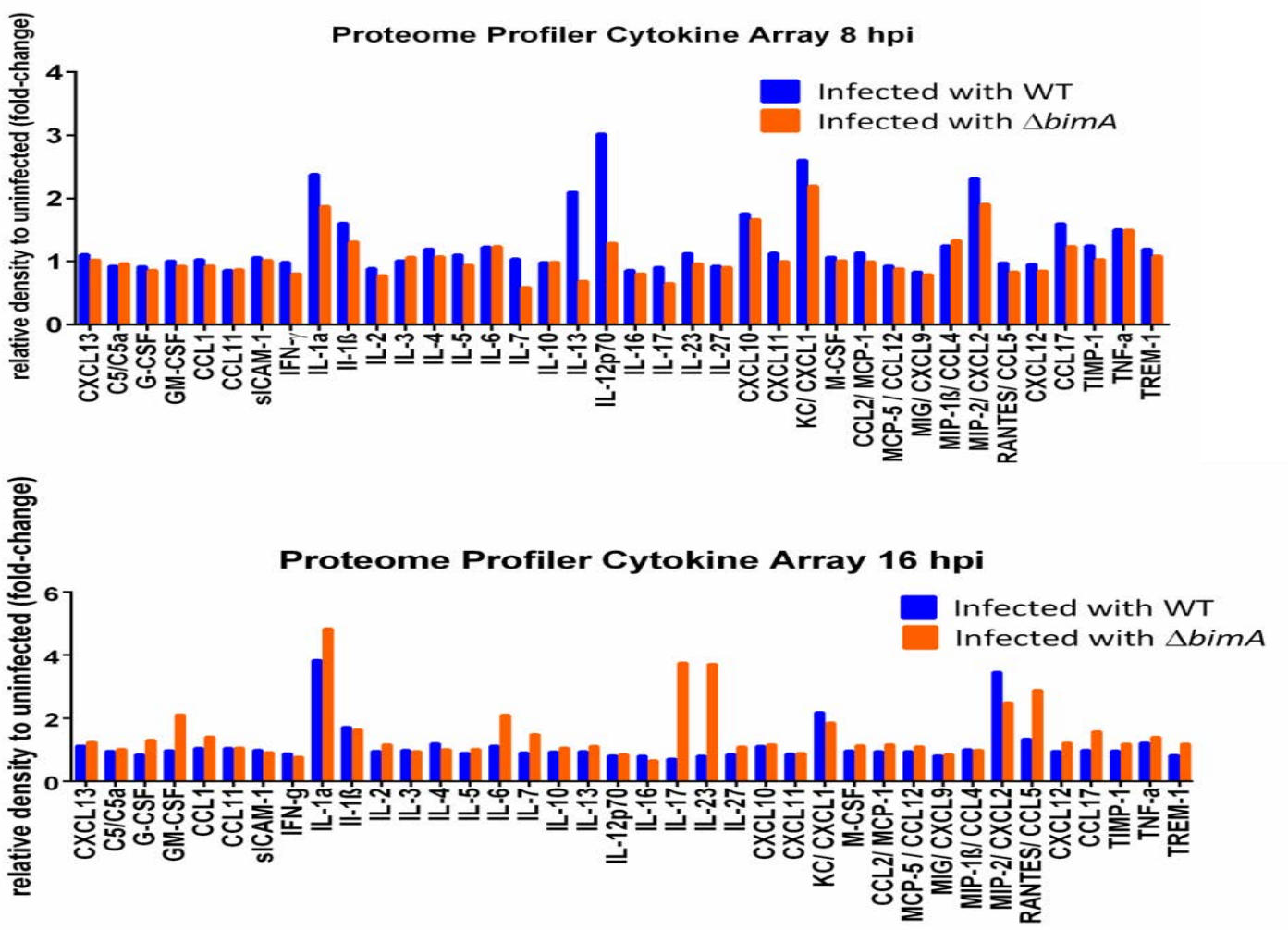

Figure 4.3 Relative levels of different cytokines/chemokines using a Proteome Profiler Cytokine Array. The cytokines/chemokines in the cell lysates of BMDMs infected either with *B. pseudomallei* WT (blue) or Δ*bimA* (orange) were compared with those in uninfected BMDMs at 8 hpi (top) and 16 hpi (bottom). Data obtained from a single experiment.

4.2.3 MyD88 depletion and inhibition do not affect the intracellular survival of *B. pseudomallei*

To investigate the role of MyD88-dependent signalling in response to intracellular *B. pseudomallei*, we utilised RNA interference (RNAi) to silence MyD88 gene expression post-transcriptionally in BALB/C BMDM cells. There is no available BALB/C MyD88 knockout mouse, hence the need for gene silencing instead. In the cell cytoplasm, exogenous dsRNA is initially recognised by the Dicer protein, an RNase that processes the dsRNA into 21-23 nucleotide short interfering RNA molecules (siRNA). The siRNAs and target RNA form a complex with the RNA-induced silencing complex (RISC) which cleaves any complementary mRNA, thus silencing the target gene. Delivery of exogenous siRNA into primary macrophages is technically difficult and challenging, but there are several reports of successful gene silencing in primary macrophages using lipid-based transfection methods (Jensen *et al*, 2014; Troegeler *et al*, 2014; Zhang *et al*, 2009). Electroporation is less preferable as this method can cause a high proportion of cell death (Jensen *et al*, 2014). A short siRNA sequence of less than 30 base pairs should not induce a potent interferon response, an innate immune response of macrophages in recognition of viral RNA (Reynolds *et al*, 2006). Furthermore, the transfection of a low concentration of synthetic RNA (<100μM) does not detrimentally affect cell viability (Jensen *et al*, 2014; Reynolds *et al*, 2006).

Pre-designed MyD88 siRNA was purchased from Ambion Life Technology (Silencer Select Pre-designed siRNA). siRNA was then delivered into BMDMs using Lipofectamine RNAiMAX (Invitrogen), a transfection reagent that consistently gives the best target gene-knockdown with minimal cytotoxicity and IFN-induced response as reported by Jensen *et al* (2014). Lipofectamine reagents are formulated from cationic lipids which form liposomes in aqueous conditions. The positively charged liposomes form complexes with nucleic acid to form liposome: nucleic acid transfection complexes which interact with the negatively charged cell membrane before entering cells through endocytosis. These 'liposomes' not only assist the cellular uptake of siRNA but also prevent endogenous enzymatic degradation during endocytosis (Gooding *et al*, 2012). The BMDMs were transfected with a mixture of Lipofectamine: siRNA at a final concentration of 70μM for 24 hours. The medium was then replaced with fresh medium and the cells cultured for a further 24 hours before being infected with *B. pseudomallei* WT or the Δ*bimA* strain. These conditions were used to minimise the off-

target effects caused by the transfection reagents as demonstrated in Jensen *et al* (2014). We included MISSION Universal Negative siRNA control (Sigma-Aldrich) at the same concentration in each experiment as a non-targeting siRNA control. This siRNA control does not share homology with any known mammalian gene. Transfection with the siRNA targeting mouse MyD88 resulted in statistically significant knockdown of 70% in BALB/C BMDMs as compared to the non-targeting negative control (Figure 4.4 (A) and (B)). The efficiency of gene silencing was determined by RT-PCR (reverse transcriptase PCR) and normalised to the expression of β-actin. The role of MyD88 in phagocytosis remains in debate as one study reported that MyD88-deficiency reduces the phagocytic activity of macrophages (Blander & Medzhitov, 2006), whilst Laroux *et al* (2005) found no difference in phagocytosis of MyD88-deficient macrophages by FACS-based analysis. In our studies, depletion of *MyD88* does not obviously impair the phagocytic activity of BMDMs as observed by confocal microscopy (Figure 4.4 (C)).

After establishing the conditions for MyD88 gene silencing in BMDMs, we measured bacterial intracellular survival by carrying out the kanamycin-protection assay as described previously. The experiment showed that depletion of MyD88 did not improve the intracellular survival of either the *B. pseudomallei* WT or Δ*bimA* mutant strain, as there was no difference in CFU between MyD88-depleted and non-depleted BMDMs at all three time points of 2 hpi, 8 hpi and 16 hpi (Figure 4.5). These data suggest that the impaired survival of the Δ*bimA* mutant at 16 hpi is not dependent on MyD88, as depletion of MyD88 does not rescue the bacterial intracellular survival defect.

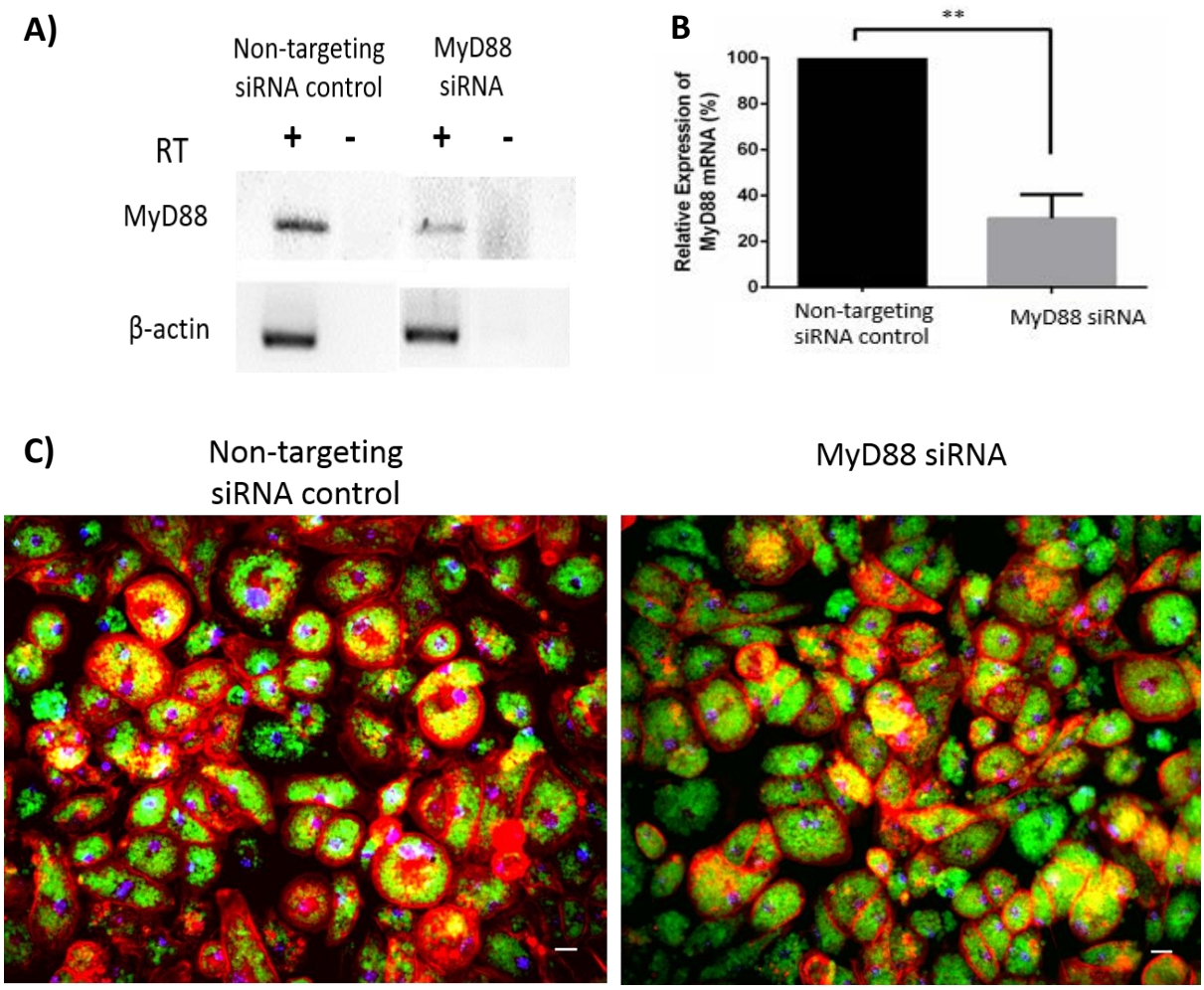

Figure 4.4 Knockdown efficiency of siRNA targeting MyD88 in BALB/C BMDMs and phagocytosis assay of siRNA-treated BMDMs. (A) RT-PCR analysis of MyD88 knockdown efficiency in BMDMs as compared to the control. BMDMs were seeded at density of 5 x 10^5 cells per well in 24-well plates. BMDMs were then transfected with MyD88 siRNA or non-targeting siRNA control using Lipofectamine as described in *Materials and Methods 2.14.1*. The β-actin gene was used as a control gene for normalisation. Densitometric quantification was performed using Image J software and is represented by the bar chart (B). (B) Bar chart represents the means + S.E. of three independent experiments. Statistical analysis was done using unpaired Student's t-test between MyD88 siRNA-treated and non-targeting siRNA-treated as a control, **$p<0.01$. (C) Confocal microscopy images of BALB/C BMDMs with phagocytosed fluorescently-labelled Zymosan beads (green). BMDMs were seeded on coverslips at 5 x 10^5 per well in 24-well plates. BMDMs were pre-treated with non-targeting siRNA (left) or MyD88 siRNA (right) before incubating with the beads for an hour, followed by fixation as described in *Materials and Methods 2.14.1 and 2.4*. The cell nuclei were stained with DAPI (blue) and the actin was stained with phalloidin (red). Images were captured using a Leica DMLB fluorescence microscope and analysed with Image J software as described in *Materials and Methods 2.9*. Scale bar represents 20μm.

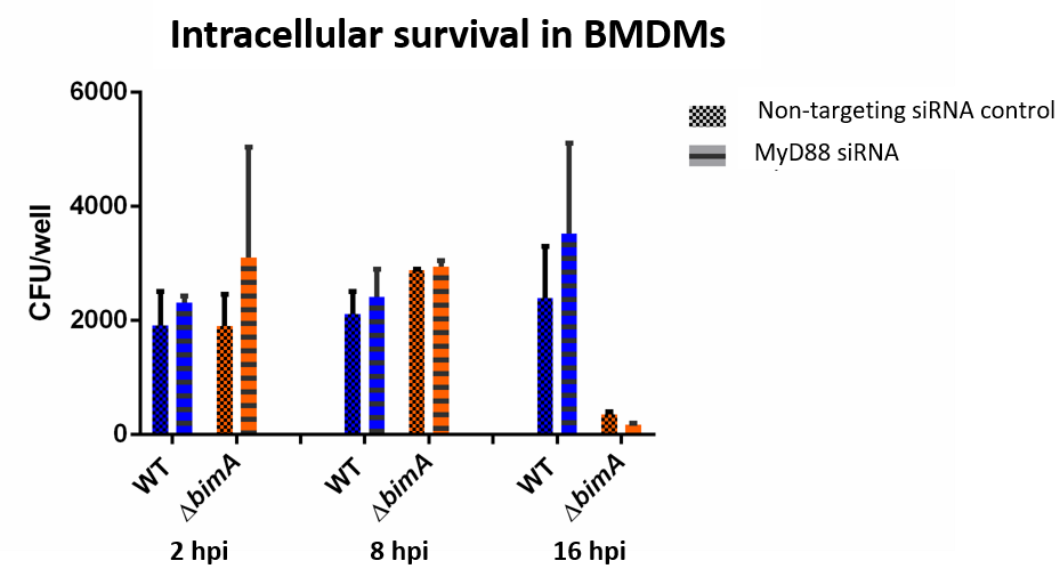

Figure 4.5 Bacterial intracellular survival in siRNA-treated BMDMs. BMDMs pre-treated with non-targeting siRNA (checked bars) or MyD88 siRNA (horizontal striped bars) were infected with *B. pseudomallei* WT (blue bar) or the Δ*bimA* mutant strain (orange bar) at an MOI of 2, for 2 hpi, 8 hpi and 16 hpi. The assay was carried out in a kanamycin-protection manner as described previously in *Materials and Methods 2.6*. The data represent the means + SE from two independent experiments. Statistical analysis was done using unpaired Student's t-test between CFU in negative control- and MyD88-siRNA treated BMDMs of the respective strains and time points.

Depletion of MyD88 mRNA may not necessarily correlate with reduced protein levels within the BMDMs so we also performed experiments using a pharmacological inhibitor of MyD88 activity. We inhibited MyD88 pharmacologically in BALB/C BMDMs using the MyD88 homodimerisation inhibitor purchased from Novus Biologicals (NBP2-29328). The MyD88 protein possesses a death domain (DD) at the N-terminus and a Toll/IL-1R receptor (TIR) domain at the C-terminus separated by a short linker domain. The TIR domain is also present in the TLR/IL-1R receptor where upon ligand stimulation, MyD88 is recruited to the receptor by this TIR-TIR interaction. TIR domains of both MyD88 and the receptor TLR/IL-1R have a common structure composed of five β-strands alternating with five α-helices, connected by loops. A loop known as the BB loop connects the second β-strand and the second α-helix and is crucial for MyD88 homodimerisation, and activation of the TLR/MyD88 signalling pathway (Loiarro *et al*, 2005; Xu *et al*, 2000; Poltorak *et al*, 1998). The MyD88 inhibitor is designed to bind to the TIR domain of MyD88 to block its homodimerisation. The inhibitor contains a sequence from the MyD88 TIR homodimerisation domain (RDVLPGT) (Loiarro *et al*, 2005) preceded by a protein transduction sequence derived from *Drosophila* known as the Antennapedia homeodomain (RQIKIWFQNRRMKWKK) to facilitate the translocation of the peptide through the cell membrane (Derossi *et al*, 1994). The control peptide in this experiment was a peptide consisting of the Antennapedia sequence only.

We pre-treated the BMDMs with 100μM inhibitory peptide or its peptide control for 24 hours as recommended by the manufacturer and also as described previously (Murshid *et al*, 2015; Nguyen *et al*, 2010). This was then followed by stimulation with 4μg/ml TLR2 agonist Pam3-Cys-Ser-Lys4 (Pam3CSK4) for the next 24 hours. Pam3CSK4 is a synthetic bacterial lipopeptide which is the prototype ligand for the heterodimeric TLR1/TLR2 complex. TLR2 propagates its signalling solely through the MyD88 adaptor protein and does not appear to use a MyD88-independent arm for signal transduction (reviewed in Takeda & Akira, 2004). Upon ligand binding to TLR, the downstream signalling cascade via MyD88 induces activation of the transcription factor NF-κB or AP-1, leading to expression of various proinflammatory cytokines such as IL-6 and IL-1β. IL-6 and IL-1β expression are dependent on MyD88 as macrophages from MyD88-knockout mice are unable to produce such cytokines upon activation with LPS (Kawai *et al*, 1999). To demonstrate that the MyD88 peptide was active in our hands, we measured the mRNA expression of IL-6 and IL-1β by qPCR. We determined that in the presence of the TLR2 agonist Pam3CSK4 alone, that the mRNA expression of IL-6 and IL-1β increased by approximately 400- and 70- fold as compared to unstimulated BMDMs

(Figure 4.6). In the presence of both the MyD88 peptide inhibitor and TLR2 agonist, we achieved a reduction in IL-6 and IL-1β mRNA expression of about 35% and 25% respectively, as compared to the peptide control (Figure 4.7). Phagocytic activity was not affected by the MyD88-blocking peptide as shown in Figure 4.8. This is the optimum reduction that we could achieve since increasing the peptide concentration did not lead to a further increase in inhibition of the TLR2 response, in fact it resulted in more cell death (data not shown). Even use of the MyD88-control peptide and MyD88-inhibitory peptide at 100μM resulted in 22.7±2.99 % and 21.5±2.98% cell cytotoxicity respectively, as determined using an LDH release assay (data not shown).

To evaluate the impact of MyD88 inhibition on *B. pseudomallei* intracellular survival in BMDMs, we performed a kanamycin protection assay as described previously. After pre-treating the BMDMs with MyD88 inhibitor or the control peptide for 24 hours, the BMDMs were infected with *B. pseudomallei* and viable counts obtained at 2 hpi, 8 hpi and 16 hpi. The results show that MyD88 is unlikely to play a role in intracellular survival of either the *B. pseudomallei* WT or the Δ*bimA* mutant strain at any of the time points tested. There was no difference in CFU numbers in BMDMs-treated with the MyD88 inhibitor compared to the control peptide, similar to the result obtained using siRNA targeted gene knockdown (figure 4.9). Despite the importance of MyD88 in innate immune pathways, we found that MyD88 deficiency in BMDMs fails to increase the growth of *B. pseudomallei* intracellularly, indicating that alternative pathways are likely required for detection and elimination of the bacterium. An alternative explanation could be that knocking down the gene by siRNA did not abrogate the gene expression enough to lead to an effect. The small amount of residual MyD88 gene expression could be adequate for MyD88-dependent signalling. Similarly, the imperfect blocking of MyD88 function may not have resulted in a significant suppression of the function of the MyD88-mediated immune response. The latter possibility could be tested in future by application of CRISPR-Cas9 (Clustered Regularly Interspaced Short Palindromic Repeats-CRISPR associated protein-9 nuclease) gene editing to delete the MyD88-encoding gene in BMDMs.

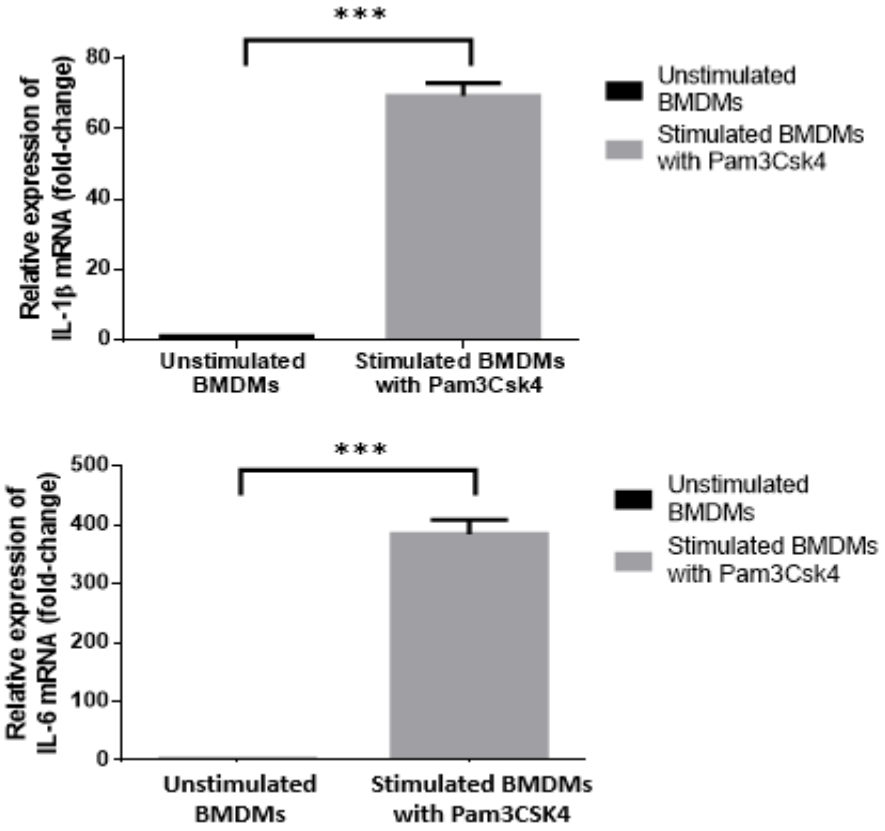

Figure 4.6 Relative expression of IL-1β (top) and IL-6 (bottom) as determined by qPCR in the presence of TLR2 agonist Pam3CSK4 as compared to unstimulated BMDMs. Total RNA from BMDMs was extracted after stimulation with (grey bar) or without Pam3CSK4 (black bar) for 24 hours as described in *Materials and Methods 2.16.* cDNA was then synthesised from the total RNA and qPCR was carried out as described in *Materials and Methods 2.17 and 2.19* respectively. GAPDH was used as a reference gene for normalisation. The data represent the means + SE of two independent experiments. Unpaired Student's t-test was used to determine the statistical significance in gene expression in the presence of TLR2 agonist as compared to unstimulated control without the agonist (***$p<0.001$).

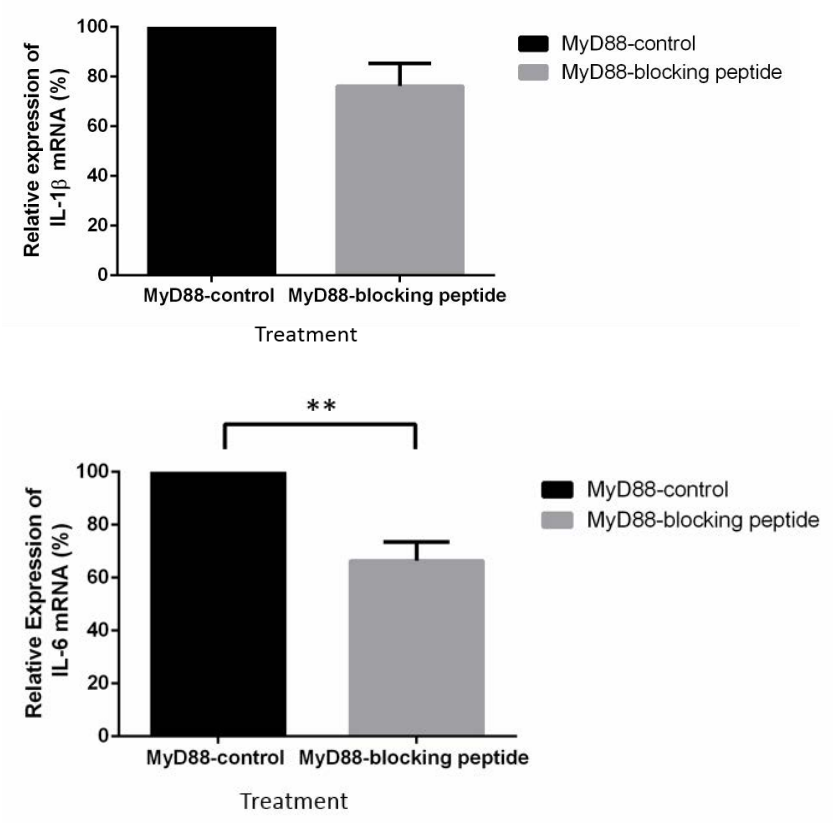

Figure 4.7 Relative expression of IL-1β (top) and IL-6 (bottom) genes as determined by qPCR upon different peptide treatments. Total RNA from BMDMs treated with MyD88-blocking peptide (black bar) or MyD88-control peptide (grey bar) was extracted after stimulation with TLR2 agonist Pam3CSK4 for 24 hours as described in *Material and Methods 2.16*. cDNA was then synthesised from the total RNA and qPCR was carried out as described in *Materials and Methods 2.17 and 2.19* respectively. GAPDH and Csnk2a2 were used as reference genes for normalisation. The data represent the means + SE of three independent experiments. Unpaired Student's t-test was used to determine the statistical significance in gene expression between the two different treatments (**$p<0.01$).

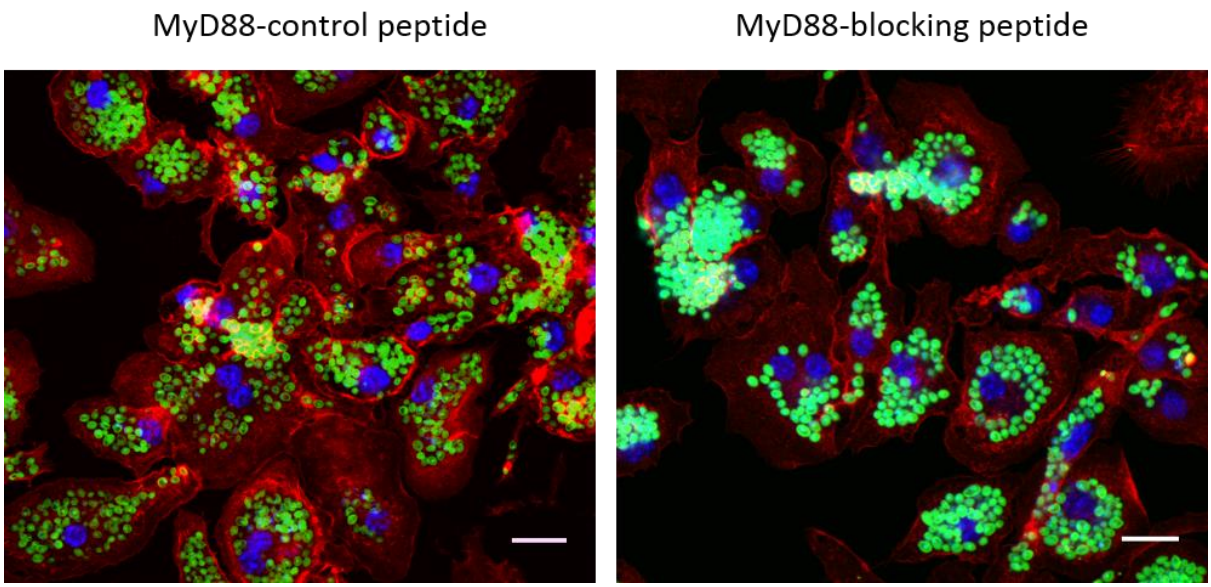

Figure 4.8 Phagocytosis assay of BMDMs pre-treated with control peptide (left) or MyD88-blocking peptide (right). Confocal microscopy images of BALB/C BMDMs with phagocytosed fluorescently-labelled Zymosan beads (green). BMDMs were seeded on coverlips at density of 5 x 10^5 per well in 24-well plates. BMDMs were first pre-treated with the respective peptide for 24 hours before incubating with the beads for an hour and fixation as described in *Materials and Methods 2.4*. The cell nuclei were stained with DAPI (blue) and the actin was stained with phalloidin (red) as shown in *Materials and Methods 2.9*. Images of a single plane were captured using a Zeiss LSM confocal laser scanning microscope and analysed with Image J software. Scale bar represents 20μm.

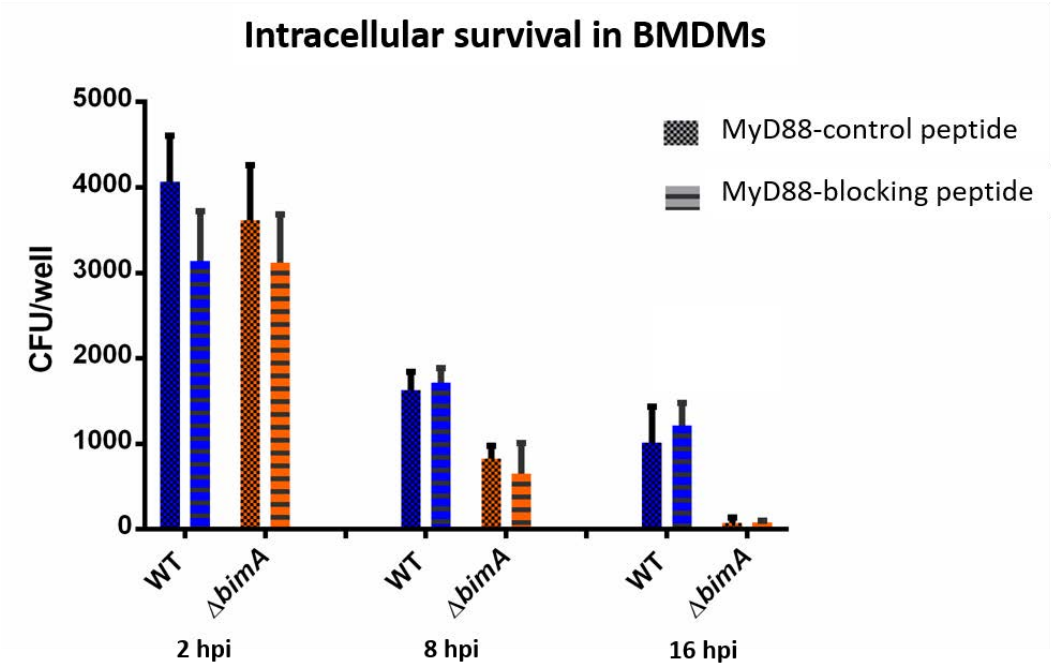

Figure 4.9 Bacterial intracellular survival in BMDMs pre-treated with MyD88-control peptide (checked bar) or MyD88-blocking peptide (horizontal-striped bar). The peptide-treated BMDMs were infected with *B. pseudomallei* WT (blue bar) or Δ*bimA* mutant (orange bar) at an MOI of 2, for three different time points of 2 hpi, 8 hpi and 16 hpi. The assay was carried out in a kanamycin-protection manner as described previously in *Materials and Methods 2.6*. The data represent the mean + SE from three independent experiments. Statistical analysis was performed using an unpaired Student's t-test between CFU in BMDMs pre-treated with two different peptides of respective strains and time points.

4.2.4 The TRIF-dependent pathway may be involved in the intracellular survival of *B. pseudomallei*

We next investigated the importance of the TRIF-adaptor protein in the host cell response to *B. pseudomallei*. We hypothesised that BMDMs may utilise TRIF-dependent TLRs to recognise and initiate the bacterial clearance. To investigate this, we used a TRIF-inhibitor known as Pepinh-TRIF (purchased from InvivoGen) to block TRIF-dependent signalling. As described for the MyD88-blocking peptide previously, Pepinh-TRIF is also designed to contain amino acids that correspond to the sequence of the BB loop of TRIF (FCEEFQVPGRGELH) (Toshchakov *et al*, 2005) linked to the cell-penetrating segment of the Antennapedia homeodomain (RQIKIWFQNRRMKWKK) (Derossi *et al*, 1994). This Pepinh-TRIF inhibitor blocks the TIR-TIR interaction of the TLR and the TRIF protein while the control peptide contains a scrambled peptide sequence (SLHGRGDPMEAFII) preceded with the Antennapedia homeodomain. TLR3 is the only TLR that is known to exert its effects through TRIF (MyD88-independent) alone (reviewed in Takeda & Akira, 2004). TLR3 recognises double-stranded RNA (dsRNA), a PAMP associated with viral infection and poly(I:C) is a synthetic analogue of dsRNA. Downstream of TLR3, TRIF activation of the interferon (IFN) regulatory factor (IRF)-3/7 pathway leads to secretion of Type I IFN (IFNα/IFNβ) (Yamamoto *et al*, 2003). Therefore, the effect of abrogating TRIF-dependent signalling can be determined by measuring IFNβ mRNA expression. To determine the efficiency of Pepinh-TRIF to block activity, we measured the gene expression of IFNβ after stimulation of BMDMs with the TLR3 agonist poly(I:C) (polyinosinic-polyctidylic acid). In the presence of poly(I:C), IFNβ mRNA expression increased by approximately 9-fold compared to unstimulated BMDMs (Figure 4.10).

We next pre-treated BMDMs with 40μM Pepinh-TRIF, or Pepinh-control as recommended by the manufacturer for 4 hours. Treating BMDMs with Pepinh-control and Pepinh-TRIF resulted in low cell cytotoxicity of 15.0$\pm$0.9 % and 16.2$\pm$2.88 % respectively, as determined by LDH release assay (data not shown). After incubation with the peptides for 4 hours, the cells were then stimulated with 25μg/ml of poly(I:C) for 6 hours. We then isolated the RNA from BMDMs and carried out qPCR to measure the expression of IFNβ. Application of the Pepinh-TRIF blocker to the Poly(I:C)-induced BMDMs resulted in a significant

reduction in IFNβ expression by approximately 60% (Figure 4.11 (A)), while the phagocytic activity was not affected by the inhibitor (Figure 4.11 (B)).

To assess whether the inhibitory activity of Pepinh-TRIF affects the course of intracellular survival of *B. pseudomallei*, we pre-treated the BMDMs with Pepinh-TRIF or the control peptide for 4 hours, followed by infection with *B. pseudomallei* strains. Viable counts were obtained at 2, 8 and 16 hpi in a kanamycin-protection manner as described previously. We included the *B. pseudomallei* Δ*bimA* mutant strain to investigate if the apparent intra-macrophage growth defect observed for the Δ*bimA* mutant is dependent on TRIF-dependent signalling. We hypothesised that if TRIF-dependent signalling is essential for cellular defence against *B. pseudomallei*, the bacterial intracellular load would be higher in the presence of the Pepinh-TRIF inhibitor compared to that in the presence of control peptide. The bar graph in Figure 4.12 shows that at 2 hpi and 8 hpi, the peptide inhibitor had no effect on bacterial survival as there were no differences in CFU counts in cells pre-treated with the control peptide or TRIF inhibitor. However, there was greater than a 3-fold increase in WT *B. pseudomallei* at the 16 hour time point in BMDMs pre-treated with Pepinh-TRIF inhibitor compared to the Pepinh-control. As expected, far fewer Δ*bimA* mutant bacteria were recovered compared to the WT strain at this time point. However, intracellular survival of the Δ*bimA* mutant was unaffected by the presence of the Pepinh-TRIF inhibitor. Although there was no statistically significant difference in CFU counts of WT bacteria between cells treated with Pepinh-TRIF and Pepinh-control, we believe that more independent repeats may reduce the high variability in the data and the results may become statistically significant. We hypothesise that TRIF-dependent signalling plays a role in intracellular survival of *B. pseudomallei*, but this pathway is less prominent for the Δ*bimA* mutant strain. Unfortunately, due to time constraints of the project we were unable to pursue this avenue of investigation any further.

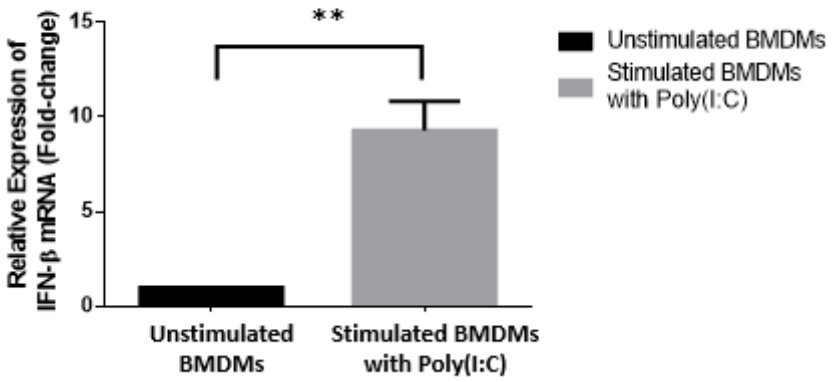

Figure 4.10 Relative expression of IFNβ in BMDMs as determined by qPCR in the presence of TLR3 agonist poly(I:C) as compared to unstimulated BMDMs. Total RNA from BMDMs was extracted after stimulation with or without poly(I:C) for 6 hours as described in *Materials and Methods 2.16*. cDNA was then synthesised from the total RNA and qPCR was carried out as described in *Materials and Methods 2.17 and 2.19* respectively. GAPDH and Csnk2a2 were used as reference genes for normalisation. The data represent the mean + SE of three independent experiments. Unpaired Student's t-test was used to determine the statistical significance in gene expression in the presence of poly(I:C) compared to unstimulated control (**$p<0.01$).

(A)

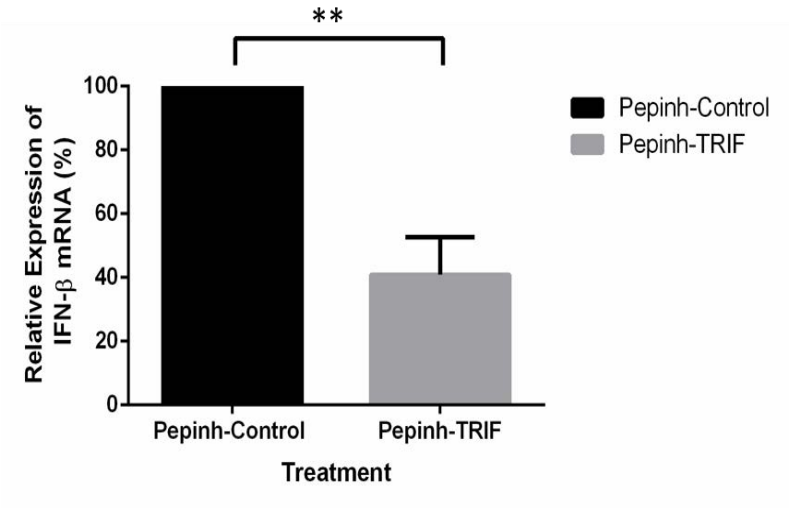

(B)

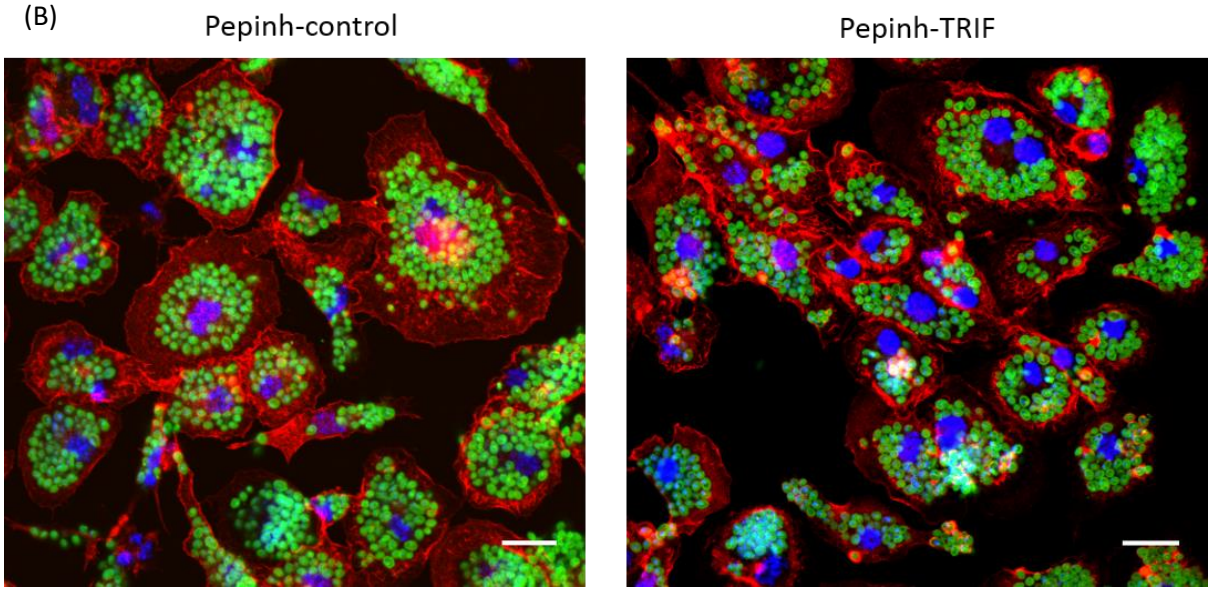

Figure 4.11 Relative expression of IFNβ and phagocytosis assay of BMDMs treated with different peptides. (A) Total RNA from BMDMs treated with Pepinh-control (black bar) or Pepinh-TRIF (grey bar) was extracted after stimulation with TLR3 agonist Poly(I:C) as described in *Materials and Methods 2.16.* cDNA was then synthesised from the total RNA and qPCR was carried out as described in *Materials and Methods 2.17 and 2.19* respectively. GAPDH and Csnk2a2 were used as reference genes for normalisation. The data represent the mean +_SE of three independent experiments. Student's t-test was used to determine the statistical significance in gene expression between the two different treatments. **p<0.01. (B) Confocal microscopy images of BALB/C BMDMs with phagocytosed fluorescently-labelled Zymosan beads (green). BMDMs were seeded on coverslips at density of 5 x 10^5 cells per well in 24-well plates. BMDMs were then pre-treated with Pepinh-control (left) or Pepinh-TRIF (right) before incubating with the beads for an hour and fixation as described in *Materials and Methods 2.4*. The cell nuclei were stained with DAPI (blue) and the actin was stained with phalloidin (red) as shown in *Materials and Methods 2.9*. Images were captured using a Zeiss LSM confocal laser scanning microscope and analysed with Image J software. Scale bar represents 20μm.

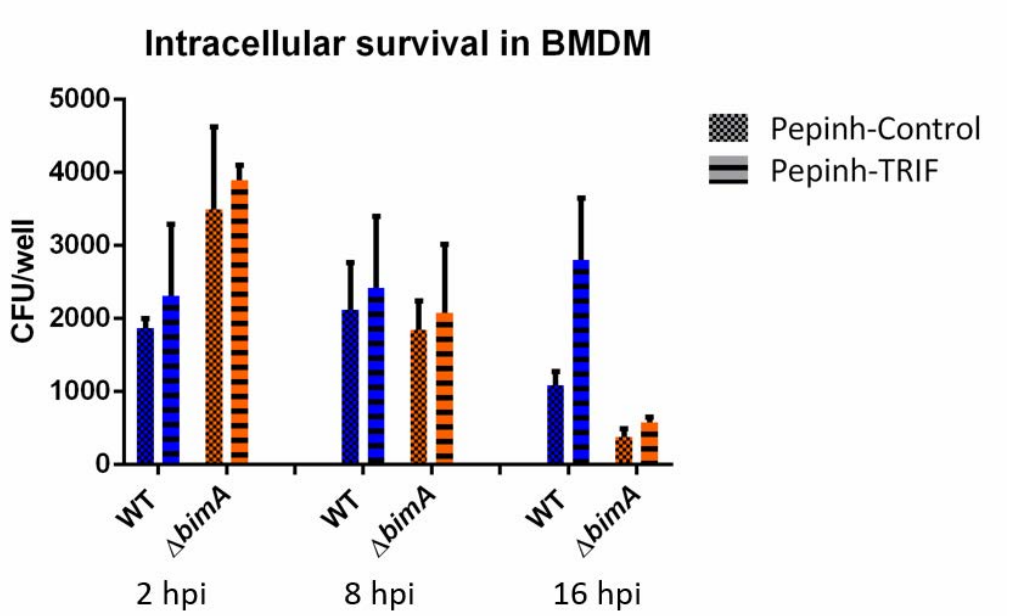

Figure 4.12 Bacterial intracellular survival in BMDMs pre-treated with Pepinh-control (left-bar) or Pepinh-TRIF (right bar). The pre-treated BMDMs were infected with *B. pseudomallei* WT (blue bar) or Δ*bimA* strains (orange bar) at an MOI of 2, for 2, 8 and 16 hpi. The assay was carried out in a kanamycin-protection manner as described previously in *Materials and Methods 2.6*. The data represent the mean + SE from three independent experiments. Statistical analysis was done using Student's t-test between CFU in pre-treated BMDMs with two different peptides of the respective strains and time points.

4.2.5 Non-canonical inflammasome activation upon *B. pseudomallei* infection of BALB/C BMDMs

Partially blocking the TRIF adaptor protein led to a trend towards improving the survival of intracellular *B. pseudomallei* at 16hpi, suggesting this pathway could be involved in the cellular response to *B. pseudomallei*. Several studies have shown that TRIF along with Type I IFNs mediate non-canonical inflammasome activation in response to the presence of Gram-negative bacteria namely *Escherichia coli, Citrobacter rodentium, Salmonella* Typhimurium and *Shigella flexneri* (Rathinam *et al*, 2012; Gurung *et al*, 2012; Broz *et al*, 2012) (Figure 4.13). The inflammasome is a multiprotein complex that assembles with members of the NOD-like receptor (NLR) and PYHIN protein families in response to PAMPs or danger signals. Upon inflammasome activation, procaspase-1 is cleaved to its active form of caspase-1 which then promotes the maturation of pro-inflammatory cytokines such as IL-1β and IL-18 (reviewed in Latz *et al*, 2013). The inflammasome is regarded as a key component of cytosolic surveillance. Recently, a new non-canonical inflammasome pathway has been described that activates caspase-11, a caspase-1 related protease (reviewed in Broz & Monack, 2013). Several studies suggest that bacterial LPS mediates the priming of caspase-11 and that activation is dependent on TRIF and Type I IFN (Casson *et al*, 2015; Kayagaki *et al*, 2013). At the transcriptional level, caspase-11 and genes involved in interferon signalling were found to be significantly up-regulated in BMDMs infected with *B. pseudomallei* (WT and Δ*bimA*) as demonstrated by our microarray analysis (refer to Chapter 5). Furthermore, the involvement of interferon-mediated signalling in infected BALB/C BMDMs as described in Chapter 5 is further supported by *in vivo* tissue transcriptomic changes in an acute animal model of melioidosis in BALB/C mice (Chin *et al*, 2010). The contribution of caspase-11-dependent mechanism in the pathogenesis of *B. pseudomallei* infection has been reported by Bast *et al* (2014). These findings together suggest that the non-canonical inflammasome pathway could potentially be an innate mechanism activated in response to intracellular *B. pseudomallei*.

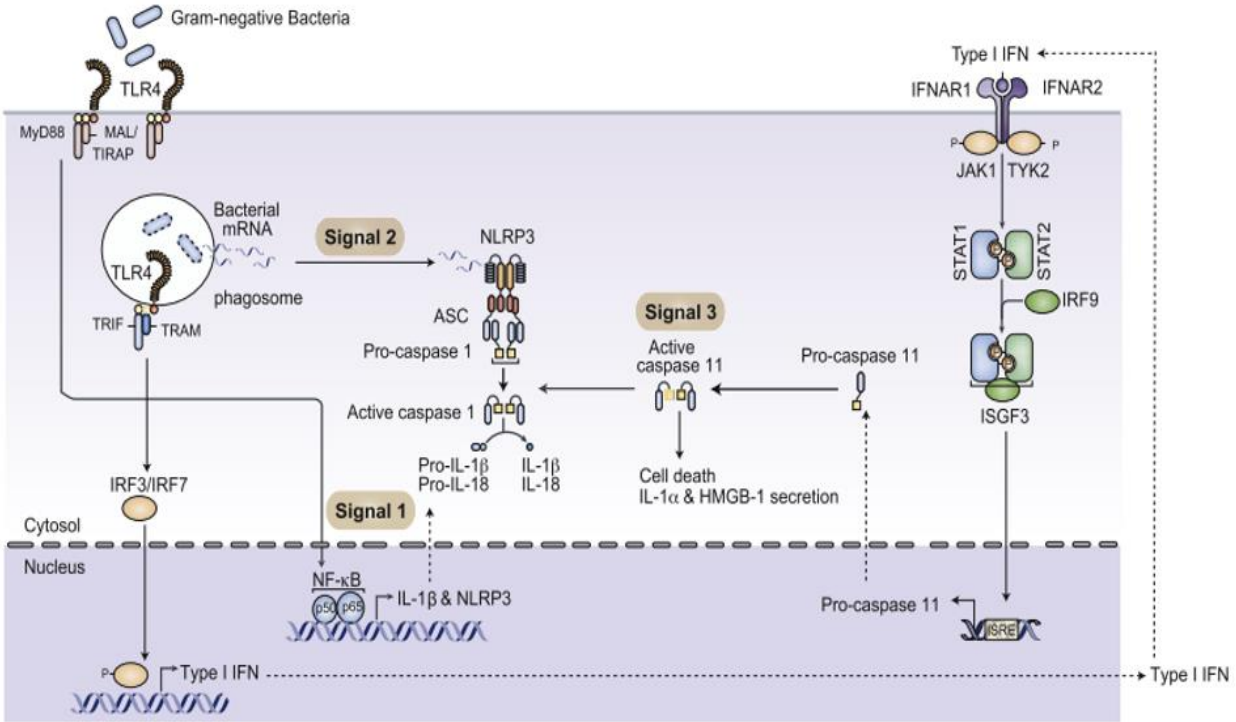

Figure 4.13 Proposed integrative model of TLR and NLR pathways during the inflammatory response to Gram-negative bacteria. Activation of the TLR4-TRIF-dependent pathway in sensing cytosolic Gram-negative bacteria upregulates the expression of Type I IFN. Increase in Type I IFN signalling induces the expression of caspase-11 and its processing into active caspase-11 (signal 3), which leads to cell death and secretion of endogenous alarmins IL-1α and HMGB-1. While activation of TLR4 through the MyD88 adaptor protein switches on the transcription of IL-1β and Nlrp3 mRNA (signal 1). Different stimuli such as bacterial mRNA in the cytosol triggers NLRP3 inflammasome assembly (signal 2). The NLRP3 complex together with activated caspase-11 synergises the activation of caspase-1 and maturation of pro-inflammatory cytokines IL-1β and IL-18 (figure reprinted from Rathinam, V.A.K. *et al* (2012). TRIF licenses caspase-11-dependent NLRP3 inflammasome activation bu Gram-negative bactreia. *Cell*, 150(12), 606-619, Copyright © 2012, with permission from Elsevier).

To directly examine the activation of the non-canonical inflammasome by *B. pseudomallei*, we analysed caspase-11 maturation in cell lysates of BMDMs infected with *B. pseudomallei* WT and the Δ*bimA* mutant strain. Pro-caspase-11 transcription is largely induced through activation of Type I IFN signalling via the TRIF-adaptor protein (Rathinam *et al*, 2012; Broz *et al*, 2012). Nevertheless, resting macrophages or dendritic cells (DCs) still express low levels of pro-caspase-11, as additional pathways could also contribute to its expression (Freigang *et al*, 2013; Broz *et al*, 2012). However, whether the processing of procaspase-11 into its active form involves an auto-activation mechanism (Rathinam *et al*, 2012) or requires an as yet undefined bacterial signal (Broz *et al*, 2012) remains controversial. We carried out Western blots to detect the level of pro-caspase-11 (43kDa) and its processing into active caspase-11 (30kDa) from three independent experiments (Figure 4.14). We then measured the intensity of the indicated bands and carried out relative densitometry analysis using ImageJ software.

The caspase-11 locus encodes two isoforms of 43kDa and 38kDa, but the antibody used in this studies only detects the 43kDa species according to the manufacturer's description. The processed form of caspase-11 is about 30kDa. Pro-caspase-11 levels were slightly higher in BMDMs infected with the *B. pseudomallei* Δ*bimA* mutant in one experiment. However, when the experiment was repeated a further two times, there was no statistical difference in pro-caspase-11 in BMDMs infected with either the Δ*bimA* strain or the WT strain in comparison to uninfected BMDMs at all-time points (Figure 4.12 (A)). Despite no statistical significance in the data we observed a trend towards higher levels of cleaved caspase 11 at 8 hours post-infection of cells with the Δ*bimA* mutant strain (Figure 4.12 (B)). Later, we carried out a more sensitive ELISA assay to measure the secretion of IL-1α as a product of activation of caspase-11.

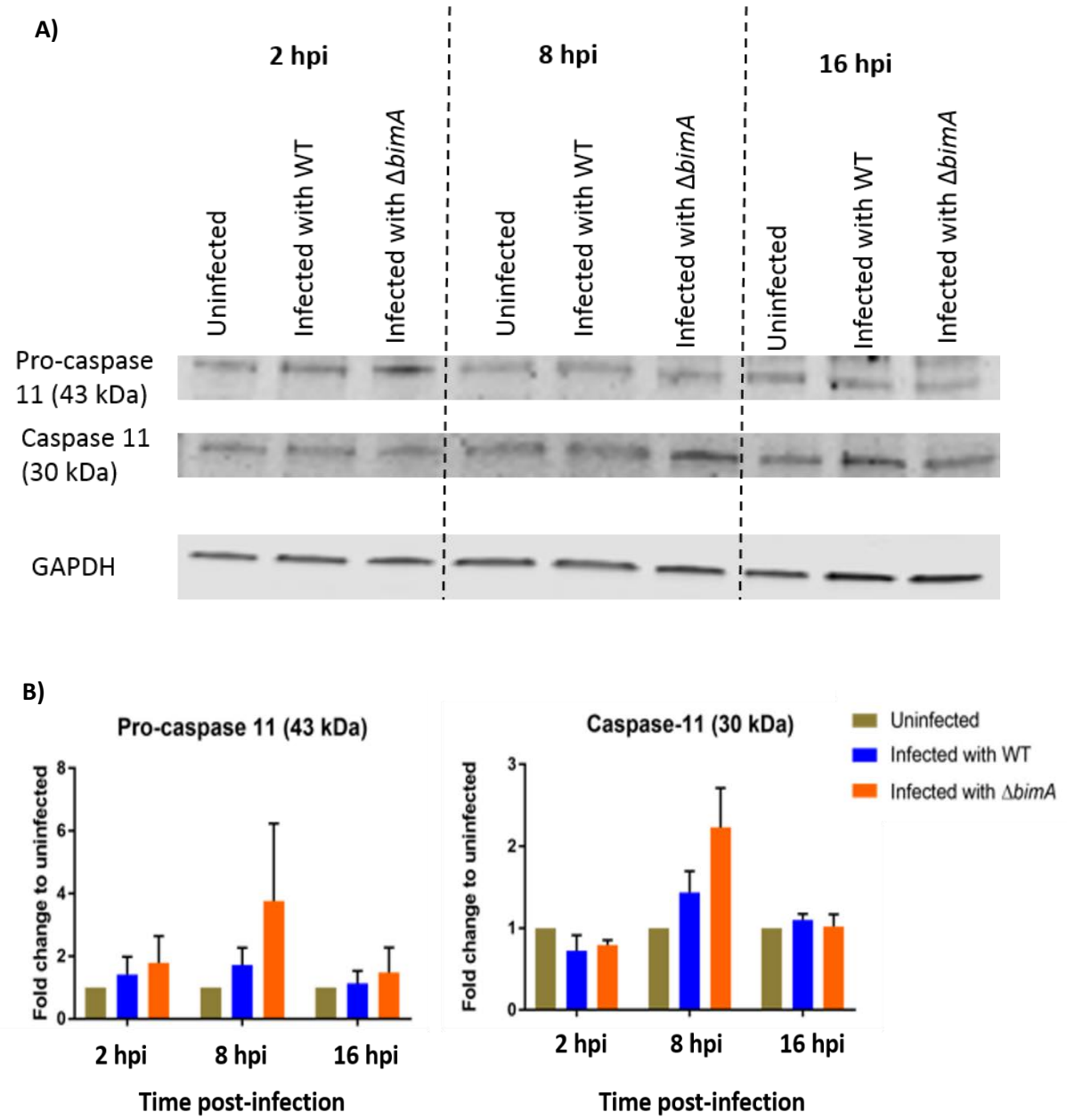

Figure 4.14 Immunoblot analysis of pro-caspase 11 and cleaved caspase 11 in BMDMs upon *B. pseudomallei* infection. (A) BMDMs were infected with *B. pseudomallei* WT or Δ*bimA* mutant strains at an MOI of 2 for 2, 8 and 16 hpi as described previously in *Materials and Methods 2.6*. Presence of pro-caspase 11 at the protein level and the activation by cleavage into caspase-11 was determined by Western blotting of cell lysates. (B) The bar chart shows the mean densitometric measurements of the pro-caspase 11 (left) and cleaved caspase-11 (right) in infected lysates as a fold change from that in uninfected cell lysate. The mean was taken from three independent experiments and the error bars represent the standard error. GAPDH is the loading control. Student's t-test was used to determine the statistical significance comparing levels in an infected cell lysate to an uninfected lysate at a respective time point.

Activation of caspase-11 has also been shown to lead to the secretion of endogenous alarmins namely IL-1α and high mobility group B1 (HMGB) (Kayagaki *et al*, 2011). In our analysis using the Proteomic Profiler Array we found a higher expression of IL-1α in infected cell lysates compared to uninfected cell lysates at 8 hpi and 16 hpi. Following on from this analysis, we measured the concentration of IL-1α in the supernatant of uninfected and infected cells by ELISA from three independent experiments. At 2 hpi and 8 hpi, the secretion of IL-1α was minimal (<5pg/ml) from both infected and uninfected BMDMs. We included a positive control where we stimulated the BMDMs with the TLR4 agonist LPS (500ng/ml) for 8 hours, which led to significant secretion of IL-1α at a concentration of ~43 pg/ml. However, at 16hpi, the BMDMs infected with WT *B. pseudomallei* showed a significant increase in IL-1α secretion compared to the uninfected BMDMs and also to BMDMs infected with the Δ*bimA* mutant (Figure 4.15). The higher amount of IL-1α secretion in BMDMs infected with the WT strain compared to the mutant strain could be associated with the higher bacterial burden of WT *B. pseudomallei* in these cells at this time point (Figure 3.3). In these experiments with naïve non-primed BMDMs, we were able to detect the secretion of IL-1α upon infection suggesting that the non-canonical inflammasome is activated as a global response to *B. pseudomallei* rather than a specific response to the Δ*bimA* mutant. The non-canonical inflammasome could be an important host innate mechanism against *B. pseudomallei* which protects the host cell at later time points post-infection.

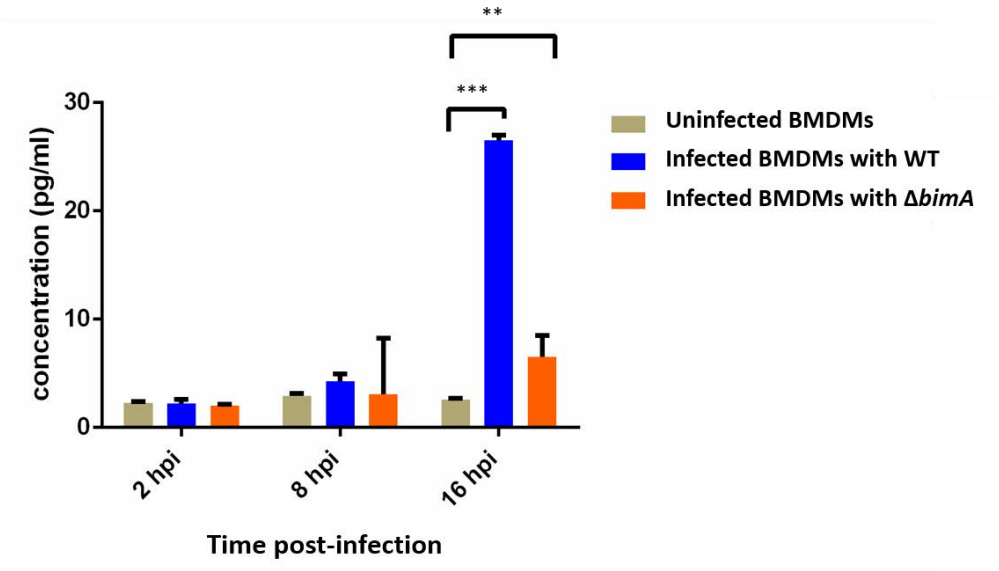

Figure 4.15 Secretion of the inflammatory cytokine IL-1α by ELISA. BMDMs were seeded at 1 x 10^5 cells per well in 96-well plate, followed by infection with *B. pseudomallei* WT (blue) or the Δ*bimA* mutant (orange) at 2, 8 and 16 hpi. The concentrations of IL-1α (pg/ml) in the supernatant of uninfected BMDMs (beige) or infected BMDMs were determined by ELISA as described in *Materials and Methods 2.11*. The bar chart represents the mean + SE from three independent experiments. The statistical analysis was performed using Student's t-test between two groups as indicated **p<0.01, ***p<0.001.

Caspase-11 does not process pro-IL-1β directly; however it is required for the activation of caspase-1 by promoting the assembly of the NLRP3 inflammasome complex (Kang *et al*, 2000). Our microarray analysis in Chapter 5 shows that *B. pseudomallei* infection in BALB/C BMDMs induces the expression of IL-1β transcript while at the protein level, we found a small fold increase of IL-1β in infected lysates as compared to the uninfected lysate, as determined using a Profiler Mouse Cytokine Array (Figure 4.2). We carried out an IL-1β ELISA to detect secretion of IL-1β in cell supernatants to investigate if such transcriptional induction leads to its maturation into active IL-1β. However, we were not able to detect any IL-1β in cell supernatants by ELISA in all samples (both uninfected and infected BMDMs with *B. pseudomallei* WT and Δ*bimA* mutant) (data not shown). Surprisingly, we detected a huge increase in expression of IL-1β in the positive control containing LPS (500ng/ml) using the Profiler Cytokine Array, but we observed no secreted IL-1β in the cell supernatants. This leads us to suggest that there is a defect in activation of the IL-1β-converting caspase-1 in BALB/C BMDMs.

We also carried out Western blotting using a caspase-1 antibody that can detect both the pro-caspase-1 precursor and the cleaved caspase-1. We could detect pro-caspase-1, however, we were unable to detect any cleaved caspase-1 in any of the samples, including the positive control (Figure 4.16). For the positive control, we primed the BMDMs with LPS for 4 hours to increase the cellular expression of NLRP3 via NF-κB signalling. We then added ATP for the next 30 minutes to activate the NLRP3 inflammasome as described in Boriushkin *et al* (2016). However, we still could not detect any cleaved caspase-1 in the positive control lysate, leading us to believe that the canonical inflammasome in our cell system might be inhibited by an unknown mechanism. Recently, Boriushkin *et al* (2016) demonstrate that such inflammasome activation and IL-1β maturation in BMDMs can be suppressed by endogenous molecular chaperone $p58^{IPK}$. $p58^{IPK}$ has been shown to inhibit the double-stranded RNA dependent protein kinase (PKR) protein, where PKR is important in mediating inflammasome activation and also the TLR4 induction of NF-κB and JNK MAPK pathways. However, further studies are needed in future to confirm if the inhibition of canonical inflammasome activation in BALB/C BMDMs we have observed is mediated by $p58^{IPK}$.

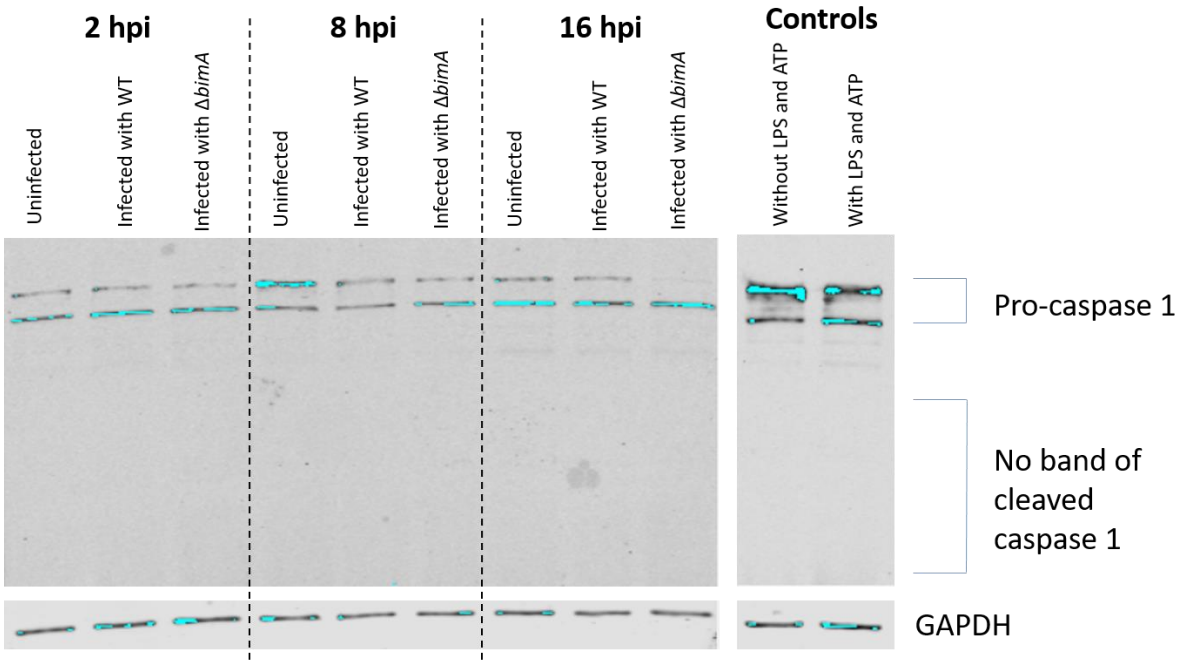

Figure 4.16 Western blot of pro-caspase 1 in BMDMs upon B. *pseudomallei* infection. (A) BMDMs were infected with *B. pseudomallei* WT or Δ*bimA* mutant strains at an MOI of 2 for 2, 8 and 16 hpi as described previously in *Materials and Methods 2.6*. Presence of pro-caspase 1 at the protein level was determined by Western blotting of cell lysates. However, none of the samples showed band of cleaved active caspase-1 including the positive control where the BMDMs were primed with LPS, followed by activation of inflammasome by ATP. Activated canonical inflammasome cleaves the procaspase-1 into active caspase-1 at 30kDa (partially cleaved) or 20kDa/ 10kDa (fully cleaved). GAPDH is the loading control.

4.3 DISCUSSION

Innate immune signalling constitutes the frontline of host defence against infection. The innate immune system is not specific and depends on recognition of conserved features of pathogens known as PAMPs. TLRs occupy a prominent position in the innate immune system by virtue of their ability to recognise various bacterial components and drive the expression of many pro- and anti-inflammatory cytokines, which together orchestrate the inflammatory response. In septicaemic melioidosis, there is increased expression of TLR1, TLR2, TLR4 and CD14 on the surfaces of circulating monocytes and granulocytes and increased levels of mRNA encoding TLR1, TLR2, TLR3, TLR4, TLR5, TLR8, TLR10, CD14 and MD-2 in leukocytes (Wiersinga *et al*, 2007). Melioidosis patients have elevated pro-inflammatory cytokines including IL-12, IL-18 and IL-15, IFNγ and TNFα (Lauw *et al*, 1999; Supputtamongkol *et al*, 1992), and patients who die from melioidosis have excessive serum levels of IL-6 and IL-8 compared to those who survive (Lauw *et al*, 1999; Friedland *et al*, 1992). In a murine melioidosis model, TLR2, TLR4 and TLR5 have been implicated in the recognition of *B. pseudomallei* (West *et al*, 2013; West *et al*, 2012; West *et al*, 2008; Wiersinga *et al*, 2007) and expression of IL-1β, IL-6 and TNFα is increased in the liver of mice infected with *B. pseudomallei* (Ulett *et al* , 2000).

TLR signalling can proceed via two distinct routes either through the MyD88- or TRIF-adaptor protein. Infection with *B. pseudomallei* has previously been shown to activate TLRs through the MyD88-dependent pathway rather than the TRIF-dependent pathway both *in vitro* and *in vivo* (Tangsudjai *et al*, 2010; Wiersinga *et al*, 2008). Wiersinga *et al* (2008) demonstrated that MyD88-, but not TRIF-dependent signalling contributes to host protection against *B. pseudomallei* in mice, at least in part by rapidly recruiting activated neutrophils towards the primary site of infection for bacterial clearance. As compared to wild-type mice, the MyD88 knockout mouse shows increased mortality accompanied with significant bacterial burden in the lung, liver and blood (Wiersinga *et al*, 2008). However, *in vitro* studies in the RAW264.7 macrophage cell line show that WT *B. pseudomallei* induced expression of genes downstream of the MyD88-dependent pathway, indicating MyD88 is an important adaptor protein of TLRs in controlling *B. pseudomallei* in this immortalised macrophage-like cell line (Tangsudjai *et al*, 2010). Despite the importance of MyD88 in controlling *B. pseudomallei in vitro* and *in vivo*, however, we were unable to demonstrate the same role of MyD88 in BALB/C BMDMs. We

knocked down MyD88 gene expression using siRNA technology and also in a separate experiment using a MyD88 homodimerisation inhibitor to block the MyD88-mediated signalling cascade. MyD88 siRNA transfection did not attain 100% gene silencing while the MyD88 homodimerisation inhibitor did not fully inhibit the downstream pathway. It is important to highlight here that in combination of incomplete abrogation of the MyD88 function with relatively low infection rate of *B. pseudomallei* in BMDMs (as discussed in Chapter 3), these collectively may reduce the impact of the findings. The residual activation of MyD88-dependent pathway may be adequate to compensate the low number of infected BMDMs. Alternatively, utilising CRISPR-Cas9 (Clustered Regularly Interspaced Short Palindromic Repeats- CRISPR associated protein-9 nuclease) gene editing technology to delete the MyD88-encoding gene in BMDMs could be considered in future. In our experimental system with the incomplete depletion of MyD88, we believe that MyD88 is not needed for controlling *B. pseudomallei* (both WT and Δ*bimA* mutant) in BALB/C BMDMs. In support of this statement, it should be noted that we were unable to observe any difference in downstream activation of NF-κB transcription factor in infected lysates (both WT and Δ*bimA* mutant) as compared to the uninfected in BALB/C BMDMs. This activation of NF-κB was determined by Western blot on the nuclear translocation of the p65 component of the complex (data not shown).

MyD88 is regarded as a major protein adaptor of TLRs as it signals downstream of all TLRs except TLR3 and some TLR4. MyD88-mediated signalling contributes to expression of many cytokines including TNFα. We found that the production of TNFα in the supernatant of cells infected with *B. pseudomallei* strain is about 5-fold less than the cells stimulated with *E. coli* LPS as measured by ELISA. This suggests that *B. pseudomallei* contributes to a weaker level of macrophage activation compared to BMDMs stimulated with *E. coli* LPS, which could explain why MyD88 may not seem important in controlling the pathogen in BALB/C BMDMs. Furthermore, the Proteome Profiler Mouse Cytokine Array identified only a few candidate proinflammatory cytokines and chemokines as elevated upon infection with *B. pseudomallei*, while there were many more expressed with much higher fold-change in *E. coli* LPS stimulated BMDMs . Utaisincharoen *et al* (2001) demonstrated that infection of *B. pseudomallei* in RAW264.7 cells leads to poor secretion of TNF-α as well as low expression of inducible nitric oxide synthase (iNOS). Consistent with this data, we were unable to detect secreted nitric oxide by Griess assay in *B. pseudomallei*-infected BMDM (both with WT and Δ*bimA*) at any experimental time points (data not shown). By being a weaker macrophage activator, *B.*

pseudomallei can be inconspicuous to the host immune system, potentially allowing the pathogen to persist intracellularly for a period of time.

TRIF is an adaptor protein mainly for TLR3 and for some TLR4. TRIF-dependent signalling drives the expression of Type I IFN including IFNβ. The TRIF-dependent signalling pathway also mediates NF-κB and MAPK signalling pathways similar to the MyD88-dependent pathway, but with delayed kinetics. Interestingly, recent findings suggest that TRIF-IFNβ signalling is associated later with the non-canonical inflammasome pathway. This non-canonical inflammasome pathway is dependent on activation of caspase-11, and later secretion of IL-1α. In a murine melioidosis model, Wiersinga *et al* (2008) reported that TRIF-dependent signalling does not protect the host, but Aachoui *et al* (2013) recently demonstrate that Casp11$^{-/-}$ knockout mice succumbed to death upon *B. pseudomallei* challenge, indicating that caspase-11 is critical for host survival against *B. pseudomallei*. In our *in vitro* model using BALB/C BMDMs, the WT bacteria appear to proliferate better (albeit at a statistically non-significant difference) when the TRIF-dependent pathway is inhibited, indicating that TRIF may be required for controlling *B. pseudomallei* intracellular fate.

In terms of non-canonical inflammasome activation, we found a slightly higher, but not statistically significant, level of caspase-11 cleavage in infected BMDMs at 8hpi compared to uninfected BMDMs. Activation of caspase-11 leads to secretion of IL-1α, suggesting that more caspase-11 cleavage would lead to secretion of more IL-1α. We found more secretion of IL-1α in BMDMs infected with both the WT and Δ*bimA* mutant strains compared to uninfected BMDMs at 16hpi. These data together suggest that the TRIF-IFNβ-non-canonical inflammasome pathway could potentially be involved in immunity against intracellular *B. pseudomallei*, but not specifically towards the Δ*bimA* mutant in BALB/C BMDMs. However, more evidence and experiments are needed before we could firmly conclude that the TLR/TRIF-IFNβ-non canonical inflammasome pathway contributes to the host cell innate response against *B. pseudomallei*.

On the other hand, the canonical inflammasome depends on the activation of caspase-1 and leads to secretion of IL-1β. In our hands, we could not promote activation of caspase-1 as demonstrated by Western blot analysis nor the secretion of IL-1β by ELISA, including in the positive control samples that were stimulated with *E.coli* LPS and ATP. We predict that there is a defect in activation of the IL-1β-converting enzyme caspase-1 in BALB/C BMDMs to secrete mature IL-1β.

Both canonical and non-canonical inflammasome pathways induce a lytic form of programmed cell death called 'pyroptosis'. We have measured cell death by LDH release assay as stated in the previous chapter. However, we do not observe any significant cell death upon *B. pseudomallei* infection at any experimental time point. This could be due to the fact that we have used naïve BMDMs without a priming agent. This may result in poor levels of inflammasome activation relative to BMDMs primed with an agent such as IFNγ, IFNβ or LPS (Finethy *et al*, 2015; Hagar *et al*, 2013). Several studies also reported that in the absence of a priming agent, the expression of caspase-11 in unstimulated macrophages is low; therefore investigation of its function requires a priming step (Broz *et al*, 2012; Gurung *et al*, 2012; Rathinam *et al*, 2012). Another explanation could be due to the low MOI used in this study where the activation of the canonical and/or non-canonical inflammasome is not distinct or obvious, therefore it is not noticeable if there is a difference upon *B. pseudomallei* infection. Bast *et al* (2014) have successfully demonstrated pyroptosis in BMDMs infected with *B. pseudomallei* but with a very high MOI of 200. However, such cell death was not observed when carrying out the same infection experiment at MOI of 2, the MOI used for infection in this thesis.

Aachoui *et al* (2013) demonstrate that caspase-11 contributes to host protection against *B. pseudomallei* in a murine model of melioidosis. Activation of the non-canonical inflammasome pathway has been observed in response to a number of other Gram-negative bacteria namely *Escherichia coli*, *Citrobacter rodentium*, *Shigella flexneri*, and *Salmonella* Typhimurium (Broz *et al*, 2012; Rathinam *et al*, 2012; Kayagaki *et al*, 2011). However, such activity is not observed with Gram-positive bacteria, indicating that the pathway is a conserved mechanism for the detection of Gram-negative bacteria. This also suggests that the Gram negative bacterial LPS could be the caspase-11 agonist. Consistently, transfection of ultrapure *Salmonella* LPS into BMDMs results in caspase-11 dependent pyroptosis (Hagar *et al*, 2013). This process requires TLR4 and TRIF-dependent interferon production. TRIF is required but MyD88 is dispensable for the pathway (Rathinam *et al*, 2012). In some scenarios, this TRIF-dependent-non-canonical inflammasome pathway requires another arm of Type I Interferon signalling as reported in several studies (reviewed in Broz & Monack, 2013; Rathinam *et al*, 2012; Kayagaki *et al*, 2011). Our analysis here is further supported in Chapter 5 by our microarray analysis, where we found that the Type I Interferon signalling pathway is involved as a global response to *B. pseudomallei*. At this point, we would predict that the non-canonical inflammasome could be

involved in host protection against *B. pseudomallei*. Unfortunately, none of the above mechanisms discussed above was responsible for the clearance of the Δ*bimA* at 16 hpi.

Interestingly, a recent study suggests that caspase-11 activation is also dependent on the small IFN-inducible GTPases termed guanylate-binding proteins (GBPs) in response to intracellular bacteria (Kim *et al*, 2016; Finethy *et al*, 2015; Pilla *et al*, 2014; Meunier *et al*, 2014). Meunier *et al* (2014) have shown that GBP helps to promote the lysis of vacuoles containing pathogens which subsequently exposes the LPS to the cytosol for downstream detection by the inflammasome machinery. This GBP-dependent LPS detection could be an alternative mechanism for bacterial LPS that bypasses the recognition by TLR4 receptor in a TRIF-independent fashion (Meunier *et al*, 2014). As described previously, *B. pseudomallei* is a weak macrophage activator, possibly due to its unique LPS structure that poorly engages with TLR4 (West *et al*, 2008; Matsuura *et al*, 1996). In fact, TLR4 knockout mice are as resistant to *B. pseudomallei* infection as wild-type mice (Wiersinga *et al*, 2007). We propose that this GBP-dependent LPS detection coupled with non-canonical inflammasome activation could also be a backup host innate mechanism in response to invading *B. pseudomallei*. In fact, the family of GBPs has also been shown to be required for cell autonomous immunity to limit the replication of *Mycobacterium bovis*, *Listeria monocytogenes* and *Salmonella* Typhimurium (reviewed in Kim *et al*, 2016; reviewed in Randow *et al*, 2013; Rupper & Cardelli, 2008). In addition to vacuolar lysis, a few studies have revealed that at least one family of the GBPs can complex with the inflammasome and promote inflammasome assembly in response to intracellular pathogens (Kim *et al*, 2016; Finethy *et al*, 2015; Shenoy *et al*, 2012). However, the stimulus involved in GBP-dependent inflammasome activation is as yet undefined (Shenoy *et al*, 2012). In the next chapter, we have found that several GBPs are elevated at the transcriptional level in response to infection of BALB/C BMDMs with *B. pseudomallei,* namely GBP1, GBP2, GBP2a, and GBP5. With the knowledge of the various roles played by GBP family members in inflammasome activation and host defence, it is tempting to investigate in future the importance of GBPs in melioidosis.

5 CHAPTER 5: PROFILING MACROPHAGE TRANSCRIPTOMIC RESPONSES TO INFECTION WITH *BURKHOLDERIA PSEUDOMALLEI*

5.1 INTRODUCTION

The complex interaction between a microbial pathogen and a host is the underlying basis of pathogenesis. When host cells respond to the presence of a pathogen, phenotypic changes are often manifested by marked changes in gene expression. Gene expression profiling by the advent of DNA microarray technology and the more recent introduction of RNA sequencing approaches has greatly expanded the ability of scientists to monitor the transcriptional changes in the host that accompany infection at a genome-wide scale. Microarray technology has been used extensively in studies of host responses to different pathogens including *Mycobacterium tuberculosis* (Xu *et al*, 2003), *Salmonella* (Eckmann *et al*, 2000), *Listeria monocytogenes* (Ng *et al*, 2005), adenovirus (Zhao *et al*, 2003), human immunodeficiency virus 1 (Geiss *et al*, 2000) as well as the parasite *Trypanosoma cruzi* (Mukherjee *et al*, 2003). In fact, Jenner and Young commented in 2005 that at least 160 papers had been published by that time on host transcriptomic profiling following infection with 26 different bacterial species, 30 different types of viruses as well as yeasts, protozoa and helminths (Jenner & Young, 2005). Although nowadays next generation sequencing such as RNA-sequencing (RNA-Seq) also holds great potential for defining host-pathogen interactions, a microarray approach still offers a number of advantages over RNA-Seq. These include a fast pipeline from sample preparation to result analysis, lower cost and the requirement for simpler bioinformatics.

Microarray technology has revolutionised our understanding of host responses during *B. pseudomallei* pathogenesis, as well as the virulence mechanisms or adaptations deployed by the pathogen for the survival in different host environments. Multiple *in vitro* studies have been designed to mimic diverse host environments and whole-genome microarray used to identify expression of genes that may be necessary for *B. pseudomallei* growth under a specific condition. For example, *B. pseudomallei* adapts to low-iron conditions by increasing the expression of genes associated with pyochelin- and hydroxamate-mediated iron-acquisition for

efficient iron uptake during infection and also by utilising alternative metabolic pathways for energy production (Tuanyok *et al*, 2005). Similar findings have been observed in an *in vivo* gene expression study of *B. pseudomallei* in a hamster model of melioidosis (Tuanyok *et al*, 2006). Besides, Chieng *et al* (2012) investigated the global *B. pseudomallei* transcriptome profile during infection of human macrophage-like U937 cells, an *in vitro* assay used to mimic cellular host defence. *B. pseudomallei* rapidly adapts to the intracellular milieu through reducing its metabolic activity and growth rate, as well as evading host immune responses by shutting down expression of known virulence factors such as the capsular polysaccharide, lipopolysaccharide (LPS) and flagella (Chieng *et al*, 2012). Furthermore, Ooi *et al* (2013) have integrated whole genome transcriptional data of *B. pseudomallei* exposed to more than 80 diverse physical, chemical and biological conditions to generate a transcriptional condition compendium of *B. pseudomallei* as a community resource for biological discovery.

A number of studies have been carried out to study the host transcriptome changes upon *B. pseudomallei* infection both *in vitro* and *in vivo*. Chin *et al* (2010) used the BALB/C mouse model of melioidosis to determine host gene signatures in the spleen and liver during acute melioidosis by microarray. They found numerous cellular processes were altered in *B. pseudomallei* intravenously-infected mice which included genes involved in the immune response, stress response, cell cycle regulation, proteosomal degradation, cellular metabolism, and signal transduction pathways (Chin *et al*, 2010). Most notably, Toll-like receptor (TLR2) expression was greatly enhanced, the dysregulation of innate immunity via TLR2 has been postulated to underlie the tissue damage observed during acute infection. Besides the mouse model, Lee *et al* (2013) have studied the global host transcriptomic changes in *Caenorhabditis elegans* following infection with *B. pseudomallei*. In their study, they identified that in a *B. pseudomallei* T3SS dependent manner, the bacterium targets a specific cellular transcription factor known as ELT-2 for ubiquitin-proteosomal degradation. ELT-2 protein is a key regulator of innate immune responses through its activity as a GATA transcription factor (Shapira *et al*, 2006), therefore degradation of this factor means a reduction in the host's ability to produce an effective antimicrobial defence and therefore leads to immune suppression (Lee *et al*, 2013).

Several *in vitro* experiments have been conducted in different cell models namely A549 human lung epithelial cells (Vellasamy *et al*, 2016), THP-1 human monocytes (Perumal Samy *et al*, 2015), and primary human monocytes (Kulsantiwong *et al*, 2016). In A549 cells infected with *B. pseudomallei*, Vellasamy *et al* (2016) found an increase in the activation of host carbohydrate metabolism and apoptosis after 3 hours of infection, but a suppression in several

components of the innate immune response. The bacteria utilise the host metabolic pathways to gain energy sources and metabolites to promote their proliferation and survival inside the host cell. Additionally, this metabolic regulation can be associated with cellular responses such as specific innate immune responses and inflammation (reviewed in Eisenreich *et al*, 2013). Apoptosis is regarded as a host defence mechanism to prevent bacterial replication within the host, while suppression of several components in innate immune response increases the chances of immune evasion by the bacteria (Vellasamy *et al*, 2016). Unlike innate immune suppression in *B. pseudomallei*-infected A549 cells, *B. pseudomallei* infection in THP-1 monocytes (Perumal Samy *et al*, 2015) and primary human monocytes (Kulsantiwong *et al*, 2016) resulted in upregulation of host innate immune response. Perumal Samy *et al* (2015) reported several inflammatory genes were differentially expressed in the host when infected with *B. pseudomallei* namely IL-1β, TNFα, IL-8, IL-6, IL-13 and many others. Kulsantiwong *et al* (2016) reported in comparison to a *B. pseudomallei* LPS mutant, a *B. pseudomallei* wild-type (WT) strain led to expression of significantly more IL-23 in infected primary human monocytes.

Macrophages are important host immune cells in the control of *B. pseudomallei*, yet the pathogen is also capable of manipulating host responses to promote its own survival. Here, in this thesis, utilisation of BALB/C BMDMs as an *in vitro* model may provide insights into the macrophage cellular response following infection with *B. pseudomallei* and also the bacterial evasion of host responses in a BimA-dependent manner. It has been described in the previous chapter that a strain lacking the *bimA* gene had impaired survival in BALB/C BMDMs when compared to the WT strain. Hence, using microarray technology in this chapter we aim:

1. To profile the global macrophage transcriptomic response to *Burkholderia pseudomallei* strain 10276
2. To identify any specific macrophage response at the transcriptomic level elicited by the Δ*bimA* mutant strain
3. To validate a subset of differentially expressed genes by qPCR

5.2 RESULTS

5.2.1 Introduction to the microarray technology and choice of optimal time points for sampling

This thesis has applied the recent technology of GeneChip microarray, to be precise the GeneChip Mouse Gene 2.0 ST Array. GeneChips (Affymetrix, Santa Clara, CA) comprise high-density *in-situ* synthesised oligonucleotide microarrays. Because *in-situ* synthesised probes are typically short (20-25 base pairs), multiple probes per transcript are included to improve sensitivity, specificity and statistical accuracy (Dalma-Weiszhausz *et al*, 2006). In the GeneChip Mouse Gene 2.0 ST Array, each unique probe is 25 bases in length where each transcript is designed with a median of 22 unique probes. This means that the array measures a median of 550 bases per transcript, interrogates across entire genes or exons and hence, provides extremely high coverage of the transcribed genome.

As it was of interest to investigate the transcriptomic changes associated with detection and elimination of the Δ*bimA* mutant, we first determined the optimal time points for sampling for microarray analysis. As presented in Chapter 3, the intracellular survival of the Δ*bimA* mutant was significantly impaired compared to the WT strain in BALB/C BMDMs at 16 hpi, but not significantly different at 8hpi. A pilot study was conducted to include more time points between 8 hpi and 16 hpi to identify the time point where the intracellular survival of Δ*bimA* mutant began to differ from that of the parental strain. The time points included in the studies were 8 hpi, 10 hpi, 12 hpi, 14 hpi and 16 hpi. BMDMs were infected at an MOI of 2 in a kanamycin-protection manner as described previously in Section 3.2.2. At the indicated time point of post-infection, the infected cell monolayers were subsequently lysed with 0.1% Triton X-100 in PBS, serially diluted and plated on Luria-Bertani (LB) agar. Bacterial colony forming units (CFUs) were recorded after 2 days incubation at 37^{o}C. This pilot study was conducted twice and the results suggested that the intracellular survival of the Δ*bimA* mutant started to differ from the WT strain as early as 12 hpi, but not at 10 hpi (data not shown). Similar intracellular survival assays were then repeated taking viable counts at 8 hpi and 12 hpi as shown in Figure 5.1. The intracellular survival between the *B. pseudomallei* WT and the Δ*bimA* strain was not statistically different at 8 hpi, but started to differ significantly at 12 hpi.

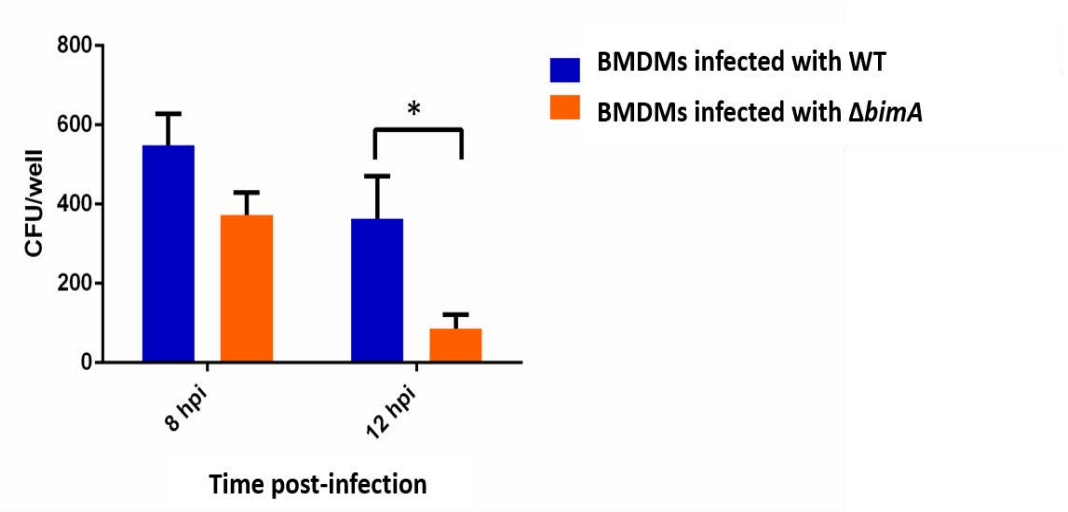

Figure 5.1 Intracellular survival of WT (blue) and Δ*bimA* mutant (orange) in BALB/C BMDMs. The mean bacterial recoveries (cfu ± standard error) per well of a 96-well plate from four independent experiments at 8 hpi and 12 hpi. Kanamycin-resistant bacteria were recovered at 8 hpi and 12 hpi after infection of BALB/C BMDMs at an MOI of 2 as described in *Materials and Methods 2.6*. Statistical significance was determined using an unpaired Student t-test *$p<0.05$, **$p<0.01$.

5.2.2 Assessing the quality of the cellular RNA

For this study, three independent experiments were carried out to generate biological replicates for analysis by microarray. In each experiment RNA was harvested from uninfected BMDMs and BMDMs infected at an MOI of 2 with *B. pseudomallei* WT or the Δ*bimA* mutant strain, at two different time points (8 hpi and 12 hpi). This experimental design gave a total of 18 samples for analysis. Total RNA of the infected or uninfected BMDMs was isolated using an RNeasy Plus Mini Kit (Qiagen). This RNeasy technology integrates unique gDNA Eliminator spin columns to eliminate gDNA contamination during isolation, hence avoiding the need for DNase digestion. In addition, QIAshredder homogenisers were used to homogenise cell lysates to further improve the RNA yields. Each sample was pooled from two or three wells of a 24-well plate (where each well contained approximately 5 x 10^5 cells per well) to provide enough total RNA for microarray (2µg of each, with a concentration of approximately 100ng/µl). The concentration was quantified using a Nanodrop ND-100 (NanoDrop Technologies). The samples were then outsourced to SourceBioscience (Nottingham, UK) for assessment of the RNA quality, as well as the processes of complementary RNA (cRNA) amplification, labelling, hybridisation and array scanning.

The RNA integrity was verified by Source BioSciences using an Agilent 2100 Bioanalyser (Agilent Technologies). All the samples used for microarray passed the QC requirement (Table 5.1). All 18 samples prepared were high quality producing two major peaks when assessed by the Bioanalyser, corresponding to the 2 major ribosomal RNA species of 28S and 18S (Figure 5.2). Low quality RNA would show a broad peak or multiple peaks. All the samples were free from protein and genomic DNA contamination, as well as organic solvent contamination as they had 260/280 ratio >2.0 and 260/230 ratio >1.5 respectively, as determined using a Nanodrop ND-100 (Table 5.1). It is crucial in the beginning to prepare high quality samples as low quality samples with the presence of contaminants can severely affect the processing steps in a typical microarray experiment.

After RNA isolation, the RNA samples were transformed into cRNA using an *in vitro* transcription (IVT) method, which provides amplification of the target. This IVT technology was originally described by Eberwine and colleagues (Van Gelder *et al*, 1990). Prior to hybridisation, cRNA was labelled with biotin and fragmented to 50- to 200-base fragments (Figure 5.3 (b)). All these steps were performed using an Affymetrix GeneChip WT PLUS

reagent Kit, following the manufacturer's instructions at Source BioSciences. These cRNA fragments were added to the hybridisation cocktail which contains salts, blocking agents and bacterial RNA spike-in controls, subsequently injected into the GeneChip array hybridisation chamber and incubated at 45°C for 16 hours. Next, the arrays were subjected to a series of washing and staining steps, where the fluorescent dyes were attached to the biotin labels. These processes were automated using an Affymetrix Fluidics station. This results in an increase in abundance of biotinylated cRNA molecules on the probes. The intensity of fluorescence, which corresponds to the abundance of cRNA fragments hybridised to the probe, was then determined by scanning the array, inferring the relative abundance of specific mRNA sequences in a sample (Figure 5.3(a)). Next, raw signal intensities for each probe pair were randomly permuted to create *CEL* files and the *CEL* files were supplied for the downstream analysis carried out at the Roslin Institute. The *CEL* files corresponding to the 18 individual samples were then imported into the Affymetric Expression Console software for preprocessing steps.

Sample ID	Description	RNA integrity number (RIN) by Agilent Bioanalyser		RNA Quality by NanoDrop		
		RIN Number	Pass/Fail	260/280	260/230	Pass/Fail
A2	Uninfected BMDMs 8 hours	10	Pass	2.1	1.67	Pass
A3		10	Pass	2.06	1.85	Pass
A4		Not provided	Pass	2.09	1.76	Pass
B2	BMDMs infected with *B. pseudomallei* WT 8hpi	10	Pass	2.08	1.88	Pass
B3		10	Pass	2.07	1.63	Pass
B4		Not provided	Pass	2.11	1.66	Pass
C2	BMDMs infected with *B. pseudomallei* Δ*bimA* 8hpi	10	Pass	2.09	1.72	Pass
C3		10	Pass	2.07	1.73	Pass
C4		10	Pass	2.07	1.79	Pass
D2	Uninfected BMDMs 12 hours	10	Pass	2.1	1.69	Pass
D3		10	Pass	2.11	1.77	Pass
D4		10	Pass	2.06	1.89	Pass
E1	BMDMs infected with *B. pseudomallei* WT 12hpi	10	Pass	2.08	1.59	Pass
E2		10	Pass	2.06	1.81	Pass
E4		10	Pass	2.11	1.87	Pass
F1	BMDMs infected with *B. pseudomallei* Δ*bimA* 12hpi	10	Pass	2.08	1.66	Pass
F2		10	Pass	2.12	1.7	Pass
F4		10	Pass	2.07	1.51	Pass

Table 5.1 RNA integrity and quality of the samples. RNA integrity number (RIN) estimates the RNA integrity of the samples, provided by Agilent Bioanalyser software. Nanodrop estimates the RNA quality of the samples. This QC report is provided by the Source BioScience.

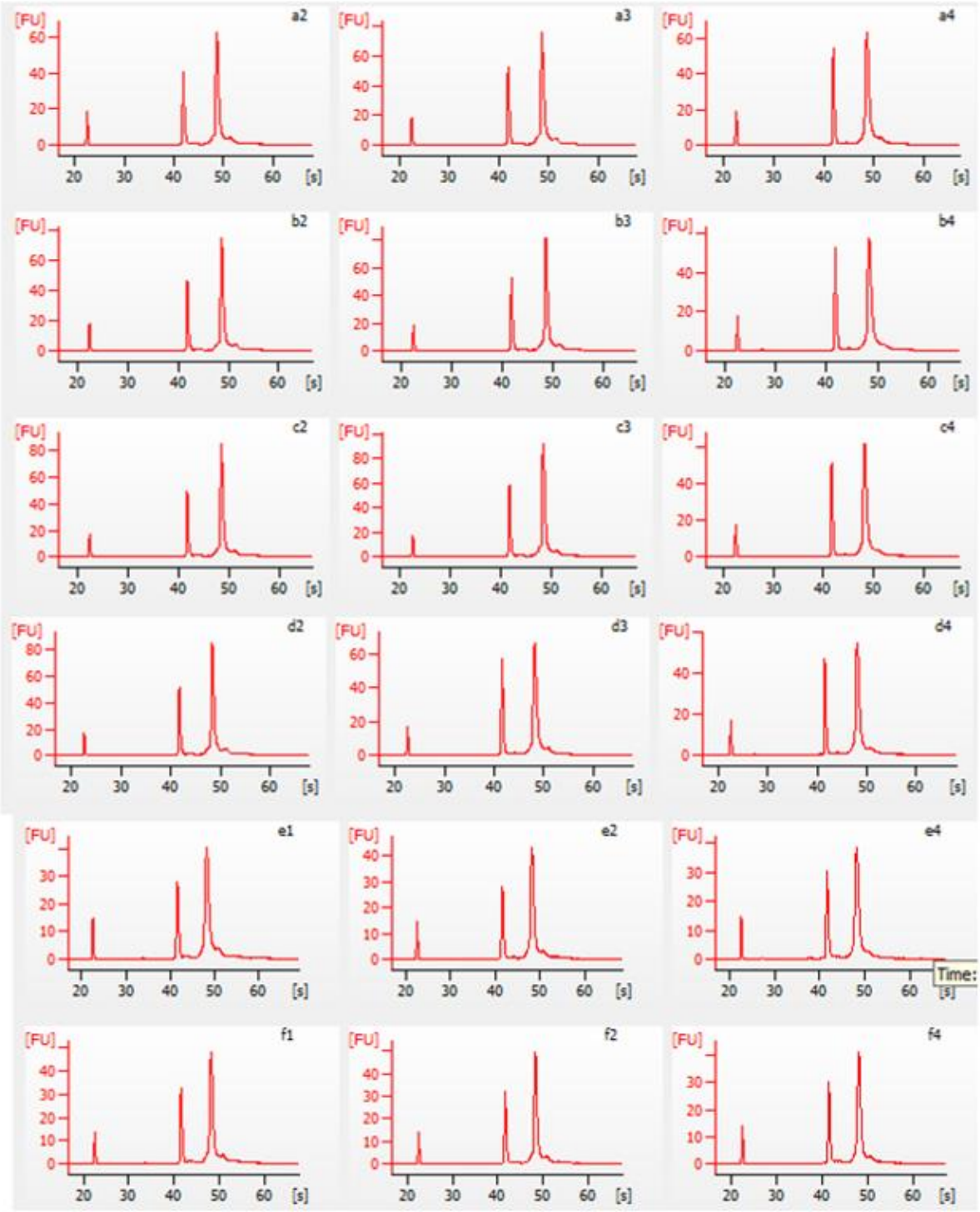

Figure 5.2 Electropherograms of RNA samples generated by the Agilent Bioanalyser. RNA samples were separated by electrophoresis on a micro-fabricated chip and detected via laser-induced fluorescence emission. All 18 samples show high-quality intact RNA with two distinct ribosomal peaks (18S and 28S), and a flat baseline between the marker (the most left small peak) and the ribosomal peaks. This QC report was provided by SourceBioScience.

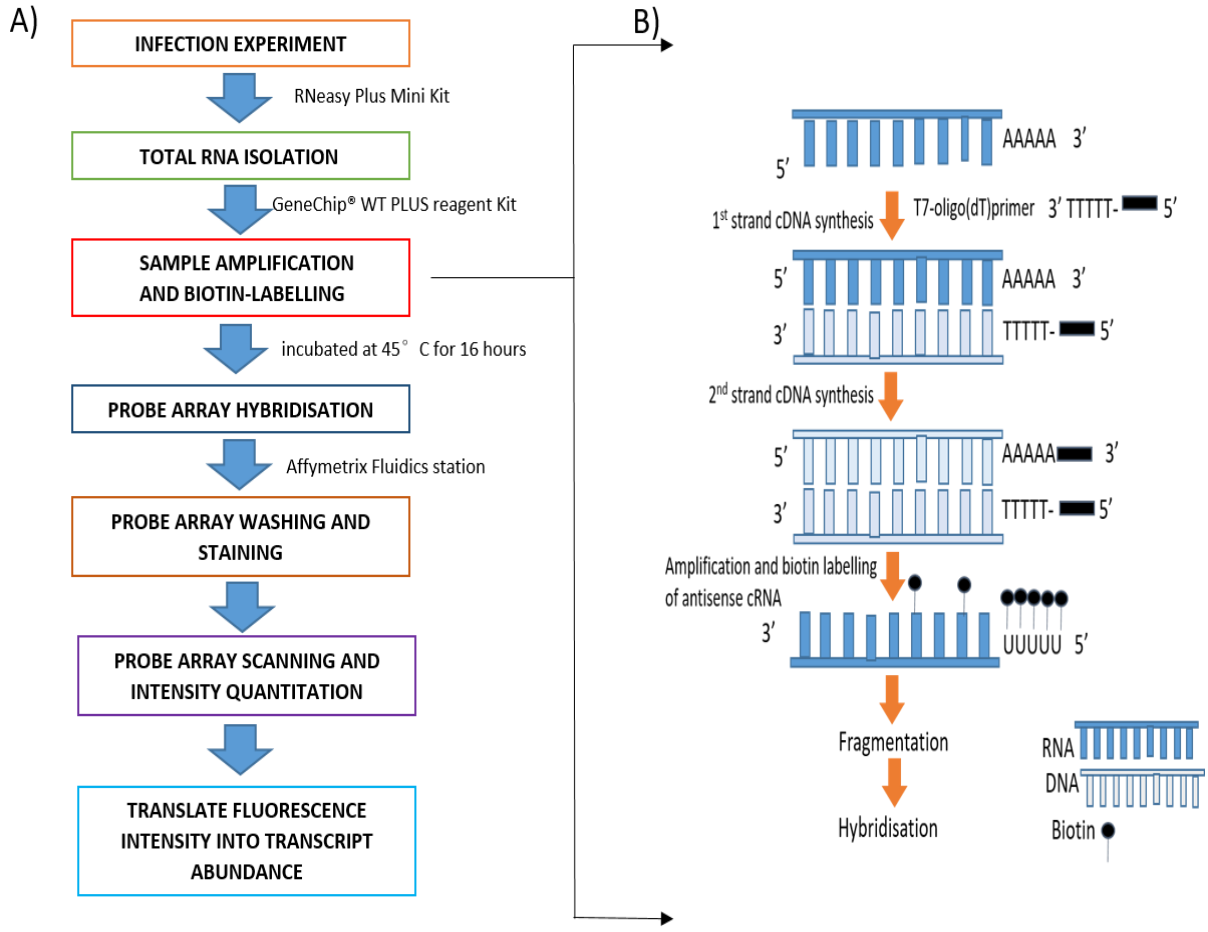

Figure 5.3 Flowchart of a typical genechip system microarray experiment. (A) Once the total RNA has been isolated and the QC determined for its integrity and quality, the samples were amplified and labelled with biotin. This labelled sample was then injected into the array and hybridised overnight in the hybridisation oven. This was followed by probe array washing and staining on the fluidics system. Finally, the arrays were scanned and the fluorescence intensity were translated into transcript abundance. (B) Flowchart of sample amplification and biotin-labelling. The first strand of cDNA was reverse-transcribed from T7-oligo(dT) primer, a primer that consists of poly(T) tail and a T7 polymerase-binding site. This was then followed by the synthesis of second cDNA by RNaseH and *E.coli* DNA polymerase I, producing a double-stranded cDNA. This cDNA was then made blunt-ended with T4 DNA polymerase and later used as a template for *in vitro* transcription (IVT) using T7 RNA polymerase and biotinylated ribonucleotides, forming biotin-labelled cRNA sample. The biotin-labelled cRNA was then purified and fragmented before hybridised to the array (both figure (A) and (B) were self-drawn).

5.2.3 Affymetrix Expression Console Software: Preprocessing steps

The microarray data presented in this thesis were RMA (Robust Multi-array Average) - background adjusted, normalised across arrays by quantile normalisation, and summarised by the median polish algorithm using Affymetrix Expression Console Software 1.4.1. This software can be accessed for free from Affymetrix Software Downloads. Normalisation is needed to reduce any sources of variation that could arise due to differences in sample preparation, production and processing of arrays. The intensity of the individual probe signals were then summarised into a single expression of each probe set in the form of $\log_2$ transformed values. This probe set summarisation was then converted into *CHP* files from the *CEL* files using GeneChip Command Console (AGCC) for further downstream analysis. Relevant NetAffx library files were downloaded from the Affymetrix website and imported into the software for the probe set annotation.

Once the probe set summarisation was completed, quality evaluation was necessary to identify poor-quality arrays or outlier arrays. Boxplots were used to look at individual arrays to detect any with divergent probe intensity distributions (Figure 5.4). All of the boxplots generated from the data from the 18 arrays were properly aligned and no obvious divergence from the median value were seen (the red line) (Figure 5.4(C)), hence none of the arrays were considered to be an outlier and all were included for further downstream analysis.

In addition to generating box plots, Expression Console Analysis software also includes several other Quality Control (QC) functionalities, namely hybridisation control (Figure 5.5 (A)) and labelling control (Figure 5.5 (B)). The hybridisation efficiency of the samples on the arrays was assessed through the use of Hybridisation Controls termed bacterial spikes. These bacterial spikes are mRNA transcripts derived from genes in the biotin synthesis pathway of *E. coli* (*bioB, bioC* and *bioD*) and *cre* is the recombinase gene from P1 bacteriophage. These mRNAs were biotinylated and fragmented independently from the starting RNA samples and injected directly into the hybridisation cocktail onto the GeneChip probe arrays to assess the consistency of hybridisation, washing and staining procedures across all samples, hence the overall microarray performance. The probe set for these genes were represented on the GeneChips. The hybridisation controls were added at different concentrations (1.5pM, 5pM, 25pM and 100pM for *bioB, bioC, bioD* and *cre* respectively), and the signal intensity increased

according to their relative concentration indicating the hybridisation passed this quality control step (AFFX-r2-Ec-*bioB*<*bioC*<*bioD*<*cre*) (Figure 5.5 (A)).

The efficiency of target labelling can be evaluated by using exogenous positive control Poly-A RNAs spikes, where these RNAs were spiked in to the starting RNA prior to cDNA synthesis and were amplified and labelled together with the RNA samples. These poly-A mRNA spikes are *in vitro* synthesised polyadenylated transcripts for *B. subtilis* genes that are absent in eukaryotic samples (*lys, phe, thr*, and *dap*). The probe set for these genes were represented on the GeneChips. The controls were added in different proportions to the isolated RNA (1:100,000, 1:50,000, 1:25,000 and 1:7,500 for *lys, phe, thr,* and *dap* respectively), and therefore, the labelling was considered to have passed the quality control when the signal values increased in the order AFFX-r2-Bs-*lys*<*phe*<*thr*<*dap* (Figure 5.5 (B)). The *lys* gene was added at the lowest proportion (1:100,000 of the total RNA) which is close to the sensitivity level of microarray. From the data presented in Figure 5.5, all 18 arrays showed the expected results, indicating that both hybridisation and labelling met the QC criteria for Affymetrix GeneChips.

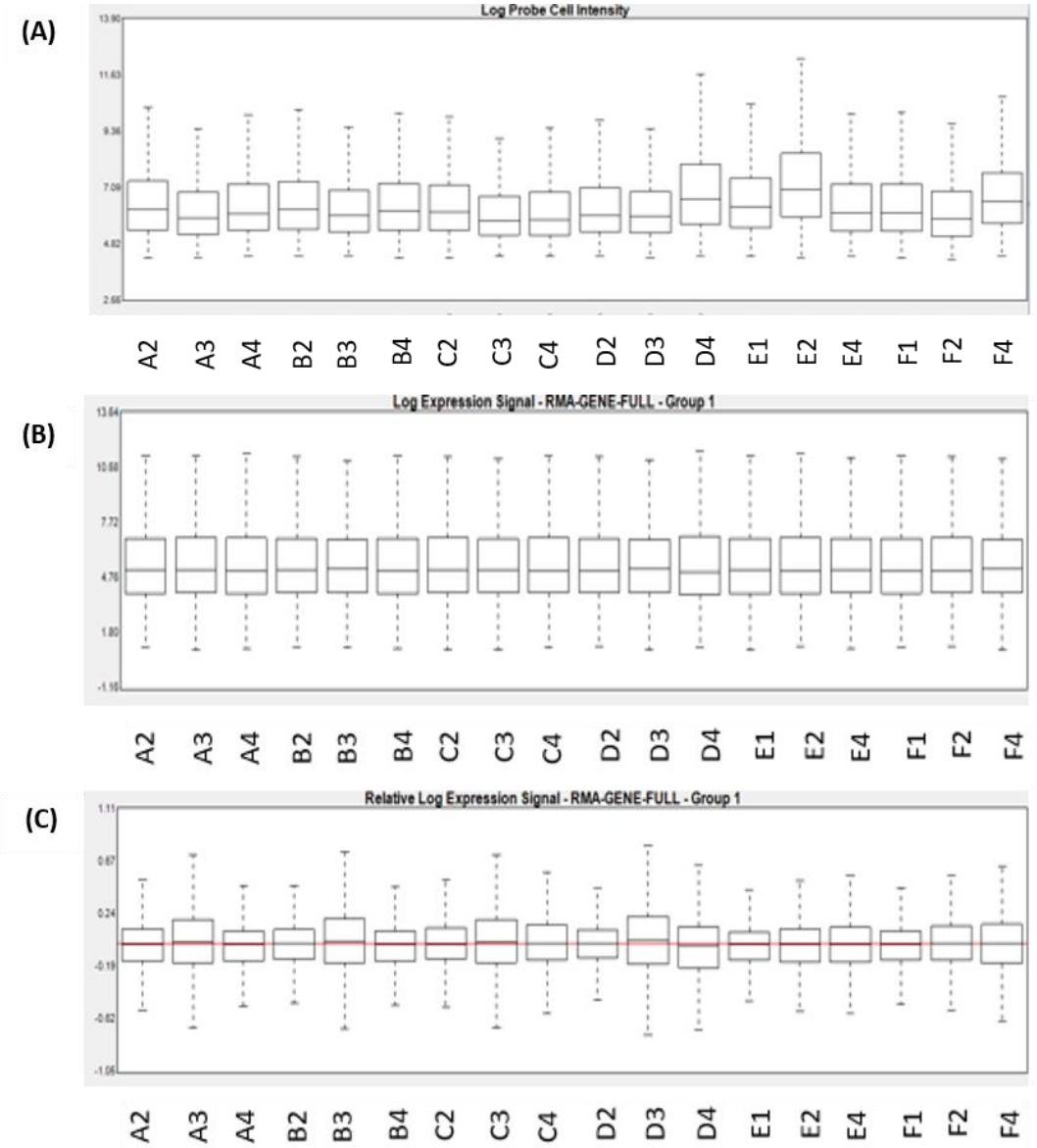

Figure 5.4 Boxplots of log-intensity distribution across all 18 GeneChips. (A) The probe cell intensity box plots were generated from *CEL* files before normalisation, therefore some differences in the distributions are to be expected. Figure (B) shows the Signal Box Plot produced from the summarised probe set signal values in *CHP* files. The x-axis shows the GeneChip with sample identity and y-axis shows the log2 intensity of probes for (A) and (B). Figure (C) shows the Relative Signal Box Plot where the distribution of probe set signal values on each array is set to the median array for the group, hence identifying any array with unusual signal distribution.

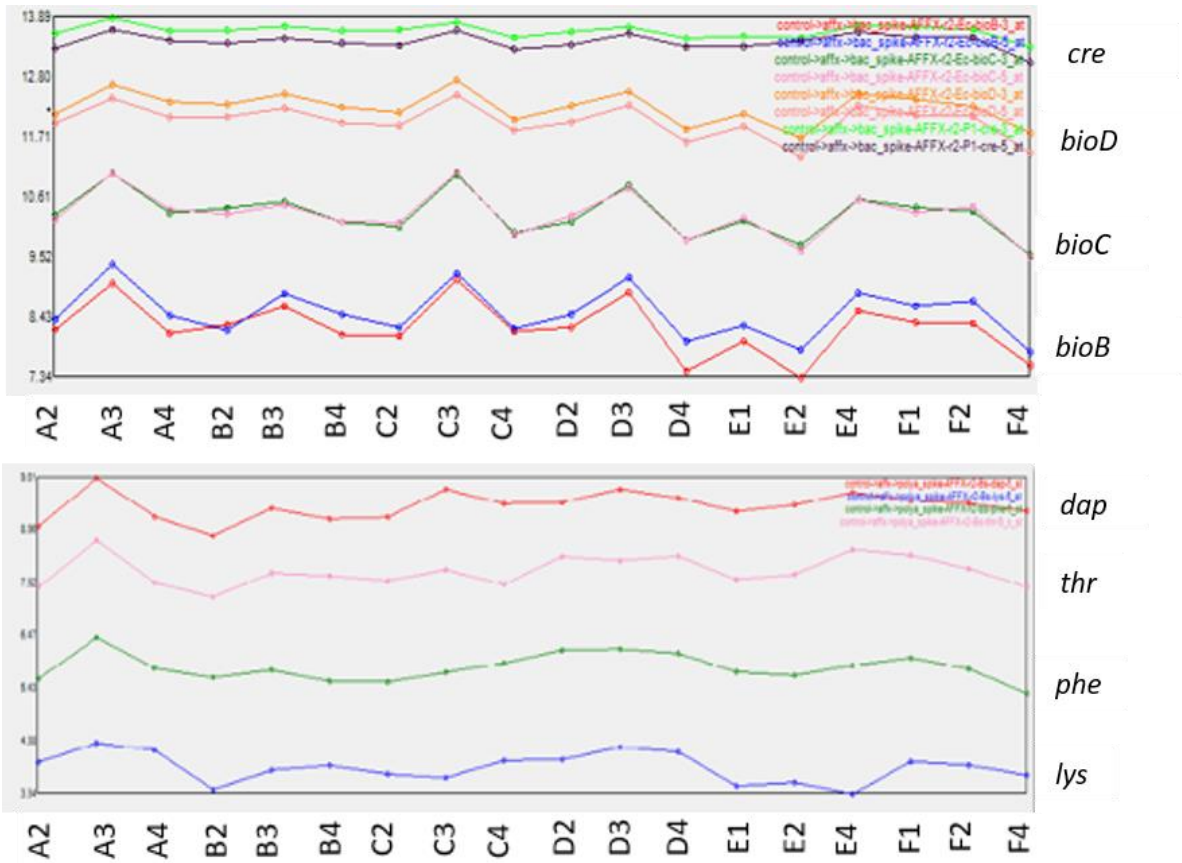

Figure 5.5 Hybridisation and polyA controls. The x-axis is the GeneChips with sample identity while the y-axis is the signal intensity of these genes that have been log2 transformed. (A) shows line graphs of signal intensity of hybridisation controls with increasing intensity from bioB<bioC<bioD<Cre. (B) shows line graphs of signal intensity of PolyA spike controls with increasing signal intensity from lys<phe<thr<dap.

5.2.4 Principal Component Analysis

Principal component analysis (PCA) is an exploratory multivariate statistical tool to visualise any variations, and hence the patterns among the samples used for transcriptome analysis. The fundamental principle of PCA is to reduce the dimensionality of the data matrix by identifying a new set of variables (PCA1, PCA2, PCA3) that account for as much of the variance in the original data set (Raychaudhuri *et al*, 2000). The first principal component (PCA1) samples the largest sources of gene expression signal variance in the data. While the remaining variability that is not accounted for by PCA1 is represented by PCA2. PCA3 captures the remaining variability from PCA2. The PCA plot in figure 5.6 was derived from log-transformed intensity data of 18 arrays; three independent biological replicates of six different cell populations that were addressed in the present study ((i) uninfected BMDMs at 8 hours, (ii) BMDMs infected with WT strain at 8 hpi, (iii) BMDMs infected with *ΔbimA* strain at 8hpi, (iv) uninfected BMDMs at 12 hours, (v) BMDMs infected with WT strain at 12hpi and (vi) BMDMs infected with *ΔbimA* strain at 12hpi). It would be ideal if the PCA data demonstrated six distinct clusters representing each of the cell populations. However, in our analysis, no obvious separate clustering between the populations could be observed (Figure 5.6), but instead all the cell populations were mixed between replicates and between experimental conditions. By analysing the data more closely, the uninfected BMDM samples at 8 hours were paired with uninfected BMDM samples at 12 hours in at least two sets of samples. Likewise, the WT-infected BMDMs was paired with the BMDMs infected with Δ*bimA* at respective time points, indicating that there was only a small variance of gene expression in the host cells when infected either with WT *B. pseudomallei* or the Δ*bimA* strain. In general, these data imply that variables between the replicates rather than the experimental factor itself accounted for the non-clustering within the plot. Differences in serum-containing cell culture, variation in cells grown and differentiation of BMDMs, differences in sample collection or sample handling, all these factors can affect the sensitivity of the high-throughput microarray, to a degree that can dominate biological changes, making it difficult to maintain consistent, reproducible results (Coombes *et al*, 2005). In addition, the variance of PCA1, PCA2 and PCA3 were relatively small (total of 33.4%) indicating that there were not many differences in gene expression between the cell populations studied.

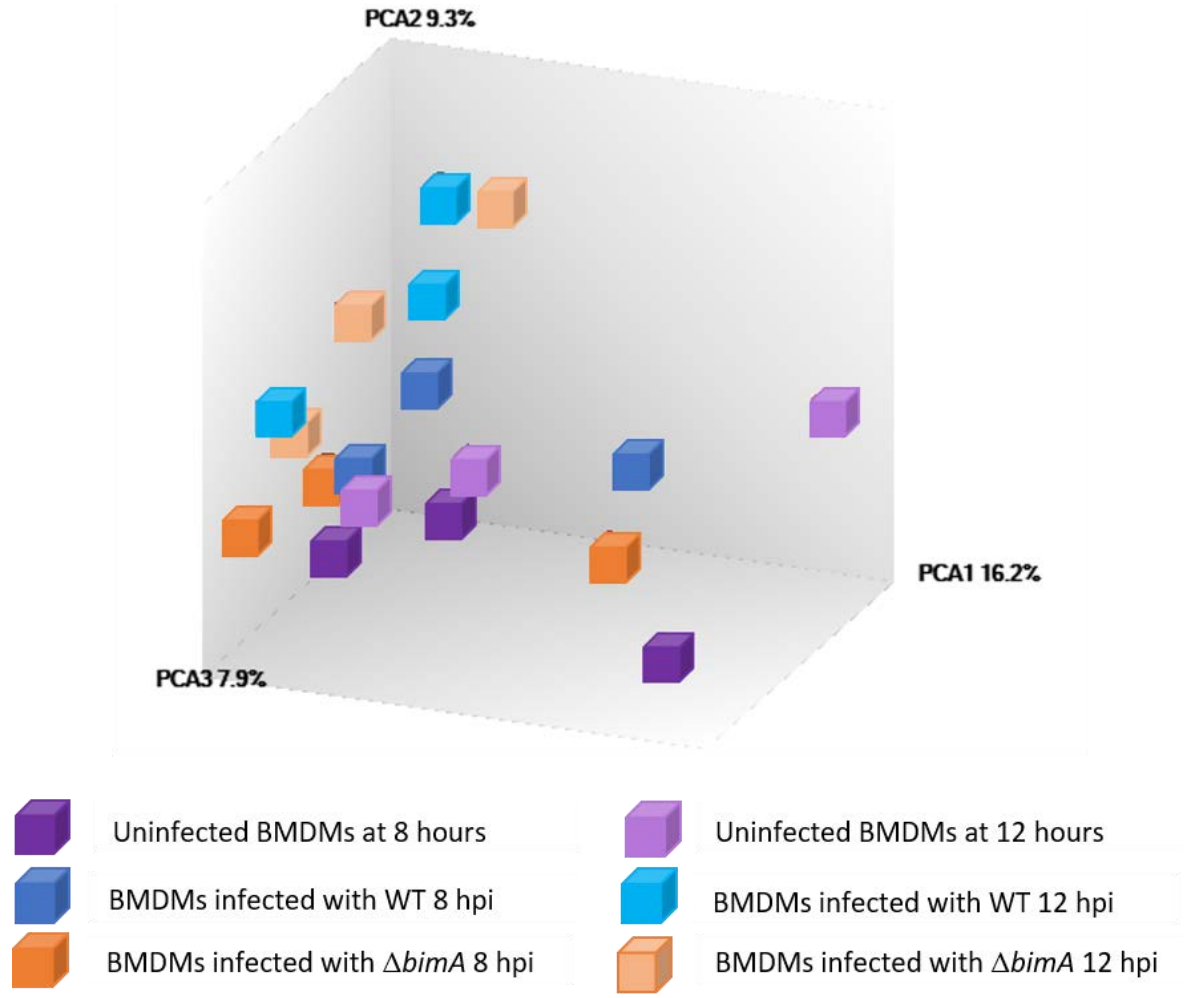

Figure 5.6 Principal component analysis (PCA) of 18 samples. Samples are coloured according to the sample populations. The percent variations accounted for by the first (PCA1), second (PCA2) and third (PCA3) axes are indicated.

5.2.5 Identifying the Differentially Expressed Genes using Affymetrix TAC Software

Affymetrix Transcriptomic Analysis Console (TAC) is a user-friendly software provided by Affymetrix Corporation for researchers to identify differentially expressed genes (DEGs). Firstly, the *CHP* files generated from the Expression Console (EC) software were imported into the TAC software. The imported files were then grouped to the appropriate group window; biological replicates for each experimental condition were considered in the same group. There were two different analyses performed; the first included three separate groups (i.e. uninfected BMDMs, BMDMs infected with WT strain, and BMDMs infected with *ΔbimA* strain) at 8 hpi while the second analysed the 12 hpi data. The workflow for the microarray analyses is illustrated in figure 5.7. Gene-level analysis was performed to compute differential expression between the three groups. Next, pairwise comparison was selected between two groups; WT infected BMDMs versus uninfected BMDMs, and *ΔbimA* infected BMDMs versus uninfected BMDMs (Figure 5.7). DEGs were selected if the p-value was <0.05, and fold change exceeded 1.5 (both upregulated and downregulated) between two groups (Table 5.2). The level of significance was tested using the One-Way ANOVA p-value. The average intensity of all the samples in a condition was based on Tukey's Bi-Weight Average Signal. The Volcano Plot Graph of each comparison pair was included to identify changes in datasets. Table 5.2 shows a summary of the number of DEGs in the pairwise comparison. Tables 5.3 to 5.10 list the top 30 genes that were upregulated and downregulated for each comparison.

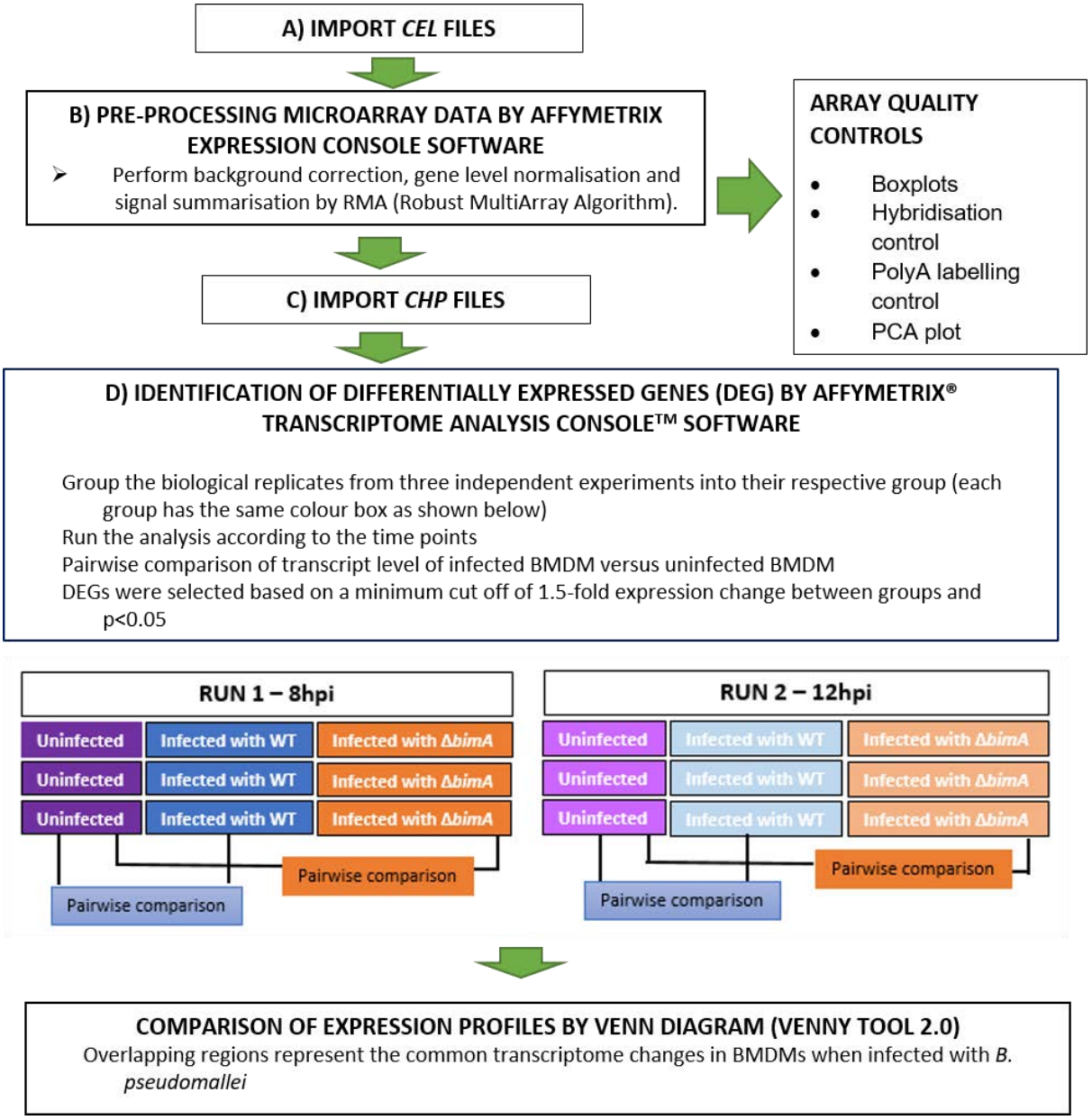

Figure 5.7 Workflow of microarray data analyses. The *CEL* files were first imported into Affymetrix Expression Console (ES) software for pre-processing the microarray data. QC of the arrays were also determined by generating box plots, line graphs for hybridisation and polyA labelling controls, as well as PCA plot. When the arrays met the quality control criteria, the output data in the form of CHP files were imported into Affymetrix Transcriptomic Analysis Software (TAC) to identify the differential expressed genes (DEGs). The transcript level was compared pairwise between the infected BMDMs versus uninfected BMDMs. DEGs were selected when the fold expression change exceeded 1.5 with a p-value <0.05. The expression profiles were then compared by Venn diagram to identify the common genes that were changed upon infection with *B. pseudomallei*.

8hpi

	BMDMs infected with WT vs uninfected BMDMs	BMDMs infected with Δ*bimA* vs uninfected BMDM
Number of up-regulated genes	141	153
Number of down-regulated genes	36	39
Total number of genes	**177**	**192**

12hpi

	BMDMs infected with WT vs uninfected BMDM	BMDMs infected with Δ*bimA* vs uninfected BMDM
Number of up-regulated genes	231	239
Number of down-regulated genes	106	93
Total number of genes	**337**	**332**

Table 5.2 Number of differential expressed genes (DEGs) that met the criteria of p-value <0.05 and fold change exceeding 1.5 for each pairwise comparison

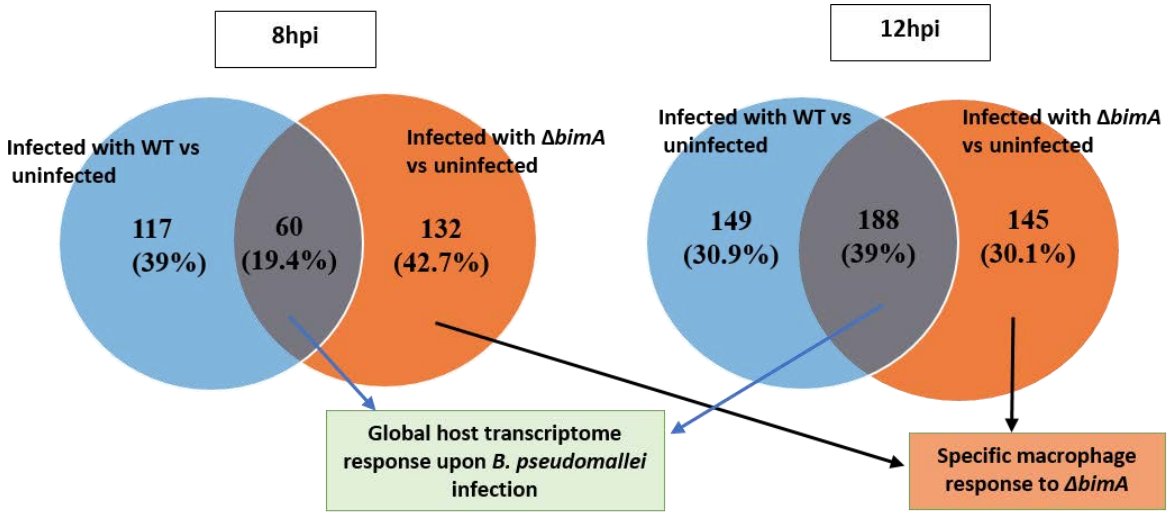

Figure 5.8 Venn diagram comparison of DEGs identified from Affymetrix TAC software. Blue and orange circles represent the DEGs in BMDMs when infected with WT and Δ*bimA* strains respectively. Numbers represent total genes that were significantly up or down -regulated in comparison to uninfected cells. The number shown in the overlap of the Venn circles denotes the common host transcriptomic changes upon infection with *B. pseudomallei*. The non-overlapping orange circle represents the genes that were differentially expressed specifically when the host cells encounter the Δ*bimA* mutant.

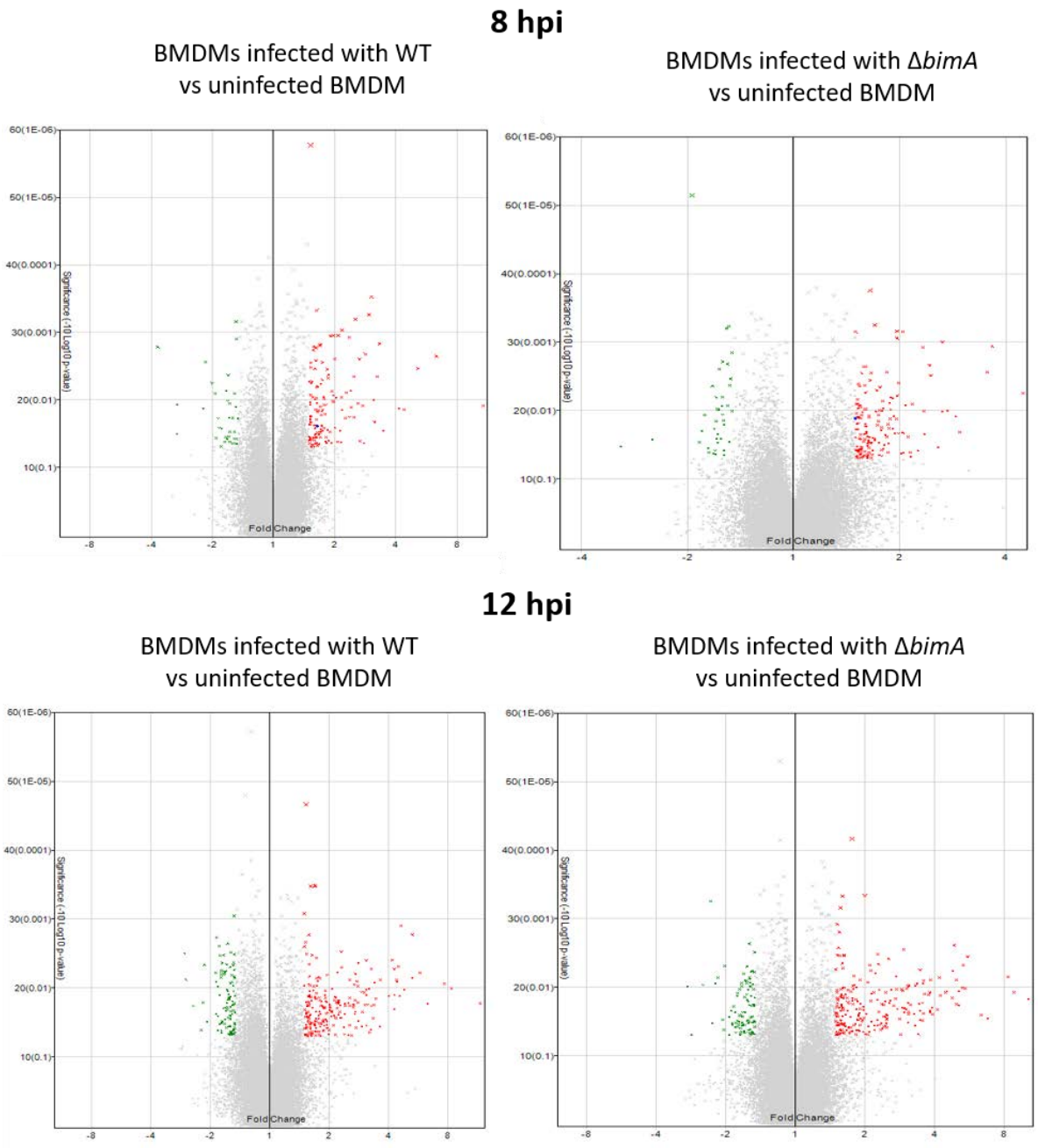

Figure 5.9 Volcano Plots of each comparison pair. X-axis is the linear fold change from comparison pair and Y-axis is $-10\log_{10}$ p-value of the ANOVA p-values. Red dots represent the upregulated transcripts while the green dots represent the downregulated transcripts.

With the cut-off described above, 177 genes (141 upregulated and 36 downregulated) and 192 genes (153 upregulated and 39 downregulated) were identified as differentially expressed in BMDMs infected with WT strain and *ΔbimA* strain respectively at 8hpi. At at 12hpi, more DEGs were identified with 337 genes (231 upregulated and 106 downregulated) and 332 genes (239 upregulated and 93 downregulated) in BMDMs infected with WT strain and *ΔbimA* strain respectively (summarised in Table 5.2). By comparing the time points, the number of DEGs were much greater (approximately 1.5 fold) at 12hpi as compared to 8hpi. The majority of the genes that were differentially expressed were upregulated, and only about 20-30% were downregulated (Table 5.2). The Volcano plots also demonstrate this trend (Figure 5.9). Upregulated genes demonstrated up to an 11-fold change, especially at the later time point of 12hpi, but the majority of downregulated genes were below a -3.0-fold change, regardless of any pairwise comparison (Figure 5.9).

In general, the upregulated genes that were consistently present in all groups were pro-inflammatory mediators namely interleukin-6 (Il-6), interleukin-1 beta (IL-1β), interleukin-1 alpha (IL-1α), prostaglandin-endoperoxide synthase 2 (PTGS2), and the chemokine ligand 3 (CXCL3). This cluster of genes constitutes a general 'alarm signal' for inflammatory responses (Jenner & Young, 2005). Several IFN-stimulating genes (ISGs) and IFN-inducible chemokine genes were also upregulated, which were more profound in cells infected at 12 hours with both the WT and Δ*bimA* strains. This cluster of genes includes ISG15, OASL1 (2',5'-oligoadenylate synthetase-like 1), OASL2, OAS2 and CXCL10. This expression signature has been shown to be upregulated in macrophages that have been stimulated with other bacteria, and highlights its importance in defence against bacteria (Jenner & Young, 2005). However, the downregulated genes were difficult to analyse since many of them were predicted genes that have not yet been characterised. Besides, the genes listed as down-regulated were not obviously associated with innate mechanisms.

The resulting lists of genes were then compared between the BMDMs infected with WT and *ΔbimA* at each time point by generating Venn diagrams using VENNY tool version 2.1, an interactive tool developed by Juan Carlos Oliveros in 2007 (http://bioinfogp.cnb.csic.es/tools/venny/index.html) (Figure 5.8). The list of DEGs in the overlapping region of the Venn diagram represents the common response of BMDMs towards *B. pseudomallei.* While the non-overlapping regions are where the genes were unique to either infection with the WT or the *ΔbimA* mutant strain. Of these, for infection at 8 hpi, 39% were unique to the WT strain versus uninfected, 19.4% were shared with both strains and 42.7%

were unique to Δ*bimA*. While for infection at 12 hpi, more genes were found in the overlapping region with a percentage of 39%, about 31% were unique to the WT strain, and the remaining 30% were unique to Δ*bimA* (Figure 5.8). Although the total number of DEGs were not different between the macrophages infected with WT or the Δ*bimA* mutant, surprisingly the percentage of genes shared with both strains was relatively small (20% at 8hpi and 40% at 12hpi). These DEGs were then grouped into biological pathways using Ingenuity Pathway Analysis.

Table 5.3 Top 30 upregulated transcripts in BMDMs infected with WT versus uninfected at 8 hpi

Gene Name	Description	Fold Change	ANOVA p-value
IL-6	interleukin 6	10.74	1.22E-02
IL-1β	interleukin 1 beta	6.33	2.26E-03
PTGS2	prostaglandin-endoperoxide synthase 2	5.14	3.42E-03
IL-12β	interleukin 12b	4.40	1.40E-02
IL-1α	interleukin 1 alpha	4.13	1.34E-02
IFIT1	interferon-induced protein with tetratricopeptide repeats 1	3.48	2.86E-02
CMPK2	cytidine monophosphate (UMP-CMP) kinase 2, mitochondrial	3.32	1.47E-03
RSAD2	radical S-adenosyl methionine domain containing 2	3.24	4.49E-03
CXCL1	chemokine (C-X-C motif) ligand 1	3.15	2.12E-02
FPR1	formyl peptide receptor 1	3.12	1.00E-02
CXCL3	chemokine (C-X-C motif) ligand 3	3.03	2.96E-04
RTP4	receptor transporter protein 4	2.96	5.48E-04
GBP2B	guanylate binding protein 2b	2.85	2.10E-03
GBP5	guanylate binding protein 5	2.79	4.32E-02
OASL2	2-5 oligoadenylate synthetase-like 2	2.65	2.48E-03
GM22197	predicted gene, 22197	2.65	4.07E-02
NOS2	nitric oxide synthase 2, inducible	2.60	1.13E-02
IRG1	immunoresponsive gene 1	2.53	6.42E-04
GBP2	guanylate binding protein 2	2.49	1.83E-02
FPR2	formyl peptide receptor 2	2.41	1.28E-02
OLR1	oxidised low density lipoprotein (lectin-like) receptor 1	2.39	7.35E-03
IFI44L	interferon-induced protein 44 like	2.37	1.81E-02
CLEC4E	C-type lectin domain family 4, member e	2.36	1.17E-03
OASL1	2-5 oligoadenylate synthetase-like 1	2.29	7.84E-03
GM22023	predicted gene, 22023	2.25	1.86E-02
IFI204	interferon activated gene 204	2.17	1.41E-02
ISG15	ISG15 ubiquitin-like modifier	2.17	9.17E-04
GBP3	guanylate binding protein 3	2.16	9.25E-03
GM4745	predicted gene 4745	2.14	4.24E-02
GM23601	predicted gene, 23601	2.13	2.85E-02

Table 5.4 Top 30 downregulated transcripts in BMDMs infected with WT versus uninfected at 8hpi

Gene Name	Description	Fold Change	ANOVA p-value
TCRG-V4	T cell receptor gamma, variable 4	-3.72	1.65E-03
TRGJ1	T cell receptor gamma joining 1	-2.99	3.16E-02
GM22571	predicted gene, 22571	-2.98	1.16E-02
GM17655	predicted gene, 17655	-2.22	1.34E-02
GM24334	predicted gene, 24334	-2.17	2.74E-03
GM24763	predicted gene, 24763	-2.00	5.66E-03
GM22321	predicted gene, 22321	-1.93	8.05E-03
P2RY12	purinergic receptor P2Y, G-protein coupled 12	-1.91	3.69E-02
VMN1R157	vomeronasal 1 receptor 157	-1.87	1.89E-02
GM22769	predicted gene, 22769	-1.85	2.59E-02
MIR541	microRNA 541	-1.81	4.88E-02
GM25914	predicted gene, 25914	-1.80	2.64E-02
KLRA9	killer cell lectin-like receptor subfamily A, member 9	-1.74	4.18E-02
MYH4	myosin, heavy polypeptide 4, skeletal muscle	-1.72	3.56E-02
OLFR390	olfactory receptor 390	-1.71	7.28E-03
OLFR99	olfactory receptor 99	-1.69	3.78E-02
GM25796	predicted gene, 25796	-1.68	1.03E-02
SPEER2	spermatogenesis associated glutamate (E)-rich protein 2	-1.67	4.30E-03
n-R5S52	nuclear encoded rRNA 5S 52	-1.66	3.47E-02
GM24384	predicted gene, 24384	-1.66	1.84E-02
MUP4	major urinary protein 4	-1.64	4.20E-02
GM23325	predicted gene, 23325	-1.59	4.39E-02
IGHV1-73	immunoglobulin heavy variable 1-73	-1.56	4.43E-02
SULT2A2	sulfotransferase family 2A, dehydroepiandrosterone (DHEA)-preferring, member 2	-1.56	8.09E-03
GM15758	predicted gene 15758	-1.56	2.95E-02
GM22805	predicted gene, 22805	-1.56	3.78E-02
HIST1H2BM	histone cluster 1, H2bm	-1.53	3.78E-02
LIFR	leukaemia inhibitory factor receptor	-1.53	6.92E-04
GM22586	predicted gene, 22586	-1.53	1.27E-02
PTGER3	prostaglandin E receptor 3 (subtype EP3)	-1.52	1.25E-03

Table 5.5 Top 30 upregulated transcripts in BMDMs infected with Δ*bimA* versus uninfected at 8hpi

Gene Name	Description	Fold Change	ANOVA p-value
IL-6	interleukin 6	4.47	5.56E-03
IL-1β	interleukin 1 beta	3.66	1.15E-03
PTGS2	prostaglandin-endoperoxide synthase 2	3.54	2.75E-03
GBP5	guanylate binding protein 5	2.96	2.06E-02
IL-12β	interleukin 12b	2.89	1.19E-02
RSAD2	radical S-adenosyl methionine domain containing 2	2.74	1.01E-02
GM22271	predicted gene, 22271	2.65	9.96E-04
IL-1α	interleukin 1 alpha	2.64	1.03E-02
GBP2B	guanylate binding protein 2b	2.57	3.41E-02
FPR1	formyl peptide receptor 1	2.45	3.05E-03
RTP4	receptor transporter protein 4	2.43	2.18E-03
CMPK2	cytidine monophosphate (UMP-CMP) kinase 2, mitochondrial	2.35	2.22E-02
NOS2	nitric oxide synthase 2, inducible	2.34	1.01E-02
CXCL3	chemokine (C-X-C motif) ligand 3	2.33	1.19E-03
GBP2	guanylate binding protein 2	2.25	3.81E-02
GM20461	predicted gene 20461	2.17	8.03E-03
GBP3	guanylate binding protein 3	2.15	4.70E-02
ADAM23	a disintegrin and metallopeptidase domain 23	2.14	4.11E-02
IFI44L	interferon-induced protein 44 like	2.11	2.40E-02
OASL2	2-5 oligoadenylate synthetase-like 2	2.08	8.36E-03
FNBP1L	formin binding protein 1-like	2.05	2.17E-02
OLFR344	olfactory receptor 344	2.05	4.09E-02
IRG1	immunoresponsive gene 1	2.04	7.04E-04
USP18	ubiquitin specific peptidase 18	2.02	4.25E-02
DDX60	DEAD (Asp-Glu-Ala-Asp) box polypeptide 60	1.99	3.97E-03
4930433I11RIK	RIKEN cDNA 4930433I11 gene	1.99	2.16E-02
CXCL1	chemokine (C-X-C motif) ligand 1	1.97	6.10E-03
GM24651	predicted gene, 24651	1.97	6.90E-04
IFI204	interferon activated gene 204	1.96	1.32E-02
CLEC4E	C-type lectin domain family 4, member e	1.96	8.75E-04

Table 5.6 Top 30 downregulated transcripts in BMDMs infected with Δ*bimA* versus uninfected at 8hpi

Gene Symbol	Description	Fold Change	ANOVA p-value
TRGJ1	T cell receptor gamma joining 1	-3.10	3.33E-02
TCRG-V4	T cell receptor gamma, variable 4	-2.52	2.65E-02
GM6909	predicted gene 6909	-1.95	7.00E-06
GM24727	predicted gene, 24727	-1.85	2.90E-02
PRL2C5	prolactin family 2, subfamily c, member 5	-1.82	1.99E-02
OLFR390	olfactory receptor 390	-1.79	1.15E-02
SNORA44	small nucleolar RNA, H/ACA box 44	-1.75	3.54E-02
MYH4	myosin, heavy polypeptide 4, skeletal muscle	-1.74	4.06E-02
GM24384	predicted gene, 24384	-1.70	4.37E-03
SNORD110	small nucleolar RNA, C/D box 110	-1.69	4.21E-02
KLK1B22	kallikrein 1-related peptidase b22	-1.68	1.82E-02
SNORD61	small nucleolar RNA, C/D box 61	-1.67	4.37E-02
AKR1CL	aldo-keto reductase family 1, member C-like	-1.66	1.44E-02
1700023C21RIK	RIKEN cDNA 1700023C21 gene	-1.66	6.42E-03
IGJ	immunoglobulin joining chain	-1.65	9.49E-03
DEFB2	defensin beta 2	-1.65	2.58E-02
SNORD42B	small nucleolar RNA, C/D box 42B	-1.64	2.92E-02
INS2	insulin II	-1.64	2.20E-02
GM25276	predicted gene, 25276	-1.63	2.46E-03
PRR27	proline rich 27	-1.63	9.79E-03
DEFB10	defensin beta 10	-1.61	2.59E-02
OLFR135	olfactory receptor 135	-1.60	8.52E-03
ZFP763	zinc finger protein 763	-1.59	1.15E-02
GM16066	predicted gene 16066	-1.59	6.35E-03
MRGPRA3	MAS-related GPR, member A3	-1.59	1.93E-03
GM561	predicted gene 561	-1.58	3.83E-02
GM24314	predicted gene, 24314	-1.58	1.39E-02
KRTAP5-2	keratin associated protein 5-2	-1.58	4.47E-02
OLFR1362	olfactory receptor 1362	-1.55	6.33E-04
GM23803	predicted gene, 23803	-1.54	8.53E-03

Table 5.7 Top 30 upregulated transcripts in BMDMs infected with WT versus uninfected at 12hpi

Gene Symbol	Description	Fold Change	ANOVA p-value
IL-6	interleukin 6	11.66	1.68E-02
IFIT1	interferon-induced protein with tetratricopeptide repeats 1	8.30	1.01E-02
PTGS2	prostaglandin-endoperoxide synthase 2	7.61	8.71E-03
TRIM30D	tripartite motif-containing 30D	6.28	1.71E-02
IL-1β	interleukin 1 beta	5.75	6.06E-03
RTP4	receptor transporter protein 4	5.27	1.67E-03
IL-1α	interleukin 1 alpha	4.77	1.06E-02
OASL2	2-5 oligoadenylate synthetase-like 2	4.61	1.24E-03
CXCL3	chemokine (C-X-C motif) ligand 3	4.54	1.30E-02
RSAD2	radical S-adenosyl methionine domain containing 2	4.49	4.88E-03
CXCL10	chemokine (C-X-C motif) ligand 10	4.39	8.16E-03
CMPK2	cytidine monophosphate (UMP-CMP) kinase 2, mitochondrial	4.37	7.65E-03
OASL1	2-5 oligoadenylate synthetase-like 1	4.29	1.27E-02
ISG15	ISG15 ubiquitin-like modifier	4.27	5.31E-03
IFI44L	interferon-induced protein 44 like	4.26	2.03E-02
OAS3	2-5 oligoadenylate synthetase 3	4.18	3.96E-03
GBP5	guanylate binding protein 5	4.01	1.29E-02
MNDA	myeloid cell nuclear differentiation antigen	3.63	7.65E-03
IRF7	interferon regulatory factor 7	3.60	3.63E-02
OAS2	2-5 oligoadenylate synthetase 2	3.44	1.43E-02
GM12250	predicted gene 12250	3.39	8.29E-03
CXCL5	chemokine (C-X-C motif) ligand 5	3.36	1.76E-02
IFI205	interferon activated gene 205	3.34	2.74E-02
DDX58	DEAD (Asp-Glu-Ala-Asp) box polypeptide 58	3.27	5.28E-03
IFI204	interferon activated gene 204	3.27	1.84E-02
TRIM30C	tripartite motif-containing 30C	3.25	4.04E-02
SLFN1	schlafen 1	3.20	4.37E-02
IFIT2	interferon-induced protein with tetratricopeptide repeats 2	3.19	1.03E-02
MX2	myxovirus (influenza virus) resistance 2	3.14	1.75E-02
EPSTI1	epithelial stromal interaction 1 (breast)	3.10	1.27E-02

Table 5.8 Top 30 downregulated transcripts in BMDMs infected with WT versus uninfected at 12hpi

Gene Name	Description	Fold Change	ANOVA p-value
TCRG-V4	T cell receptor gamma, variable 4	-2.68	3.17E-03
CD34	CD34 antigen	-2.66	7.58E-03
CD209A	CD209a antigen	-2.43	1.85E-02
RGS18	regulator of G-protein signalling 18	-2.17	1.62E-02
VWA5B2	von Willebrand factor A domain containing 5B2	-2.14	4.61E-03
PTPN22	protein tyrosine phosphatase, non-receptor type 22 (lymphoid)	-2.07	3.12E-02
OLFR458	olfactory receptor 458	-1.88	6.04E-03
GM22305	predicted gene, 22305	-1.87	2.37E-02
GM23763	predicted gene, 23763	-1.86	8.14E-03
OLFR1216	olfactory receptor 1216	-1.85	1.86E-03
MAGEB1	melanoma antigen, family B, 1	-1.83	9.60E-03
DEFA-PS13	defensin, alpha, pseudogene 13	-1.83	4.13E-02
RGS2	regulator of G-protein signalling 2	-1.82	2.59E-02
GM24839	predicted gene, 24839	-1.80	2.46E-03
SNORD37	small nucleolar RNA, C/D box 37	-1.79	3.38E-02
CDH1	cadherin 1	-1.79	1.26E-02
ALOX5	arachidonate 5-lipoxygenase	-1.78	3.36E-03
FCRLS	Fc receptor-like S, scavenger receptor	-1.76	5.76E-03
GM22236	predicted gene, 22236	-1.76	7.00E-03
TRGV2	T cell receptor gamma variable 2	-1.76	6.30E-03
GM8126	predicted gene 8126	-1.76	4.12E-02
OLFR136	olfactory receptor 136	-1.75	4.50E-02
CCR2	chemokine (C-C motif) receptor 2	-1.74	4.33E-03
SNORA33	small nucleolar RNA, H/ACA box 33	-1.74	3.05E-02
GM23819	predicted gene, 23819	-1.74	5.59E-03
ASGR2	asialoglycoprotein receptor 2	-1.73	3.08E-03
OLFR803	olfactory receptor 803	-1.73	3.08E-02
CD300E	CD300e antigen	-1.71	6.30E-03
VRK1	vaccinia related kinase 1	-1.71	3.34E-03
SUGCT	succinyl-CoA glutarate-CoA transferase	-1.71	1.99E-02

Table 5.9 Top 30 upregulated transcripts in BMDMs infected with Δ*bimA* versus uninfected at 12hpi

Gene Name	Description	Fold Change	ANOVA p-value
IL-6	interleukin 6	10.20	1.49E-02
IFIT1	interferon-induced protein with tetratricopeptide repeats 1	8.86	1.18E-02
PTGS2	prostaglandin-endoperoxide synthase 2	8.35	7.07E-03
TRIM30D	tripartite motif-containing 30D	6.78	2.86E-02
TRIM30C	tripartite motif-containing 30C	6.40	2.55E-02
RTP4	receptor transporter protein 4	5.58	3.57E-03
CXCL10	chemokine (C-X-C motif) ligand 10	5.44	1.04E-02
RSAD2	radical S-adenosyl methionine domain containing 2	5.35	4.76E-03
GBP5	guanylate binding protein 5	5.29	1.02E-02
IL-1β	interleukin 1 beta	5.11	1.14E-02
IFI204	interferon activated gene 204	5.09	1.84E-02
CMPK2	cytidine monophosphate (UMP-CMP) kinase 2, mitochondrial	5.00	7.82E-03
IFI44L	interferon-induced protein 44 like	4.98	1.77E-02
OASL2	2-5 oligoadenylate synthetase-like 2	4.87	2.45E-03
IFIT2	interferon-induced protein with tetratricopeptide repeats 2	4.81	5.78E-03
GBP4	guanylate binding protein 4	4.52	1.14E-02
MX2	myxovirus (influenza virus) resistance 2	4.48	1.19E-02
IL-1α	interleukin 1 alpha	4.23	1.32E-02
ISG15	ISG15 ubiquitin-like modifier	4.21	7.26E-03
EPSTI1	epithelial stromal interaction 1 (breast)	4.12	2.12E-02
IIGP1	interferon inducible GTPase 1	3.93	2.49E-02
GM12250	predicted gene 12250	3.91	1.98E-02
OAS3	2-5 oligoadenylate synthetase 3	3.86	7.85E-03
CXCL3	chemokine (C-X-C motif) ligand 3	3.84	2.31E-02
OASL1	2-5 oligoadenylate synthetase-like 1	3.83	1.19E-02
IFI205	interferon activated gene 205	3.82	2.20E-02
MNDA	myeloid cell nuclear differentiation antigen	3.77	1.30E-02
GM4951	predicted gene 4951	3.62	1.26E-02
GBP9	guanylate-binding protein 9	3.59	2.44E-02
DDX60	DEAD (Asp-Glu-Ala-Asp) box polypeptide 60	3.58	8.04E-03

Table 5.10 Top 30 downregulated transcripts in BMDMs infected with Δ*bimA* versus uninfected at 12hpi

Gene Name	Description	Fold Change	ANOVA p-value
TCRG-V4	T cell receptor gamma, variable 4	-2.94	9.73E-03
TRGJ1	T cell receptor gamma joining 1	-2.81	4.97E-02
CD34	CD34 antigen	-2.51	9.32E-03
GM23763	predicted gene, 23763	-2.32	5.54E-04
ALOX5	arachidonate 5-lipoxygenase	-2.22	8.82E-03
TCRG-C3	T cell receptor gamma, constant 3	-2.16	7.24E-03
GM24142	predicted gene, 24142	-2.06	2.30E-02
PTPN22	protein tyrosine phosphatase, non-receptor type 22 (lymphoid)	-2.04	4.20E-02
CCR2	chemokine (C-C motif) receptor 2	-2.02	4.91E-03
MAGEB1	melanoma antigen, family B, 1	-1.93	2.71E-02
GM25799	predicted gene, 25799	-1.93	4.96E-02
RAB26OS	RAB26, member RAS oncogene family	-1.89	2.20E-02
SNORA33	small nucleolar RNA, H/ACA box 33	-1.88	3.37E-02
SNORD37	small nucleolar RNA, C/D box 37	-1.87	3.54E-02
CD209A	CD209a antigen	-1.85	1.91E-02
GM26345	predicted gene, 26345	-1.82	2.31E-02
GM22797	predicted gene, 22797	-1.82	3.83E-02
RGS18	regulator of G-protein signalling 18	-1.81	4.61E-02
GM25970	predicted gene, 25970	-1.81	3.29E-02
FCRLS	Fc receptor-like S, scavenger receptor	-1.79	1.35E-02
CDH1	cadherin 1	-1.78	3.11E-02
GM26354	predicted gene, 26354	-1.78	3.79E-02
AKR1C19	aldo-keto reductase family 1, member C19	-1.77	1.22E-02
GM5643	heterogeneous nuclear ribonucleoprotein A1 pseudogene	-1.76	3.46E-02
GM20461	predicted gene 20461	-1.75	3.16E-02
MIR743	microRNA 743	-1.74	1.07E-02
CD300E	CD300e antigen	-1.74	2.55E-02
MCM7	minichromosome maintenance deficient 7	-1.74	4.97E-02
GM22303	predicted gene, 22303; topoisomerase (DNA) II alpha	-1.72	2.60E-02

5.2.6 Functional Classification of Differentially Expressed Genes by IPA

The next step after differential expression analysis was to categorise the list of DEGs into functions, interactions and pathways that reflect the underlying biological processes. This process is known as Functional Enrichment Analysis where a statistical algorithm is used to find functional annotations that the set of genes are significantly associated with. Nowadays, there are several Pathway Analysis Software (PAS) available for biologists to carry out such analysis without requiring advanced computer skills. Among the common ones are the free online web interface **D**atabase for **A**nnotation, **V**isualisation and **I**ntegrated **D**iscovery (DAVID) and the commercial software **I**ngenuity **P**athway **A**nalysis (IPA) (QIAGEN). This analysis relies on biological databases where DAVID and IPA functional enrichment annotate pathways based on the DAVID Knowledgebase and IPA's proprietary Knowledgebase respectively (Sherman *et al*, 2007). The data presented here were analysed using IPA software, where this software provides additional graphical representation of biological pathways, a feature which is not available in DAVID. This feature is invaluable to researchers as it visualises the networks of interacting genes, hence allowing insights into specific molecular/cellular pathways based on known biological interactions.

A list of DEGs in each group were uploaded and imported into IPA. *Core Analysis* was performed with default settings in IPA. Right-tailed Fisher's exact tests were used to calculate a p-value for each of the biological functions assigned to the uploaded list of DEGs. The Canonical Pathway Analysis in IPA associates the genes with canonical pathways in Ingenuity's Knowledgebase and returns three measures of association: (1) a list of associated molecules that maps to the pathway, (2) a p-value of the Fisher's exact test and (3) ratio of DEGs mapping to each specific pathway divided by the total number of genes in the pathway.

Out of 60 DEGs that represent the common host response to both strains at 8 hpi, 55 were mapped by IPA and resulted in 69 canonical pathways. Table 5.11 shows the ranking of the top 30 IPA canonical pathways of common host responses to infection at 8hpi. The majority of the top ranking IPA-identified canonical pathways were involved in immune-related signalling and communication associated with host innate and adaptive immune responses. Among them are '*Communication Between Innate and Adaptive Immune Cells'* which was identified at the top of the analysis, '*Role of Cytokines in Mediating Communication between Immune Cells*' (rank 5), '*Crosstalk between Dendritic Cells and Natural Killer Cells'* (rank

11), '*TREM1 Signalling'* and '*Toll-like Receptor Signalling'* (rank 18) in which the pro-inflammatory mediators IL-6, IL-1β, IL-1α, and Tumor Necrosis factor (TNF) were the common associated molecules between them. Some of these signalling pathways were also found at 12hpi (Table 5.11).

At 12hpi, 166 DEGs were found in the overlapping region of differential transcripts to both strains, of which 150 were mapped by IPA and generated 58 canonical pathways. Table 5.12 shows the ranking of the top 30 IPA canonical pathways of common host responses to infection by *B. pseudomallei* at 12hpi. IPA analysis identified several pathways related to Interferon signalling in response to *B. pseudomallei* at 12hpi (Table 5.12). The most significantly enriched canonical pathway in this category is '*Activation of Interferon Regulatory Factors (IRF) by Cytosolic Pattern Recognition Receptors'* followed by '*Interferon Signalling*'. Interestingly, this interferon-dependent cellular pathway is mainly involved in the host recognition of viral PAMPs, yet it was also upregulated in response to *B. pseudomallei.* The genes that were upregulated in the pathway include the cytosolic PRRs retinoic acid inducible gene-1 (RIG-1) (also known as DDX58) and RIG-1 like receptors (RLR), namely melanoma differentiation gene-5 (MDA-5) (also known as IFIH) and laboratory of genetics and physiology 2 (LGP2) (also known as DHX58). Upon RNA recognition, RIG-1 and MDA-5 are recruited to mitochondria to bind with the adaptor protein MAVS (mitochondrial anti-viral signalling). This results in a signalling cascade leading to nuclear translocation of the transcription factors Interferon Regulatory Factor 3 (IRF3) and IRF7 (reviewed in Reikine *et al*, 2014). IRF3 and IRF7 induce the expression of interferon and interferon-stimulated genes (ISGs), of which IFNα4 and ISG15 were among the genes upregulated in the dataset. Genes encoding transcription factors involved in generating an IFN response namely STAT1 and STAT2, together with their partner IRF9, were also found to be significantly upregulated (reviewed in Platanias, 2005). In addition to the involvement of PRR-signalling through RIG-1 and RLRs, the analysis also identified more PRR-related signalling pathways namely '*Role of Pattern Recognition Receptors in Recognition of Bacteria and Viruses*' (3rd rank) and '*Toll-like receptor signalling'* (13th rank). Given the previously identified role of programmed cell death during *B. pseudomallei* infection *in vitro* (Bast *et al*, 2014), '*Death receptor signalling'* was identified at 17th rank. Several poly-(ADP)ribose polymerase (PARP) molecules were associated with the pathway namely PARP9 (BAL1), PARP10, PARP12 and PARP14 (BAL2) which were also found in other pathways namely '*Retinoic Acid Mediated Apoptosis Signalling*' (rank 6th) and '*UVA-induced MAPK signalling*' (rank 16th). The PARP proteins are involved

in post-translational modification of ADP-ribose protein using NAD^+ as a substrate, a process known as poly(ADP-ribosyl)ation. This mechanism is important in modulating several intracellular pathways including the DNA damage response, protein stability and cell death (Vyas & Chang, 2014; Schreiber *et al*, 2006).

For the canonical pathways that were identified uniquely to the *B. pseudomallei* WT strain, they were generally similar to the canonical pathways of common host response to both strains as described above, but with additional specific molecules. Interferon-related immune canonical pathways '*Activation of IRF by Cytosolic Pattern Recognition Receptors'* and '*Role of RIG1-like receptors in Antiviral Innate Immunity'* were also identified at both 8hpi and 12hpi in this category (Table 5.13 and 5.14). Interestingly, both cytoplasmic sensors of viral nucleic acids Interferon Induced with Helicase C domain 1 (IFIH1) and Z-DNA binding protein 1 (ZBP-1/DAI) were found to be uniquely increased at 8hpi in response to *B. pseudomallei* WT strain. At 12 hpi, the transcription factor IRF7 involved in expression of interferon-related genes was found to be significantly expressed along with the pro-inflammatory cytokine TNF (tumour necrosis factor). Noticeably, the inhibitory gene *NFKBIE* of the NF-kB signalling pathway was found to be upregulated in this category both at 8 hpi and 12 hpi. An increase in the expression of such an inhibitory gene is an equally important aspect of the response to re-balance the host cell to its inactivated state when the inflammatory stimulus is no longer present.

In contrast, very few IPA canonical pathways with significant p-value (less than 0.05) could be mapped with the list of DEGs describing the specific response of macrophages to the Δ*bimA* mutant (2 pathways for 8 hpi and 12 pathways for 12 hpi) (Table 5.15 and 5.16). Up to 40% of the genes were not characterised in IPA pathways. 53 genes out of 132 DEGs and 52 genes from 149 DEGs, identified at 8hpi and 12hpi respectively, could not be mapped by IPA. This indicates that the genes involved in detection and elimination of the *B. pseudomallei* Δ*bimA* mutant are likely to be novel. The *NOS2* (Type 2 nitric oxide synthase, also known as iNOS) gene was upregulated specifically in response to Δ*bimA*, and was mapped to '*Citrulline-Nitric Oxide Cycle'* and '*Superpathway of Citrulline Metabolism'* pathways based on IPA analysis. Nos2/iNOS enzyme is expressed in activated macrophages, synthesises nitric oxide (NO) production for controlling replication of other Gram-negative bacteria such as *E. coli* and *S. typhi*, but not in response to *B. pseudomallei* (Utaisincharoen *et al*, 2001). *B. pseudomallei* has previously been shown to be capable of evading Nos2/iNOS-dependent macrophage killing (Utaisincharoen *et al*, 2001), hence, an increase in the expression here could be a specific

response to the Δ*bimA* strain. Additionally, the FAS gene was also increased in expression in this study where Fas protein is expressed on the surface of macrophages to interact with its ligand (FasL), resulting in FasL-induced apoptosis. This apoptotic mechanism effectively controlled the intracellular viability of *Mycobacterium tuberculosis* (Oddo *et al*, 1998), hence could represent a potential mechanism to the reduced intracellular survival of the Δ*bimA* mutant. The FAS gene was mapped to three different IPA canonical pathways namely, '*p53 signalling'*, '*Type I Diabetes Mellitus Signalling'*, '*Allograft Rejection Signalling*' and '*Aryl Hydrocarbon Receptor Signalling'*. In addition to NOS2 and FAS, *FNBP1L* (formin binding protein-1 like) gene (also known as TOCA-1) was also differentially expressed in response to Δ*bimA* at 12hpi, but was not mapped to any canonical pathway. TOCA-1 was shown to have a role in antibacterial autophagy to restrict intracellular replication of *Salmonella enterica* serovar Typhimurium (Huett *et al*, 2009), hence, another potential innate mechanism to target the *B. pseudomallei* Δ*bimA* mutant.

Table 5.11 Top 30 IPA canonical pathways of common host responses to infection by *B. pseudomallei* at 8hpi. The table ranks the pathways from the lowest to the highest p-value based on Fisher's exact test. The ratio is calculated as the number of DEGs in the given pathway (listed as associated molecules) divided by the total number of genes annotated in each canonical pathway in IPA.

	Canonical pathways from IPA	p-value	Ratio	Associated molecules
1	Communication Between Innate and Adaptive Immune Cells	6.13E-12	8/63 (0.127)	CCL5, CCR7, CD40, IL-6, IL-12β, IL-1α, IL-1β, TNF
2	Granulocyte Adhesion and Diapedesis	8.59E-12	10/151 (0.066)	CCL5, CCL20, CXCL2, CXCL3, FPR1, FPR2, IL-1α, IL-1β, MMP25, TNF
3	Role of Hypercytokinemia/ Hyperchemokinemia in the Pathogenesis of Influenza	8.87E-11	6/27 (0.222)	CCL5, IL-6, IL-12β, IL-1α, IL-1β, TNF
4	Differential Regulation of Cytokine Production in Macrophages and T Helper cells by IL-17A and IL-17F	3.74E-10	5/15 (0.333)	CCL5, IL-6, IL-12β, IL-1β, TNF
5	Role of Cytokines in Mediating Communication between Immune Cells	4.49E-08	5/36 (0.139)	IL-6, IL-12β, IL-1α, IL-1β, TNF
6	Altered T cell and B cell Signalling in Rheumatoid Arthritis	6.41E-08	6/77 (0.078)	CD40, IL-6, IL-12β, IL-1α, IL-1β, TNF
7	Dendritic Cell Maturation	1.37E-07	7/146 (0.048)	CCR7, CD40, IL-6, IL-12β, IL-1α, IL-1β, TNF
8	Activation of IRF by Cytosolic Pattern Recognition Receptors	2.45E-07	5/50 (0.100)	CD40, DHX58, IL-6, ISG15, TNF
9	LXR/RXR Activation	4.85E-07	6/108 (0.056)	IL-6, IL-1α, IL-1β, NOS2, PTGS2, TNF
10	Role of PRR in Recognition of Bacteria and Viruses	7.03E-07	6/115 (0.052)	CCL5, IL-6, IL-12β, IL-1α, IL-1β, TNF
11	Crosstalk between Dendritic Cells and Natural Killer Cells	1.16E-06	5/68 (0.074)	CCR7, CD40, IL-6, IL-12β, TNF
12	Atherosclerosis Signalling	1.25E-05	5/110 (0.045)	CD40, IL-6, IL-1α, IL-1β, TNF
13	Graft-versus-Host disease Signalling	2.20E-06	4/34 (0.118)	IL-6, IL-1α, IL-1β, TNF
14	HMGB1 Signalling	1.37E-05	5/112 (0.045)	IL-6, IL-12β, IL-1α, IL-1β, TNF
15	T-helper Cell Differentiation	2.50E-05	4/62 (0.065)	CD40, IL-6, IL-12β, TNF
16	IL-10 Signalling	3.01E-05	4/65 (0.062)	IL-6, IL-1α, IL-1β, TNF
17	TREM1 Signalling	3.60E-05	4/68 (0.059)	CD40, IL6, IL1B, TNF
18	Toll-like Receptor Signalling	4.04E-05	4/70 (0.057)	IL-12β, IL-1α, IL-1β, TNF
19	Haematopoiesis from Pluripotent Stem cells	5.45E-05	3/27 (0.111)	IL-6, IL-12β, IL-1α
20	Hepatic Cholestasis	5.58E-05	5/150 (0.033)	IL-6, IL-12β, IL-1α, IL-1β, TNF
21	Systemic Lupus Erythematous Signalling	6.93E-05	5/157 (0.032)	CD40, IL-6, IL-1α, IL-1β, TNF

22	Glucocorticoid Receptor Signalling	7.81E-05	6/258 (0.023)	CCL5, IL-6, IL-1β, NOS2, PTGS2, TNF
23	PPAR Signalling	1.04E-04	4/89 (0.045)	IL-1α, IL-1β, PTGS2, TNF
24	Role of Macrophages, Fibroblasts and Endothelial Cells in Rheumatoid Arthritis	1.19E-04	6/283 (0.021)	CCL5, IL-6, IL-1α, IL-1β, NOS2, TNF
25	Cholecystokinin/Gastrin-mediated Signalling	1.45E-04	4/97 (0.041)	IL-1α, IL-1β, PTGS2, TNF
26	Type I Diabetes Mellitus Signalling	1.45E-04	4/97 (0.041)	IL-12β, IL-1β, NOS2, TNF
27	Allograft Rejection Signalling	1.66E-04	3/39 (0.077)	CD40, H2-M2, TNF
28	MSP-RON Signalling	2.23E-04	3/43 (0.07)	IL-12β, NOS2, TNF
29	IL-6 Signalling	2.60E-04	4/113 (0.035)	IL-6, IL-1α, IL-1β, TNF
30	IL-12 Signalling and Production in macrophages	2.69E-04	4/114 (0.035)	CD40, IL-12β, NOS2, TNF

Table 5.12 Top 30 IPA canonical pathways of common host responses to infection by *B. pseudomallei* at 12hpi. The table ranks the pathways from the lowest to the highest p-value based on Fisher's exact test. The ratio is calculated as the number of DEGs in the given pathway (listed as associated molecules) divided by the total number of genes annotated in each canonical pathway in IPA.

	Canonical Pathways from IPA	p-value	Ratio	Associated molecules
1	Activation of IRF by Cytosolic Pattern Recognition Receptors	4.96E-17	13/50 (0.26)	ADAR, CD40, DDX58/RIG-1, DHX58/LGP2, IL-6, ISG15, IFIH1/MDA-5, IFIT2, IRF9, STAT1, STAT2, IFNα4, ZBP1
2	Interferon Signalling	4.97E-11	8/30 (0.267)	IFIT1, IRF1, IRF9, ISG15, OAS1, STAT1, STAT2, TAP1
3	Role of Pattern Recognition Receptors in Recognition of Bacteria and Viruses	8.03E-11	12/115 (0.104)	IL-1α, IL-1β, OAS1, OAS2, OAS3, Oas1b, CCL5, DDX58/RIG-1, IFNα4
4	Granulocyte Adhesion and Diapedesis	1.93E-09	12/151 (0.079)	CCL5, CXCL12, CXCL3, CXCL6, CXCL9, CXCL10, CXCL11, FPR1, FPR2, IL-1α, IL-1β, SDC4
5	Agranulocyte Adhesion and Diapedesis	4.24E-08	11/160 (0.069)	CCL5, CD34, CXCL2, CXCL3, CXCL6, CXCL9, CXCL10, CXCL11, IL-1α, IL-1β, SDC4
6	Retinoic Acid Mediated Apoptosis Signalling	1.02E-06	6/44 (0.136)	IFNα4, IRF1, PARP9, PARP10, PARP12, PARP14
7	Role of Hypercytokinemia/ Hyperchemokinemia in the Pathogenesis of Influenza	4.75E-08	6/27 (0.222)	CCL5, CXCL10, IFNα4, IL-6, IL-1α, IL-1β
8	Communication Between Innate and Adaptive immune cells	8.60E-06	6/63 (0.095)	CCL5, CD40, CXCL10, IL-6, IL-1α, IL-1β
9	Role of RIG1-like Receptors in Antiviral Innate Immunity	7.80E-05	4/30 (0.133)	DDX58/RIG-1, DHX58/LGP2, IFIH1, IFNα4
10	Role of Cytokines in Mediating Communication Between Immune Cells	1.62E-04	4/36 (0.111)	IFNα4, IL6, IL-1α, IL-1β
11	Role of IL-17F in Allergic Inflammation Airway Disease	1.80E-04	4/37 (0.108)	CXCL6, CXCL10, IL-6, IL-1β
12	Differential regulation of cytokine production in macrophages and T helper cells by IL-17A and IL-17F	1.88E-04	3/15 (0.2)	CCl5, IL-6, IL-1β
13	Toll-like receptor Signalling	2.04E-04	5/70 (0.071)	IL-1α, IL-1β, TNFAIP3, TRAF1, EIF1AK2
14	Atherosclerosis signalling	2.04E-04	6/110 (0.055)	ALOX5, CCR2, CD40, IL-6, IL-1α, IL-1β
15	Differential Regulation of Cytokine Production in Intestinal Epithelial Cells by IL-17A and IL-17F	2.78E-04	3/17 (0.176)	CCL5, IL-1α, IL-1β
16	UVA-Induced MAPK Signalling	5.24E-04	5/86 (0.058)	PARP9, PARP10, PARP12, PARP14, STAT1
17	Death Receptor Signalling	5.53E-04	5/87 (0.057)	DAXX, PARP9, PARP10, PARP12, PARP14

18	IL-15 production	7.96E-04	3/24 (0.125)	IL-6, IRF1, STAT1
19	Pathogenesis of Multiple Sclerosis	8.60E-04	2/6 (0.333)	CCL5, CXCL10
20	Dendritic Cell Maturation	9.23E-04	6/146 (0.041)	CD40, IL-6, IL-1α, IL-1β, STAT1, STAT2
21	CD40 Signalling	1.39E-03	4/63 (0.063)	CD40, PTGS2, TNFAIP3, TRAF1
22	Role of Lipids/Lipid Rafts in the Pathogenesis of Influenza	2.03E-03	2/9 (0.222)	IFNα4, RSAD2
23	Graft-versus-Host disease Signalling	2.23E-03	3/34 (0.088)	IL-6, IL-1α, IL-1β
24	Hepatic fibrosis/Hepatic Stellate Cell Activation	2.33E-03	6/175 (0.034)	CCL5, CD40, IL-6, IL-1α, IL-1β, STAT1
25	Altered T cell and B cell Signalling in Rheumatoid Arthritis	2.92E-03	4/77 (0.052)	CD40, IL-6, IL-1α, IL-1β
26	Role of PKR in Interferon Induction and Antiviral Response	3.31E-03	3/39 (0.077)	EIF2AK2, IRF1, STAT1
27	Role of IL-17A in Arthritis	6.30E-03	3/49 (0.061)	CCL5, CXCL6, PTGS2
28	Systemic Lupus Erythematosus Signalling	7.29E-03	5/157 (0.032)	CD40, IFNα4, IL-6, IL-1α, IL-1β
29	NF-KB Signalling	7.88E-03	5/160 (0.031)	CD40, EIF2AK2, IL-1α, IL-1β, TNFAIP3
30	LXR/RXR Activation	9.63E-03	4/108 (0.037)	IL-6, IL-1α, IL-1β, PTGS2

Table 5.13 Top 30 IPA canonical pathways exclusive to the WT strain of *B. pseudomallei* at 8hpi. The table ranks the pathways from the lowest to the highest p-value based on Fisher's exact test. The ratio is calculated as the number of DEGs in the given pathway (listed as associated molecules) divided by the total number of genes annotated in each canonical pathway in IPA.

	Canonical Pathways from IPA	p-value	Ratio	Associated molecules
1	Activation of IRF by Cytosolic Pattern Recognition Receptors	8.90E-06	4/50 (0.08)	IFIH1, NFKBIE, STAT1, ZBP1
2	UVA-Induced MAPK Signalling	1.51E-03	3/86 (0.035)	PARP9, PARP12, STAT1
3	Death Receptor Signalling	1.56E-03	3/87 (0.034)	NFKBIE, PARP9, PARP12
4	TNFR2 Signalling	2.64E-03	2/29 (0.069)	NFKBIE, TRAF1
5	Role of RIG1-like Receptors in Antiviral Innate Immunity	2.82E-03	2/30(0.067)	IFIH1, NFKBIE
6	2-1BB Signalling in T Lymphocytes	2.82E-03	2/30 (0.067)	NFKBIE, TRAF1
7	Interferon Signalling	2.82E-03	2/30 (0.067)	IFIT1, STAT1
8	TWEAK Signalling	3.41E-03	2/33 (0.061)	NFKBIE, TRAF1
9	Role of Pattern Recognition Receptors in Recognition of Bacteria and Viruses	3.44E-03	3/115 (0.026)	IFIH1, OAS2, OAS3
10	G-Protein Coupled Receptor Signalling	4.31E-03	4/252 (0.016)	ADORA2A, NFKBIE, PYRY12, PTGER3
11	April-Mediated Signalling	4.50E-03	2/38 (0.053)	NFKBIE, TRAF1
12	Role of PKR in Interferon Induction and Antiviral Response	4.73E-03	2/39 (0.051)	NFKBIE, STAT1
13	B Cell Activating Factor Signalling	4.97E-03	2/40 (0.05)	NFKBIE, TRAF1
14	iNOS Signalling	5.73E-03	2/43 (0.047)	NFKBIE, STAT1
15	Retinoic Acid Mediated Apoptosis Signalling	5.99E-03	2/44 (0.045)	PARP9, PARP12
16	Dendritic Cell Maturation	6.69E-03	3/146 (0.021)	NFKBIE, STAT1, STAT4
17	CNTF Signalling	6.81E-03	2/47 (0.043)	LIFR, STAT1
18	PPARα/RXRα Activation	9.35E-03	3/165 (0.018)	HELZ2, MEF2C, NFKBIE
19	Acetate Conversion to Acetyl-CoA	1.05E-02	1/4 (0.25)	ACSL1
20	Induction of Apoptosis by HIV1	1.06E-02	2/59 (0.034)	NFKBIE, TRAF1
21	T Helper Cell Differentiation	1.16E-02	2/62 (0.032)	STAT1, STAT4
22	CD40 Signalling	1.20E-02	2/63 (0.032)	NFKBIE, TRAF1
23	FLT3 Signalling in Hematopoietic Progenitor Cells	1.50E-02	2/71 (0.028)	STAT1, STAT4
24	Small Cell Lung Cancer Signalling	1.50E-02	2/71 (0.028)	NFKBIE, TRAF1
25	JAK/STAT Signalling	1.55E-02	2/72 (0.028)	STAT1, STAT4
26	cAMP-mediated signalling	1.83E-02	3/212 (0.014)	ADORA2A, P2RY12, PTGER3
27	Type I Diabetes Mellitus Signalling	2.70E-02	2/97 (0.021)	NFKBIE, STAT1
28	Fatty Acid Activation	3.12E-02	1/12 (0.083)	ACSL1
29	p38 MAPK Signalling	3.40E-02	2/110 (0.018)	MEF2C, STAT1
30	Type II Diabetes Mellitus Signalling	3.57E-02	2/113 (0.018)	ACSL1, NFKBIE

Table 5.14 Top 30 IPA canonical pathways exclusive to the WT strain of *B. pseudomallei* at 12hpi. The table ranks the pathways from the lowest to the highest p-value based on Fisher's exact test. The ratio is calculated as the number of DEGs in the given pathway (listed as associated molecules) divided by the total number of genes annotated in each canonical pathway in IPA.

	Canonical Pathways from IPA	p-value	Ratio	Associated molecules
1	Role of RIG1-like receptors in Antiviral Innate Immunity	1.70E-04	3/30 (0.1)	IRF7, NFKBIE, TRIM25
2	Activation of IRF by Cytosolic Pattern Recognition Receptors	7.79E-04	3/50(0.06)	IRF7, NFKBIE, TNF
3	Dendritic Cell Maturation	1.91E-03	4/146 (0.027)	HLA-A, LY75, NFKBIA, TNF
4	Cyclins and Cell Cycle Regulation	2.52E-03	3/75 (0.04)	CCNA2, CCND1, CDKN2C
5	Estrogen-mediated S-phase Entry	3.36E-03	2/24 (0.083)	CCNA2, CCND1
6	PPAR Signalling	4.08E-03	3/89 (0.034)	NFKBIA, PDGFC, TNF
7	Antigen Presentation Pathway	4.25E-03	2/27 (0.074)	HLA-A, NLRC5
8	TNFR2 Signalling	4.89E-03	2/29 (0.069)	NFKBIA, TNF
9	Type I Diabetes Mellitus Signalling	5.19E-03	3/97 (0.031)	HLA-A, NFKBIA, TNF
10	Glioma Signalling	5.19E-03	3/97 (0.031)	CCND1, CDKN2C, PDGFC
11	Graft-versus-host disease Signalling	6.68E-03	2/34 (0.059)	HLA-A, TNF
12	Neuroprotective Role of THOP1 in Alzheimer's Disease	7.07E-03	2/35 (0.057)	HLA-A, MME
13	Role of PKR in Interferon Induction and Antiviral Response	8.27E-03	2/39 (0.051)	NFKBIA, TNF
14	Allograft Rejection Signalling	8.72E-03	2/39 (0.051)	HLA-A, TNF
15	Aryl Hydrocarbon Receptor Signalling	1.13E-02	3/129 (0.023)	CCNA2, CCND1, TNF
16	TNFR1 Signalling	1.25E-02	2/47 (0.043)	NFKBIA, TNF
17	eNOS Signalling	1.28E-02	3/135 (0.022)	CCNA2, KDR, PDGFC
18	OX40 Signalling	1.41E-02	2/50 (0.04)	HLA-A, NFKBIA
19	Airway Inflammation in Asthma	1.44E-02	1/4 (0.25)	TNF
20	Regulation of Cellular Mechanics by Calpain Protease	1.63E-02	2/54 (0.037)	CCNA2, CCND1
21	PXR/RXR Activation	1.80E-02	2/57 (0.035)	CYP2C9, TNF
22	Role of Macrophages, Fibroblasts, and Endothelial Cells in Rheumatoid Arthritis	1.91E-02	4/283 (0.014)	CCND1, NFKBIA, PDGFC, TNF
23	Acute Phase Response Signalling	1.91E-02	3/157 (0.019)	CP, NFKBIA, TNF
24	Induction of Apoptosis by HIV1	1.92E-02	2/59 (0.034)	NFKBIA, TNF
25	NF-kB Signalling	2.01E-02	3/160 (0.019)	KDR, NFKBIA, TNF
26	Cell Cycle: G1/5 Checkpoint Regulation	2.05E-02	2/61 (0.033)	CCND1, CDKN2C
27	Airway Pathology in Chronic Obstructive Pulmonary Disease	2.15E-02	1/6 (0.167)	TNF
28	Communication between Innate and Adaptive Immune Cells	2.17E-02	2/63 (0.032)	HLA-A, TNF

29	Hypoxia Signalling in the Cardiovascular System	2.17E-02	2/63 (0.032)	NFKBIA, UBE2L6
30	IL-10 Signalling	2.31E-02	2/65 (0.031)	NFKBIA, TNF

Table 5.15 IPA canonical pathways exclusive to the Δ*bimA* strain of *B. pseudomallei* at 8hpi. The table ranks the pathways from the lowest to the highest p-value based on Fisher's exact test. The ratio is calculated as the number of DEGs in the given pathway (listed as associated molecules) divided by the total number of genes annotated in each canonical pathway in IPA.

Canonical Pathways from IPA	p-value	Ratio	Associated molecules
Role of IL-17A in Psoriasis	1.71E-02	1/7 (0.143)	CXCL6
Role of Pattern Recognition Receptors of Bacteria and Viruses	3.26E-02	2/115 (0.017)	DDX58/RIG-1, OAS1B

Table 5.16 IPA canonical pathways exclusive to the Δ*bimA* strain of *B. pseudomallei* at 12hpi. The table ranks the pathways from the lowest to the highest p-value based on Fisher's exact test. The ratio is calculated as the number of DEGs in the given pathway (listed as associated molecules) divided by the total number of genes annotated in each canonical pathway in IPA.

Canonical pathways from IPA	p-value	Ratio	Associated molecules
p53 signalling	5.19E-03	3/94 (0.032)	CHEK1, DRAM1, FAS
Type I Diabetes Mellitus Signalling	5.67E-03	3/97 (0.031)	FAS, NOS2, SOCS1
Allograft Rejection Signalling	9.56E-03	2/39 (0.051)	FAS, H2-M2
Aryl Hydrocarbon Receptor Signalling	1.29E-03	3/129 (0.023)	CHEK1, FAS, MCM7
Citrulline-Nitric Oxide Cycle	1.48E-03	1/4 (0.25)	NOS2
Role of Macrophages, Fibroblasts and Endothelial Cells in Rheumatoid Arthritis	2.12E-02	4/283 (0.014)	LEF1, NOS2, SOCS1, VCAM1
ILK signalling	2.67E-02	3/173 (0.017)	ITGB7, LEF1, NOS2
Role of BRCA1 in DNA damage response	3.34E-02	2/77 (0.026)	CHEK1, MSH2
Superpathway of Citrulline Metabolism	4.81E-02	1/13 (0.077)	NOS2
Cholesterol Biosynthesis	4.81E-02	1/13 (0.077)	DHCR7
Cholesterol Biosynthesis II (via 24,25-dihyrolanosterol)	4.81E-02	1/13 (0.077)	DHCR7
Cholesterol Biosynthesis III (via Desmosterol)	4.81E-02	1/13 (0.077)	DHCR7

5.2.7 Validating Differentially Expressed Genes by SYBR-Green Real-Time PCR

5.2.7.1 Reverse transcription of total RNAs into complementary DNA (cDNA)

Microarray results are influenced by several factors at different steps starting from array production, RNA extraction, probe labelling, hybridisation of targets on the probes and image analysis, which may lead to false positive expression differences (Tusher *et al*, 2001; Rajeevan *et al*, 2001). Therefore, DEGs need to be validated with another method such as conventional reverse transcription-polymerase chain reaction (RT-PCR) or, the current state-of-the-art for gene quantification, real-time PCR (qPCR). In this thesis, qPCR was used to validate several DEGs from three independent experiments. The qPCR that was performed here was two-step qPCR as the total RNA was first reverse transcribed into cDNA by Reverse Transcriptase (RT) separately from the PCR reaction itself.

qPCR was performed on cDNA generated from the same RNA samples that were prepared primarily for microarray analysis. Total RNA (100ng) was reversed transcribed using random oligo (dT) primer with GoScript Reverse Transcriptase that were provided in the GoScript Reverse Transcription System (Promega). The oligo(dT) primers are about 15-20 bases and are comprised of thymine bases which anneal to the poly(A) tail at the 3' end of mRNA transcripts and initiates cDNA synthesis. Reverse transcriptase catalyses the addition of dNTPs to generate a complementary strand of DNA. The cDNA molecules were then aliquoted into small single-use volumes and frozen at -80^{o}C to prevent the need for multiple freeze-thaw cycles which can cause cDNA degradation. For each sample, a non-enzyme control (no RT) was generated as a negative control, where samples were tested by PCR to check for gDNA contamination of the template RNA. Figure 5.10 shows PCR amplification of a 350bp fragment of beta-actin (β-actin) after reverse transcription with- or without RT enzyme. The β-actin primers were designed spanning an exon-exon boundary. If there was contamination of genomic DNA in the RNA samples, a slightly higher band of about ~440bp should appear in the no-RT control lane. All 18 samples were free from genomic DNA contamination as none of the samples showed a species around ~440bp in the no-RT control lanes.

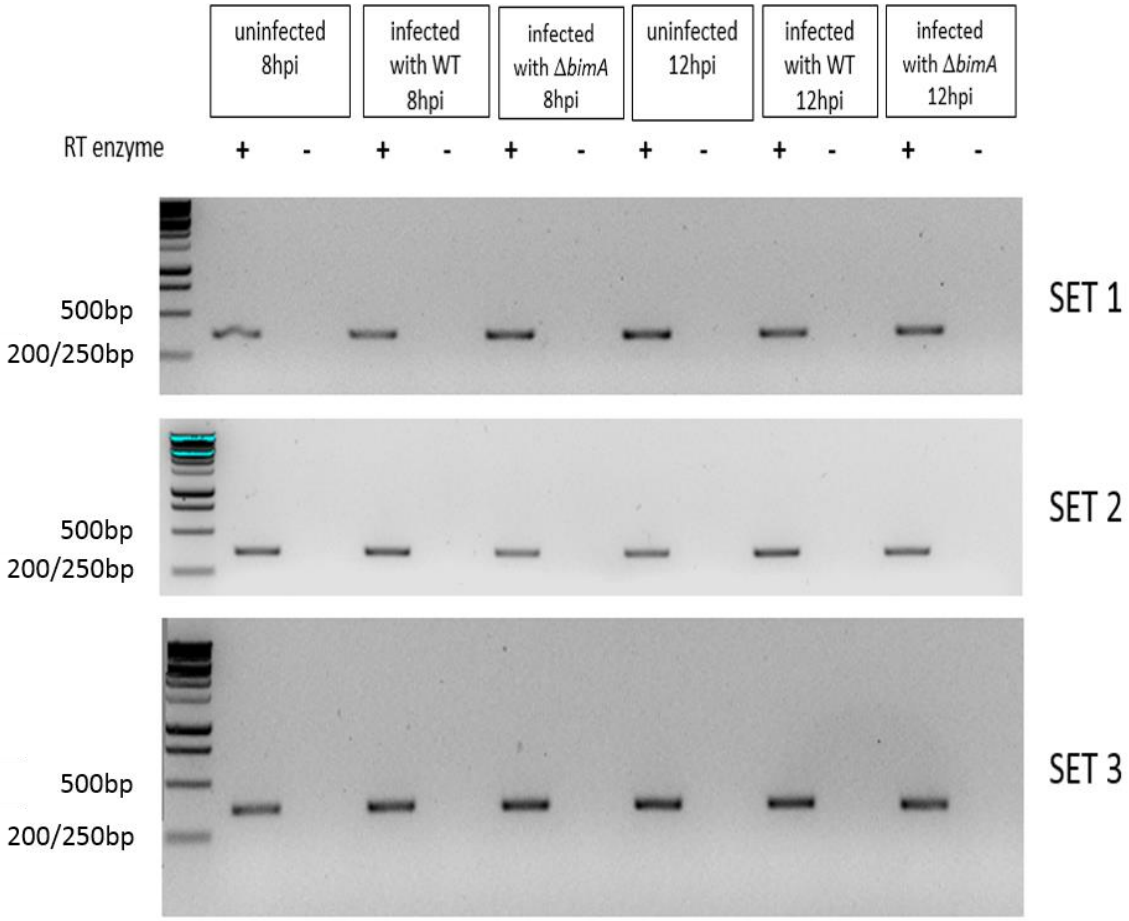

Figure 5.10 Agarose gel electrophoresis of cDNA template. There were 18 samples in total of RNA isolated from three independent experiments. All 18 samples were reverse transcribed into cDNA with- or without RT (reverse transcriptase) enzyme, followed by PCR amplification specific for β-actin. PCR products were then visualised using 2.5% agarose gel electrophoresis. Amplification of β-actin from cDNA gives a band product at approximately 350bp.

5.2.7.2 Primer design and optimisation for qPCR

In qPCR reactions, two different fluorescent reporter molecules can be used; a sequence specific probe containing a fluorescent reporter dye at the 5' end and a quencher dye at the 3' end, such as a TaqMan probe, or a non-specific DNA binding dye such as SYBR Green which binds to double-stranded DNA to produce fluorescence. SYBR Green I reporter molecule was used in the qPCR assays presented in this thesis. SYBR green dye binds to double-stranded DNA, as more double-stranded amplicons are produced, the intensity of the fluorescence increases. SYBR Green I dye gives substantial sensitivity for target quantification, it is easy to use, reproducible and cost effective.

One of the limitations in DNA-binding dye chemistry assay is the inherent non-specificity. The dye can bind to any double-stranded DNA including primer-dimers, hence, the efficiency of the qRT-PCR is highly dependent on the primers used. The primers were carefully self-designed and analysed using Beacon Designer software (PREMIER Biosoft International) to check if the primer sets (forward and reverse primer of the target) could form any secondary DNA structures namely a primer-dimer (self-dimer, or cross-dimer) or hairpin structure. The primers were designed to span exon-exon boundaries, thus avoiding the detection of target from residual genomic DNA in the initial RNA sample. The primers were also checked with the NCBI BLAST database search tool to ensure that they did not anneal to any non-specific DNA targets. Nine different concentrations of reverse and forward primers were tested (two-by-two combinations of 100, 200 or 300nM) to obtain the optimum concentration for each pair where it gave the lowest threshold cycle (Ct) but maximum amplification with minimum non-specific amplification. The criteria that were taken into account when designing the primers are described in more detail in the *Materials and Methods 2.18.*

A non-specific signal cannot always be prevented, but the specificity can be determined easily by melt-curve analysis (known as the dissociation curve) on the PCR products from every experiment. As the temperature increases, the double-stranded PCR products with the incorporated dye begin to dissociate, resulting in decreasing fluorescence intensity. The temperature at which the DNA dissociates is dependent on the length and sequence of the PCR products generated. Therefore, a single unique peak represents the PCR products with homogenous length and sequence (the amplicons), while multiple peaks indicate non-specific amplification where more than one population of PCR products have been generated including

primer-dimer artifacts. Figure 5.11 shows an example of a dissociation curve of Interleukin-1α gene from 18 samples. Dissociation curve analysis was performed in every qPCR experiment to confirm that only a single-peak was generated every time, hence increasing the reliability of the qPCR results. The qPCR reaction is described in more detail in the *Materials and Methods 2.19*.

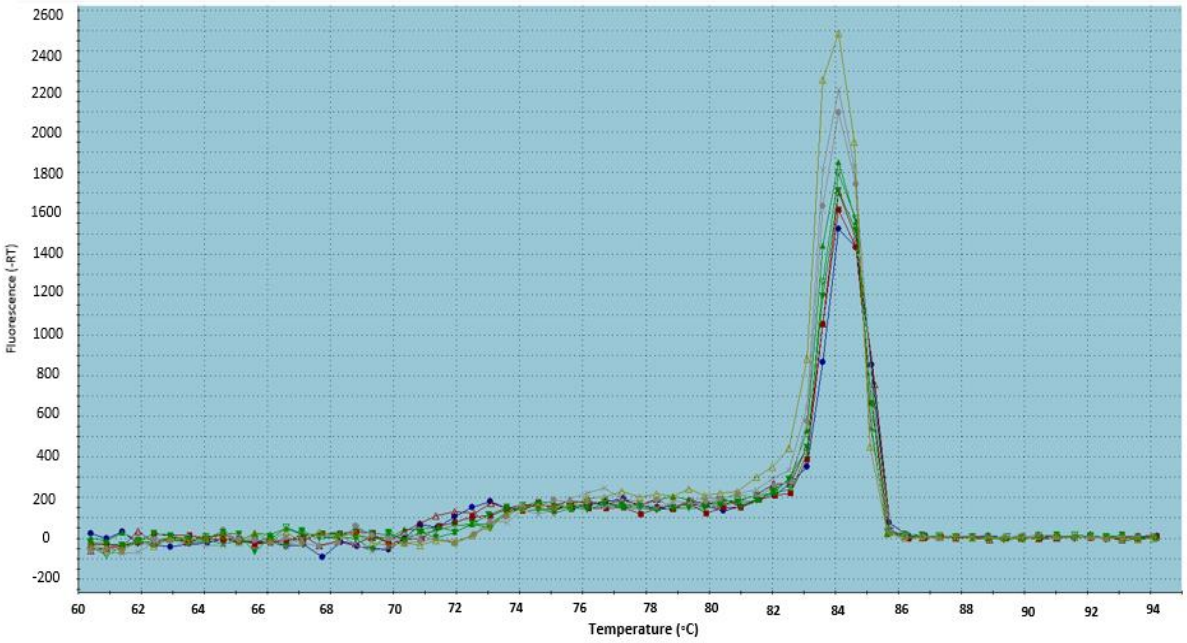

Figure 5.11 Melt curves from qPCR of IL-1α gene from 18 samples over the entire temperature range. The x-axis is temperature and y-axis is the fluorescence intensity. Total RNA was isolated from uninfected and infected BMDMs with *B. pseudomallei* WT or Δ*bimA* at 8 hpi and 12 hpi, with three replicates to give a total of 18 samples. The total RNA was then reverse transcribed into cDNA followed by qPCR as described in *Materials and Methods 2.19*. Melt-curve anlaysis was carried out in every PCR run to assess the dissociation-characteristics of double-stranded DNA during heating, hence the specificity of the PCR products. SYBR green fluorophore was used to quantify the double-stranded DNA. As the temperature increases, the double stranded DNA begins to dissociate and the fluorescence intensity starts to decrease. As the melt curves from all the samples produce a single-peak, indicating a single, specific product is generated.

5.2.7.3 Evaluation of Reference Gene Expression Stability

Normalisation is crucial for a reliable qPCR assay as it helps to correct for variations in the amount of starting material, reverse-transcription yield, and amplification efficiency, thus enabling comparisons of mRNA concentrations across different samples. Samples can be normalised to sample size, or total RNA, but the use of endogenous reference genes (often referred as housekeeping genes) is commonly accepted as the most appropriate normalisation strategy (Bustin *et al*, 2009). Normalisation involves reporting the ratios of the mRNA concentrations of the GOI (genes of interest) to those of the reference genes. Hence, the main criteria for reference genes is that they must be stably expressed, and should not vary widely in different species, tissues or in response to experimental conditions. Their abundances should be representative of the total amounts of mRNA present in the samples. Traditionally, many studies presumed the constitutively expressed housekeeping genes such as β-actin (ACTB) and glyceraldehyde-3-phosphate dehydrogenase (GAPDH) were stably expressed and were therefore used as normalising controls. However, many publications have demonstrated that these endogenous housekeeping genes can quantitatively vary, depending on the experimental conditions (Kozera & Rapacz, 2013; Thellin *et al*, 1999). Therefore, there is a need for systematic validation of internal reference genes for each specific experimental design. Furthermore, validation of the reference genes are important criteria required in MIQE (**M**inimum **I**nformation for Publication of **Q**uantitative Real-Time PCR **E**xperiments). MIQE is a guideline that describes minimum information necessary for evaluating qPCR experiments, hence ensures its relevance, accuracy and reproducibility (Bustin *et al*, 2009).

The stability of candidate internal reference genes may be assessed using a variety of different algorithms namely geNorm, NormFinder and BestKeeper (De Spiegelaere *et al*, 2015; Vandesompele *et al*, 2002). In this study, we implemented GeNorm using qBase+ software from BioGazelle to evaluate a set of reference genes to use in the qPCR experiments. GeNorm (Primer Design Ltd), developed in 2002, calculates the gene expression stability (M) for each reference gene based on the average pairwise variation (V) between all studied reference genes across all samples. Following calculation of the M value, the programme then ranks the genes from the most stable gene characterised by the lowest M value, to the least stable with the highest M value. In addition, geNorm can determine the optimal number of reference genes for qPCR normalisation by finding the smallest needed to minimise mean variation as presented

by geNormV chart. This optimal number of reference genes (n) is found when the pairwise variation V(n/n+1) drops below 0.15 (Vandesompele *et al*, 2002). Six different reference gene/ primer sets were purchased commercially from PrimerDesign Ltd for use with SYBR green, known as the Mouse geNormPLUS 6 gene kit. The reference genes provided in this kit are stated in the *Materials and Methods 2.18.*

All 18 samples were assayed in duplicate with each reference gene at the recommended optimal concentration of 300nM. The Ct values were then exported into qBase+ software and geNorm program was selected for the analysis. From the geNorm M graph (Figure 5.12), the software identified that glyceraldehyde-3-phosphate dehydrogenase (GAPDH) and casein kinase 2 (Csnk2a2) were the most stable reference genes. From data presented in the geNormV bar chart (Figure 5.13), the optimal number of reference targets in this experimental situation is two (geNormV <0.15) when comparing a normalisation factor based on the 2 or 3 most stable targets. As such, the optimal normalisation factor can be calculated as the geometric mean of reference targets GAPDH and Csnk2a2.

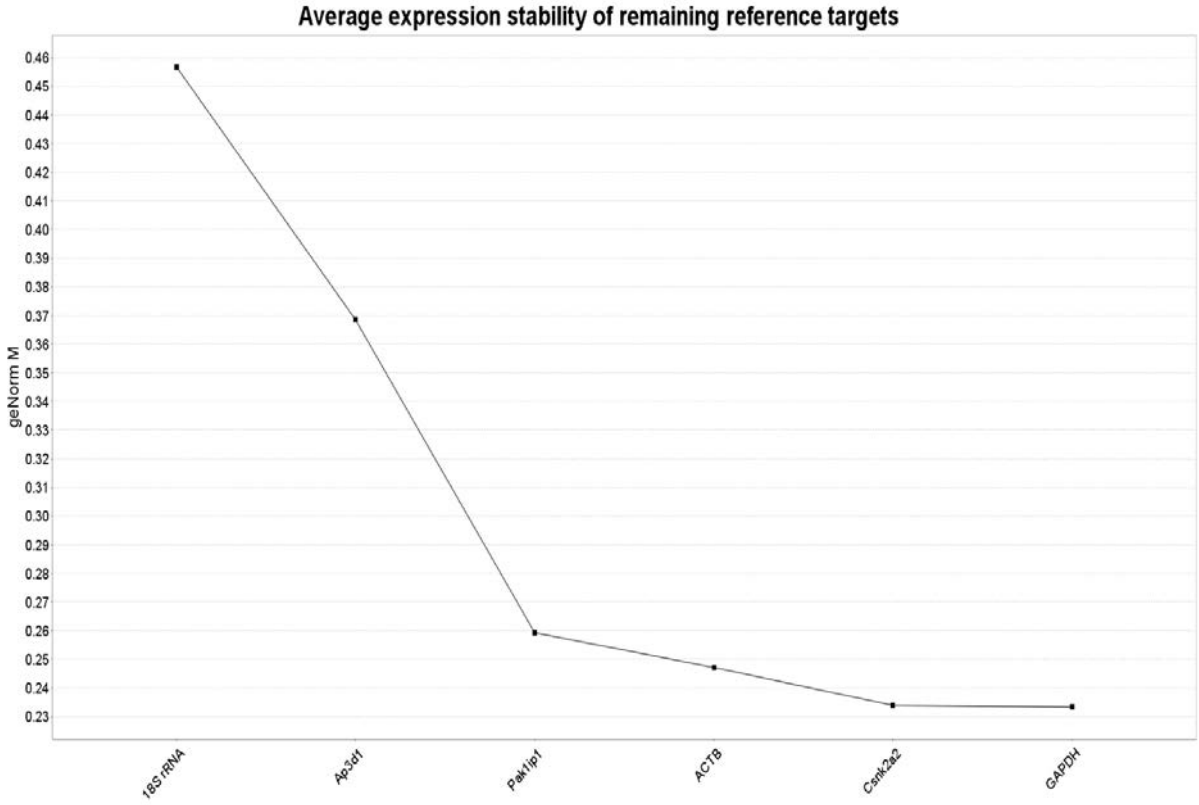

Figure 5.12 Average expression stability values of reference genes. The geNorm programme ranks the reference genes from the least stable (highest M value on the left) to the most stable gene (lowest M value on the right). The program identified GAPDH and Csnk2a2 as the most stable genes to be used as reference genes for qPCR normalisation.

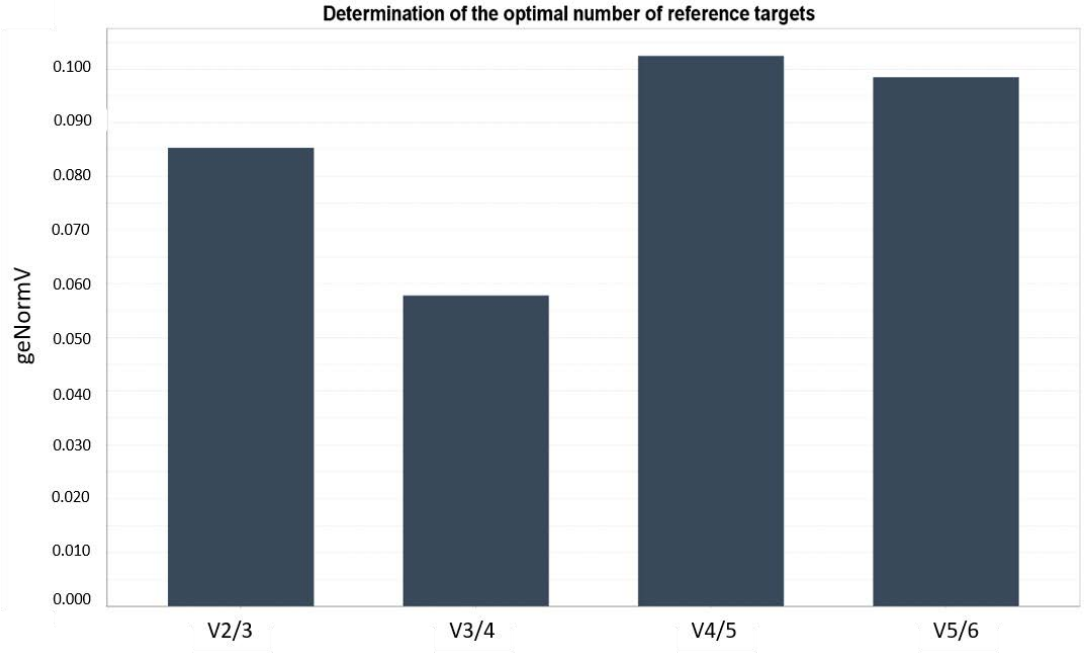

Figure 5.13 geNorm V bar chart shows the optimal number of reference targets. The lower the variable V is (on y-axis), the less variation. Vandesompele *et al* (2002) proposed a cut off at 0.15. X-axis indicates the the variation in normalisation factor. V2/3 indicates the variation in normalisation factor with 2 vs 3 reference genes. Two reference genes were sufficient for qPCR normalisation.

5.2.7.4 Quantification of Real-Time PCR (qPCR)

After determining the optimal concentration of primers to use in each reaction, it is important to test the performance of the qPCR reaction in terms of amplification efficiency. The amplification efficiency (E) can be determined from the slope of a standard curve of the GOI (gene of interest) and the reference genes. A standard curve was produced from the PCR-generated product (10^{-1} to 10^{-5} ng). An acceptable range for percentage of efficiency is between 90-100%. This E-value was taken into account for more accurate gene quantification as explained below.

Relative quantification strategy was chosen for qPCR data presented here. Relative quantification (also known as comparative quantification) calculates the relative quantities of targets to the calibrator (which is the uninfected BMDM cells at the respective time point). There are two different mathematical models established to calculate the expression of the target gene in relation to reference genes; Delta-delta Ct (ΔΔCt) and Pfaffl methods. ΔΔCt method assumes the amplification efficiency of both GOI and reference gene is 100% and the amplification factor = 2. In contrast, the Pfaffl method is an efficiency-corrected comparative quantification, which permits the incorporation of different amplification efficiency/factor into the mathematical model. In this study, standard curves have been determined for each target and reference gene (they ranged from 90-100% efficiency). Since the standard curves did not meet 100% amplification efficiency, it is more appropriate to use the Pfaffl method for quantification. A slight modification on Pfaffl modelling has been proposed by Vandesompele *et al* (2002), which permits the normalisation with multiple reference genes. The denominator of the Pfaffl method is replaced with the geometric mean of the normalisation factor of two or more reference genes (GAPDH and CSNK2A2 in this study). This modified Pfaffl method (also known as the Vandesompele method) was used for the quantification of qPCR in this study.

$$\text{Normalised Relative Quantity (NRQ)} = \frac{(E_{target})^{\Delta Ct\ target\ (calibrator - sample)}}{\sqrt[n]{\prod (E_{refgene})^{\Delta Ct\ refgene\ (calibrator - sample)}}}$$

Geometric mean

A panel of ten immune-related genes were selected for validation by real-time qPCR (table 5.17). 5/10 are pro-inflammatory cytokine genes (IL-6, IL-1β, IL-1α, CD40, and IL-12β), 2/10 are members of the interferon signalling pathway (ISG15 and IFIH1) and the remaining three genes were shown to be upregulated specifically in response to the Δ*bimA* mutant at 12hpi (NOS2, FNBP1L, and FAS). All the genes selected were indicated to be upregulated by the microarray analysis. In terms of direction of fold change, all the genes validated by qPCR displayed directionally concordant gene expression profiles between both methods. None of the genes tested showed a down-regulation, consistent with the fact that DEGs with negative fold change were not validated by qPCR in this study. In most cases, the magnitude of fold change by qPCR is much higher compared to fold change obtained from microarray analysis, in agreement with the higher sensitivity of qPCR in gene quantification (Bustin *et al*, 2005). However, some of the genes that were not represented on the microarray as significantly expressed showed a substantial increase in expression. For examples, *NOS2, FNBP1L*, and *FAS* genes that were thought to be specifically increased in response to the Δ*bimA* mutant at 12hpi, were also significantly increased in fold change expression in response to the WT strain. This is possible as both microarrays and qPCR are influenced by several factors which affect the correlation of gene expression between the two methods. One of the fundamental differences is the method of normalisation with microarray requiring global normalisation while qPCR calibrates the gene expression against reference genes (Morey *et al,* 2006; Etienne *et al*, 2004; Irrisarry *et al*, 2003; Vandesompele *et al*, 2002). Besides, the data reported for microarray and qPCR were averaged in different manners. The value obtained from microarray was derived from the composite array in which each feature of the replicate arrays underwent a weighted averaging based on feature quality analysed by the software. On the other hand, qPCR data were unweighted averages from replicates. In addition, each method has individual inherent pitfalls. Microarray is easily prone to errors such as cross hybridisation of labelled target to the probes, while amplification biases and the formation of primer-dimers are errors that are inherent to qPCR. Differences in reverse transcriptase and priming methods also contribute to the low correlation between microarray and qPCR. Nevertheless, good laboratory technique and proper controls can reduce these errors to obtain as high a correlation as possible.

The 32 sets of paired-data highlighted in bold in table 5.17 were then subjected to statistical analyses to determine the correlation between the microarray and qPCR results. Statistical analysis was performed using Spearman's Rho non-parametric test using Minitab 17 Statistical Software. Overall, a significant correlation was observed between microarray and

qPCR with a correlation coefficient (r) of 0.734 (Spearman's Rho, $p<0.0001$, $n=32$). This highly significant correlation indicates acceptable validation of the microarray results as determined in Morey *et al*, 2006.

Table 5.17 Genes selected for validation of the microarray data by qPCR

	Infected with WT 8hpi (fold change)			Infected with *ΔbimA* 8hpi (fold change)			Infected with WT 12hpi (fold change)			Infected with *ΔbimA* 12hpi (fold change)	
	Microarray	**qPCR**		**Microarray**	**qPCR**		**Microarray**	**qPCR**		**Microarray**	**qPCR**
IL-6	**10.74**	**39.3 ± 13.5**		**4.47**	**32.1 ± 10.5**		**11.66**	**35.2 ± 2.4**		**10.2**	**41.2 ± 8.8**
IL-1β	**6.33**	**8.85 ± 2.57**		**3.66**	**8.38 ± 2.62**		**5.75**	**6.61 ± 0.83**		**5.11**	**6.34 ± 1.73**
IL-1α	**4.13**	**6.61 ± 2.27**		**2.64**	**5.04 ± 1.66**		**4.77**	**15.3 ± 11.4**		**4.23**	**13.66 ± 10.2**
CD40	**1.71**	**3.99 ± 0.99**		**1.5**	**4.3 ± 1.07**		**2.15**	**6.99 ± 4.51**		**2.01**	**6.72 ± 4.09**
ISG15	**2.17**	**4.72 ± 1.17**		**1.87**	**4.03 ± 1.14**		**4.27**	**12.5 ± 7.2**		**4.21**	**12.0 ± 5.6**
IFIH1/MDA-5	**1.81**	**1.08 ± 0.40**		not DE	1.05 ± 0.35		**2.42**	**2.55 ± 1.08**		**2.89**	**2.41 ± 0.96**
IL-12β	**4.4**	**22.5 ± 10.9**		**2.89**	**20.8 ± 7.9**		not DE	12.6 ± 1.7		not DE	15.3 ± 0.01
Nos2	**2.6**	**10.7 ± 6.4**		**2.34**	**7.22 ± 5.49**		not DE	3.62 ± 0.53		**2.83**	**2.99 ± 1.05**
Fnbp1L	**1.61**	**4.47 ± 1.97**		**2.05**	**6.20 ± 1.98**		not DE	3.66 ± 1.52		**2.56**	**4.04 ± 2.36**
Fas	not DE	1.82 ± 0.23		not DE	2.02 ± 0.65		not DE	1.55 ± 0.60		**1.52**	**1.46 ± 0.48**

Quantification of qPCR was given as an average fold change based on three independent experiments ± Standard Error

*not DE= not differentially expressed based on microarray analysis. Therefore, these values (non-bold numbers) are excluded from Spearman's Rho statistical analysis

5.2.8 Investigating the role of FNBP1L in limiting the intracellular survival of Δ*bimA* in BMDMs

One of the key reasons the microarray experiment was carried out was to identify potential mechanism/s involved in the detection and elimination of the *B. pseudomallei* Δ*bimA* mutant in BALB/C BMDMs. As explained previously, not many genes in this category were mapped to IPA canonical pathways, and very few pathways were identified from the analysis. Microarray analysis found that FNBP1L (Formin-binding protein 1-like) (also known as Toca-1) was among those upregulated genes specific to infection of cells with the Δ*bimA* mutant strain. Although qPCR analysis showed that there was no significant difference in *FNBP1L* gene expression between cells infected with either the WT or Δ*bimA* strain, there was a slightly higher expression in cells infected with the Δ*bimA* mutant compared to the WT strain. With the recent findings of a novel role of FNBP1L in anti-*Salmonella* autophagy (Huett *et al*, 2009), we then selected FNBP1L for functional validation to investigate if the protein is involved in limiting the intracellular survival of *B. pseudomallei* Δ*bimA* specifically.

FNBP1L protein, a transducer of Cdc42-dependent actin assembly, has been identified as a novel component of the autophagic apparatus in mammalian cells through a yeast-human network analysis performed by Huett *et al* (2009). FNBP1L has been shown to interact with Atg3 (autophagy-related protein 3) via its functional domain protein-kinase C-related kinase HR1 (homology domain 1) in a similar fashion to the characterised FNBP1L ligand Cdc42. ATG3 acts as an ubiquitin-carrier protein (E2) enzyme that catalyses the lipidation of LC3-I into LC3-II, an essential molecule in autophagosome formation. Interestingly, this FNBP1L-mediated autophagy targeting *Salmonella enterica* Typhimurium (*S.* Typhimurium) is independent from ubiquitination signals required for canonical autophagy as described previously in Chapter 3. Detailed microscopic examination identified significant colocalisation of *S.* Typhimurium with LC3 molecules. However, the colocalisation was largely absent following FNBP1L siRNA knockdown and could be fully rescued by restoration of FNBP1L expression (Huett *et al*, 2009). This observation is paralleled with their gentamycin intracellular survival assay in HeLa cells where the bacteria were shown to replicate more in the FNBP1L-deficient cells compared to the control-treated cells. These data together demonstrate the novel role of FNBP1L in restricting the intracellular survival of *S.* Typhimurium via an autophagy-dependent mechanism (Huett *et al*, 2009). Therefore, we investigated if FNBP1L plays a

similar role in clearing the Δ*bimA* mutant in BALB/C BMDMs at 16 hpi by confocal microscopy.

BALB/C BMDMs were infected with *B. pseudomallei* WT or the Δ*bimA* mutant at an MOI of 2 for 8 hpi and 16 hpi in a kanamycin-protection manner as described previously. The infected BMDMs on the coverslip were then stained with *B. pseudomallei* antibody (red) and anti-FNBP1L (green). Analysis of confocal images revealed no significant colocalisation of FNBP1L with either intracellular WT or Δ*bimA* bacteria at either 8 hpi or 16 hpi (Figure 5.14). Similarly, the Δ*bimA* mutant did not colocalise with LC3 molecules as demonstrated in Chapter 3, adding more evidence that autophagy via FNBP1L/LC3 is unlikely to be responsible for the impaired survival of the Δ*bimA* mutant in BMDM cells.

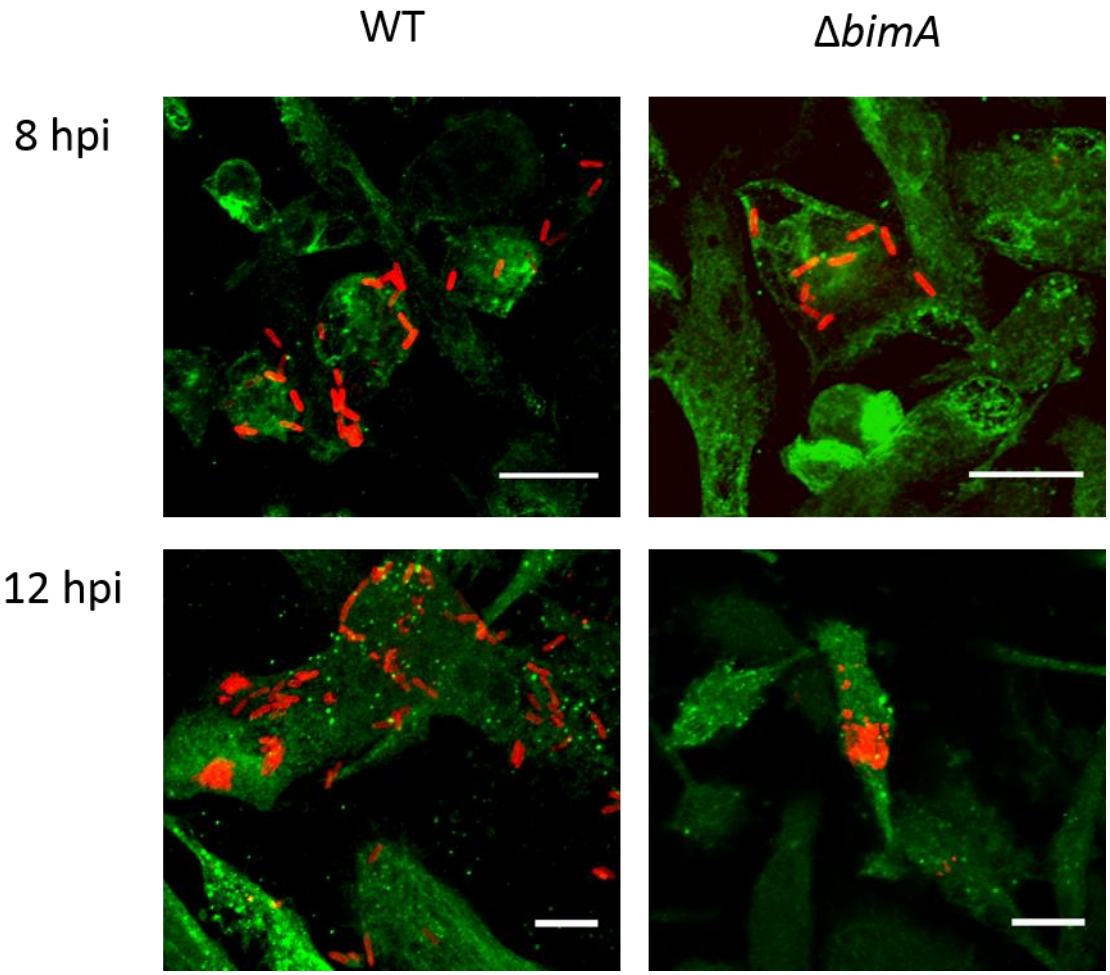

Figure 5.14 Representative z-stack confocal microscopy images of BMDMs infected with *B. pseudomallei* WT and Δ*bimA* mutant bacteria for FNBP1L co-localisation. BMDMs infected with WT and Δ*bimA* mutant bacteria were incubated for the indicated times before fixing and staining for confocal microscopy. Bacteria were stained red with mouse anti-*B. pseudomallei* LPS and anti-mouse Ig-Alexa 568 antibodies. FNBP1L was stained green with rabbit anti-FNBP1L and anti-rabbit Ig-Alexa Fluor 488. Scale bar = 10μm

5.3 DISCUSSION

The responses of host cells to pathogens are often accompanied by marked reprogramming of their transcriptome. The advent of DNA microarray technology allows us to investigate transcriptional profiling of BALB/C BMDMs when infected with *B. pseudomallei* WT and Δ*bimA* mutant strains. The microarray analysis was carried out at two different time points (8 and 12hpi) chosen based on the intracellular CFU counts, where the number of WT bacteria and Δ*bimA* mutant were not different (at 8hpi) and started to differ significantly (at 12hpi) respectively. Using this approach, we have presented in this chapter a global overview of the changes in transcript abundance in response to the *B. pseudomallei* 10276 strain as well as specific response to the Δ*bimA* mutant that resulted in significantly decreased intracellular survival.

Analysis of global gene expression in response to *B. pseudomallei* (both WT and Δ*bimA* mutant strains) at the earlier time point of 8hpi identified that among the top ranking DEGs are those encoding pro-inflammatory cytokines. These include IL-6, IL-1α, IL-1β, CD40, TNF, and IL-12β which were also found to be elevated at 12hpi following *B. pseudomallei* infection. Many of these genes, together with several other genes, were selected for validation at the transcriptional level using quantitative real-time PCR (qPCR). With 10 genes being tested, we have obtained significant correlation between microarray and qPCR (Spearman's Rho coefficient of 0.734), indicating acceptable validation of the microarray analysis. In addition, there are also other inflammatory chemokines that were induced in infected host cells, to name several; CXCL3 (also termed as Macrophage Inflammatory Protein 2β (MIP2β)), CXCL2 (MIP2α), CCL5 (RANTES), CCR7, CCL20 (MIP3α). These chemokines and cytokines together form a cluster of inflammatory mediators that could be designated as a 'common host immune response', representing a general 'alarm signal' for inflammatory infections. This set of genes is also found to be upregulated in different cell types upon infection with several different pathogens such as *Mycobacterium tuberculosis* (Magee *et al*, 2012), *Listeria monocytogenes* (Cohen *et al*, 2000), *Brucella abortus* (Eskra *et al*, 2003), and *Staphylococcus aureus* (Matussek *et al*, 2005). IPA Functional analysis of this cluster of inflammatory-associated genes suggests that they are involved in communication between innate and adaptive immune cells. For example, IL-6 is a pleiotropic inflammatory cytokine which has been reported to be important in the resolution of innate immunity and also as a key immunological

switch to orchestrate transition from innate to acquired immune processes (Jones, 2005). The chemokines listed above are required for chemotactic activity to recruit more inflammatory and immune effector cells such as neutrophils and natural killer (NK) cells.

The interferon (IFN)-mediated response was reported as the most prominent pathway identified at 12hpi in response to infection with both *B. pseudomallei* WT and the Δ*bimA* mutant strains. In IPA analysis, several pathways are mentioned related to the interferon-mediated response which include '*Activation of IRF by Cytosolic Pattern Recognition Receptors'* (1st rank), *'Interferon Signalling'* (2nd rank) and *'Role of RIG1-like Receptors in Antiviral Innate Immunity'*(3rd rank). Type I and Type II IFN are the main classes of the IFN family, which separately bind to their respective receptors. Expression of some genes are regulated by both Type I and II IFNs such as IFITM1, whereas others are selectively regulated by distinct IFNs. For example, only Type I IFNs drive the expression of 2',5'-oligoadenylate synthetase 1 (OAS1) gene while expression of the IFN-regulatory factor 1 (IRF1) gene is preferentially induced by Type II IFNγ (Horiuchi *et al*, 2011). All the genes mentioned here were found to be upregulated in BMDMs infected with both WT and Δ*bimA* strains, suggesting that both Type I and Type II IFN signalling pathways are crucial for host responses against *B. pseudomallei*.

In melioidosis studies, it is well-known that IFNγ plays an important immunoregulatory role in melioidosis. IFNγ is a potent macrophage activator which is essential in mediating antibacterial host defence. *In vivo* studies using a mouse model show that depleting IFNγ with neutralising antibody significantly increases host susceptibility to melioidosis (Santanirand *et al*, 1999). In human studies, plasma IFN-γ concentration, which is usually undetectable in plasma of normal controls, was greatly increased in melioidosis patients (Lauw *et al*, 1999). A similar report on elevated levels of circulating IFNγ in melioidosis patients is described by Brown *et al* (1991). In addition, one of the IFNγ-inducing cytokines IL-12p40 was found to be significantly higher in melioidosis patients (Lauw *et al*, 1999). Our microarray analysis also found upregulation of the gene encoding IL-12p40 in this category. Our *in vitro* system does not include IFN-γ as a macrophage activator, hence, the upregulation of gene transcription in IFN-γ signalling indicates a distinct host response to infection.

Whilst IFN-γ plays an important role in the pathogenesis of melioidosis, the role for Type I IFN is not well described. IFNα4 was upregulated specifically in our microarray dataset as a global response to infection with *B. pseudomallei*. Besides, our microarray analysis has shown

upregulation of the cytosolic RNA sensor RIG-1 (RNA helicase retinoic acid inducible gene 1 protein, also known as Ddx58) and RIG-1-like (RLR) protein MDA-5 (melanoma differentiation-associated gene 5, also known as Ifih1) upon *B. pseudomallei* infection of BMDM cells. RIG-1 and MDA-5 both contain a DExD/H box RNA helicase domain that recognises dsRNA, and two caspase recruiting domain (CARD)-like domains to relay the signal. Bacterial mRNA is distinct from eukaryotic RNA as bacterial mRNA is not capped and contains triphosphates at the 5' end, rendering it a perfect ligand for the RIG-1 receptor (Hagmann *et al*, 2013). Upon RNA recognition, RIG-1 and MDA-5 are recruited to the outer membrane of mitochondria, where they encounter adaptor protein IPS-1 (also known as MAVS, CARDIF or VISA) that regulates downstream Type I IFN signalling. Although these sensors are typically thought to detect viruses, it is increasingly evident that they are also involved in the innate immune response to intracellular bacterial pathogens. It has been reported that *Legionella pneumophila* (Monroe *et al*, 2009) and *Listeria monocytogenes* (Hagmann *et al*, 2013) can secrete RNA and translocate it into the host cell cytoplasm, where it triggers the immunosurveillance RIG-1/MDA-5 pathway. In *L. pneumophila*, the translocation of bacterial RNA was shown to be mediated by a Type IV Secretion system, whereas *L. monocytogenes* secretes the RNA via a SecA2 secretion system (Hagmann *et al*, 2013; Monroe *et al*, 2009). To our knowledge, this cytosolic RNA-sensing pathway has not been reported previously to be associated with melioidosis. It will be interesting to examine in future studies how *B. pseudomallei* induces a Type I interferon response via the RIG-1/MDA5 pathway. The activation mechanism could result from direct recognition of bacterial RNA or an indirect host response due to secretion of other bacterial effectors.

In addition to interferon signalling, our microarray analysis also observed higher transcription of several genes encoding poly(ADP-ribose)-polymerase (PARP) proteins that are associated with three different IPA canonical pathways; '*Retinoic Acid Mediated Apoptosis Signalling* ', '*Death Receptor Signalling*' and '*UVA-Induced MAPK Signalling'*. These include PARP9, PARP10, PARP12 and PARP14. These genes and their associated pathways are observed most profoundly at 12hpi as a global response to both *B. pseudomallei* WT and the Δ*bimA* mutant. PARP enzymes comprise a catalytic domain ADP-ribosyl transferase which transfer negatively charged ADP-ribose moieties from donor NAD+ molecules onto the acceptor protein, a mechanism known as poly(ADP-ribosylation) (PARylation). This post-translational modification is essential in controlling a wide array of cellular processes; DNA repair, chromatin modulation and transcriptional regulation, cell division and roles in cellular

stress response and inflammation (Gibson & Kraus, 2012; Schreiber *et al*, 2006). PARPs are categorised largely on the basis of their domain architecture and their functional motifs. Some PARPs namely PARP1, PARP2 and PARP3 are localised in the nucleus where their primary function is to sense DNA breaks and transmit signals for DNA repair. However, in a situation of genotoxic stress, PARP-1 can be activated excessively which leads to cell death (David *et al*, 2009;D'Amours *et al*, 2001). PARP9 and PARP14 are examples of macroPARPs, containing a macrodomain fold which are high-affinity ADP-ribose-binding modules that can assist the migration of these PARPs to sites of poly- and possibly mono(ADP-ribosyl)ation (Karras *et al*, 2005). PARP 9 localisation is not known, but PARP 14 is present in stress granules in the cytosol. Interestingly, very recent findings by Iwata *et al* (2016) identified PARP9 and PARP14 as key regulators of macrophage activation, both in humans and mouse. PARP 9 was shown to promote IFN-γ induced responses, but PARP 14 suppressed the IFN-γ response. This cross-regulation of macrophage activation is important for a balance of pro-inflammatory and anti-inflammatory processes in host cells (Iwata *et al*, 2016). PARP 12 is an example of a CCCH PARP which have a Cys-Cys-Cys-His zinc finger that bind to RNA, as well as Trp-Trp-Glu domains for PAR binding activity. PARP10 is not categorised in any subfamily but found to be a partner protein of proto-oncoprotein c-Myc which inhibits cell proliferation and transformation (Yu *et al*, 2005). These together show the importance of PARPs in which their activity is a key component of cellular stress responses that lead to physiological or pathological outcomes. Like other post-translational modifications such as ubiquitination, phosphorylation, acetylation, and SUMOylation, ADP-ribosylation has profound effects on cellular functions.

To identify potential mechanism/s involved in clearing the *B. pseudomallei* Δ*bimA* mutant in infected BALB/C BMDMs, we selected one candidate for functional validation known as FNBP1L (Formin-binding protein-1 like, also known as TOCA-1) by confocal microscopy to assess the colocalisation of FNBP1L with the bacteria. From the literature, FNBP1L protein is required to limit replication of *Salmonella enterica* serovar Typhimurium (*S.* Typhimurium) in epithelial cells through an autophagy-dependent mechanism (Huett *et al*, 2009). However, this anti-*Salmonella* autophagy mechanism is independent from ubiquitin signalling as described previously in Chapter 3. FNBP1L was shown to interact with ATG3 (autophagy-related protein 3), which plays a role as an ubiquitin carrier enzyme mediating lipidation of LC3-I molecules to form LC3-II molecules during autophagosomes biogenesis (Huett *et al*, 2009). Interestingly, this FNBP1L molecule is non-essential for classical autophagic induction by

rapamycin or serum-starvation. However, our preliminary confocal images analysis do not show that the Δ*bimA* mutant colocalises with FNBP1L protein. As shown previously in Chapter 3 the Δ*bimA* mutant also does not significantly colocalise with LC3 molecules, which further confirms that autophagy via FNBP1L protein and LC3 molecules is not involved in restricting the intracellular survival of the Δ*bimA* mutant in BMDM cells. Furthermore, the studies performed by Huett and colleagues were conducted in non-phagocytic immortalised HEK293T and HeLa cells (Huett *et al*, 2009). It is possible that the pro-autophagy activity of FNBP1L observed during infection with *S.* Typhimurium is cell type-dependent. It would be interesting in future to study the role of this protein against *B. pseudomallei* in those cell lines. Although in other studies, FNBP1L has been described as a protein required for *Shigella flexneri* actin polymerisation (Leung *et al*, 2008), here we did not investigate if the protein was recruited to the actin tails of *B. pseudomallei*.

In relation to the autophagy pathway as described in Chapter 3, Klionsky *et al* (2015) demonstrate that the induction of autophagy in certain circumstances is accompanied by an increase in the mRNA levels of certain autophagy-related genes (ATG), such as ATG5 (beclin 1, a protein crucial for autophagy initiation), ATG7 (the activating enzyme for Atg8 conjugation), ATG8/LC3, ATG9 (involves in autophagosomes formation), ATG12 (ubiquitin-like modifier that conjugate with Atg5) and ATG14 (recruits other ATG proteins at the early stages of autophagasome formation) (Klionsky *et al*, 2015). However, the global transcriptomic microarray analysis here found that none of these genes is differentially expressed in infected BMDMs cells with either WT *B. pseudomallei* or Δ*bimA*. This finding adds further evidence demonstrating that autophagy is not important in controlling the intracellular survival of *B. pseudomallei* in BALB/C BMDMs. If any of the genes listed above had been shown to be upregulated upon infection, it would have been desirable to knock down the gene/s by siRNA transfection, followed by subsequent investigation of the effect of knockdown on bacterial intracellular survival.

Microarray analysis suggested that NOS2 and FAS were among those genes specifically upregulated in response to infection with the Δ*bimA* mutant strain. NOS2 encodes for inducible, nitric oxide synthase enzyme (iNOS) which is responsible for the production of nitric oxide, an antimicrobial compound. Whereas FAS (also known as APO-1/CD95) is a member of the TNF receptor family where its interaction with the ligand FasL results in the transduction of cell signalling leading to apoptosis (Nagata, 1997). However, validation by qPCR identified that the NOS gene was significantly elevated in cells infected with both WT and Δ*bimA* mutant

strains, at 8hpi and 12hpi, with the fold change ranging from 7.22 to 20.2. Although the fold-change amplitude of the gene expression is considerably high, we were not able to detect nitrite in the supernatants of infected cells by Griess assay, presumably because the nitrite produced is below the limit of detection of the assay (as mentioned in Chapter 4). *B. pseudomallei* was found previously to suppress the production of nitric oxide, unlike other Gram-negative bacteria such as *E. coli* and *Salmonella* Typhi (Utaisincharoen *et al*, 2001). Besides, the production of nitric oxide requires macrophage priming by IFN-γ and LPS, which were not included in our assay (Utaisincharoen *et al*, 2001;Lowry & Goldberg, 1998). On the other hand, qPCR validation of the FAS gene found the gene was expressed slightly higher (amplitude less than 2-fold), not just in cells infected with the Δ*bimA* mutant strain, but also with the WT strain.

Up to 40% of the genes that were classified as DEGs specifically upregulated in response to the Δ*bimA* mutant were not characterised, and those characterised were mapped to very few canonical pathways in the IPA analysis. This suggests that the innate mechanism/s involved in the cellular response to the Δ*bimA* mutant could be novel or mediated by host post-translational modification, which is beyond the capability of the DNA microarray used in this chapter. Another important point to note is that in our microarray analysis, the RNA that was analysed was a mixture of RNA from both infected and uninfected macrophages. Approximately only 0.5% of the BMDMs were infected based on the CFU counts in the kanamycin protection assay. This consequently limits the experimental power to identify innate mechanism/s activated upon infection. The increase in signals detected between uninfected and infected groups could reflect a 'bystander effect' where the signals emanating from infected cells may be perturbing gene expression in uninfected cells to make them more anti-microbial. Therefore, the altered gene expression identified in the infected group is either due to a direct effect upon infection, or an indirect bystander effect. It would be better if the infected BMDMs were sorted out from the uninfected ones by FACS before isolating the RNA. However, this is not possible as working with a hazard group 3 pathogen does not allow us to bring the pathogen out from the Containment Level 3 (CL3) facility and contaminate the in-house FACS machine. Hence, although quite a number of DEGs were identified between groups, it should be noted that these signals may be confounded by the small proportion of infected cells in the samples, as well as bystander effects.

In addition, analysis from the PCA plot suggests the variations between replicates are more profound than the variations observed between groups of uninfected and BMDMs infected with either *B. pseudomallei* WT or the Δ*bimA* strain at respective time points. We

would think that differentiating bone-marrow cells into mature macrophages (BMDMs) in the presence of GM-CSF and foetal-calf serum (FCS) on different days for independent biological repeats results in true day-to-day biological variations of the primary cultures. This could account for the primary source of such variability rather than the microarray methodology itself such as RNA isolation or array hybridisation. To overcome such variation, Depke *et al* (2014) suggested using a standardised culture system to differentiate BMDMs in which they successfully produced highly reproducible biological replicates. This could be implemented in future for studying global expression analysis in BMDMs. While subtle gene-expression responses were highly sensitive to changes in primary BMDMs, remarkably we found no convincing evidence of induction of a specific gene expression response in cells infected with *B. pseudomallei* incapable of forming actin-tails.

6 CHAPTER 6: GENERAL DISCUSSION

Melioidosis, an infectious disease that affects both humans and animals is caused by the bacterium *Burkholderia pseudomallei*. Current treatment for melioidosis is limited by the intrinsic antibiotic resistance of *B. pseudomallei* and there is no effective and safe vaccine available for human use. Effective innate immune responses are critical for controlling the early phase of infection. Diabetic patients who have defective innate immune responses are more susceptible to melioidosis (Currie *et al*, 2010; Chanchamroen *et al*, 2009). The innate immune system is designed to detect invading pathogens, and send endogenous alarm signals from the infected cells to trigger recruitment of more immune cells to the site of infection for pathogen clearance. When this innate immune system fails to clear the infection, the adaptive immune system comes into play as a second line of defence to continue the unresolved host-pathogen battle. Macrophages are important host innate immunity cells, yet *B. pseudomallei* can survive within such cells, particularly those of diabetic patients. The main aim of this thesis is to provide more understanding of the macrophage: bacterium interaction. The thesis also aimed to understand how actin-based motility mediated by the bacterial factor BimA could help the bacteria to evade the macrophage's protective cell-autonomous immunity pathways. Discovering such an evasion mechanism would facilitate the development of immune-based host-directed therapies, which in turn could benefit the treatment of a range of intracellular bacteria refractory to antibiotic treatment including *B. pseudomallei*. Throughout studies in this thesis, bone-marrow derived macrophages (BMDMs) differentiated from the bone marrow cells of BALB/C mice, which represent an acute murine melioidosis model, were used for the investigations.

In Chapter 3, we consistently observe BimA-dependent actin tail formation (Figure 3.5) and survival of *B. pseudomallei* in BALB/C BMDMs (Figure 3.3). No actin structures were associated with cytoplasmic Δ*bimA* mutant (Figure 3.5) and the Δ*bimA* mutant is impaired in intracellular survival at 16 hpi (hours of post infection) (Figure 3.3), making this a robust system to address the objectives to identify the BimA-dependent evasion mechanisms of *B. pseudomallei*. This phenotype however, can be restored upon inducible expression of BimA *in trans*, consistent with a role for the BimA protein in actin-based motility (Figure 3.5). We observed that the defect in the intracellular survival of the Δ*bimA* strain is not due to phagosomal killing as determined by kanamycin and chloroquine protection assay (Figure 3.6)

but rather, an unknown cell-autonomous innate mechanism is thought to be involved in detection and elimination of the Δ*bimA* mutant.

6.1 Autophagy and future directions

Whilst there are numerous strategies to evade different cell-autonomous defence pathways, cytosol-adapted *Listeria monocytogenes* and *Shigella flexneri* use actin-based motility to avoid host autophagy recognition and elimination (Yoshikawa *et al*, 2009; Ogawa *et al*, 2005). Whilst autophagy has previously been implicated in targeting phagosomal *B. pseudomallei* in an LC3-associated phagocytosis (LAP) -dependent manner, cytoplasmic *B. pseudomallei* has been shown to be capable of escaping canonical autophagy (Gong *et al*, 2011; Cullinane *et al*, 2008). With a traditional 'hypothesis-driven' approach, we speculated that autophagy evasion could be dependent on the BimA-mediated actin-based motility. Whilst autophagy has been shown to target mutants of *L. monocytogenes* and *S. flexneri* incapable of actin-based motility for degradation, the present studies have clearly demonstrated that autophagy does not play a role in the clearance of the *B. pseudomallei* Δ*bimA* mutant from infected BMDMs. The studies presented in this thesis included LC3-conversion assay by Western blot (Figure 3.9) and confocal imaging for colocalisation of LC3 with bacteria (Figure 3.10) as well as the autophagic adaptor protein p62 with bacteria (Figure 3.12). Prior to autophagy-mediated degradation of the actin-based motility deficient *L. monocytogenes* mutant, the mutant is extensively ubiquitinated when compared to the WT strain. However, such selective ubiquitination is not observed for the *B. pseudomallei* Δ*bimA* mutant as the majority of both *B. pseudomallei* WT and the Δ*bimA* mutant are similarly ubiquitinated (Figure 3.10). Besides marking cytosolic bacteria with ubiquitin as a signal to initiate autophagy, bacterial glycans in the cytoplasm can be recognised by galectin molecules, in which galectin-8 has been demonstrated to link into the autophagy pathway (Thurston *et al*, 2012). Some other adaptor proteins namely, NDP52 and optineurin, are also worth investigation in the future (Kraft *et al*, 2010). The importance of autophagy in innate sensing mechanisms highlights the emerging link between cytoskeletal elements and the host defence mechanism. Interestingly, septin proteins have also been identified to be recruited to intracytoplasmic *Shigella flexneri,* which cage the non-motile bacteria and promote autophagy (Mostowy *et al*, 2010). This phenomenon is known as septin-caging and therefore warrants further investigations in relation to its role in control of *B. pseudomallei* in future.

6.2 Cellular signalling pathways and future directions

Host cell-autonomous immunity begins when the receptor (PRR) senses microbial components (PAMPs) or danger molecules (DAMPs) which then mediate downstream intracellular signalling networks for bacterial elimination. In Chapter 4, the aim was to investigate the role of Toll-like Receptors (TLR) in recognition and elimination of the *B. pseudomallei* Δ*bimA* mutant. Instead of investigating individual TLRs, the studies focused on the contribution of the TLR adaptor proteins; MyD88 and TRIF. A gene silencing technique using short interfering RNAs (siRNAs) (Figure 4.4) was used to knockdown MyD88 gene expression, and in a separate experiment MyD88- or TRIF-blocking peptide were used to inhibit the respective signalling pathway (Figure 4.7 and Figure 4.10 respectively). In addition to the role of the TLRs, the investigation included the involvement of canonical and non-canonical inflammasome pathways which result in pyroptotic cell death. Instead of investigating the individual inflammasome-associated receptors (NLRs), the studies in this thesis only focused on the associated caspase maturation and also the end products of specific cytokine secretion (Figure 4.14 and figure 4.15). However, none of these pathways were shown to be promising candidate pathways involved in clearance of the Δ*bimA* mutant from infected BMDMs. The TRIF-IFNβ-non-canonical inflammasome pathway may be required for controlling *B. pseudomallei* intracellular fate, this cell-autonomous response is unlikely to be specific to the Δ*bimA* mutant.

We also propose that the host innate mechanism that targets the Δ*bimA* mutant may require post-translational modifications (PTM) which is beyond the capability of experiments carried out in this thesis. Host genes translated into proteins are often subject to PTMs, which exert an additional layer of regulation. Therefore, a proteomic approach for global profiling of host protein modification during infection would be a superior tool to understand host-pathogen interactions. As such, mass spectrometry (MS)-based proteomics serves as a high sensitivity high-throughput approach for global protein profiling as well as identification of relevant PTMs (Angel *et al*, 2012). In terms of PTMs, phosphorylation is the most recognised modification and a central regulator of various cellular signalling pathways (Angel *et al*, 2012). Protein phosphorylation is a reversible PTM, regulated by kinases and phosphatases. Protein phosphorylation is known to be involved in transcriptional and translational regulation, cellular signalling and communication as well as many other cellular processes including energy metabolism, apoptosis, cell cycle progression, cell differentiation and cytoskeleton regulation (Hunter, 2000). MS-based phosphoproteomics is an excellent tool for revealing such global

changes in cellular phosphoproteomes. Bacterial pathogens evolve mechanisms through toxins, effector molecules or virulence factors to modulate and hijack signalling pathways for their own benefits and survival. In the innate immune system, recognition of microbial associated PAMPs or DAMPs by specific PRRs triggers the phosphorylation-based signalling cascades which result in the production of cytokines and chemokines, inflammasome activation, apoptosis or other forms of cell death to restrict the survival of the invading pathogen. For example, activation of TLRs results in the activation of many kinases including interleukin-1 receptor-associated kinases (IRAK), mitogen-activated protein kinases (MAPKs), extracellular-signal regulated kinases (ERK, also known as classical MAPKs) and IκB kinase (IKK), followed by subsequent phosphorylation of the master transcriptional regulators AP-1 and NFκB. Some pathogens such as *Yersinia spp* have been shown to attenuate the immune response by irreversible inactivation of MAPKs and IKK (Mukherjee *et al*, 2006). *Shigella flexneri* has been shown to dephosphorylate p38 MAPK and ERK via its T3SS effector protein OspF in infected epithelial cells. Such dephosphorylation results in attenuation of pro-inflammatory cytokine IL-8 (Schmutz *et al*, 2013). Similarly, *Salmonella* Typhimurium prevents apoptosis by targeting kinases Akt and RSK1 (protein downstream of ERK phosphorylation) through its T3SS effector protein SopB, as determined by global phosphoproteomics analysis (Rogers *et al*, 2011). Therefore, we propose a large-scale phosphoproteomics approach to provide insight into the regulation of the host-pathogen interactions and the cell signalling pathways, specifically in response to the Δ*bimA* mutant. MS-based phosphoproteomics is also capable of discovery of novel cell signalling circuits. The findings from the phosphoproteomics data could then be confirmed with functional studies involving small interfering RNAs (siRNAs) and relevant kinase inhibitors.

6.3 Host transcriptomic studies and future directions

From the traditional 'hypothesis-driven' approaches described above, we moved to an unbiased high-throughput method using microarray (Chapter 5). The technology provides an overview of the expression pattern of thousands of differentially expressed genes during infection, which in turn offers more insight into pathways and networks for host-pathogen interactions. Global transcriptional profiling by microarray revealed that the BALB/C BMDMs mount innate immune responses to infection with both *B. pseudomallei* WT and the Δ*bimA* mutant when compared to uninfected control cells during the experimental time points

of 8 and 12 hpi. A microarray dataset presented by table 5.10 and 5.11, found a similar cohort of core inflammatory 'alarm signal' molecules comprised of various pro-inflammatory cytokines and chemokines, as a similar suite of genes induced in THP-1 human monocytic-like cells (Perumal Samy *et al*, 2015), as well as in murine tissues infected with a *B. pseudomallei* WT strain (Chin *et al*, 2010). These inflammatory signals also serve as a means for communication between innate and adaptive immune response (Table 5.10). At later time points of infection, the predominant response has pervasive similarities to the transcriptional programme mediated by interferon-related signalling (Table 5.11). The involvement of interferon-mediated signalling in infected BALB/C BMDMs in our *in vitro* assays is mirrored with the *in vivo* host transcriptomic changes in the acute melioidosis BALB/C mouse model (Chin *et al*, 2010). IFNγ has been shown to be essential for resistance to *B. pseudomallei* both *in vitro* and *in vivo* (Utaisincharoen *et al*, 2004; Santanirand *et al*, 1999). In fact, IFNγ and its inducing cytokines IL-12β were found to be significantly higher in melioidosis patients (Lauw *et al*, 1999; Brown *et al*, 1991). Whilst there are extensive investigations on the role of IFNγ in the pathogenesis of melioidosis, the role of Type I IFN is not well described. Very few studies reported on the importance of IFNβ in suppressing the intracellular growth of *B. pseudomallei* when added exogenously (Utaisincharoen *et al*, 2003), however, it is believed that *B. pseudomallei* infection is unlikely to induce host TLR/TRIF-dependent pathways to produce Type I IFN (Tangsudjai *et al*, 2010; Wiersinga *et al*, 2008; Utaisincharoen *et al*, 2003). The identification of upregulated genes encoding RNA sensors of the RLR family (RIG-1 and MDA-5) in the present microarray dataset is an interesting finding. As far as we are aware no literature has been published regarding the role of any of these cytosolic RNA sensors in detecting the presence of *B. pseudomallei* to produce Type I IFN, which we postulate to be a specific response by BALB/C BMDMs upon *B. pseudomallei* infection. Therefore, this thesis is the first report identifying the possible involvement of RIG-1 and MDA-5 receptors in sensing cytosolic RNA as well as related interferon signalling in melioidosis. Recently, it has been demonstrated that RIG-1/MDA5 signalling pathways can also result in a programmed cell death known as apoptosis (Chattopadhyay & Sen, 2017) which has not being investigated in this thesis. Nevertheless, we would wish to pursue future validation and functional characterisation for the candidate receptors and interferon mediators.

The second goal of the microarray experiment was to identify an innate immune response that specifically targets the Δ*bimA* mutant, however, we found no conclusive evidence at the transcriptional level. To our surprise, very few functional pathways were identified for this

category, with very few molecules associated with each pathway (Table 5.14 and Table 5.15). We were unable to identify clusters that could be considered specific to the presence of cytoplasmic bacteria that are unable to form actin tails. Many of the differentially expressed genes identified as being specific to the Δ*bimA* mutant have no previously known role. This suggests that the host mechanisms targeting the Δ*bimA* mutant are likely to be novel. Besides, it could be possible that the specific genes involved are not present on microarrays or the transcript abundance is too low to be detected, representing some of the pitfalls of the microarray technology. Therefore the more expensive next generation sequencing technologies such as RNA-seq could be used in future to overcome such limitations. Additionally, future experiments would be more powerful if RNA from the infected cells could be isolated from the uninfected as discussed in Chapter 5. As microarray technology detects the known transcripts with existing genomic sequencing information, RNA-seq on the other hand, is ideal for exploring novel transcripts. Besides, RNA-seq delivers much lower background signal as compared to microarray, therefore capable of overcoming common hybridisation issues seen with microarrays.

6.4 Final conclusions

In conclusion, the present studies provide evidence that *B. pseudomallei bimA*-dependent elimination in BALB/C BMDMs is unlikely to involve autophagy, TLR-dependent signalling, canonical inflammasome nor non-canonical inflammasome pathways. Although studies of global transcriptome profiling by microarray have proven powerful tools in the study of host-pathogen interactions, they cannot fruitfully assist discovery of novel genes as well as mechanisms that rely on protein post-translational modification. Besides, there are other possible cell-autonomous immunity pathways that may be involved in targeting *bimA*-deficient bacteria such as galectins and septin caging. The future also requires more combinations of various 'omics' techniques such as MS-proteomics and RNA-seq technologies. These strategies together will provide valuable information about host-pathogen interactions, which can be utilised in the development of immune-based host-directed therapies as viable alternatives to antimicrobials.

7 BIBLIOGRAPHY

Aachoui, Y., Leaf, I. a, Hagar, J. a, Fontana, M. F., Campos, C. G., Zak, D. E., … Miao, E. a. (2013). Caspase-11 protects against bacteria that escape the vacuole. *Science*, *339*(6122), 975–978.

Abbink, F. C., Orendi, J. M., & Beaufort, A. J. (2001). Mother-to-child transmission of *Burkholderia pseudomallei. New England Journal of Medicine*, *344*(15), 1171.

Allwood, E. M., Devenish, R. J., Prescott, M., Adler, B., & Boyce, J. D. (2011). Strategies for intracellular survival of *Burkholderia pseudomallei*. *Frontiers in Microbiology*, *2*, 1–19.

Angel, T. E., Aryal, U. K., Hengel, S. M., Baker, E. S., Kelly, R. T., Robinson, W., & Smith, R. D. (2012). Mass spectrometry based proteomics: existing capabilities and future directions. *Chemical Society Reviews*, *41*(10), 3912–3928.

Arjcharoen, S., Wikraiphat, C., Pudla, M., Limposuwan, K., Woods, D. E., Sirisinha, S., & Utaisincharoen, P. (2007). Fate of a *Burkholderia pseudomallei* lipopolysaccharide mutant in the mouse macrophage cell line RAW 264.7: possible role for the O-antigenic polysaccharide moiety of lipopolysaccharide in internalization and intracellular survival. *Infection and Immunity*, *75*(9), 4298–4304.

Austyn, J. M., & Gordon, S. (1981). F4/80, a monoclonal antibody directed specifically against the mouse macrophage. *European Journal of Immunology*, *11*, 805–815.

Bäckhed, F., & Hornef, M. (2003). Toll-like receptor 4-mediated signaling by epithelial surfaces: Necessity or threat? *Microbes and Infection*, *5*(11), 951–959.

Balder, R., Lipski, S., Lazarus, J. J., Grose, W., Wooten, R. M., Hogan, R. J., … Lafontaine, E. R. (2010). Identification of *Burkholderia mallei* and *Burkholderia pseudomallei* adhesins for human respiratory epithelial cells. *BMC Microbiology*, *10*, 250.

Barker, J. R., Koestler, B. J., Carpenter, V. K., Burdette, D. L., Waters, C. M., Vance, R. E., & Valdivia, R. H. (2013). STING-dependent recognition of cyclic di-AMP mediates type I interferon responses during *Chlamydia trachomatis* infection. *mBio*, *4*(3), 1–11.

Barnes, J. L., Williams, N. L., & Ketheesan, N. (2008). Susceptibility to *Burkholderia pseudomallei* is associated with host immune responses involving tumor necrosis factor receptor-1 (TNFR1) and TNF receptor-2 (TNFR2). *FEMS Immunology and Medical Microbiology*, *52*(3), 379–388.

Barnett, J. B., & Brundage, K. M. (2010). Evaluating macrophages in immunotoxicity testing. *Methods in Molecular Biology (Clifton, N.J.)*, *598*, 75–94.

Barth, S., Glick, D., & Macleod, K. F. (2010). Autophagy: Assays and artifacts. *Journal of Pathology*, *221*(2), 117–124.

Bast, A., Krause, K., Schmidt, I. H. E., Pudla, M., Brakopp, S., Hopf, V., … Steinmetz, I. (2014). Caspase-1-Dependent and -Independent cell death pathways in *Burkholderia pseudomallei* infection of macrophages. *PLoS Pathogens*, *10*(3), e1003986.

Benanti, E. L., Nguyen, C. M., & Welch, M. D. (2015). Virulent *Burkholderia* species mimic host actin polymerases to drive actin-based motility. *Cell*, 161, 348-360.

Berghaus, L. J., Moore, J. N., Hurley, D. J., Vandenplas, M. L., Fortes, B. P., Wolfert, M. A., & Boons, G.-J. (2010). Innate immune responses of primary murine macrophage-lineage cells and RAW 264.7 cells to ligands of

Toll-like receptors 2, 3, and 4. *Comparative Immunology, Microbiology and Infectious Diseases*, *33*(5), 1–13.

Blander, J. M., & Medzhitov, R. (2006). On regulation of phagosome maturation and antigen presentation. *Nat Immunol*, *7*(10), 1029–1035.

Boh, B. K., Ng, M. Y., Leck, Y. C., Shaw, B., Long, J., Sun, G. W., … Hagen, T. (2011). Inhibition of cullin RING ligases by cycle inhibiting factor : Evidence for interference with Nedd8-induced conformational control. *Journal of Molecular Biology*, *413*(2), 430–437.

Boriushkin, E., Wang, J. J., Li, J., Bhatta, M., & Zhang, S. X. (2016). p58(IPK) suppresses NLRP3 inflammasome activation and IL-1beta production via inhibition of PKR in macrophages. *Scientific Reports*, *6*(April), 25013.

Breen, J. D., & Karchmer, A. W. (1995). *Staphylococcus aureus* infections in diabetic patients. *Infectious Disease Clinicals of North America*, *9*(1), 11–24.

Breitbach, K., Klocke, S., Tschernig, T., Van Rooijen, N., Baumann, U., & Steinmetz, I. (2006). Role of inducible nitric oxide synthase and NADPH oxidase in early control of *Burkholderia pseudomallei* infection in mice. *Infection and Immunity*, *74*(11), 6300–6309.

Breitbach, K., Rottner, K., Klocke, S., Rohde, M., Jenzora, A., Wehland, J., & Steinmetz, I. (2003). Actin-based motility of *Burkholderia pseudomallei* involves the Arp 2/3 complex, but not N-WASP and Ena/VASP proteins. *Cellular Microbiology*, *5*(6), 385–393.

Breitbach, K., Sun, G. W., Köhler, J., Eske, K., Wongprompitak, P., Tan, G., … Steinmetz, I. (2009). Caspase-1 mediates resistance in murine melioidosis. *Infection and Immunity*, *77*(4), 1589–1595.

Breitbach, K., Wongprompitak, P., & Steinmetz, I. (2011). Distinct roles for nitric oxide in resistant C57BL/6 and susceptible BALB/c mice to control *Burkholderia pseudomallei* infection. *BMC Immunology*, *12*, 20.

Brett, P. J., DeShazer, D., & Woods, D. E. (1998). *Burkholderia thailandensis* sp. nov., a *Burkholderia pseudomallei*-like species. *International Journal of Systematic Bacteriology*, *48*, 317–320.

Brown, A. E., Dance, D. A. B., Suputtamongkol, Y., Chaowagul, W., Kongchareon, S., Webster, H. K., & White, N. J. (1991). Immune cell activation in melioidosis - increased serum levels of interferon-gamma and soluble interleukin-2 receptors without change in soluble Cd8 protein. *Journal of Infectious Diseases*, *163*(5), 1145–1148.

Broz, P., & Monack, D. M. (2013). Noncanonical inflammasomes: Caspase-11 activation and effector mechanisms. *PLoS Pathogens*, *9*(2), 9–12.

Broz, P., Ruby, T., Belhocine, K., Bouley, D. M., Kayagaki, N., Dixit, V. M., & Monack, D. M. (2012). Caspase-11 increases susceptibility to *Salmonella* infection in the absence of caspase-1. *Nature*, *490*(7419), 288–91.

Burdette, D. L., & Vance, R. E. (2013). STING and the innate immune response to nucleic acids in the cytosol. *Nature Immunology*, *14*(1), 19–26.

Burtnick, M. N., Brett, P. J., Harding, S. V., Ngugi, S. A., Ribot, W. J., Chantratita, N., … DeShazer, D. (2011). The cluster 1 type VI secretion system is a major virulence determinant in *Burkholderia pseudomallei*. *Infection and Immunity*, *79*(4), 1512–1525.

Burtnick, M. N., Brett, P. J., Nair, V., Warawa, J. M., Woods, D. E., & Gherardini, F. C. (2008). *Burkholderia pseudomallei* type III secretion system mutants exhibit delayed vacuolar escape phenotypes in RAW 264.7 murine macrophages. *Infection and Immunity*, *76*(7), 2991–3000.

Bustin, S. A., Benes, V., Garson, J. A., Hellemans, J., Huggett, J., Kubista, M., … Wittwer, C. T. (2009). The MIQE guidelines: Minimum Information for Publication of Quantitative Real-Time PCR experiments. *Clinical Chemistry*, *55*(4), 611–622.

Bustin, S. A., Benes, V., Nolan, T., & Pfaffl, M. W. (2005). Quantitative real-time RT-PCR - A perspective. *Journal of Molecular Endocrinology*, *34*(3), 597–601.

Case, C. L., Kohler, L. J., Lima, J. B., Strowig, T., de Zoete, M. R., Flavell, R. A., … Roy, C. R. (2013). Caspase-11 stimulates rapid flagellin-independent pyroptosis in response to L*egionella pneumophila*. *Proceedings of the National Academy of Sciences of the United States of America*, *110*(5), 1851–1856.

Casson, C. N., Yu, J., Reyes, V. M., Taschuk, F. O., Yadav, A., Copenhaver, A. M., … Shin, S. (2015). Human caspase-4 mediates noncanonical inflammasome activation against gram-negative bacterial pathogens. *Proceedings of the National Academy of Sciences*, *112*(21), 6688–6693. 2

Ceballos-Olvera, I., Sahoo, M., Miller, M. A., del Barrio, L., & Re, F. (2011). Inflammasome-dependent pyroptosis and IL-18 protect against *Burkholderia pseudomallei* lung infection while IL-1Beta is deleterious. *PLoS Pathogens*, *7*(12), e1002452.

Cervantes, J., Nagata, T., Uchijima, M., Shibata, K., & Koide, Y. (2008). Intracytosolic *Listeria monocytogenes* induces cell death through caspase-1 activation in murine macrophages. *Cellular Microbiology*, *10*(1), 41–52.

Chamberlain, L. M., Godek, M. L., Gonzalez-Juarrero, M., & Grainger, D. W. (2009). Phenotypic non-equivalence of murine (monocyte-) macrophage cells in biomaterial and inflammatory models. *Journal of Biomedical Materials Research - Part A*, 88(4), 858-871.

Chanchamroen, S., Kewcharoenwong, C., Susaengrat, W., Ato, M., & Lertmemongkolchai, G. (2009). Human polymorphonuclear neutrophil responses to *Burkholderia pseudomallei* in healthy and diabetic subjects. *Infection and Immunity*, *77*(1), 456–463.

Charuchaimontri, C., Suputtamongkol, Y., Nilakul, C., Chaowagul, W., Chetchotisakd, P., Lertpatanasuwun, N., … Woods, D. E. (1999). Antilipopolysaccharide II: an antibody protective against fatal melioidosis. *Clinical Infectious Diseases : An Official Publication of the Infectious Diseases Society of America*, *29*(4), 813–818.

Chattopadhyay, S., & Sen, G. C. (2017). RIG-I-like receptor-induced IRF3 mediated pathway of apoptosis (RIPA): a new antiviral pathway. *Protein and Cell*, *8*(3), 165–168.

Chen, H. Y., Weng, I. C., Hong, M. H., & Liu, F. T. (2014). Galectins as bacterial sensors in the host innate response. *Current Opinion in Microbiology*, *17*(1), 75–81.

Cheng, A. C., & Currie, B. J. (2005). Melioidosis: Epidemiology, pathophysiology, and management. *Clinical Microbiology Reviews*, *18*(2), 383–416.

Chieng, S., Carreto, L., & Nathan, S. (2012). *Burkholderia pseudomallei* transcriptional adaptation in macrophages. *BMC Genomics*, *13*(1), 1–13.

Chin, C.-Y., Monack, D. M., & Nathan, S. (2010). Genome wide transcriptome profiling of a murine acute melioidosis model reveals new insights into how *Burkholderia pseudomallei* overcomes host innate immunity. *BMC Genomics*, *11*(1), 672.

Coenye, T., & Vandamme, P. (2003). Diversity and significance of *Burkholderia* species occupying diverse ecological niches. *Environmental Microbiology*, *5*(9), 719–729.

Cohen, P., Bouaboula, M., Bellis, M., Jbilo, O., Poinot-chazel, C., Galie, S., … Casellas, P. (2000). Monitoring cellular responses to Listeria monocytogenes with oligonucleotides arrays. *The Journal of Biological Chemistry*, *275*(15), 11181–11190.

Collins, C. A., De Mazière, A., Van Dijk, S., Carlsson, F., Klumperman, J., & Brown, E. J. (2009). Atg5-independent sequestration of ubiquitinated mycobacteria. *PLoS Pathogens*, *5*(5), 1000430.

Coombes, K. R., Morris, J. S., Hu, J., Edmonson, S. R., & Baggerly, K. A. (2005). Serum proteomics profiling--a young technology begins to mature. *Nature Biotechnology*, *23*(3), 291–2.

Cullinane, M., Gong, L., Li, X., Lazar Adler, N. R., Tra, T., Wolvetang, E., … Adler, B. (2008). Stimulation of autophagy suppresses the intracellular survival of *Burkholderia pseudomallei* in mammalian cell lines. *Autophagy*, *4*(6), 744–753.

Cullinane, M., Gong, L., Li, X., Lazar-Adler, N., Tra, T., Wolvetang, E., … Adler, B. (2008). Stimulation of autophagy suppresses the intracellular survival of Burkholderia pseudomallei in mammalian cell lines. *Autophagy*, *4*(6), 744–753.

Currie, B. J. (2008). Advances and remaining uncertainties in the epidemiology of Burkholderia pseudomallei and melioidosis. *Transactions of the Royal Society of Tropical Medicine and Hygiene*, *102*, 225–227.

Currie, B. J., Fisher, D. A., Anstey, N. M., & Jacups, S. P. (2000). Melioidosis: acute and chronic disease, relapse and re-activation. *Transactions of the Royal Society of Tropical Medicine and Hygiene*, *94*, 301–304.

Currie, B. J., Fisher, D. A., Howard, D. M., Burrow, J. N. C., Selvanayagam, S., Snelling, P. L., … Mayo, M. J. (2000). The epidemiology of melioidosis in Australia and Papua New Guinea. In *Acta Tropica* (pp. 121–127).

Currie, B. J., & Jacups, S. P. (2003). Intensity of rainfall and severity of melioidosis, Australia. *Emerging Infectious Diseases*, *9*(12), 1538–1542.

Currie, B. J., Mayo, M., Anstey, N. M., Donohoe, P., Haase, A., & Kemp, D. J. (2001). A cluster of melioidosis cases from an endemic region is clonal and is linked to the water supply using molecular typing of *Burkholderia pseudomallei* isolates. *American Journal of Tropical Medicine and Hygiene*, *65*(3), 177–179.

Currie, B. J., Ward, L., & Cheng, A. C. (2010). The epidemiology and clinical spectrum of melioidosis: 540 cases from the 20 year darwin prospective study. *PLoS Neglected Tropical Diseases*, *4*(11), e900.

D'Amours, D., Sallmann, F. R., Dixit, V. M., & Poirier, G. G. (2001). Gain-of-function of poly(ADP-ribose) polymerase-1 upon cleavage by apoptotic proteases: implications for apoptosis. *Journal of Cell Science*, *114*(Pt 20), 3771–3778.

Dalma-Weiszhausz, D. D., Warrington, J., Tanimoto, E. Y., & Miyada, C. G. (2006). The Affymetrix GeneChip Platform: An Overview. *Methods in Enzymology*, *410*(06), 3–28.

Dance, D. (2014). Treatment and prophylaxis of melioidosis. *International Journal of Antimicrobial Agents*, *43*(4), 310–318.

Darveau, R. P., Pham, T. T. T., Lemley, K., Reife, R. A., Bainbridge, B. W., Coats, S. R., … Hajjar, A. M. (2004). Porphyromonas gingivalis lipopolysaccharide contains multiple lipid A species that functionally interact with both toll-like receptors 2 and 4. *Infection and Immunity*, *72*(9), 5041–5051.

David, K. K., Andrabi, S. A., Dawson, T. M., & Dawson, V. L. (2009). Parthanatos, a messenger of death. *Frontiers in Bioscience (Landmark Edition)*, *14*, 1116–28.

De Spiegelaere, W., Dern-Wieloch, J., Weigel, R., Schumacher, V., Schorle, H., Nettersheim, D., … Fink, C. (2015). Reference gene validation for RT-qPCR, a note on different available software packages. *PLoS ONE*, *10*(3), 1–13.

DeFilippis, V. R., Alvarado, D., Sali, T., Rothenburg, S., & Früh, K. (2010). Human cytomegalovirus induces the interferon response via the DNA sensor ZBP1. *Journal of Virology*, *84*(1), 585–98.

Depke, M., Breitbach, K., Dinh, K., Dang, H., Brinkmann, L., Salazar, M. G., … Völker, U. (2014). Bone marrow-derived macrophages from BALB/c and C57BL/6 mice fundamentally differ in their respiratory chain complex proteins, lysosomal enzymes and components of antioxidant stress systems ☆. *Journal of Proteomics*, *103*(7), 72–86.

Derossi, D., Joliot, A. H., Chassaing, G., & Prochiantz, A. (1994). The third helix of the Antennapedia homeodomain translocates through biological membranes. *Journal of Biological Chemistry*, *269*(14), 10444–10450.

DeShazer, D. (2007). Virulence of clinical and environmental isolates of *Burkholderia oklahomensis* and *Burkholderia thailandensis* in hamsters and mice. *FEMS Microbiology Letters*, *277*, 64–69.

Di Lella, S., Sundblad, V., Cerliani, J. P., Guardia, C. M., Estrin, D. A., Vasta, Gerardo, R., & Rabivonich, G. A. (2011). When galectins recognise glycans: from biochemistry to physiology and back again. *Biochemistry*, *50*(37), 7842–7857.

Dixit, E., & Kagan, J. C. (2013). Intracellular pathogen detection by RIG-I-like receptors. *Advances in Immunology*, *117*, 99–125.

Dooley, K. E., & Chaisson, R. E. (2009). Tuberculosis and diabetes mellitus: convergence of two epidemics. *Lancet Infectious Disease*, *9*(12), 737–746.

Dupont, N., Lacas-gervais, S., Bertout, J., Paz, I., Freche, B., Nhieu, G. T. Van, … Lafont, F. (2009). Article *Shigella* phagocytic vacuolar membrane remnants participate in the cellular response to pathogen invasion and are regulated by autophagy. *Cell Host and Microbe*, *6*(2), 137–149.

Easton, A., Haque, A., Chu, K., Lukaszewski, R., & Bancroft, G. J. (2007). A critical role for neutrophils in resistance to experimental infection with *Burkholderia pseudomallei*. *The Journal of Infectious Diseases*, *195*(1), 99–107.

Eckmann, L., Smith, J. R., Housley, M. P., Dwinell, M. B., & Kagnoff, M. F. (2000). Analysis by high density cDNA arrays of altered gene expression in human intestinal epithelial cells in response to infection with the invasive enteric bacteria *Salmonella* 2. *J.Biol.Chem.*, *275*(19), 14084–14094.

Egile, C., Loisel, T. P., Laurent, V., Li, R., Pantaloni, D., Sansonetti, P. J., & Carlier, M. F. (1999). Activation of the CDC42 effector N-WASP by the *Shigella flexneri* IcsA protein promotes actin nucleation by Arp2/3 complex and bacterial actin-based motility. *The Journal of Cell Biology*, *146*(6), 1319–1332.

Eisenreich, W., Heesemann, J., Rudel, T., & Goebel, W. (2013). Metabolic host responses to infection by intracellular bacterial pathogens. *Frontiers in Cellular and Infection Microbiology*, *3*(July), 24.

Ekchariyawat, P., Pudla, S., Limposuwan, K., Arjcharoen, S., Sirisinha, S., & Utaisincharoen, P. (2005). *Burkholderia pseudomallei*-induced expression of Suppressor of Cytokine Signaling 3 and Cytokine-Inducible Src Homolgy 2-Containing protein in mouse macrophages: A possible mechanism for suppression of the response to Gamma interferon stimulation. *Society*, *73*(11), 7332–7339.

Eskra, L., Mathison, A., & Splitter, G. (2003). Microarray analysis of mRNA levels from RAW264. 7 macrophages infected with *Brucella abortus*. *Infection and Immunity*, *71*(3), 1125–1133.

Essex-Lopresti, A. E., Boddey, J. A., Thomas, R., Smith, M. P., Hartley, M. G., Atkins, T., … Titball, R. W. (2005). A type IV Pilin, PilA, contributes to adherence of Burkholderia pseudomallei and virulence in vivo. *Infection and Immunity*, *73*(2), 1260–1264.

Etienne, W., Meyer, M. H., Peppers, J., & Meyer, R. A. (2004). Comparison of mRNA gene expression by RT-PCR and DNA microarray. *BioTechniques*, *36*(4), 618–626.

Fernandez-Prada, C. M., Hoover, D. L., Tall, B. D., Hartman, A. B., Kopelowitz, J., & Venkatesan, M. M. (2000). *Shigella flexneri* IpaH7.8 facilitates escape of virulent bacteria from the endocytic vacuoles of mouse and human macrophages. *Infection and Immunity*, *68*, 3608–3619.

Feterl, M., Govan, B. L., & Ketheesan, N. (2008). The effect of different *Burkholderia pseudomallei* isolates of varying levels of virulence on toll-like-receptor expression. *Transactions of the Royal Society of Tropical Medicine and Hygiene*, *102 Suppl* , S82–8.

Finethy, R., Jorgensen, I., Haldar, A. K., De Zoete, M. R., Strowig, T., Flavell, R. A., … Coers, J. (2015). Guanylate binding proteins enable rapid activation of canonical and noncanonical inflammasomes in *Chlamydia*-infected macrophages. *Infection and Immunity*, *83*(12), 4740–4749.

Freigang, S., Ampenberger, F., Weiss, A., Kanneganti, T.-D., Iwakura, Y., Hersberger, M., & Kopf, M. (2013). Fatty acid-induced mitochondrial uncoupling elicits inflammasome-independent IL-1α and sterile vascular inflammation in atherosclerosis. *Nature Immunology*, *14*(10), 1045–53.

Friedland, J. S., Suputtamongkol, Y., Remick, D. G., Chaowagul, W., Strieter, R. M., Kunkel, S. L., … Griffin, G. E. (1992). Prolonged elevation of interleukin-8 and interleukin-6 concentrations in plasma and of leukocyte interleukin-8 mRNA levels during septicemic and localized Pseudomonas pseudomallei infection. *Infection and Immunity*, *60*(6), 2402–2408.

Fujimuro, M., Sawada, H., & Yokosawa, H. (1994). Production and characterization of monoclonal antibodies specific to multi-ubiquitin chains of polyubiquitinated proteins. *FEBS Letters*, *349*(2), 173–180. 4

Gaffen, S. L. (2008). An overview of Il-17 function and signaling. *Cytokine*, *43*(3), 402–407.

Geerlings, S. E., & Hoepelman, a I. (1999). Immune dysfunction in patients with diabetes mellitus (DM). *FEMS Immunology and Medical Microbiology*, *26*(3-4), 259–265.

Geiss, G. K., Bumgarner, R. E., An, M. C., Agy, M. B., van 't Wout, a B., Hammersmark, E., … Katze, M. G. (2000). Large-scale monitoring of host cell gene expression during HIV-1 infection using cDNA microarrays. *Virology*, *266*(1), 8–16.

Gibson, B. A., & Kraus, W. L. (2012). New insights into the molecular and cellular functions of poly(ADP-ribose) and PARPs. *Nature Reviews Molecular Cell Biology*, *13*(7), 411–424.

Glass, M. B., Gee, J. E., Steigerwalt, A. G., Cavuoti, D., Barton, T., Hardy, R. D., … Wilkins, P. P. (2006). Pneumonia and septicemia caused by *Burkholderia thailandensis* in the United States. *Journal of Clinical Microbiology*, *44*(12), 4601–4604.

Godoy, D., Randle, G., Simpson, A. J., Aanensen, D. M., Pitt, T. L., Kinoshita, R., & Spratt, B. G. (2003). Multilocus sequence typing and evolutionary relationships among the causative agents of melioidosis and glanders, *Burkholderia pseudomallei* and *Burkholderia mallei. Journal of Clinical Microbiology*, *41*(5), 2068–2079. 3

Goley, E. D., Rodenbusch, S. E., Martin, A. C., & Welch, M. D. (2004). Critical conformational changes in the Arp2/3 complex are induced by nucleotide and nucleation promoting factor. *Molecular Cell*, *16*, 269–279.

Gong, L., Cullinane, M., Treerat, P., Ramm, G., Prescott, M., Adler, B., … Devenish, R. J. (2011). The *Burkholderia pseudomallei* type III secretion system and BopA are required for evasion of LC3-associated phagocytosis. *PLoS ONE*, *6*(3), e17852.

Gooding, M., Browne, L. P., Quinteiro, F. M., & Selwood, D. L. (2012). siRNA Delivery: From lipids to cell-penetrating peptides and their mimics. *Chemical Biology and Drug Design*, *80*(6), 787–809.

Green, D. R., & Levine, B. (2014). To be or not to be? How selective autophagy and cell death govern cell fate. *Cell*, *157*(1), 65–75.

Groß, O., Yazdi, A. S., Thomas, C. J., Masin, M., Heinz, L. X., Guarda, G., … Tschopp, J. (2012). Inflammasome activators induce interleukin-1α secretion via distinct pathways with differential requirement for the protease function of caspase-1. *Immunity*, *36*(3), 388–400.

Gurung, P., Subbarao Malireddi, R. K., Anand, P. K., Demon, D., Vande Walle, L., Liu, Z., … Kanneganti, T. D. (2012). Toll or interleukin-1 receptor (TIR) domain-containing adaptor inducing interferon-β (TRIF)-mediated caspase-11 protease production integrates toll-like receptor 4 (TLR4) protein- and Nlrp3 inflammasome-mediated host defense against enteropathogens. *Journal of Biological Chemistry*, *287*(41), 34474–34483.

Gutierrez, M. G., Master, S. S., Singh, S. B., Taylor, G. A., Colombo, M. I., & Deretic, V. (2004). Autophagy is a defense mechanism inhibiting BCG and *Mycobacterium tuberculosis* survival in infected macrophages. *Cell*, *119*(6), 753–766.

Hagar, J. A., Powell, D. A., Aachoui, Y., Ernst, R. K., & Miao, E. A. (2013). Cytoplasmic LPS activates caspase-11: implications in TLR4-independent endotoxic shock. *Science*, *341*(6151), 1250–1253.

Haglund, C. M., Choe, J. E., Skau, C. T., Kovar, D. R., & Welch, M. D. (2010). Rickettsia Sca2 is a bacterial formin-like mediator of actin-based motility. *Nature Cell Biology*, *12*(11), 1057–1063. 9

Hagmann, C. A., Herzner, a. M., Abdullah, Z., Zillinger, T., Jakobs, C., Schuberth, C., … Schlee, M. (2013). RIG-I detects triphosphorylated RNA of *Listeria monocytogenes* during infection in non-immune cells. *PLoS ONE*, *8*(4), 1–11.

Hall, P. A., & Russell, S. E. H. (2004). The pathobiology of the septin gene family, 489–505.

Hancock, G. E., Schaedler, R. W., & MacDonald, T. T. (1986). *Yersinia enterocolitica* infection in resistant and susceptible strains of mice. *Infection and Immunity*, *53*(1), 26–31.

Harley, V. S., Dance, D. A., McCrossan, M. V., & Drasar, B. S. (1998). An ultrastructural study of the phagocytosis of *Burkholderia pseudomallei*. *Microbios*, *94*(377), 35–45.

Heeb, S., Blumer, C., & Haas, D. (2002). Regulatory RNA as mediator in GacA / RsmA-dependent global control of exoproduct formation in *Pseudomonas* fluorescens CHA0. *Journal of Bacteriology*, *184*(4), 1046–56.

Henry, T., Brotcke, a, Weiss, D. S., Thompson, L. J., & Monack, D. M. (2007). Type I interferon signaling is required for activation of the inflammasome during *Francisella* infection. *J Exp Med*, *204*(5), 987–994.

Henry, T., Kirimanjeswara, G. S., Ruby, T., Jones, J. W., Perret, M., Ho, L., … Dennis, W. (2010). Type I Interferon signaling constrains IL-17A/F secretion by γδ T cells during bacterial infections. *J Immunol.*, *184*(7), 3755–3767.

Hiura, T. S., Kempiak, S. J., & Nel, a E. (1999). Activation of the human RANTES gene promoter in a macrophage cell line by lipopolysaccharide is dependent on stress-activated protein kinases and the IkappaB kinase

cascade: implications for exacerbation of allergic inflammation by environmental pollutant. *Clinical Immunology (Orlando, Fla.)*, *90*(3), 287–301.

Hodgson, K. A., Govan, B. L., Walduck, A. K., Ketheesan, N., & Morris, J. L. (2013). Impaired early cytokine responses at the site of infection in a murine model of type 2 diabetes and melioidosis comorbidity. *Infection and Immunity*, *81*(2), 470–477.

Hodgson, K. A., Morris, J. L., Feterl, M. L., Govan, B. L., & Ketheesan, N. (2011). Altered macrophage function is associated with severe *Burkholderia pseudomallei* infection in a murine model of type 2 diabetes. *Microbes and Infection*, *13*(14-15), 1177–1184.

Holt, M. (2001). Cell motility: proline-rich proteins promote protrusions. *Trends in Cell Biology*, *11*(1), 38–46.

Hoppe, I., Brenneke, B., Rohde, M., Kreft, A., Ußler, S. H., Reganzerowski, A., & Steinmetz, A. I. (1999). Characterization of a murine model of melioidosis: comparison of different strains of mice. *Infection and Immunity*, *67*(6), 2891–2900.

Horiuchi, M., Itoh, A., Pleasure, D., Ozato, K., & Itoh, T. (2011). Cooperative contributions of Interferon regulatory factor 1 (IRF1) and IRF8 to interferon-γ-mediated cytotoxic effects on oligodendroglial progenitor cells. *Journal of Neuroinflammation*, *8*(8), 1–16.

Howe, C., Sampath, A., & Spotnitz, M. (1971). The *pseudomallei* group: a review. *The Journal of Infectious Diseases*, *124*(6), 598–606.

Huett, A., Ng, A., Cao, Z., Kuballa, P., Komatsu, M., Daly, M. J., … Xavier, R. J. (2009). A novel hybrid yeast-human network analysis reveals an essential role for FNBP1L in antibacterial autophagy. *Journal of Immunology (Baltimore, Md. : 1950)*, *182*(8), 4917–4930.

Hunter, T. (2000). Signaling--2000 and beyond. *Cell*, *100*(1), 113–127.

Inglis, T. J. J. (2010). The treatment of melioidosis. *Pharmaceuticals*, *3*, 1296–1303.

Inglis, T. J. J., Garrow, S. C., Henderson, M., Clair, A., Sampson, J., O'Reilly, L., & Cameron, B. (2000). *Burkholderia pseudomallei* traced to water treatment plant in Australia. *Emerging Infectious Diseases*, *6*(1), 56–59.

Inglis, T. J. J., Mee, B. J., & Chang, B. J. (2001). The environmental microbiology of melioidosis. *Reviews in Medical Microbiology*, *12*(1), 13–20.

Inglis, T. J. J., Robertson, T., Woods, D. E., Dutton, N., & Chang, B. J. (2003). Flagellum-mediated adhesion by *Burkholderia pseudomallei* precedes invasion of Acanthamoeba astronyxis. *Infection and Immunity*, *71*(4), 2280–2282.

Irving, A. T., Mimuro, H., Kufer, T. A., Lo, C., Wheeler, R., Turner, L. J., … Kaparakis-Liaskos, M. (2014). The immune receptor NOD1 and kinase RIP2 interact with bacterial peptidoglycan on early endosomes to promote autophagy and inflammatory signaling. *Cell Host and Microbe*, *15*(5), 623–635.

Ishikawa, H., Ma, Z., & Barber, G. N. (2009). STING regulates intracellular DNA-mediated, type I interferon-dependent innate immunity. *Nature*, *461*(7265), 788–92.

Iwata, H., Goettsch, C., Sharma, A., Ricchiuto, P., Goh, W., Halu, A., … Aikawa, M. (2016). PARP9 and PARP14 cross-regulate macrophage activation via STAT1 ADP-ribosylation. *Nat Communications*, *7*(12849), 1–19.

Jarvelainen, H. A., Galmiche, A., & Zychlinsky, A. (2003). Caspase-1 activation by *Salmonella*. *Trends in Cell Biology*, *13*(4), 204–209.

Jehl, S. P., Nogueira, C. V., Zhang, X., & Starnbach, M. N. (2012). IFN-Gamma inhibits the cytosolic replication of *Shigella flexneri* via the cytoplasmic RNA Sensor RIG-I. *PLoS Pathogens*, *8*(8), e1002809.

Jenner, R. G., & Young, R. a. (2005). Insights into host responses against pathogens from transcriptional profiling. *Nature Reviews. Microbiology*, *3*(4), 281–294.

Jensen, K., Anderson, J. a., & Glass, E. J. (2014). Comparison of small interfering RNA (siRNA) delivery into bovine monocyte-derived macrophages by transfection and electroporation. *Veterinary Immunology and Immunopathology*, *158*(3-4), 224–232.

Jiang, X., Shen, C., Yu, H., Karunakaran, K. P., & Brunham, R. C. (2010). Differences in innate immune responses correlate with differences in murine susceptibility to *Chlamydia muridarum* pulmonary infection. *Immunology*, *129*(4), 556–566.

Jitprasutwit, N., Zainal-Abidin, N., Vander Broek, C., Kurian, D., Korbsrisate, S., Stevens, M. P., & Stevens, J. M. (2016). Identification of Candidate Host Cell Factors Required for Actin-Based Motility of *Burkholderia pseudomallei*. *Journal of Proteome Research*, *15*(12), 4675–4685.

Jo, E. K., Yuk, J. M., Shin, D. M., & Sasakawa, C. (2013). Roles of autophagy in elimination of intracellular bacterial pathogens. *Frontiers in Immunology*, *4*(97), 1–9.

Jones, A. L., Beveridge, T. J., & Woods, D. E. (1996). Intracellular survival of Burkholderia pseudomallei. *Infection and Immunity*, *64*(3), 782–790.

Jones, S. A. (2005). Directing transition from innate to acquired immunity: Defining a role for IL-6. *The Journal of Immunology*, *175*(6), 3463–3468.

Jovanovic, D. V, Di Battista, J. A., Martel-Pelletier, J., Jolicoeur, F. C., He, Y., Zhang, M., … Pelletier, J. P. (1998). IL-17 stimulates the production and expression of proinflammatory cytokines, IL-beta and TNF-alpha, by human macrophages. *Journal of Immunology (Baltimore, Md. : 1950)*, *160*(7), 3513–21.

Kang, S.-J., Wang, S., Hara, H., Peterson, E. P., Namura, S., Amin-Hanjani, S., … Yuan, J. (2000). Dual role of caspase-11 in mediating activation of caspase-1 and caspase-3 under pathological conditions. *The Journal of Cell Biology*, *149*(3), 613–622.

Karras, G. I., Kustatscher, G., Buhecha, H. R., Allen, M. D., Pugieux, C., Sait, F., … Ladurner, A. G. (2005). The macro domain is an ADP-ribose binding module. *The EMBO Journal*, *24*(11), 1911–20.

Katz, J., Zhang, P., Martin, M., Vogel, S. N., Michalek, S. M., & Mmun, I. N. I. (2006). Toll-Like Receptor 2 Is required for inflammatory responses to *Francisella tularensis* LVS, *74*(5), 2809–2816.

Kaur, G., & Dufour, J. M. (2012). Cell lines: Valuable tools or useless artifacts. *Spermatogenesis*, *2*(1), 1–5.

Kawai, T., Adachi, O., Ogawa, T., Takeda, K., & Akira, S. (1999). Unresponsiveness of MyD88-deficient mice to endotoxin. *Immunity*, *11*(1), 115–122.

Kawai, T., & Akira, S. (2010). The role of pattern-recognition receptors in innate immunity: update on Toll-like receptors. *Nature Immunology*, *11*(5), 373–84.

Kawai, T., & Akira, S. (2011). Toll-like Receptors and their crosstalk with other innate receptors in infection and immunity. *Immunity*, *34*(5), 637–650.

Kayagaki, N., Warming, S., Lamkanfi, M., Walle, L. Vande, Louie, S., Dong, J., … Dixit, V. M. (2011). Non-canonical inflammasome activation targets caspase-11. *Nature*, *479*(7371), 117–121.

Kayagaki, N., Wong, M. T., Stowe, I. B., Ramani, S. R., Gonzalez, L. C., Akashi-takamura, S., … Dixit, V. M. (2013). Noncanonical inflammasome activation by intracellular LPS independent of TLR4. *Science*, *341*, 1246–1249.

Kazazian, N. H. (2014). NLRP3 inflammasome activation by crystal structures. *BioSciences Master Reviews*, 1–8.

Kespichayawattana, W., Intachote, P., Utaisincharoen, P., & Sirisinha, S. (2004). Virulent *Burkholderia pseudomallei* is more efficient than avirulent *Burkholderia thailandensis* in invasion of and adherence to cultured human epithelial cells. *Microbial Pathogenesis*, *36*(5), 287–92.

Kespichayawattana, W., Rattanachetkul, S., Wanun, T., Utaisincharoen, P., & Sirisinha, S. (2000). *Burkholderia pseudomallei* induces cell fusion and actin-associated membrane protrusion: A possible mechanism for cell-to-cell spreading. *Infection and Immunity*, *68*(9), 5377–5384.

Kihara, A., Noda, T., Ishihara, N., & Ohsumi, Y. (2001). Two distinct Vps34 phosphatidylinositol 3-kinase complexes function in autophagy and carboxypeptidase y sorting in Saccharomyces cerevisiae. *Journal of Cell Biology*, *152*(3), 519–530.

Kim, B.-H., Chee, J. D., Bradfield, C. J., Park, E.-S., Kumar, P., & MacMicking, J. D. (2016). Interferon-induced guanylate-binding proteins in inflammasome activation and host defense. *Nature Immunology*, *17*(5), 481–489.

Klionsky, D. J., Abdelmohsen, K., Abe, A., Abedin, J., Abeliovich, H., Arozena, A. A., … Besteiro, S. (2015). Guidelines for the use and interpretation of assays for monitoring autophagy (3rd edition). *Autophagy*, *8627*, 1–222.

Kozera, B., & Rapacz, M. (2013). Reference genes in real-time PCR. *Journal of Applied Genetics*, *54*(4), 391–406.

Kraft, C., Peter, M., & Hofmann, K. (2010). Selective autophagy: ubiquitin-mediated recognition and beyond. *Nature Cell Biology*, *12*(9), 836–841.

Kruse, A., Kirchner, H., Zawatzky, R., & Domke-Opitz, I. (1989). In vitro development of bone-marrow-derived macrophages. Influence of mouse genotype on response to colony-stimulating factors and autocrine interferon induction. *Scandinavian Journal of Immunology*, *30*, 731–740.

Kulsantiwong, P., Pudla, M., Boondit, J., Wikraiphat, C., Dunachie, S. J., Chantratita, N., & Utaisincharoen, P. (2016). *Burkholderia pseudomallei* induces IL-23 production in primary human monocytes. *Medical Microbiology and Immunology*, *205*(3), 255–260.

Kunakorn, M., Jayanetra, P., & Tanphaichitra, D. (1991). Man-to-man transmission of melioidosis. *The Lancet*, *337*(8752), 1290–1291.

Laroux, F. S., Romero, X., Wetzler, L., Engel, P., & Terhorst, C. (2005). Gram-Negative bacteria NADPH Oxidase function and killing of cutting edge: MyD88 controls phagocyte cutting edge: MyD88 controls phagocyte NADPH oxidase function and killing of Gram-Negative bacteria 1. *J Immunol References*, *1755596*(9), 5596–5600.

Latz, E., Ts, X., & Stutz, A. (2013). Activation and regulation of the inflammasomes. *Nature Reviews Immunology*, *13*(6), 1–31.

Lauw, F. N., Simpson, a J., Prins, J. M., Smith, M. D., Kurimoto, M., van Deventer, S. J., … van der Poll, T. (1999). Elevated plasma concentrations of interferon (IFN)-gamma and the IFN-gamma-inducing cytokines interleukin (IL)-18, IL-12, and IL-15 in severe melioidosis. *The Journal of Infectious Diseases*, *180*(II), 1878–1885.

Leakey, A. K., Ulett, G. C., Hirst, R. G., & Leakey, A. K. (1998). BALB/c and C57Bl/6 mice infected with virulent *Burkholderia pseudomallei* provide contrasting animal models for the acute and chronic forms of human melioidosis. *Microbial Pathogenesis*, *24*, 269–275.

Lee, S.-H., Wong, R.-R., Chin, C.-Y., Lim, T.-Y., Eng, S.-A., Kong, C., … Nathan, S. (2013). *Burkholderia pseudomallei* suppresses *Caenorhabditis elegans* immunity by specific degradation of a GATA transcription factor. *Proceedings of the National Academy of Sciences of the United States of America*, *110*(37), 15067–72.

Lee, Y. H., Chen, Y., Ouyang, X., & Gan, Y.-H. (2010). Identification of tomato plant as a novel host model for Burkholderia pseudomallei. *BMC Microbiology*, *10*, 28–38.

Lertpatanasuwan, N., Sermsri, K., Petkaseam, A., Trakulsomboon, S., Thamlikitkul, V., & Suputtamongkol, Y. (1999). Arabinose-positive *Burkholderia pseudomallei* infection in humans: case report. *Clinical Infectious Diseases*, *28*, 928–929.

Leung, Y., Ally, S., & Goldberg, M. B. (2008). Bacterial actin assembly requires Toca-1 to relieve N-WASP autoinhibition. *Cell Host Microbiology*, *17*(1), 39–47.

Levine, B., & Kroemer, G. (2008). Autophagy in the Pathogenesis of Disease. *Cell*, *132*, 27–42.

Limmathurotsakul, D., Golding, N., Dance, D. A. B., Messina, J. P., Pigott, D. M., Moyes, C. L., … Hay, S. I. (2016). Predicted global distribution of *Burkholderia pseudomallei* and burden of melioidosis. *Nature Microbiology*, *1*(January), 1–5.

Lin, Y.-T., Wang, F.-D., Wu, P.-F., & Fung, C.-P. (2013). *Klebsiella pneumoniae* liver abscess in diabetic patients: association of glycemic control with the clinical characteristics. *BMC Infectious Diseases*, *13*(1), 56.

Lippmann, J., Rothenburg, S., Deigendesch, N., Eitel, J., Meixenberger, K., Van Laak, V., … Opitz, B. (2008). IFN-beta responses induced by intracellular bacteria or cytosolic DNA in different human cells do not require ZBP1 (DLM-1/DAI). *Cellular Microbiology*, *10*(12), 2579–2588.

Liu, B., Koo, G. C., Yap, E. H., Chua, K. L., & Gan, Y. (2002). Model of differential susceptibility to mucosal *Burkholderia pseudomallei* infection model of differential susceptibility to mucosal *Burkholderia pseudomallei* infection. *Infection and Immunity*, *70*(2), 504–511.

Liu, T., Nishimura, H., Matsuguchi, T., & Yoshikai, Y. (2000). Differences in interleukin-12 and -15 production by dendritic cells at the early stage of *Listeria monocytogenes* infection between BALB/c and C57 BL/6 mice. *Cellular Immunology*, *202*(1), 31–40.

Loiarro, M., Sette, C., Gallo, G., Ciacci, A., Fantó, N., Mastroianni, D., … Ruggiero, V. (2005). Peptide-mediated interference of TIR domain dimerization in MyD88 inhibits interleukin-1-dependent activation of NF-κB. *Journal of Biological Chemistry*, *280*(16), 15809–15814.

Lowry, M. a R., & Goldberg, J. I. (1998). Induction of nitric oxide (NO) synthesis in murine macrophages requires potassium. *Sciences-New York*, *4*, 597–603.

Maegraith, B. G., & Leithead, C. S. (1964). Melioidosis: A case-report. *The Lancet*, *283*(7338), 862–863.

Magee, D. a., Taraktsoglou, M., Killick, K. E., Nalpas, N. C., Browne, J. a., Park, S. D. E., … MacHugh, D. E. (2012). Global gene expression and systems biology analysis of bovine monocyte-derived macrophages in response to *in vitro* challenge with *Mycobacterium bovis*. *PLoS ONE*, *7*(2).

Mahla, R. S., Reddy, M. C., Vijaya Raghava Prasad, D., & Kumar, H. (2013). Sweeten PAMPs: Role of sugar complexed PAMPs in innate immunity and vaccine biology. *Frontiers in Immunology*, *4*(SEP), 1–16.

Maltez, V. I., & Miao, E. a. (2016). Reassessing the evolutionary importance of inflammasomes. *Journal of Immunology*, *196*(3), 956–962.

Man, S. M., & Kanneganti, T.-D. (2015). Regulation of inflammasome activation. *Immunological Reviews*, *265*(1), 6–21.

Mancuso, G., Midiri, a., Biondo, C., Beninati, C., Zummo, S., Galbo, R., … Teti, G. (2007). Type I IFN signaling Is crucial for host resistance against different species of pathogenic bacteria. *The Journal of Immunology*, *178*(5), 3126–3133.

Marathe, S. a., Sen, M., Dasgupta, I., & Chakravortty, D. (2012). Differential modulation of intracellular survival of cytosolic and vacuolar pathogens by curcumin. *Antimicrobial Agents and Chemotherapy*, *56*(11), 5555–5567.

Martinez, F. O., & Gordon, S. (2014). The M1 and M2 paradigm of macrophage activation: time for reassessment. *F1000Prime Reports*, *6*(13).

Matsuura, M., Kawahara, K., Ezaki, T., & Nakano, M. (1996). Biological activities of lipopolysaccharide of *Burkholderia (Pseudomonas) pseudomallei. FEMS Microbiology Letters*, *137*(1), 79–83.

Matussek, A., Strindhall, J., Stark, L., Rohde, M., Geffers, R., Buer, J., … Löfgren, S. (2005). Infection of human endothelial cells with *Staphylococcus aureus* induces transcription of genes encoding an innate immunity response. *Scandinavian Journal of Immunology*, *61*(6), 536–544.

Mays, E. E., & Ricketss, E. A. (1975). Melioidosis: Recrudescence associated with Bronchonic Carcinoma twenty-six years following initial geographic exposure. *CHEST*, *68*(2), 261–263.

McCormick, J. B., Sexton, D. J., McMurray, J. G., Carey, E., Hayes, P., & Feldman, R. A. (1975). Human-to-human transmission of *Burkholderia pseudomallei*. *Annuals of Internal Medicine*, *83*, 512–513.

Mehrpour, M., Esclatine, A., Beau, I., & Codogno, P. (2010). Overview of macroautophagy regulation in mammalian cells. *Cell Research*, *20*(7), 748–62.

Meunier, E., Dick, M. S., Dreier, R. F., Schürmann, N., Kenzelmann Broz, D., Warming, S., … Broz, P. (2014). Caspase-11 activation requires lysis of pathogen-containing vacuoles by IFN-induced GTPases. *Nature*, *509*(7500), 366–70.

Miao, E. A., Leaf, I. A., Treuting, P. M., Mao, D. P., Dors, M., Sarkar, A., … Aderem, A. (2010). Caspase-1-induced pyroptosis is an innate immune effector mechanism against intracellular bacteria. *Nat Immunol*, *11*(12), 1136–1142.

Mishra, B. B., Li, Q., Steichen, A. L., Binstock, B. J., Metzger, D. W., Teale, J. M., & Sharma, J. (2013). Galectin-3 functions as an alarmin : Pathogenic role for sepsis development in murine respiratory tularemia, *8*(3), 1–12.

Mizushima, N., & Yoshimori, T. (2007). How to Interpret LC3 Immunoblotting. *Autophagy*, *3*(6), 542–545.

Mizushima, N., Yoshimori, T., & Levine, B. (2010). Methods in mammalian autophagy research. *Cell*, *140*, 313–326.

Monroe, K. M., McWhirter, S. M., & Vance, R. E. (2009). Identification of host cytosolic sensors and bacterial factors regulating the type I interferon response to *Legionella pneumophila*. *PLoS Pathogens*, *5*(11).

Morey, J. S., Ryan, J. C., & Van Dolah, F. M. (2006). Microarray validation: factors influencing correlation between oligonucleotide microarrays and real-time PCR. *Biological Procedures Online*, *8*(1), 175–93.

Mostowy, S., Bonazzi, M., Hamon, M. A., Tham, T. N., Mallet, A., Lelek, M., … Cossart, P. (2010). Entrapment of intracytosolic bacteria by septin cage-like structures. *Cell Host and Microbe*, *8*, 433–444.

Muangsombut, V., Suparak, S., Pumirat, P., Damnin, S., Vattanaviboon, P., Thongboonkerd, V., & Korbsrisate, S. (2008). Inactivation of *Burkholderia pseudomallei bsaQ* results in decreased invasion efficiency and delayed escape of bacteria from endocytic vesicles. *Archives of Microbiology*, *190*, 623–631.

Mukherjee, S., Belbin, T. J., Spray, D. C., Iacobas, D. A., Weiss, L. M., Kitsis, R. N., … Tanowitz, H. B. (2003). Microarray analysis of changes in gene expression in a murine model of chronic chagasic cardiomyopathy. *Parasitology Research*, *91*(3), 187–196.

Mukherjee, S., Keitany, G., Li, Y., Wang, Y., Ball, H. L., Goldsmith, El. J., & Orth, K. (2006). *Yersinia* YopJ acetylates and inhibits kinase activation by blocking phosphorylation. *Science*, *312*(5777), 1211–1214.

Murshid, A., Gong, J., Prince, T., Borges, T. J., & Calderwood, S. K. (2015). Scavenger receptor SREC-I mediated entry of TLR4 into lipid microdomains and triggered inflammatory cytokine release in RAW 2647 cells upon LPS activation. *PLoS ONE*, *10*(4), 1-24.

Myers, J. T., Tsang, A. W., & Swanson, J. A. (2003). Localized reactive oxygen and nitrogen intermediates inhibit escape of *Listeria monocytogenes* from vacuoles in activated macrophages. *Journal of Immunology*, *171*(10), 5447–5453.

Nagata, S. (1997). Apoptosis by death factor. *Cell*, *88*(3), 355–365.

Nakagawa, I., Amano, A., Mizushima, N., Yamamoto, A., Yamaguchi, H., Kamimoto, T., … Yoshimori, T. (2004). Autophagy defends cells against invading group A Streptococcus. *Science (New York, N.Y.)*, *306*(5698), 1037–40.

Nakatogawa, H., Suzuki, K., Kamada, Y., & Ohsumi, Y. (2009). Dynamics and diversity in autophagy mechanisms: lessons from yeast. *Nature Reviews. Molecular Cell Biology*, *10*, 458–467.

Nelson, M., Prior, J. L., Lever, M. S., Jones, H. E., Atkins, T. P., & Titball, R. W. (2004). Evaluation of lipopolysaccharide and capsular polysaccharide as subunit vaccines against experimental melioidosis. *Journal of Medical Microbiology*, *53*(12), 1177–1182.

Netea, M. G., Simon, A., Van De Veerdonk, F., Kullberg, B. J., Van Der Meer, J. W. M., & Joosten, L. A. B. (2010). IL-1beta processing in host defense: Beyond the inflammasomes. *PLoS Pathogens*, *6*(2), 1–9.

Ng, H. H., Frantz, C. E., Rausch, L., Fairchild, D. C., Shimon, J., Riccio, E., … Mirsalis, J. C. (2005). Gene expression profiling of mouse host response to *Listeria monocytogenes* infection. *Genomics*, *86*(6), 657–667.

Ngauy, V., Lemeshev, Y., Sadkowski, L., & Crawford, G. (2005). Cutaneous melioidosis in a man who was taken as a prisoner of war by the Japanese during World War II. *Journal of Clinical Microbiology*, *43*(2), 970–972.

Nguyen, D. T., de Witte, L., Ludlow, M., Yüksel, S., Wiesmüller, K. H., Geijtenbeek, T. B. H., … de Swart, R. L. (2010). The synthetic bacterial lipopeptide Pam3CSK4 modulates respiratory syncytial virus infection independent of TLR activation. *PLoS Pathogens*, *6*(8), 43–44.

Nikolov, D., Hu, S., Lin, J., Gasch, A., Hoffmann, A., Horikoshi, M., Chua.N., Roeder, G., Burley, S. (1992). A novel heterodimeric cysteine protease is required for interleukin-1B processing in monocytes. *Nature*, *360*, 40–46.

Novem, V., Shui, G., Wang, D., Bendt, A. K., Siew, H. S., Liu, Y., … Tan, G. (2009). Structural and biological diversity of lipopolysaccharides from *Burkholderia pseudomallei* and *Burkholderia thailandensis*. *Clinical and Vaccine Immunology*, *16*(10), 1420–1428.

Novikov, A., Cardone, M., Thompson, R., Shenderov, K., Kirschman, K. D., Mayer-Barber, K. D., … Feng, C. G. (2011). *Mycobacterium tuberculosis* triggers host type I IFN signaling to regulate IL-1β production in human macrophages. *Journal of Immunology (Baltimore, Md. : 1950)*, *187*(5), 2540–7.

O'Connell, R. M., Saha, S. K., Vaidya, S. a, Bruhn, K. W., Miranda, G. a, Zarnegar, B., … Cheng, G. (2004). Type I interferon production enhances susceptibility to *Listeria monocytogenes* infection. *J.Exp.Med.*, *200*(0022-1007), 437–445.

O'Neill, L. a J., & Bowie, A. G. (2007). The family of five: TIR-domain-containing adaptors in Toll-like receptor signalling. *Nature Reviews. Immunology*, *7*(5), 353–64.

Oddo, M., Renno, T., Attinger, a, Bakker, T., MacDonald, H. R., & Meylan, P. R. (1998). Fas ligand-induced apoptosis of infected human macrophages reduces the viability of intracellular *Mycobacterium tuberculosis*. *Journal of Immunology (Baltimore, Md. : 1950)*, *160*(11), 5448–54.

Oficjalska, K., Raverdeau, M., Aviello, G., Wade, S. C., Hickey, A., Sheehan, K. M., … Creagh, E. M. (2015). Protective role for caspase-11 during acute experimental murine colitis. *Journal of Immunology (Baltimore, Md. : 1950)*, *194*(3), 1252–60.

Ogawa, M., Yoshimori, T., Suzuki, T., Sagara, H., Mizushima, N., & Sasakawa, C. (2005). Escape of intracellular *Shigella* from autophagy. *SCIENCE*, *307*, 727–731.

Ogura, Y., Inohara, N., Benito, A., Chen, F. F., Yamaoka, S., & Núñez, G. (2001). Nod2, a Nod1/Apaf-1 Family member that Is restricted to monocytes and activates NF-kappaB. *Journal of Biological Chemistry*, *276*(7), 4812–4818.

Ooi, W. F., Ong, C., Nandi, T., Kreisberg, J. F., Chua, H. H., Sun, G., … Tan, P. (2013). The condition-dependent transcriptional landscape of *Burkholderia pseudomallei. PLoS Genetics*, *9*(9), e1003795.

Parameswaran, N., & Patial, S. (2010). Tumor necrosis factor-α signaling in macrophages. *Critical Reviews in Eukaryotic Gene Expression*, *20*(2), 87–103.

Patel, N., Conejero, L., De Reynal, M., Easton, A., Bancroft, G. J., & Titball, R. W. (2011). Development of vaccines against *Burkholderia pseudomallei. Frontiers in Microbiology*, *2*(198).

Peng, J., Yuan, Q., Lin, B., Panneerselvam, P., Wang, X., Luan, X. L., … Ding, J. L. (2010). SARM inhibits both TRIF- and MyD88-mediated AP-1 activation. *European Journal of Immunology*, *40*(6), 1738–1747.

Perrin, A. J., Jiang, X., Birmingham, C. L., So, N. S. Y., & Brumell, J. H. (2004). Recognition of bacteria in the cytosol of mammalian cells by the ubiquitin system. *Current Biology*, *14*, 806–811.

Perry, A. K., Chen, G., Zheng, D., Tang, H., & Cheng, G. (2005). The host type I interferon response to viral and bacterial infections. *Cell Research*, *15*(6), 407–422.

Perumal Samy, R., Manikandan, J., Pachiappan, A., Ooi, E. E., Aw, L. T., Stiles, B. G., … Chow, V. T. (2015). Gene microarray analyses of *Daboia russelli russelli* Daboiatoxin treatment of THP-1 human macrophages Infected with *Burkholderia pseudomallei. Current Molecular Medicine*, *15*(10), 961–974.

Platanias, L. C. (2005). Mechanisms of type-I- and type-II-interferon-mediated signalling. *Nature Reviews. Immunology*, *5*(5), 375–86.

Plumlee, C. R., Lee, C., Beg, A. a., Decker, T., Shuman, H. a., & Schindler, C. (2009). Interferons direct an effective innate response to *Legionella pneumophila* infection. *Journal of Biological Chemistry*, *284*(44), 30058–30066.

Poltorak, A., He, X., Smirnova, I., Liu, M.-Y., Van Huffell, C., Du, X., … Beutler, B. (1998). Defective LPS signaling in C3H/HeJ and C57BL/10ScCr mice: mutations in Tlr4 gene. *Science*, *282*(5396), 2085–2088.

Pruksachartvuthi, S., Aswapokee, N., & Thankerngpol, K. (1990). Survival of *Pseudomonas pseudomallei* in human phagocytes. *Journal of Medical Microbiology*, *31*, 109–114.

Pumirat, P., Broek, C. Vander, Juntawieng, N., Muangsombut, V., Kiratisin, P., Pattanapanyasat, K., … Korbsrisate, S. (2014). Analysis of the prevalence, secretion and function of a cell cycle-inhibiting factor in the melioidosis pathogen *Burkholderia pseudomallei. PLoS ONE, 9*(5): e96298.

Puthucheary, S. D., & Nathan, S. A. (2006). Comparison by electron microscopy of intracellular events and survival of *Burkholderia pseudomallei* in monocytes from normal subjects and patients with melioidosis. *Singapore Medical Journal*, *47*(8), 697–703.

Py, B. F., Lipinski, M. M., & Yuan, J. (2007). Autophagy limits *Listeria monocytogenes* intracellular growth in the early phase of primary infection. *Autophagy*, *3*(2), 117–125.

Rainbow, L., Hart, C. A., & Winstanley, C. (2002). Distribution of type III secretion gene clusters in *Burkholderia pseudomallei, B. thailandensis* and *B. mallei. Journal of Medical Microbiology*, *51*, 374–384.

Rajeevan, M. S., Ranamukhaarachchi, D. G., Vernon, S. D., & Unger, E. R. (2001). Use of real-time quantitative PCR to validate the results of cDNA array and differential display PCR technologies. *Methods (San Diego, Calif.)*, *25*(4), 443–51.

Randow, F., MacMicking, J. D., & James, L. C. (2013). Cellular self-defense: How cell-autonomous immunity protects against pathogens. *Science*, *340*(6133-6145).

Rasmussen, S. B., Horan, K. A., Holm, C. K., Stranks, A. J., Mettenleiter, T. C., Simon, K. A., … Paludan, S. R. (2011). Activation of autophagy by alpha-herpesviruses in myeloid cells is mediated by cytoplasmic viral DNA through a mechanism dependent on STING. *Journal of Immunology*, *187*(10), 5268–5276.

Rathinam, V. a K., Vanaja, S. K., Waggoner, L., Sokolovska, A., Becker, C., Stuart, L. M., … Fitzgerald, K. a. (2012a). TRIF licenses Caspase-11-dependent NLRP3 inflammasome activation by Gram-Negative bacteria. *Cell*, *150*(3), 606–619.

Raupach, B., Peuschel, S. K., Monack, D. M., & Zychlinsky, A. (2006). Caspase-1-mediated activation of interleukin-1β (IL-1β) and IL-18 contributes to innate immune defenses against *Salmonella enterica* serovar *Typhimurium* infection. *Infection and Immunity*, *74*(8), 4922–4926.

Rayamajhi, M., Humann, J., Penheiter, K., Andreasen, K., & Lenz, L. L. (2010). Induction of IFN-alphabeta enables *Listeria monocytogenes* to suppress macrophage activation by IFN-gamma. *The Journal of Experimental Medicine*, *207*(2), 327–337.

Raychaudhuri, S., Stuart, J. M., & Altman, R. B. (2000). Principal components analysis to summarize microarray experiments: application to sporulation time series. *Pacific Symposium on Biocomputing. Pacific Symposium on Biocomputing*, 455–66.

Reikine, S., Nguyen, J. B., & Modis, Y. (2014). Pattern recognition and signaling mechanisms of RIG-I and MDA5. *Frontiers in Immunology*, *5*, 1–7.

Reynolds, A., Anderson, E. M., Vermeulen, A., Fedorov, Y., Robinson, K., Leake, D., … Khvorova, A. (2006). Induction of the interferon response by siRNA is cell type − and duplex length − dependent Induction of the interferon response by siRNA is cell type – and duplex length – dependent. *RNA*, *12*, 988–993.

Rinchai, D., Riyapa, D., Buddhisa, S., Utispan, K., Titball, R. W., Stevens, M. P., … Lertmemongkolchai, G. (2015). Macroautophagy is essential for killing of intracellular *Burkholderia pseudomallei* in human neutrophils. *Autophagy*, *11*(5), 748–755.

Riyapa, D., Buddhisa, S., Korbsrisate, S., Cuccui, J., Wren, B. W., Stevens, M. P., … Lertmemongkolchai, G. (2012). Neutrophil extracellular traps exhibit antibacterial activity against *Burkholderia pseudomallei* and are influenced by bacterial and host factors. *Infection and Immunity*, *80*(11), 3921–3929.

Rogers, L. D., Brown, N. F., Fang, Y., Pelech, S., & Foster, L. J. (2011). Phosphoproteomic analysis of *Salmonella*-infected cells identifies key kinase regulators and SopB-dependent host phosphorylation events. *Science Signaling*, *4*(191), rs9–rs9.

Rogul, M., Brendle, J. J., Haapala, D. K., & Alexander, A. D. (1970). Nucleic acid similarities among *Pseudomonas pseudomallei, Pseudomonas multivorans*, and *Actinobacillus mallei*. *Journal of Bacteriology*, *101*(3), 827–835.

Romao, S., & Munz, C. (2014). LC3-associated phagocytosis. *Autophagy*, *10*(3), 526–528.

Roque, S., Nobrega, C., Appelberg, R., & Correia-Neves, M. (2007). IL-10 underlies distinct susceptibility of BALB/c and C57BL/6 mice to *Mycobacterium avium* infection and influences efficacy of antibiotic therapy. *Journal of Imunology*, *178*(12), 8028–8035.

Rupper, A. C., & Cardelli, J. A. (2008). Induction of guanylate binding protein 5 by gamma interferon increases susceptibility to *Salmonella enterica* serovar Typhimurium-induced pyroptosis in RAW 264.7 cells. *Infection and Immunity*, *76*(6), 2304–2315.

Saijo, S., Ikeda, S., Yamabe, K., Kakuta, S., Ishigame, H., Akitsu, A., … Iwakura, Y. (2010). Dectin-2 recognition of α-mannans and induction of Th17 cell differentiation is essential for host defense against candida albicans. *Immunity*, *32*(5), 681–691.

Santanirand, P., Harley, V. S., Dance, D. a B., Drasar, B. S., & Bancroft, G. J. (1999). Obligatory role of gamma interferon for host survival in a murine model of infection with *Burkholderia pseudomallei*. *Infection and Immunity*, *67*(7), 3593–3600.

Sarovich, D. S., Ward, L., Price, E. P., Mayo, M., Pitman, M. C., Baird, R. W., & Currie, B. J. (2014). Recurrent melioidosis in the darwin prospective melioidosis study: Improving therapies mean that relapse cases are now rare. *Journal of Clinical Microbiology*, *52*(2), 650–653.

Sato, S., Ouellet, N., Pelletier, I., Rancourt, A., & Bergeron, M. G. (2002). Role of galectin-3 as an adhesion molecule for neutrophil extravasation during *Streptococcal pneumonia. Journal of Immunology*, *168*, 1813–1822.

Schattgen, S. A., & Fitzgerald, K. A. (2011). The PYHIN protein family as mediators of host defenses. *Immunological Reviews*, *243*(1), 109–118.

Schmutz, C., Ahrné, E., Kasper, C. a., Tschon, T., Sorg, I., Dreier, R. F., … Arrieumerlou, C. (2013). Systems-level overview of host protein phosphorylation during *Shigella flexneri* infection revealed by phosphoproteomics. *Molecular & Cellular Proteomics*, *12*(10), 2952–2968.

Schreiber, V., Dantzer, F., Ame, J.-C., & de Murcia, G. (2006). Poly(ADP-ribose): novel functions for an old molecule. *Nature Reviews. Molecular Cell Biology*, *7*(7), 517–28.

Schwarz, S., Singh, P., Robertson, J. D., LeRoux, M., Skerrett, S. J., Goodlett, D. R., … Mougous, J. D. (2014). VgrG-5 is a *Burkholderia* type VI secretion system-exported protein required for multinucleated giant cell formation and virulence. *Infection and Immunity*, *82*(4), 1445–1452.

Schwarz, S., West, T. E., Boyer, F., Chiang, W. C., Carl, M. A., Hood, R. D., … Mougous, J. D. (2010). *Burkholderia* type vi secretion systems have distinct roles in eukaryotic and bacterial cell interactions. *PLoS Pathogens*, *6*(8), 77–78.

Shapira, M., Hamlin, B. J., Rong, J., Chen, K., Ronen, M., & Tan, M.-W. (2006). A conserved role for a GATA transcription factor in regulating epithelial innate immune responses. *Proceedings of the National Academy of Sciences of the United States of America*, *103*(38), 14086–91. 3

Shenoy, A. R., Wellington, D. A., Kumar, P., Kassa, H., Booth, C. J., Cresswell, P., & MacMicking, J. D. (2012). GBP5 promotes NLRP3 inflammasome assembly and immunity in mammals. *Science*, *338*, 619–621.

Sherman, B. T., Huang, D. W., Tan, Q., Guo, Y., Bour, S., Liu, D., … Lempicki, R. a. (2007). DAVID Knowledgebase: a gene-centered database integrating heterogeneous gene annotation resources to facilitate high-throughput gene functional analysis. *BMC Bioinformatics*, *8*, 426.

Sitthidet, C., Korbsrisate, S., Layton, A. N., Field, T. R., Stevens, M. P., & Stevens, J. M. (2011). Identification of motifs of *Burkholderia pseudomallei* BimA required for intracellular motility, actin binding, and actin polymerization. *Journal of Bacteriology*, *193*(8), 1901–1910.

Sitthidet, C., Stevens, J. M., Chantratita, N., Currie, B. J., Peacock, S. J., Korbsrisate, S., & Stevens, M. P. (2008). Prevalence and sequence diversity of a factor required for actin-based motility in natural populations of *Burkholderia* species. *Journal of Clinical Microbiology*, *46*(7), 2418–2422.

Sitthidet, C., Stevens, J. M., Field, T. R., Layton, A. N., Korbsrisate, S., & Stevens, M. P. (2010). Actin-based motility of *Burkholderia thailandensis* requires a central acidic domain of BimA that recruits and activates the cellular Arp2/3 complex. *Journal of Bacteriology*, *192*(19), 5249–5252.

Sivalingam, S. P., Sim, S. H., Jasper, L. C. W., Wang, D., Liu, Y., & Ooi, E. E. (2008). Pre- and post-exposure prophylaxis of experimental *Burkholderia pseudomallei* infection with doxycycline, amoxicillin/clavulanic acid and co-trimoxazole. *Journal of Antimicrobial Chemotherapy*, *61*(3), 674–678.

Smith, M. F., Mitchell, A., Li, G., Ding, S., Fitzmaurice, A. M., Ryan, K., … Goldberg, J. B. (2003). Toll-like receptor (TLR) 2 and TLR5, but not TLR4, are required for *Helicobacter pylori*-induced NF-κB activation and chemokine expression by epithelial cells. *Journal of Biological Chemistry*, *278*(35), 32552–32560.

Srinivasan, A., Kraus, C. N., DeShazer, D., Becker, P. M., Dick, J. D., Spacek, L., … Thomas, D. L. (2001). Glanders in a military research microbiologist. *The New England Journal of Medicine*, *345*(4), 256–258.

Stanton, A. T., & Fletcher, W. Melioidosis, Studies from the Institute for Medical Reasearch, Federated Malay States (1932).

Stevens, J. M., Ulrich, R. L., Taylor, L. A., Wood, M. W., DeShazer, D., Stevens, M. P., & Galyov, E. E. (2005). Actin-binding proteins from *Burkholderia mallei* and B*urkholderia thailandensis* can functionally compensate for the actin-based motility defect of a *Burkholderia pseudomallei bimA* mutant. *Journal of Bacteriology*, *187*(22), 7857–7862.

Stevens, M. P., Friebel, A., Taylor, L. A., Wood, M. W., Brown, P. J., Hardt, W. D., & Galyov, E. E. (2003). A *Burkholderia pseudomallei* type III secreted protein, BopE, facilitates bacterial invasion of epithelial cells and exhibits guanine nucleotide exchange factor activity. *Journal of Bacteriology*, *185*(16), 4992–4996.

Stevens, M. P., Haque, A., Atkins, T., Hill, J., Wood, M. W., Easton, A., … Galyov, E. E. (2004). Attenuated virulence and protective efficacy of a *Burkholderia pseudomallei bsa* type III secretion mutant in murine models of melioidosis. *Microbiology*, *150*, 2669–2676.

Stevens, M. P., Stevens, J. M., Jeng, R. L., Taylor, L. A., Wood, M. W., Hawes, P., … Galyov, E. E. (2005). Identification of a bacterial factor required for actin-based motility of *Burkholderia pseudomallei*. *Molecular Microbiology*, *56*(1), 40–53.

Stevens, M. P., Wood, M. W., Taylor, L. A., Monaghan, P., Hawes, P., Jones, P. W., … Galyov, E. E. (2002). An Inv/Mxi-Spa-like type III protein secretion system in *Burkholderia pseudomallei* modulates intracellular behavior of the pathogen. *Molecular Microbiology*, *46*(3), 649–659.

Stockinger, S., Kastner, R., Kernbauer, E., Pilz, A., Westermayer, S., Reutterer, B., … Decker, T. (2009). Characterization of the interferon-producing cell in mice infected with *Listeria monocytogenes*. *PLoS Pathogens*, *5*(3), 1–10.

Sulaiman, S., Othman, M., & Aziz, A. (2000). Isolations of enteric pathogens from synanthropic flies trapped in downtown Kuala Lumpur. *Journal of Vector Ecology*, *25*(1), 90–93.

Sun, G. W., & Gan, Y.-H. (2010). Unraveling type III secretion systems in the highly versatile *Burkholderia pseudomallei*. *Trends in Microbiology*, *18*(12), 561–568.

Sun, G. W., Lu, J., Pervaiz, S., Cao, W. P., & Gan, Y. H. (2005). Caspase-1 dependent macrophage death induced by *Burkholderia pseudomallei*. *Cellular Microbiology*, *7*(10), 1447–1458.

Suparak, S., Kespichayawattana, W., Haque, A., Easton, A., Damnin, S., Lertmemongkolchai, G., … Korbsrisate, S. (2005). Multinucleated giant cell formation and apoptosis in infected host cells is mediated by *Burkholderia pseudomallei* type III secretion protein BipB. *Journal of Bacteriology*, *187*(18), 6556–6560.

Suparak, S., Muangsombut, V., Riyapa, D., Stevens, J. M., Stevens, M. P., Lertmemongkolchai, G., & Korbsrisate, S. (2011). *Burkholderia pseudomallei*-induced cell fusion in U937 macrophages can be inhibited by monoclonal antibodies against host cell surface molecules. *Microbes and Infection*, *13*(12-13), 1006–1011.

Supputtamongkol, Y., Kwiatkowski, D., Dance, D., Chaowagul, W., & White, N. J. (1992). Tumor necrosis factor in septicaemic melioidosis. *Journal of Infectious Diseases*, *165*(3), 561–564.

Suzuki, T., Franchi, L., Toma, C., Ashida, H., Ogawa, M., Yoshikawa, Y., … Nuez, G. (2007). Differential regulation of caspase-1 activation, pyroptosis, and autophagy via Ipaf and ASC in *Shigella*-infected macrophages. *PLoS Pathogens*, *3*(8), 1082–1091.

Takeda, K., & Akira, S. (2004). TLR signaling pathways. *Seminars in Immunology*, *16*(1), 3–9.

Tan, K. S., Chen, Y., Lim, Y., Tan, G., Liu, Y., Lim, Y., … Gan, Y. (2010). Suppression of host innate immune response by *Burkholderia pseudomallei* through the virulence factor TssM. *Journal of Immunology*, 1–12.

Tangsudjai, S., Pudla, M., Limposuwan, K., Woods, D. E., Sirisinha, S., & Utaisincharoen, P. (2010). Involvement of the MyD88-independent pathway in controlling the intracellular fate of *Burkholderia pseudomalle*i infection in the mouse macrophage cell line RAW 264.7. *Microbiology and Immunology*, *54*(5), 282–290.

Taylor, P. R., Tsoni, S. V, Willment, J. A., Dennehy, K. M., Rosas, M., Findon, H., … Brown, G. D. (2007). Dectin-1 is required for beta-glucan recognition and control of fungal infection. *Nature Immunology*, *8*(1), 31–38.

Thellin, O., Zorzi, W., Lakaye, B., De Dorman, B., Coumans, B., Hennen, G., … Heinen, E. (1999). Housekeeping genes as internal standars: use and limits. *Journal of Biotechnology*, *75*, 291–295.

Thurston, T. L. M., Wandel, M. P., von Muhlinen, N., Foeglein, A., & Randow, F. (2012). Galectin 8 targets damaged vesicles for autophagy to defend cells against bacterial invasion. *Nature*, *482*, 414–419.

Toesca, I. J., French, C. T., & Miller, J. F. (2014). The type VI secretion system spike protein VgrG5 mediates membrane fusion during intercellular spread by *pseudomallei* group *Burkholderia* species. *Infection and Immunity*, *82*(4), 1436–1444.

Toshchakov, V. U., Basu, S., Fenton, M. J., & Vogel, S. N. (2005). Differential involvement of BB Loops of Toll-IL-1 Resistance (TIR) domain-containing adapter proteins in TLR4- versus TLR2-mediated signal transduction. *J Immunol*, *175*(1), 494–500.

Troegeler, A., Lastrucci, C., Duval, C., Tanne, A., Cougoule, C., Maridonneau-Parini, I., … Lugo-Villarino, G. (2014). An efficient siRNA-mediated gene silencing in primary human monocytes, dendritic cells and macrophages. *Immunology and Cell Biology*, (May), 1–10.

Tsang, A. W., Oestergaard, K., Myers, J. T., & Swanson, J. a. (2000). Altered membrane trafficking in activated bone marrow- derived macrophages Abstract : Activation of macrophages with inter- leads to increased intracellular resistance to mi- Despite the requirement of the macrophage vacu- antigen processing , the rates o, *68*(October), 487–494.

Tuanyok, A., Kim, H. S., Nierman, W. C., Yu, Y., Dunbar, J., Moore, R. A., … Woods, D. E. (2005). Genome-wide expression analysis of iron regulation in *Burkholderia pseudomallei* and *Burkholderia mallei* using DNA microarrays. *FEMS Microbiology Letters*, *252*(2), 327–335.

Tuanyok, A., Tom, M., Dunbar, J., & Woods, D. E. (2006). Genome-wide expression analysis of *Burkholderia pseudomallei* infection in a hamster model of acute melioidosis. *Infection and Immunity*, *74*(10), 5465–5476.

Tusher, V. G., Tibshirani, R., & Chu, G. (2001). Significance analysis of microarrays applied to the ionizing radiation response. *Proceedings of the National Academy of Sciences of the United States of America*, *98*(9), 5116–21.

Ulett, G. C., Ketheesan, N., & Hirst, R. G. (2000). Cytokine gene expression in innately susceptible BALB/c Mice and relatively resistant C57BL/6 mice during infection with virulent *Burkholderia pseudomallei. Infection and Immunity*, *68*(4), 2034–2042.

Utaisincharoen, P., Anuntagool, N., Arjcharoen, S., Limposuwan, K., Chaisuriya, P., & Sirisinha, S. (2004). Induction of iNOS expression and antimicrobial activity by interferon (IFN)-beta is distinct from IFN-gamma in *Burkholderia pseudomallei*-infected mouse macrophages. *Clinical and Experimental Immunology*, *136*(2), 277–83.

Utaisincharoen, P., Anuntagool, N., Limposuwan, K., Chaisuriya, P., & Sirisinha, S. (2003). Involvement of Beta interferon in enhancing inducible nitric oxide synthase production and antimicrobial activity of. *Society*, *71*(6), 3053–3057.

Utaisincharoen, P., Arjcharoen, S., Limposuwan, K., Tungpradabkul, S., & Sirisinha, S. (2006). *Burkholderia pseudomallei* RpoS regulates multinucleated giant cell formation and inducible nitric oxide synthase expression in mouse macrophage cell line (RAW 264.7). *Microbial Pathogenesis*, *40*(4), 184–189.

Utaisincharoen, P., Tangthawornchaikul, N., Kespichayawattana, W., Anuntagool, N., Chaisuriya, P., & Sirisinha, S. (2000). Kinetic studies of the production of Nitric Oxide (NO) and Tumour Necrosis Factor-Alpha (TNF-a) in macrophages stimulated with *Burkholderia pseudomallei* endotoxin. *Clinical and Experimental Immunology*, *122*(3), 324–329.

Utaisincharoen, P., Tangthawornchaikul, N., Kespichayawattana, W., Chaisuriya, P., & Sirisinha, S. (2001). *Burkholderia pseudomallei* interferes with inducible nitric oxide synthase (iNOS) production: a possible mechanism of evading macrophage killing. *Microbiology and Immunology*, *45*(4), 307–313.

Van Gelder, R. N., von Zastrow, M. E., Yool, a, Dement, W. C., Barchas, J. D., & Eberwine, J. H. (1990). Amplified RNA synthesized from limited quantities of heterogeneous cDNA. *Proceedings of the National Academy of Sciences of the United States of America*, *87*(5), 1663–1667.

Vandesompele, J., De Preter, K., Pattyn, F., Poppe, B., Van Roy, N., De Paepe, A., & Speleman, F. (2002). Accurate normalization of real-time quantitative RT-PCR data by geometric averaging of multiple internal control genes. *Genome Biology*, *3*(7), RESEARCH0034.

Vellasamy, K. M., Mariappan, V., Shankar, E. M., & Vadivelu, J. (2016). *Burkholderia pseudomallei* differentially regulates host innate immune response genes for intracellular survival in lung epithelial cells. *PLOS Neglected Tropical Diseases*, *10*(7), e0004730.

Verreck, F. A. W., de Boer, T., Langenberg, D. M. L., Hoeve, M. A., Kramer, M., Vaisberg, E., … Ottenhoff, T. H. M. (2004). Human IL-23-producing type 1 macrophages promote but IL-10-producing type 2 macrophages subvert immunity to (myco)bacteria. *Proceedings of the National Academy of Sciences of the United States of America*, *101*(13), 4560–4565.

Vojo, D., & Kliewer, S. A. (2012). Autophagy as an innate immunity paradigm: expanding the scope and repertoire of pattern recognition receptors. *Current Opinion in Microbiology*, *24*(1), 21–31.

Von Moltke, J., Ayres, J. S., Kofoed, E. M., Chavarría-Smith, J., & Vance, R. E. (2013). Recognition of bacteria by inflammasomes. *Annual Review of Immunology*, *31*(1), 73–106.

Vyas, S., & Chang, P. (2014). New PARP targets for cancer therapy. *Nature Reviews Cancer*, *14*(7), 502–509.

Warawa, J. M., Fields, K., & Torres, A. G. (2010). Evaluation of surrogate animal models of melioidosis. *Frontiers in Immunology*, 1, 141-153.

Warawa, J., & Woods, D. E. (2005). Type III secretion system cluster 3 is required for maximal virulence of *Burkholderia pseudomallei* in a hamster infection model. *FEMS Microbiology Letters*, *242*, 101–108.

Warren, S. E., Mao, D. P., Rodriguez, A. E., Miao, E. A., & Aderem, A. (2008). Multiple Nod-Like receptors activate caspase 1 during *Listeria monocytogenes* infection. *Journal of Immunology*, *180*, 7558–7564.

Watson, R. O., Manzanillo, P. S., & Cox, J. S. (2012). Extracellular *M. tuberculosis* DNA targets bacteria for autophagy by activating the host DNA-sensing pathway. *Cell*, *150*(4), 803–815.

Weehuizen, T. A. F., Prior, J. L., Van Der Vaart, T. W., Ngugi, S. A., Nepogodiev, S. A., Field, R. A., … Wiersinga, W. J. (2015). Differential Toll-Like Receptor-signalling of *Burkholderia pseudomallei* lipopolysaccharide in murine and human models. *PLoS ONE*, *10*(12), 1–15.

Welch, M. D., Iwamatsu, A., & Mitchison, T. J. (1997). Actin polymerization is induced by Arp2/3 protein complex at the surface of *Listeria monocytogenes. Nature*, *385*, 265–269.

West, T. E., Chantratita, N., Chierakul, W., Limmathurotsakul, D., Wuthiekanun, V., Myers, N. D., … Skerrett, S. J. (2013). Impaired TLR5 functionality is associated with survival in melioidosis. *Journal of Immunology (Baltimore, Md. : 1950)*, *190*(7), 3373–9.

West, T. E., Chierakul, W., Chantratita, N., Limmathurotsakul, D., Wuthiekanun, V., Emond, M. J., … Skerrett, S. J. (2012). Toll-like receptor 4 region genetic variants are associated with susceptibility to melioidosis. *Genes and Immunity*, *13*(1), 38–46.

West, T. E., Ernst, R. K., Jansson-Hutson, M. J., & Skerrett, S. J. (2008). Activation of Toll-like receptors by *Burkholderia pseudomallei*. *BMC Immunology*, *9*, 46.

West, T. E., Myers, N. D., Chantratita, N., Chierakul, W., Limmathurotsakul, D., Wuthiekanun, V., … Skerrett, S. J. (2014). NLRC4 and TLR5 each contribute to host defense in respiratory melioidosis. *PLoS Neglected Tropical Diseases*, *8*(9), e3178.

Whitmore, A., & Krishnaswami, C. S. (1912). An account of the discovery of a hitherto undescribed infective disease occurring among population of Rangoon. *Indian Medical Gazette*, *47*, 262–267.

Wiersinga, W. J., Currie, B. J., & Peacock, S. J. (2012). Melioidosis. *New England Journal of Medicine*, *367*(11), 1035–1044.

Wiersinga, W. J., Wieland, C. W., Dessing, M. C., Chantratita, N., Cheng, A. C., Limmathurotsakul, D., … Van Der Poll, T. (2007). Toll-like receptor 2 impairs host defense in gram-negative sepsis caused by *Burkholderia pseudomallei* (Melioidosis). *PLoS Medicine*, *4*(7), 1268–1280.

Wiersinga, W. J., Wieland, C. W., Roelofs, J. J. T. H., & van der Poll, T. (2008). MyD88 dependent signaling contributes to protective host defense against *Burkholderia pseudomallei. PloS One*, *3*(10), e3494.

Wiersinga, W. J., Wieland, C. W., Van Der Windt, G. J. W., De Boer, A., Florquin, S., Dondorp, A., … Van Der Poll, T. (2007). Endogenous interleukin-18 improves the early antimicrobial host response in severe melioidosis. *Infection and Immunity*, *75*(8), 3739–3746.

Wileman, T. (2013). Autophagy as a defence against intracellular pathogens. *Autophagy: Molecules and Mechanisms*, *55*, 153–163.

Wong, K. T., Puthucheary, S. D., & Vadivelu, J. (1995). The histopathology of human melioidosis. *Histopathology*, *26*(1), 51–55.

Xu, Y., Tao, X., Shen, B., Horng, T., Medzhitov, R., Manley, J. L., & Tong, L. (2000). Structural basis for signal transduction by the Toll/interleukin-1 receptor domains. *Nature*, *408*(6808), 111–5.

Xu, Y., Xie, J., Li, Y., Chen, J., & Wang, H. (2003). Using a cDNA microarray to study cellular gene expression altered by *Mycobacterium tuberculosis*. *Chinese Medical Journal*, *116*(7), 1070–1073.

Yamamoto, M., Sato, S., Hemmi, H., Hoshino, K., Kaish, T., Sanjo, H., … Akira, S. (2003). Role of adaptor TRIF in the MyD88-Independent Toll-like receptor signaling pathway. *Science*, *301*(5633), 640–643.

Yoshikawa, Y., Ogawa, M., Hain, T., Yoshida, M., Fukumatsu, M., Kim, M., … Sasakawa, C. (2009). Listeria monocytogenes ActA-mediated escape from autophagic recognition. *Nature Cell Biology*, *11*(10), 1233–1240.

Yu, M., Schreek, S., Cerni, C., Schamberger, C., Lesniewicz, K., Poreba, E., … Lüscher, B. (2005). PARP-10, a novel Myc-interacting protein with poly(ADP-ribose) polymerase activity, inhibits transformation. *Oncogene*, *24*(12), 1982–1993.

Zhang, X., Edwards, J. P., & Mosser, D. M. (2009). The expression of exogenous genes in macrophages: obstacles and opportunities. *Methods in Molecular Biology*, *531*, 287–300.

Zhao, H., Granberg, F., Elfineh, L., Pettersson, U., & Svensson, C. (2003). Strategic attack on host cell gene expression during adenovirus infection. *Journal of Virology*, *77*(20), 11006–15.

Zheng, Y. T., Shahnazari, S., Brech, A., Lamark, T., Johansen, T., & Brumell, J. H. (2009a). The adaptor protein p62/SQSTM1 targets invading bacteria to the autophagy pathway. *Journal of Immunology (Baltimore, Md. : 1950)*, *183*(9), 5909–5916.

Zheng, Y. T., Shahnazari, S., Brech, A., Lamark, T., Johansen, T., & Brumell, J. H. (2009b). The adaptor protein p62/SQSTM1 targets invading bacteria to the autophagy pathway. *Journal of Immunology (Baltimore, Md. : 1950)*, *183*(9), 5909–5916.